SPATIALLY-LOCALIZED CORRELATION OF MRI AND MECHANICAL STIFFNESS TO ASSESS CARTILAGE INTEGRITY IN THE HUMAN TIBIAL PLATEAU

by

Joseph Thomas Samosky

B.S.E. Electrical Engineering, University of Pittsburgh 1985
B.S. Behavioral Neuroscience, University of Pittsburgh 1986
M.S. Electrical Engineering and Computer Science, MIT 1993

SUBMITTED TO THE HARVARD-MIT DIVISION OF HEALTH SCIENCES AND TECHNOLOGY
IN PARTIAL FULFILLMENT OF THE REQUIREMENTS FOR THE DEGREE OF

DOCTOR OF PHILOSOPHY IN MEDICAL ENGINEERING

AT THE

MASSACHUSETTS INSTITUTE OF TECHNOLOGY

JUNE 2002

ARCHIVES
MASSACHUSETTS INSTITUTE OF TECHNOLOGY
MAY 0 9 2002
LIBRARIES

© 2002 Massachusetts Institute of Technology
All rights reserved

Signature of Author ______________________________
Harvard-MIT Division of Health Sciences and Technology
March 21, 2002

Certified by ______________________________
W. Eric L. Grimson
Thesis Co-supervisor, Bernard M. Gordon Professor of Medical Engineering

Certified by ______________________________
Martha L. Gray
Thesis Co-supervisor, Edward Hood Taplin Professor of Medical and Electrical Engineering

Accepted by ______________________________
Martha L. Gray
Chair, Graduate Committee

Spatially-Localized Correlation of MRI and Mechanical Stiffness to Assess Cartilage Integrity in the Human Tibial Plateau

by

Joseph Thomas Samosky

Submitted to the Harvard-MIT Division of Health Sciences and
Technology on March 21, 2002 in Partial Fulfillment
of the Requirements for the Degree of
Doctor of Philosophy in Medical Engineering

ABSTRACT

Osteoarthritis is a painful degenerative joint disease affecting millions of people in the U.S. The pathogenesis of articular cartilage disease is characterized by softening of cartilage and loss and disruption of constituent macromolecules including proteoglycans and collagen. In current orthopaedic surgical practice, the gold standard for evaluating articular cartilage integrity is the use of a hand probe during arthroscopy. Mechanical probing, however, is invasive and requires anesthesia. Tightly confined areas of the articular surface can be difficult to reach and assess, and manual probing provides a subjective rather than a quantitative assessment of cartilage mechanical integrity.

This thesis was motivated by the desire for a noninvasive and nondestructive means to map the variation in mechanical stiffness of an articular surface. Such a method could potentially have application to guiding surgeons during procedures and quantitatively assessing the efficacy of medical and surgical therapies. It could also potentially provide patient-specific, *in vivo* tissue mechanical property data for surgical simulation and preoperative procedure planning.

The macromolecule glycosaminoglycan (GAG) is a significant determinant of cartilage stiffness. GAG content can be assessed noninvasively *in vivo* and *in vitro* by an MRI-based technique known as delayed gadolinium-enhanced magnetic resonance imaging of cartilage (dGEMRIC), which measures the MRI parameter T1 after equilibration with the ionic contrast agent $Gd(DTPA)^{2-}$. With dGEMRIC, $T1_{Gd}$ serves as an index of GAG content: we therefore examined whether cartilage stiffness could be related to dGEMRIC-measured $T1_{Gd}$ in samples of human tibial plateaus.

We developed an experimental methodology to permit indentation test sites and regions in dGEMRIC scans to be registered with submillimeter accuracy. We found that the load response to focal indentation (a measure of local stiffness) and locally-averaged $T1_{Gd}$ were in general highly correlated (Pearson correlation coefficients $r = .80, .90, .64, .81$ ($p < .002$) for four different patient samples, 130 total test locations). We further demonstrated that the observed correlation is not a simple consequence of cartilage thickness effects. We observed that the parameters of the stiffness–$T1_{Gd}$ relationship differed in some samples between the region of the tibial plateau covered by the meniscus *in vivo* and the more central region normally in contact with the femoral condyle. This suggests that another factor such as surface architecture or collagen integrity also influences the indentation response of the articular surface.

Thesis Supervisors:	William Eric Leifur Grimson, Ph.D. Bernard M. Gordon Professor of Medical Engineering, MIT
	Martha L. Gray, Ph.D. Edward Hood Taplin Professor of Medical and Electrical Engineering

Thesis Committee Members

Committee Cochair
W. Eric L. Grimson, Ph.D.
Bernard M. Gordon Professor of Medical Engineering
Associate Director, Artificial Intelligence Laboratory
Department of Electrical Engineering and Computer Science
Massachusetts Institute of Technology

Committee Cochair
Martha L. Gray, Ph.D.
Edward Hood Taplin Professor of Medical and Electrical Engineering
Co-Director, Harvard-MIT Division of Health Sciences and Technology
Massachusetts Institute of Technology

Robert D. Howe, Ph.D.
Gordon McKay Professor of Engineering
Division of Engineering and Applied Sciences
Harvard University

Scott D. Martin, M.D.
Department of Orthopaedic Surgery
Brigham and Women's Hospital/Partners Healthcare System
Instructor of Orthopedic Surgery, Harvard Medical School
Boston, Massachusetts

Sarah Frisken, Ph.D.
Senior Research Scientist
Mitsubishi Electric Research Laboratories
Cambridge, Massachusetts

Acknowledgments

Of all the pages in this thesis, these are the most enjoyable to write.

It has been a privilege to have had Eric Grimson and Martha Gray as my thesis advisors. I am deeply grateful to them for their support, insight, patience and guidance.

Eric has an unfailingly optimistic attitude and a keen editor's eye. His excitement and energy toward research are infectious and inspiring. I have learned a great deal from Eric's example about how to distill the essentials of problems, experiments and prose. I am also very grateful to Eric for financial support for this work, most especially during a critical period of time when my family needed me and I was away from the lab and MIT.

A long time ago, I sat talking with Martha in her office in building E36, long before she took over the reigns of power of the HST empire. It was during a semester when all of our HST weekly seminar presenters gave talks either about cartilage or MRI, and the standing joke at that time was that if you were a Medical Engineering student, you could save time when asking a colleague about their research by condensing the question to "Cartilage or MRI?" I recall proudly telling Martha at the time that I had no intention of being drawn into either the cartilage or MRI vortices within HST. Of course, as luck would have it, I spun into both. I am extremely appreciative to Martha for taking on a much larger role in this work as the focus shifted more toward the experimental science of cartilage. Martha's always insightful questions have challenged me and refined how I think about experiments, data and "what it all means." She also has an outlook that focuses not on what may have gone wrong, but on the next step to make things work right. It's a very valuable lesson and an ultimately very productive approach.

I am also extremely thankful to both Eric and Martha for the time they have spent reading and editing many drafts of my work over a period of many months.

I simply cannot adequately express my appreciation to Scott Martin for his helpfulness and encouragement throughout this work. Scott welcomed me into the operating room, allowing me to scrub in with him on procedures and to actually examine joints with an arthroscope and probe. He enlisted the aid of his fellow surgeon colleagues at both the Brigham and Women's Hospital and the West Roxbury VA to help obtain tissue samples. Scott is an extraordinary surgeon, an exemplary teacher and a good friend. His encouragement has been a bright beacon at many a cloudy moment and I am extremely fortunate to know and work with him.

Robert Howe clearly enjoys both mechanical design and students, and I had many valuable and enjoyable discussions with Rob about mechanics, haptics and the design of an instrumented surgical probe. Rob also allowed me use of the facilities of the Harvard Biorobotics Laboratory to test the probe, and he put me in touch with his student Anna Galea and her finite element modeling work.

Speaking of Anna—thank *you*! Anna, in addition to the intriguing combination of being a thespian, fencer and metalsmith, was extremely helpful in running the finite element models I used to examine stress distribution and thickness effects on indenter force. Many models. First in 2D, then in 3D. (We drew the line at 4D). She was extremely generous with her time through multiple iterations of the models, and I am very appreciative for her time and effort.

I am especially appreciative to Sarah Frisken for germinating the seeds that grew into this PhD. Sarah led the project team at Mitsubishi Electric Research Labs that developed a prototype arthroscopic knee surgery simulator which inspired the questions I addressed in this thesis. Sarah brought people of varied backgrounds and skills together and created a motivating and exciting research environment. I also thank Sarah for many excellent discussions.

Deborah Burstein has been an honorary sixth member of my committee and has offered many critiques of this work, in particular providing good discussions of MRI and valuable insights in how to think about quick experiments to elicit "90% results with 10% time and effort."

Thanks to Jeeva Munasinghe for many hours of help setting up and running the MRI scans, for tasty rice dishes with flavors I've never before encountered (dried Maldive fish?) and for mutually encouraging conversations when circumstances were less than encouraging.

I appreciate the time Adil Bashir spent early on in getting me oriented to the arcane mysteries of MRI. Thanks also to Bruce Po for his excellent work in creating an efficient and comprehensible T1 computation program for the lab.

Toolmaking has been long regarded as one of the signal characteristics distinguishing humans from our other animal neighbors on this planet (although some recent observations of chimps using twigs to extract tasty ants from anthills—a sort of ant fondue—casts some doubt on this.) But, ant-dipping aside, I have no doubt that artful, elegant toolmaking is a supremely human enterprise. I am deeply appreciative to the supreme humans Ron Wiken, Mark Ottensmeyer and Bill "Crash" Yerazounis for sharing the art and science of machining with me. Ron, I can't thank you enough for your teaching me how to turn lumps of aluminum and plastic into scientific tools. Pretty much everything I know about machining I owe to Ron. As manager of the AI Lab Machine Shop, Ron always dropped what he was doing when I came into his office (which also serves as the parts treasure chest for the AI Lab) and took the time to show me how to mount a tool on the lathe or solve a tricky set-up with the milling machine. (Or, most excitingly, he'd pull out his secret cache of "special tools" he kept for high-precision work and let me use these preciously guarded gems.) Mark, thank you for welcoming me into your lab and for creating devices which amazed me and showed me what a *real* machinist can aspire to. (Thanks also for always having NPR on the radio!) And Bill was unceasingly helpful in allowing me access to the machine shop at MERL and teaching me the *rest* of what I know about machining.

Of course, there are drawbacks to everything, and one consequence of my hours with Ron and Mark and Bill is that I now regard anything with less than .001 inch tolerances as downright sloppy!

Next, Rachel Oppenheimer. Wow, where do I even begin? Rachel, in addition to being one of the most thorough, careful and conscientious experimentalists I have ever worked with, also brightened the lab each day with the most innovative fashion designs ever seen at the Harvard Institutes of Medicine. Rachel was daily an absolutely invaluable asset to my experimental work, had exquisite taste in electronica and brought fun to working on even the most tedious experiments. Bill Nye rules!

I'd like to thank the patients from whose knees the cartilage I examined came. It's sometimes easy when working with these samples during long nights over many months to come to regard them as abstractions. But each of these objects was once a living part of someone's body and served them well for 60, 70 or 80 years. These samples helped these patients to dance in celebration after World War II and walk up the aisle at their weddings and play with their children. It has been a privilege to be able to employ these samples of their bodies in my work.

Nina Menezes, Allison Pettit and Amy Gillis have made the lab a fun place to be. Bob Choy solved many a Mac or PC-related problem for us. Marilyn Tessier and Bernd Comjean have made the path between wanting to order something and actually *getting* that something as straight a line as possible. (And thank you, Marilyn, for reimbursing expenses for materials that required a certain amount of explanation.) Betty Chase is an island of comfort in an often hectic sea.

There have been many, many people along this journey who have enriched my life, taught me many things, opened my eyes and made the trip very worthwhile. I especially thank Kathleen Donahue, Marie-José Belanger, Brian, Tim Davis, Naomi Chesler, Dan Sidney, Dan Sodickson, Joelle Dennie, Tom Quinn, Minerva Garcia, and Paula Ragan for their friendship and for making MIT a much, much better place.

I only wish I possessed words equal to the breadth and depth of my gratitude to Ashley Williams—my experimental results, my thesis, my appreciation of dance and the arts, my fitness, my dinners, my life and my sense of my place in the cosmos have all been made better because of you—are you sure you're just *one* person?! Thank you for being helpful in so many different ways, and for being so exceptional at all of them. Thank you especially for your patience, and kindness and friendship when I have most needed them. I'm really glad you came down from the mountains to dance by the sea.

Finally, Mom, thank you so much for your love and encouragement and for your unfailing confidence in me. Thank you for your support, whether it was your always supportive words or the exquisitely timed care package of cookies! Thank you for your example of integrity, hard work, and dedication to others, qualities shared in equal measure with Dad. Although my dad did not live to see this thesis completed, I can palpably imagine the joy and pride he would have felt. If in my life and work I can help people even a fraction as much as my dad in his simple goodness and hard work did, I will consider my life's work a to be a consummate success. I dedicate this research and this thesis to him.

Joseph T. Samosky
March 21, 2002
Cambridge, MA

Financial support of this work was provided from the National Science Foundation, the National Institutes of Health, and Mitsubishi Electric Research Laboratories (MERL).

Contents

Table of Figures

Chapter 1

Introduction

1.1 Motivation: the impact of arthritis

Movement is an essential part of being human. We are highly articulated organisms, with 254 synovial joints, those permitting the freest and widest range of movement, in each of our bodies. Each articulation depends for its smooth, painless motion on the gliding of two cartilage surfaces to allow movement of one bone relative to another. The synovial joint appears in evolutionary history at about the time that creatures moved from the oceans to the land. Without cartilage, we could not locomote, we could not dance or sing, we could not reach out with extended limbs and opposable thumbs and grasp and manipulate our environment, we could not move toward and touch one another.

Arthritis is disease of cartilage, and collectively all forms of arthritis are the main cause of disability in the U.S., accounting for nearly 18% of all disability and limiting daily activities for more than 7 million Americans (Centers for Disease Control and Prevention 2001). Approximately 43 million persons in the U.S. suffer from some form of arthritis, at a resulting cost of $65 billion in treatment and lost productivity due to disability. By 2020, an estimated 20% of the population will be affected. Arthritis is not just morning stiffness–its impact can be profound and devastating. It can compromise the ability to work, to express oneself artistically and creatively, and to be an active participant in the community. The consequences of severe arthritis can range from increased personal isolation to increased risk for cardiovascular disease due to the inability to exercise without debilitating pain. Better means to understand, diagnose and treat cartilage pathology thus offer enormous potential to improve the quality of life for millions of persons.

1.2 Motivation: applications

The research program described in this thesis had its origin in prior work as part of a project to develop a computer-based simulator for arthroscopic surgery in the knee (Figure 1-1) (Gibson, Fyock, Grimson et al. 1998). Arthoscopy is used to diagnose and treat both arthritic degeneration and traumatic pathology in the larger joints, particularly the knee and shoulder. A fundamental question faced in the simulator development effort, however, was how to obtain mechanical property data for the soft tissues of the simulated

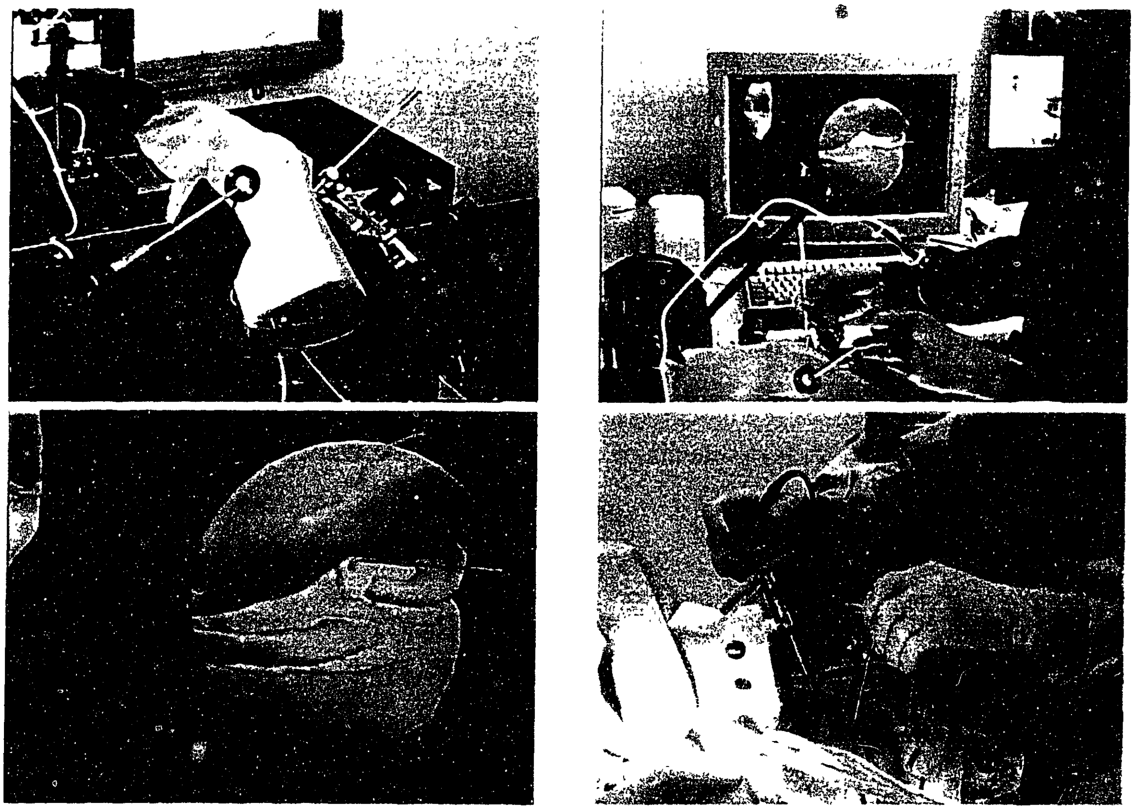

Figure 1-1 An arthroscopic surgical simulator (top, left and right) employs computer models of the knee and tools such as an arthroscope and mechanical probe. The system renders visual images (bottom left) and forces (via a haptic interface) that simulate the perceptually salient features of real arthroscopic surgery (bottom right). The simulator shown was developed by a consortium consisting of MERL – A Mitsubishi Electric Research Laboratory, MIT's AI Laboratory, CMU's Medical Robotics Laboratory and the Brigham and Women's Hospital Surgical Planning Laboratory.

knee. Most importantly, we wished to *noninvasively* assess mechanical integrity of the cartilage in a patient, so that we could model and simulate a patient-specific virtual knee, which could then be used for training, preoperative rehearsal or planning.

Beyond cartilage mechanical property measurement for simulation, the ability to assess cartilage mechanical integrity noninvasively, nondestructively and with good spatial resolution offers additional application to aiding surgeons performing diagnostic arthroscopy. The methodology of this work also has application to basic research in understanding the biomechanical behavior of normal and diseased cartilage.

Surgical simulation

Arthroscopy is the most common orthopedic procedure in the U.S., offering numerous benefits to patients compared to open surgery. It is a procedure requiring considerable skill, however, and residents face a steep learning curve due to significant constraints on visibility, instrument movement and demanding psychomotor coordination requirements. Surgical simulators, and in particular simulators utilizing three-dimensional computer graphics and force-feedback (haptic) interfaces may offer significant benefits in helping surgeons learn arthroscopic techniques progressively, comprehensively and with less risk exposure for patients.

The development and use of such computer-based simulators has received increasing recent interest (Dawson and Kaufman 1998), and numerous clinicians have advocated the use of simulation for surgical procedure training, and particularly for training in minimally invasive techniques such as arthroscopy (Satava and Jones 1998; Azar and Andrews 1997; Ota, Loftin, Saito et al. 1995; Satava 1993). Ota et al. go so far as to make the speculation that use of virtual reality simulators in surgical procedure training could potentially reduce a 5 year residency program to 3 years, owing to the increase in the number and variety of training cases (Ota, Loftin, Saito et al. 1995).

Current simulators, however, are handicapped by a lack of empirical, patient-specific tissue-property data. The noninvasive mapping of, for example, the stiffness of the cartilage surface in the knee could be used to provide data for surgical simulators employed for procedure training and rehearsal, enabling more perceptually realistic haptic simulation of a task such as probing the articular surface (Gibson, Fyock, Grimson et al.

1998). Although *in vitro* mechanical measurements of cadaveric joints or articular surfaces removed during total joint replacement could also provide material property data for surgical simulation, a noninvasive acquisition methodology could offer patient-specific, *in vivo* data to support the planning and rehearsing of procedures for specific surgeries on individual patients.

Noninvasive, comprehensive evaluation and diagnosis of articular surface pathology

The pathogenesis of early articular cartilage disease is characterized by loss and disruption of matrix macromolecules including proteoglycans and collagen. Alterations in the biochemistry and organization of the matrix cause diminished mechanical integrity of the cartilage with resulting impairment of its essential function in load bearing, load distribution and lubrication of the synovial joint. Clinically, this functional impairment presents as pain and stiffness in the affected joint, but disease progression by the time of presentation may be substantial. Clinical diagnosis of degenerative change in the articular surface is made on the basis of medical history, clinical examination, radiographic studies and, typically in more advanced and severe cases, arthroscopy. Unfortunately, the gold standard (and sole) methodology for assessing cartilage functional integrity is currently also the most invasive, namely, visualization and manual probing of the articular surface during diagnostic arthroscopy.

The round-ended probe is regarded as the arthroscopist's single most important diagnostic tool in assessing cartilage integrity (Azar and Andrews 1997; Metcalf and Sweeny 1996; Shahriaree 1992), and has been described as an extension of the surgeon's finger or hand, permitting the size and consistency of an articular surface lesion to be felt as well as seen. Through manual application of a mechanical load and observing both visually and proprioceptively the resulting deformation of the cartilage, probing reveals the relative firmness or softness of the cartilage and enables evaluation of the extent of chondromalacia present (Figure 1-2). Probing can reveal pathological softening even in cases where visual inspection reveals an apparently normal surface, such as in cases of early, low-grade (stage 1) chondromalacia (Conway, Hayes, Loughran et al. 1991), cases in which softening occurs deep to the surface or where fibrous tissue masks an underlying abnormality (Joyce and Andrews 1997). Indeed, in one study of chondromalacia patellae, no visible changes in cartilage appearance were seen in a majority (55 out of 98) of patients with quantitatively measured mechanical softening of the patellar surface (Dashefsky 1987).

In addition to being invasive, traditional arthroscopic probing is subjective, and in particular does not support quantitative assessment of cartilage mechanical properties, thus limiting its applicability to accurately map stiffness variation across an articular surface, between patients or longitudinally over time. Several instrumented devices have been developed to provide more quantitative *in vivo* assessment of cartilage mechanical function. These include an indentation elastometer fixed to the joint during open surgical

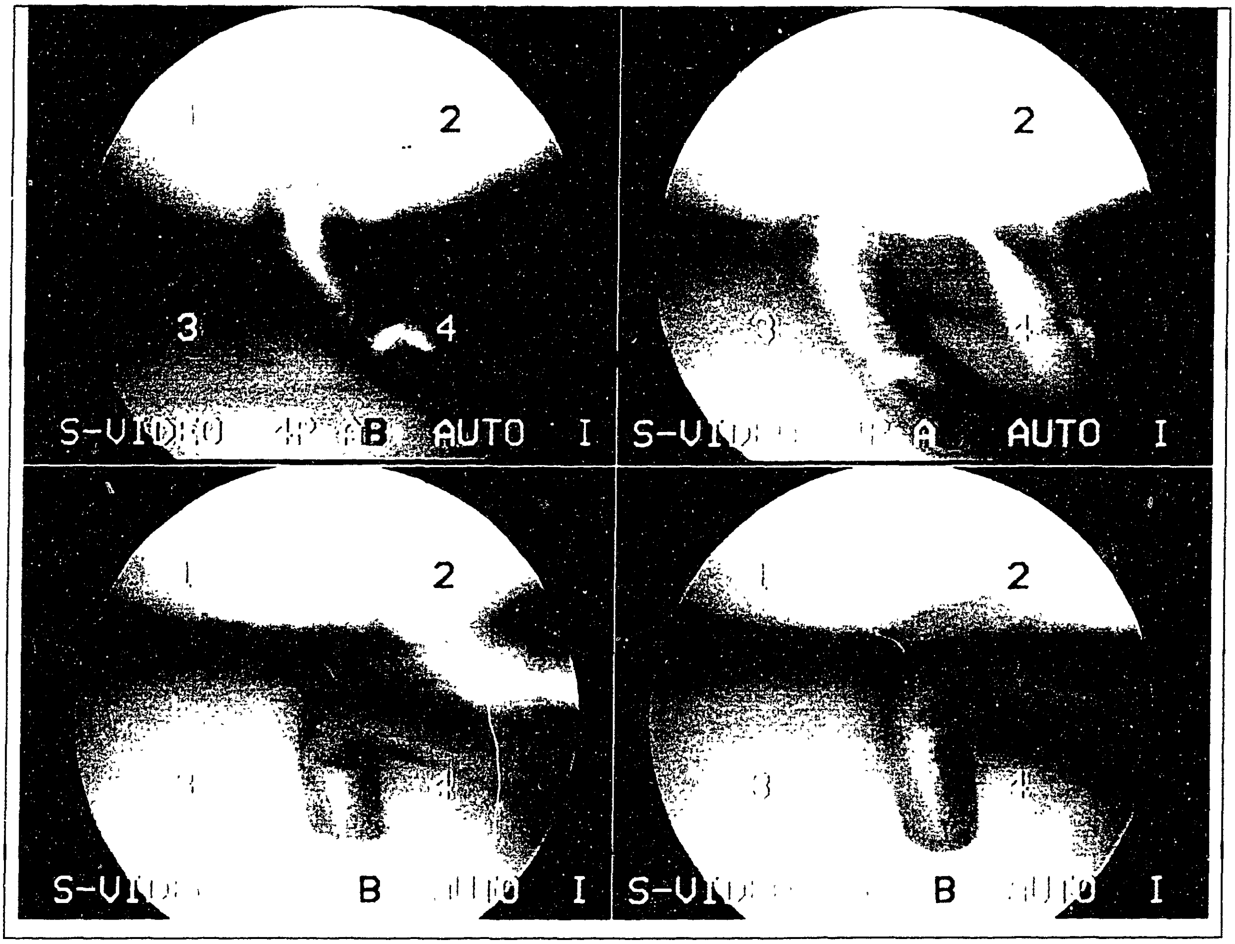

Figure 1-2 Arthroscopic video images of the diagnostic probing of the articular surfaces of the knee. The top two images show probing of relatively healthy cartilage on the femoral condyle–note the relatively slight indentation of the cartilage beneath the probe tip in the upper right frame. As the probe was then moved across the tibial plateau (bottom), the tip sank into a focal area of softened cartilage (lower left). Such regions of chondromalacia may not be apparent to visual inspection, but are revealed by probing. (Images acquired during arthroscopic surgery at the Brigham and Women's Hospital, Boston.)

procedures (Tkaczuk 1986; Tkaczuk, Norrbom and Werelind 1982), hand-held probes which indent the cartilage surface under manual pressure and measure the resulting force (Niederauer, Cristante, Niederauer et al. 1998; Lyyra, Jurvelin, Pitkanen et al. 1995; Dashefsky 1987) and a probe combining ultrasound measurement of cartilage thickness with automated displacement-controlled indentation (Fu, Youn and Suh 1998). A device exploiting the phenomenon of current-generated stress in order to characterize cartilage electromechanical response has also been demonstrated (Berkenblit, Frank, Salant et al. 1994) and work has been done to adapt the probe for *in vivo* application (Treppo, Quan, Batra et al. 1998). Instrumented probes enable direct and quantitative assessment of cartilage mechanical behavior, but require surgical invasion. Arthroscopy also imposes significant constraints on instrument maneuverability, and all mechanical probes, whether conventional or instrumented, can encounter challenges in gaining access to tightly confined areas of the articular surface such as the posterior tibial plateau or the posterior aspects of the femoral condyles.

A noninvasive method of assessing cartilage mechanical integrity would offer potential benefits in a variety of applications. Regions of the articular surface difficult to reach or inaccessible to an arthroscopic probe could be evaluated. Quantitative and comparative assessments could be made to permit longitudinal study of the evolution of patterns of degeneration and progression in early-stage disease which might be hidden from even visual inspection of the articular surface. Noninvasive tracking of changes in cartilage integrity would be a key asset in the assessment and development of both pharmacologic and surgical therapeutic interventions.

Furthermore, a noninvasive, imaging-based technique permitting distributed topographic mapping (rather than the point-wise measurement provided by a probe) would enable the creation of visual maps portraying stiffness variation across a three-dimensional rendering of the articular surface. Such visualizations could serve as useful “road maps” for surgeons for guidance during procedures, offering them, in one view, comprehensive insight into where the cartilage is healthy or soft, especially in areas difficult to access by mechanical probing, and indicating areas deserving particular attention. Such maps could save time in the operating room, and saved OR time equates to both reduced patient anesthesia and lower cost.

1.3 Objectives and specific questions addressed in this thesis

Motivated by these goals and applications, we have investigated the application of delayed $Gd(DTPA)^{2-}$ enhanced magnetic resonance imaging of cartilage (dGEMRIC), a noninvasive, clinically-applicable MRI technique, for assessing the *in situ* mechanical response of the articular surface to indentation. Recently, MRI-based methods have shown significant utility in revealing not only the anatomy and morphology of the articular surface, but allowing assessment of cartilage biochemical composition as well (Burstein, Bashir and Gray 2000). In particular, dGEMRIC has been shown to be practical for evaluating cartilage glycosaminoglycan (GAG) concentrations both *in vitro* and *in vivo* (Burstein, Velyvis, Scott et al. 2001; Allen, Burstein and Gray 1999; Bashir, Gray, Hartke et al. 1999; Bashir, Gray, Boutin et al. 1997; Bashir, Gray and Burstein 1996). Since GAG has been shown to be a determinant of cartilage stiffness, we undertook the examination of whether dGEMRIC could be used as a noninvasive means to assess the mechanical integrity of the articular surface.

Specifically, we addressed the central question of whether a correlation can be observed between the stiffness at loci on an articular surface, as measured by the load response to indentation testing, and the locally-averaged $T1_{Gd}$ at the loci, using dGEMRIC. Since dGEMRIC $T1_{Gd}$ measurement is an indicator of GAG content, we hypothesized that it could have predictive value in assessing cartilage mechanical integrity.

The following specific questions were also addressed:

Sample-specific and anatomical patterns

- If a correlation is seen between stiffness and $T1_{Gd}$, is the correlation the same across samples from different patients?
- Do human tibial plateaus show any typical spatial patterns or regional differences in stiffness variation and stiffness-$T1_{Gd}$ correlation?

Details of the relationship between load response and $T1_{Gd}$ (or GAG)

- Does the relationship between load response and local GAG concentration depend on the magnitude and time course of indentation? Specifically, does locally-averaged $T1_{Gd}$

correlate to a more or less degree with the load responses elicited by fixed-amplitude and fixed-strain pulse displacements (short-time or "instantaneous" response), fixed-amplitude and fixed-strain step displacements (equilibrium response), and sinusoidal steady-state compression at different frequencies (dynamic response)?

- Given a fixed indenter size, geometry and indentation depth, how does the correlation between stiffness and $T1_{Gd}$ vary with the depth of the region-of-interest (ROI) used for averaging $T1_{Gd}$?
- How does the ROI which maximizes load–$T1_{Gd}$ (or load–GAG) correlation compare with the stress field in the region of indentation as predicted by finite-element modeling? In particular, do we see a reasonable correspondence between the region of cartilage predicted to contain most of the stress/strain field and the ROI which maximizes the correlation between cartilage GAG and stiffness?

Examination of confounding/other variables

- How does variation in cartilage thickness affect indentation test results? Can we separate the effect of variations in thickness from the effect of local GAG concentration on measured indentation load response? What effect due to thickness variation does finite element modeling predict?
- Are other factors (besides GAG content) suggested as affecting indentation response?

Methodological questions

- How can pixels in an MR scan be registered with physically measured locations on the surface of an osteochondral sample? What tools, techniques and methodologies can be developed and applied to achieve this?
- What spatial accuracy do we obtain when positioning the indenter on the surface of a sample?
- Does our technique for positioning an indenter at a specific locus on a cartilage surface and measuring cartilage stiffness at that locus give repeatable results when the same location is tested over a short time interval (minutes to hours)? (with and without intervening movement of the indenter with respect to the sample)
- How much interoperator variability occurs when performing repeated mechanical measurements with our system?

- When performing indentation testing on a rectangular sample, how does proximity of the test locus to an edge or a corner affect measured load responses? What implications does this have for defining valid test regions on a sample?
- Do our sample handling/storage protocols affect cartilage mechanical properties? Specifically, do measurements of stiffness show change over long time intervals (weeks to months) with intervening exposure of the samples to freezing, refrigeration and room temperature?

1.4 Thesis overview

We here provide a brief overview of the central experimental methods employed in this study. Following this, a chapter-by-chapter guide is offered to orient the reader to the main points we covered herein.

Outline of overall approach

Preliminary studies to develop registration, mechanical testing and imaging methods were conducted using partially-trypsinized bovine tibial plateaus. These were equilibrated in 1 mM $Gd(DTPA)^{2-}$ and imaged at 2T using 2D saturation recovery or inversion recovery sequences. One sample was imaged using a 3D MRI study. $T1_{Gd}$ maps were computed from the MRI data and correlations were examined between locally-averaged $T1_{Gd}$ values and measures of mechanical stiffness made at a number of points selected within both the trypsinized and nondegraded regions.

The main experimental studies to test *in situ* correlation of cartilage stiffness and colocal, MRI-measured $T1_{Gd}$ or [GAG] were conducted on specimens of human tibial plateaus derived from patients undergoing total knee replacement surgery. Osteochondral specimens of human tibial plateaus were cut and mounted on specially fabricated registration plates. These plates contained marker holes which permitted registration of locations on the samples at which indentation testing was performed with regions in MRI sections through the same loci. At an array of locations on each sample, stiffness was assessed by applying a pulse displacement with a hemispherically-tipped indenter and then measuring the resulting peak load response. Next, after equilibration in 2 mM $Gd(DTPA)^{2-}$, dGEMRIC imaging was performed at 8.45Tand T1 maps were computed.

In selected cases, GAG maps were computed from the $T1_{Gd}$ maps. We then examined the correlation between the mechanical load responses at the test loci and the locally-averaged $T1_{Gd}$ of the cartilage at the sites.

Outline of the thesis

A review of the clinical and basic science background as well as a review of prior relevant work is presented in Chapter 2. A brief description of the dGEMRIC methodology is also provided.

The tissue samples studied, both bovine and human, are described in Chapter 3, along with the system employed to permit mechanical-MRI registration. Techniques for positioning the sample test loci beneath the indenter are presented, along with a discussion of positioning accuracy.

Chapters 4 and 5 present the methods used for mechanical tests and MRI measurements, respectively. Apparatus, indentation testing protocols and reproducibility results for mechanical testing are presented in Chapter 4. The flow of image data from acquisition, to $T1_{Gd}$ map computation, GAG map computation, segmentation and spatially-localized averaging of $T1_{Gd}$ (or GAG) at the test sites is presented in Chapter 5. The chapter also describes the MRI-based thickness measurements made at each test locus.

A finite element model of the indentation test was applied to examine the effect of thickness on expected load response. The results of this analysis were applied to control for the effect of thickness as a potential confounding variable in interpreting stiffness-$T1_{Gd}$ correlations. The FE model and results are the topic of Chapter 6.

The core results of the thesis are presented in Chapter 7: the correlations observed between indentation stiffness and $T1_{Gd}$. Supporting analyses and results are also included here, including examinations of the effects of ROI depth for $T1_{Gd}$ averaging, thickness (using the results of Chapter 6) and variations in integrity of the surface layer of the tibial plateau cartilage. (The tibial plateau exhibits a characteristic heterogeneity in surface condition: the area under the menisci is typically visibly smooth and shiny, the area not covered by the menisci appears to have a roughened, dull, “carpet-like” surface. We examined the effect of this difference in surface condition on our measured stiffness-$T1_{Gd}$ correlations.)

Preliminary work was also performed in 3D imaging and in the development of an instrumented surgical probe system to measure the forces and motions surgeons employ when probing an articular surface. This work, as well as additional applications and future directions are presented and discussed in the concluding chapter.

Appendices include the specifics of the experimental protocols employed, intended to provide sufficient detail to permit extension of these results in future work.

Chapter 2

Background

2.1 The knee: anatomic and clinical background

851,000 arthroscopies were performed in hospitals and ambulatory surgery clinics in the U.S. in 1995, with 685,000 (80%) performed in the knee (Praemer 1998). An approximately equal number are estimated to be performed annually in physicians' offices (for which no national reporting is done), giving a total estimate of 1.7 million arthroscopies performed yearly in the U.S. alone, with about 1.4 million in the knee. The knee is therefore an extremely important target for research aimed at improving the diagnosis and treatment of arthritic disease.

The knee is the largest and most complex joint in the human body. Figure 2-1 illustrates its basic anatomy, introduces some relevant terminology and describes some of its principal components. In addition to the structures identified in the figure, the joint is surrounded and contained by tough, fibrous bands of tissue which collectively form the joint capsule. (Note that this highly simplified description omits many additional structures, including the bursae, plicae, nerves, arteries, veins, the infrapatellar fat pad and several additional ligaments and tendons.)

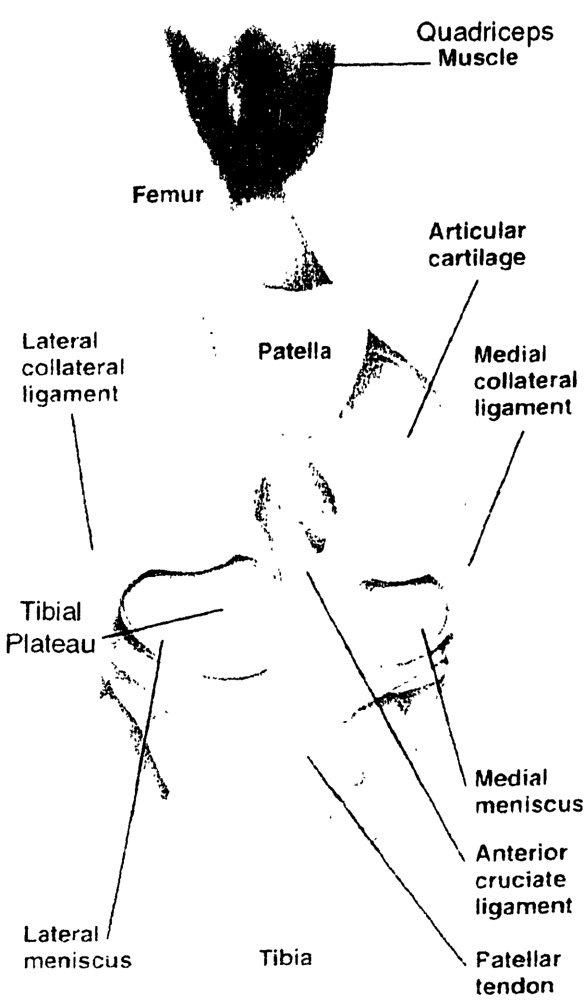

Figure 2-1 The distal (far) end of the femur is made up of two rounded **condyles** (from Greek *kondylos*, knuckle) separated by the **intercondylar notch** (not labeled). In front, the condyles are connected by a smooth cartilage-covered depression called the **trochlear surface** (Latin *trochlea*, pulley) in the middle of which runs the **trochlear groove**. The patella slides over this trochlear surface of the femur. The proximal end of the tibia is a relatively flat "table"–the **tibial plateau**–which has two slight concavites which articulate with the condyles. The medial and lateral tibial **hemi-plateaus** are separated by a craggy ridge, the **intercondylar eminence**. Anatomically and functionally, the knee is thus divided into the **medial and lateral compartments,** separated by the intercondylar eminence and intercondylar notch. The condyles and tibial plateau are covered by **articular cartilage,** ranging in depth from approx. 1 to 5 mm. The bony surface immediately subjacent to the cartilage is termed **subchondral bone**. The **menisci** are crescent-shaped structures made of highly fibrous cartilage which sit atop and partially cover the articular cartilage of the tibial plateau. Their upper surfaces conform closely to the femoral condyles. The menisci stabilize the joint and increase the effective area of contact between condyles and plateau, thereby reducing peak contact stresses. The anterior cruciate ligament and, behind it, the posterior cruciate ligament (not labeled), help to tie the joint together and constrain the anterior-posterior motion of the tibia with respect to the femur. (Figure adapted from "Knee Arthroscopy" by Krames Communications, San Bruno, CA).

Of particular note are the relatively flat regions (compared to most joint surfaces) of the tibial plateau. For indentation testing of samples, a flat surface is desirable so as to be able to maintain approximate perpendicularity of the indenter to the cartilage surface without multi-axis angular positioning of the sample (and the need to continually reorient the sample for each test locus, as would be necessary on a highly curved surface). The tibial plateau is also a common site of cartilage degeneration, and hence presents a potential source of heterogeneous cartilage integrity, supporting the experimental examination of variations in stiffness and GAG content. Finally, the tibial plateau and a subjacent layer of subchondral bone is frequently removed relatively intact and in its entirety during total knee replacement (TKR) surgery. This common procedure therefore provides a source of plateaus suitable for mechanical testing and imaging *in vitro*.

2.2 Articular cartilage: function and structure

A layer of articular cartilage covers the contact surfaces at the ends of the bones, forming a gliding surface. It provides shock absorption, a load-bearing surface and lubrication. The coefficient of friction between contacting cartilages can be as low as 0.0026, probably the lowest of any known solid material (Fung 1993). Compare, for example, that the coefficient of friction of Teflon surfaces is on the order of 0.05 – 0.1, more than an order of magnitude higher.

In the knee the average cartilage thickness is from 2 to 4 mm; this thickness varies over the articular surface, tending to be greater toward the center of the condyles and in the central areas of the tibial plateaus (the areas not covered by the menisci) (Ateshian, Soslowsky and Mow 1991). The cartilage on the undersurface of the patella is the thickest in the knee, with maximum thickness of 5-6mm (Arnoczky, Dodds and Wickiewicz 1996; Ateshian, Soslowsky and Mow 1991).

Cartilage is a remarkably complex biomaterial with correspondingly complex material properties. Despite being largely acellular and traditionally believed to lack intrinsic regenerative capacity, it must routinely bear loads of 4 to 5 times body weight and do so regularly for more than 70 years. Adult cartilage is an avascular, aneural tissue made up of a sparse number of cells embedded in an extracellular matrix (ECM) composed of collagen fibers, proteoglycans (PGs), water and ions (Figure 2-2). The network of collagen fibers is thought to be primarily responsible for the tensile strength of cartilage. The combination of the proteoglycans and water forms a viscous, gel-like substance with a high osmotic swelling pressure. Proteoglycans are macromolecules with a structure analogous to a bottle brush, with many glycosaminoglycan (GAG) molecules (sulfated polysaccharides) attached to a central protein core. The GAGs are richly negatively charged. Mutual repulsion among the strongly anionic GAGs causes them to stick out stiffly from the central core (hence, the bottle-brush image). This mutual repulsion is also responsible for the GAG's resistance to compression.

2.3 Articular cartilage biomechanics

Cartilage exhibits viscoelastic material behavior. Figure 2-3 shows the response of a

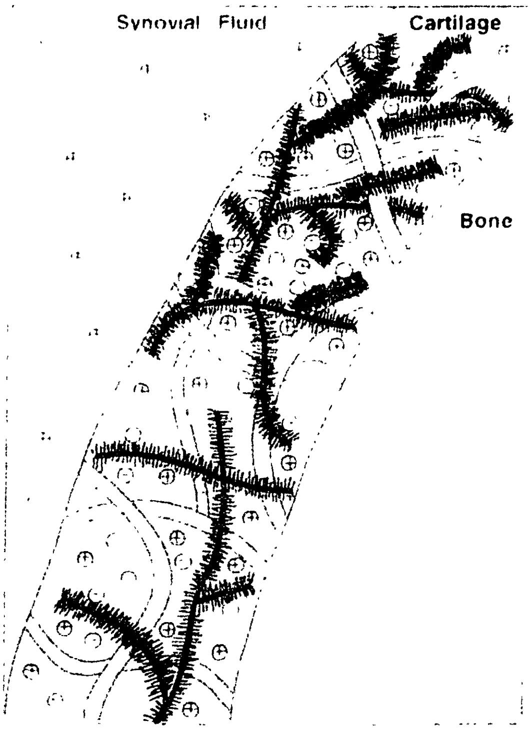

Figure 2-2 Illustration of the molecular composition of articular cartilage. The solid phase consists of a matrix of collagen fibers (gray) and a network of proteoglycans (black). Each proteoglycan molecule has many glycosaminoglycan side chains (GAGs), giving the molecule a bottle-brush appearance. The GAGs carry many negatively charged carboxyl and sulfate groups (yellow); these groups are fixed to the solid matrix. A mobile negative ion such as the MRI contrast agent Gd-DTPA^{2-} (pink negative signs) will tend to be repulsively excluded from regions rich in GAG and preferentially admitted to regions of low GAG concentration. This creates image contrast based on GAG distribution, and forms the basis for the use of Gd-DTPA^{2-} to image GAG distribution *in vivo* via MRI. From (Bashir, Gray, Boutin et al. 1997).

cartilage cylinder subjected to two different mechanical provocations. In a displacement control experiment, the sample is subjected to a fixed strain and the force needed to maintain the strain is measured over time. The decay in force illustrated in the figure is characteristic of viscoelastic materials and is termed a *stress relaxation response.* In a load control experiment, a fixed load is applied and the resulting strain is measured over time. The characteristic increase in strain to an equilibrium value is known as *creep* behavior.

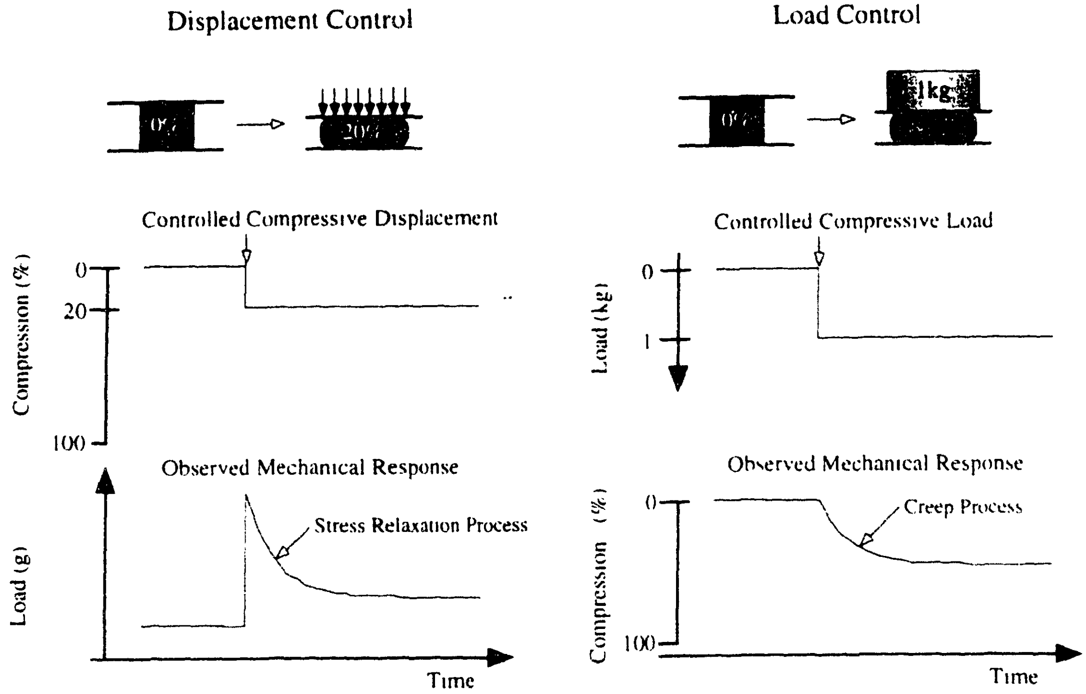

Figure 2-3 Illustration of the viscoelastic behavior of cartilage. On the left, a cylinder of cartilage is subjected to a 20% compressive strain and the force needed to maintain the strain is recorded. On the right, a fixed 1kg load is applied and the resulting compression is measured over time. Equilibrium levels of stress are reached in on the order of 25 minutes; equilibrium compression (the "creep time") is roughly 2 hours. From (Allen, Eisenberg and Gray 1998)

A plethora of models have been developed over the past 30 years to describe and predict the mechanical behavior of cartilage. The earliest work assumed a *single phase* for the material. Hayes et al. (1972) modeled cartilage as a homogeneous, isotropic, linear elastic material; they derived an analytical solution for the case in which a rigid sphere or a plane-ended cylinder indents (infinitesimally) an elastic layer of cartilage bonded to a rigid substrate. Cartilage was modeled as a linear *viscoelastic* material by

Hayes and Mockros (1971), Coletti et al. (1972) and Parsons and Black (1977). Woo et al. (1980) and Simon et al. (1984) modeled cartilage with the *quasi-linear viscoelastic* (QLV) theory developed previously by Fung (1972). (The response of a QLV material to a time-varying displacement input is found by convolution of a nonlinear, time-independent elastic response with a time-varying relaxation function.)

In the approaches just described, cartilage is viewed as a traditional single-phase elastic or viscoelastic solid. Mow et al. (1980) formulated a *biphasic* theory for cartilage in which the tissue is modeled as a mixture of a permeable, porous, linearly elastic solid phase (representing the collagen and proteoglycan) and an incompressible, inviscid fluid phase (representing the interstitial fluid). They derived a mathematical analysis of the deformation of this two-phase material under conditions of infinitesimal strain. The viscoelastic mechanical properties derive from the combination of the elastic response of the solid matrix and the flow of fluid through it. Roughly speaking, the model is similar to a wet sponge: squeezing the sponge forces redistribution of water, subject to the resistance of the solid matrix (which is inversely proportional to its permeability).

This model was subsequently generalized to include a viscoelastic model of the solid matrix (Mak 1986), and nonlinear properties, including strain-dependent permeability of the solid matrix (Lai, Mow and Roth 1981; Lai and Mow 1980), finite (rather than infinitesimal) deformation (Mow, Kwan, Lai et al. 1986) and the combination of both strain-dependent permeability and finite deformation (Cohen 1992; Kwan, Lai and Mow 1990). In the most general case, the biphasic theory includes a solid phase which is nonlinearly permeable, anisotropic, inhomogeneous and viscoelastic undergoing finite deformation, and a viscous, dissipative fluid phase (Lai, Mow and Zhu 1993). The analytic solution for the surface deformation in a creep experiment and the relaxation force in a stress-relaxation experiment has been solved for the biphasic model for indentation with a porous indenter and frictionless interface (Mow, Gibbs, Lai et al. 1989; Mak, Lai and Mow 1987). However some indication of the complexity of the modeling problem is given in the observation of the investigators themselves that "good theoretical-experimental fits are difficult to obtain early in the time response (e.g., first 200 seconds)." (Spilker, Suh and Mow 1992)

Further evidence of the complexity of cartilage behavior is given by the fact that, for the case of *finite* deformation by an impermeable indenter (such as a stainless steel surgical probe), no tractable analytic solution is known to exist, even for simple indenter geometries (Spilker, Suh and Mow 1992).

The challenge of analytic solutions has motivated finite element methods for analyzing cartilage mechanical behavior; for example a finite element formulation of the biphasic theory (Spilker and Suh 1990) has been applied to analyze the stress-relaxation response after indentation by a plane-ended cylindrical indenter, with examination of porous and permeable indenters, and frictionless and adhesive contact conditions. (Spilker, Suh and Mow 1992) (An informative review of finite element analysis of cartilage mechanical behavior is provided by Goldsmith, Hayes and Clift (1996)).

In addition to this record of analytical effort, an equally rich assortment of experimental techniques have been employed to poke, pull and squeeze cartilage. These include *indentation tests* with either porous or nonporous indenters, *tensile stress tests, unconfined compression tests* of cylindrical plugs of cartilage, and *confined compression tests* in which the cartilage is placed in a rigid, confining cylinder and pressed with a porous piston; each of these perturbations can be applied as controlled displacement or controlled load tests, as well as dynamic compression tests in which cyclical displacements are applied at varying frequencies[1]. For each of these tests, the immediate, intermediate and long-term responses exhibit distinctly different behaviors. The immediate, or short-term response, occurs before sufficient time has elapsed for appreciable water flow to occur, and exhibits approximately linearly elastic behavior. During the intermediate response, water flows and redistributes through the porous matrix and matrix consolidation (i.e., compaction) occurs; the resulting material response is viscoelastic or, more cor-

---

[1] Significantly for the long history of attempts to reconcile experiment to theory in cartilage mechanical modeling, a recent study applied a finite element formulation of the biphasic poroviscoelastic (BPVE) model to simulate the behavior of cartilage in unconfined compression, confined compression and indentation with both porous and nonporous plane-ended metal indenters. The authors of this study found that, once the parameters of the BPVE model were set so as to match model predictions to experimental results of unconfined compression stress relaxation experiments on bovine cartilage, the same model was also able to predict the results of confined compression and indentation experiments on the same tissue. This is a first demonstration that the BPVE model can account for the experimental data for multiple loading tests based on one set of data. (DiSilvestro and Suh 2001)

rectly, poroviscoelastic. After sufficient time has elapsed, fluid flow ceases and equilibrium is reached, characterizing the long-term response, which has also been successfully modeled using elastic material parameters.

2.4 Prior work

2.4.1 Relationship of cartilage biochemistry to compressive stiffness

Early work examining the relationship of GAG to cartilage mechanical behavior suggested that GAG played a primary role in supporting the resilience of cartilage to an applied compressive load. In studies of *in situ* indentation of the human femoral head, the 2-second creep modulus (determined by applying a fixed load and measuring deformation 2 seconds after load application) was found to correlate with local cartilage GAG content, chondroitin sulfate content or keratan sulfate content, but not with collagen content (Kempson, Muir, Swanson et al. 1970). The 15-second creep strain (i.e., the strain measured 15 seconds after load application) of bovine osteochondral plugs was found to increase with hyaluronidase or trypsin degradation of GAG (indicating decreased stiffness), while no significant decrease in stiffness occurred following treatment with collagenase (Harris, Parker, Radin et al. 1972). Experimental degradation of cartilage GAG also has been shown to cause an increase in creep strain measured at 1 minutes and 2 minutes post-load (Kempson 1975). In the first indentation study to use a controlled displacement (stress-relaxation) method (compared to previous controlled-load (creep) methods), a decrease in the equilibrium Young's modulus of rabbit tibial plateau cartilage was seen in the two weeks following meniscectomy, with recovery to near baseline by six months. Uronic acid content (indicative of GAG content) showed similar temporal variation and correlated closely with the equilibrium modulus (Hoch, Grodzinsky, Koob et al. 1983). More recently, it has been demonstrated that the dynamic stiffness of bovine cartilage disks shows an approximately linear relationship to bulk GAG content when tested in unconfined oscillatory compression at approximately 1 Hz, and that this relationship is independent of the mechanism used to modulate GAG content (enzymolysis or IL-1B) (Allen, Burstein and Gray 1999).

Other investigations, however, have raised questions about the precise relationship of GAG or proteoglycan (PG) to compressive stiffness and, in particular, the relative roles of GAG and collagen in determining the response of cartilage to short-time, or "instantaneous" compressive loading (a term whose precise definition is somewhat elusive in the experimental literature.) For example, in the *in situ* studies of the femoral head mentioned above, GAG depletion was found to increase both 1 minute and 2 minute creep strains to a greater extent than the strain at 0.2 seconds (Kempson 1975). In a study of unconfined compression of human femoral head and condylar cartilage, it was concluded that it was not proteoglycan content but rather the collagen fiber network that was mainly responsible for determining the instantaneous deformation (Mizrahi, Maroudas, Lanir et al. 1986). A similar conclusion was reached in an examination of the elastic stiffness and viscous damping coefficient in the human femoral head, in which it was further concluded that proteoglycans preferentially control the time-dependent viscous response (in distinction to the instantaneous response) by their role in regulating fluid transport in the matrix (Bader, Kempson, Egan et al. 1992). Similarly, in tests of the canine tibial plateau, it was found that instant shear modulus was not correlated with PG content (Jurvelin, Saamanen, Arokoski et al. 1988). (The same investigation found that equilibrium modulus, while correlated with PG content in the femur, was not correlated with PG in the tibial plateau).

This thesis is primarily concerned with relatively short-time, focal indentation, and several studies have examined the correlation between cartilage biochemical content—as measured by biochemical assay—and mechanical stiffness as assessed by use of handheld indentation instruments which typically have a small indenter footprint (on the order of 1 mm), apply a fixed displacement and measure short-term compressive load response (these instruments are intended for application *in vivo*). Using one such instrument (Artscan 1000™, Artscan Oy, Helsinki) to mechanically test bovine osteochondral plugs subjected to degradation by trypsin, chondroitinase ABC or collagenase, both PG and collagen digestion were associated with decreased measured stiffness (Lyyra, Arokoski, Oksala et al. 1999). Using the same indentation device, another group of investigators examined the regional stiffness in cadaveric human femurs at loci on the patellar groove and condyles. Osteochondral plugs were then harvested from the regions tested and analyzed for total proteoglycan and total collagen content. A correlation was not seen between measured compressive stiffness and either PG or collagen content (A correlation *was* found between stiffness and Mankin histological grading score.) (Franz, Hasler, Hagg et al. 2001). In a study employing a different hand-held indentation probe (ACTAEON™, OsteoBiologics, San Antonio, TX), the focal indentation stiffness of osteochondral plugs from human femoral condyles was measured with both a benchtop instrument and the handheld probe (Bae, Temple, Rivard et al. 2002). Each plug was then analyzed for GAG and collagen content by DMMB and hydroxyproline assays, respectively. The correlation between stiffness measurements obtained with the handheld probe and GAG content was weak ($r = 0.24$) and did not quite reach statistical significance ($p = .051$). Stiffness measurements obtained with the benchtop device demonstrated a weak ($r = 0.26$) but significant ($p < .05$) correlation between stiffness and GAG content. In this study, no significant correlation was seen between stiffness (determed via either instrument) and bulk collagen content.

2.4.2 Application of MRI to assess matrix constituents and their relationship to mechanical behavior

The key issue examined in this thesis is the relationship between cartilage mechanical behavior and a noninvasive MRI-measured index of cartilage GAG. We here briefly review relevant prior work developing MRI measurement of GAG and examining relationships between MRI-derived indices of matrix constituents and correlated mechanical properties.

MRI-based GAG measurement

MRI methods applicable to the measurement of GAG *in vitro* and *in vivo* have recently been reviewed, including methods utilizing sodium, $Gd(DTPA)^{2-}$ and other techniques (Burstein, Bashir and Gray 2000). In particular, the use of dGEMRIC-measured T1 is particularly attractive for noninvasive GAG assessment. It is a nondestructive, quantitative, sensitive, and specific measure, which has been applied both in vitro (Williams 2001; Allen, Burstein and Gray 1999) and clinically (Burstein, Velyvis, Scott et al. 2001; Tiderius, Olsson, Verdier et al. 2001; Trattnig, Mlynarik, Breitenseher et al. 1999; Bashir, Gray, Boutin et al. 1997), and has been validated via comparison to Na+ imaging (Bashir, Gray and Burstein 1996) biochemical assay (Bashir, Gray, Hartke et al.

1999) and tissue histology (Bashir, Gray, Hartke et al. 1999). It can also potentially provide fully three-dimensional mapping of GAG distribution throughout the cartilage.

Correlations between mechanical properties and MRI measures of matrix constituents

Relatively few studies have directly examined the correlation between indices of cartilage mechanical integrity and MRI-based indices of cartilage biochemical composition. In one recent investigation using dGEMRIC in a small sample of patients (n=8), cartilage showing arthroscopically visible degeneration (fibrillation and clefts) demonstrated significantly higher $Gd(DTPA)^{2-}$ uptake as reflected by lower $T1_{Gd}$ (i.e., T1 after administration of $Gd(DTPA)^{2-}$) than visibly normal cartilage (Tiderius, Olsson, Leander et al. 1999); however, no quantitative mechanical measure of cartilage integrity was made in this study. Mapping of cartilage T2 has shown sensitivity to cartilage collagen content, and collagenase degradation has been shown to cause a concomitant increase in T2 in the superficial zone and a decrease in equilibrium Young's modulus (measured using a stepwise stress-relaxation technique) (Nieminen, Toyras, Rieppo et al. 2000).

Most directly relevant to the present work is a recent study in which bulk $T1_{Gd}$ (measured using dGEMRIC) and *equilibrium* mechanical moduli were compared in cartilage disks (Nieminen, Töyräs, Laasanen et al. 2001). Adjacent pairs of disks were cut from bovine humeral heads. Average $T1_{Gd}$ was measured using dGEMRIC in one disk from each pair, equilibrium Young's modulus and aggregate modulus were measured in the adjacent disk (using optical measurements to determine Poisson's ratio and a single-step stress relaxation experiment (10% prestrain, 5% step) to determine Young's modulus). Equilibrium Young's modulus and aggregate modulus were found to be significantly correlated with $T1_{Gd}$.

2.5 dGEMRIC methodology

The dGEMRIC technique measures cartilage T1 following administration and equilibration with the anionic contrast agent $Gd(DTPA)^{2-}$ which distributes in the tissue in inverse relationship to the anionic fixed charged density. In cartilage, this fixed charged density is due to the numerous negatively-charged sulfate and carboxyl side groups (which are ionized at physiological pH) of the chondroitin sulfate and keratan sulfate components of GAG (Figure 2-2). Hence, $Gd(DTPA)^{2-}$ tends to be electrostatically repelled from regions of high GAG concentration, and preferentially admitted to regions of low GAG concentration. Since $Gd(DTPA)^{2-}$ is a paramagnetic agent which locally lowers T1, areas of cartilage with lower GAG content (less fixed negative charge) will admit more $Gd(DTPA)^{2-}$ and exhibit lower T1. Application of a modified Donnan equilibrium theory permits dGEMRIC T1 measurements to be quantitatively related to cartilage fixed-charge density, which in turn can be related to cartilage GAG concentration (Bashir, Gray, Hartke et al. 1999; Bashir, Gray and Burstein 1996).

2.6 Summary

Four decades of research have helped elucidate the complex structure of and interactions between cartilage constituents–principally collagen, proteoglycans and water–which determine its remarkable mechanical and tribological behavior. The response of cartilage to an applied load or displacement can simplistically but usefully be divided into (1) an instantaneous elastic response followed by (2) a poroviscoelastic response as water redistributes within the matrix, eventually leading to (3) an equilibrium state.

In general, the experimental evidence to date supports the view that cartilage poroviscoelastic response and equilibrium stiffness are dependent on PG content (and hence GAG content). A less definitive statement can be made regarding the relationship between PG content and "instantaneous" or short term compressive response, as the experimental literature presents disparate findings on the correlation between stiffness measured during short loading times and GAG content. Precise comparisons across studies are complicated by the multiplicity of mechanical testing protocols employed. In addition, the destructive biochemical assays employed in many studies typically require a volume of tissue quite large in comparison with the indenter footprint. This presents the question of whether sufficient colocalization has been maintained between the region of cartilage subjected to stress during mechanical testing and the region of cartilage assayed biochemically for GAG or collagen to permit valid examinations of mechanical-biochemical correlations to be made. In the work described in this thesis, this issue was specifically addressed, and methods were developed to permit loci of mechanical indentation testing to be registered (i.e., colocalized) with regions in MRI scans corresponding to the loci with high precision The apparatus and methodology developed to permit this close mechanical-MRI registration is described in detail in Chapter 3.

Chapter 3

Tissue Samples and Indentation-MRI Registration

Since the central scientific goal of this project was to determine if the mechanical response of cartilage to indentation was correlated with $T1_{Gd}$ in the region of cartilage subjected to the indentation, a key requirement was the ability to accurately and reproducibly determine what region in an MRI scan of a sample corresponded to a site of indentation. Specifically, we wanted to colocalize the region of $T1_{Gd}$ assessment with the region of tissue subjected to mechanical stress; essentially, this meant we wanted to look at $T1_{Gd}$ (or GAG) under the footprint of the indenter. We therefore developed methods and apparatus to register pixels in dGEMRIC MR images with physical locations on cartilage specimens.

To our knowledge, this is the first work to examine the relationship between an MR-derived index of a cartilage matrix constituent and a mechanical property in a highly spatially-localized way. Prior work examining the relationship of cartilage matrix constituents (or MR measures of them) to mechanical responses have typically examined bulk properties of cartilage plugs, or, when indentation studies have been employed, there has typically been a large disparity between the footprint of the indenter and the volume of tissue analyzed for GAG (or collagen) content. As was indicated in the summary of Section 2.6 (and will be addressed in more detail in Section 8.2), the failure to provide sufficient colocalization of the region subjected to biochemical assay and indenter footprint may be one underlying factor in the disparate reports of the relationship of GAG or collagen content to indentation stiffness found in the literature. The need for accurate registration of mechanical test sites and MRI data was therefore deemed central to the mission of this work.

We will first begin with a description of the essential material examined in this study: the bovine and human articular samples employed, including how they were acquired, prepared, handled and stored. We will then describe the approach we developed to permit accurate, reproducible, registration (colocalization) of spatially-localized mechanical measurements and spatially-localized MRI measurements, thereby enabling them to be meaningfully compared and correlated.

3.1 Tissue samples: bovine and human

Bovine Tibial Plateau Specimens

A total of 9 bovine knees were dissected to yield the tibial plateaus. Bovine specimens were used for preliminary research studies:

(1) to develop and refine the protocols employed for dissection, $Gd(DTPA)^{2-}$ equilibration, imaging, mechanical testing, and tissue storage,

(2) to develop and test the methods used for affixing the bone surfaces of the specimens to the registration plates, and

(3) for preliminary stiffness-$T1_{Gd}$ correlation experiments in which a portion of the sample was degraded by trypsin digestion. 5 bovine plateaus were used for trypsinization studies.[2]

Human Tibial Plateau Specimens

Osteochondral specimens of human tibial plateaus were obtained from patients undergoing total knee replacement surgery.[3] Through a collaboration with Dr. Scott Martin

---

[2] One trypsinized plateau was used in a comparative study of the time course of diffusion of Magnevist ($Gd(DTPA)^{2-}$) and Prohance (nonionic Gd) into normal and degraded cartilage. This work was done in a collaborative project with Amy Gillis, Harvard-MIT Division of Health Sciences and Technology MD program. The results have been reported separately and are not included herein.

(Department of Orthopedic Surgery, Brigham and Women's Hospital), arrangements were made to be present for surgeries of patients at both the Brigham and Women's Hospital and the West Roxbury V.A. Hospital. Typically, the entire tibial plateau was obtained in one piece. (In some cases, hemi-plateaus or smaller portions were received.) The specimens were placed in saline immediately after removal from the patients, then transported in a temperature-controlled container to the lab. Immediately, as much as possible of the remaining capsular or ligamentous soft tissue was trimmed from the specimens. Within several hours of acquisition, the samples were then either frozen for future use, or, in some cases, immediately prepared for MR imaging and mechanical testing with no intervening freezing.

A total of 12 human tibial plateaus were acquired, designated HT0 through HT11.[4] Portions of the tibial plateaus exhibiting a proximate range of visibly healthy and degraded areas were selected for further study. Based on this criterion, many plateaus proved unsuitable for study: due to severe degeneration of the cartilage to the point of exposing denuded bone (HT5, HT9), the presence of only severe disease on one half of the plateau and only pristine cartilage on the other half (HT2), or the presence of fissures or surgical instrument cuts in the cartilage surface (HT9). At least one patient had disease so severe that essentially no cartilage could be identified in the sample (HT10).

Specimens HT1, HT3, HT6, HT8 and HT11 proved to have regions of cartilage appropriate for sample preparation and experimental investigation.[5]

---

[3] All applicable procedures and rules were followed for use of human tissues, including the filing of appropriate applications with MIT's Committee on the Use of Humans as Experimental Subjects (COUHES) and adherence to their guidelines.

[4] Entire human tibial plateaus are identified with a label consisting of the prefix "HT" (Human Tibia) followed by a serial number. A particular specimen cut from a plateau is designated as, for example, HT3A, with the suffix letter A indicating the particular sample derived from the plateau HT3.

[5] Portions of additional samples, HT0, HT4 and HT7, also had potentially appropriate areas and were frozen for follow-up and future study. (HT0 and HT4 had each been frozen for over one year at the time of finalization of the experimental protocol for the current study, and were deferred in favor of specimens acquired hours to days prior to use.)

3.1.1 Tissue preparation

Bovine specimens

Fresh, intact bovine hind leg knee joints (calves 2 days to 3 weeks old) were obtained on the day of sacrifice from a local research abattoir (Research 87, Marlborough, MA). The joints were dissected, carefully removing overlying musculature, the capsule, the ligaments and menisci. The tibial plateau was then harvested by making a transverse razor saw cut approximately 5 mm below the cartilage/bone interface. A midsagittal cut was made, transecting the specimen and yielding two hemi-plateaus; each hemi-plateau was either used in full (for imaging in a 30 cm bore 2 T MR imager) or cut into smaller osteochondral samples for imaging in a 1 inch bore 8.45 T MR imager. Each osteochondral sample was rinsed well in Hank's balanced salt solution in order to remove blood (which contains naturally-occurring serum proteases and trypsin inhibitors). The cut bone surface was dried with gauze, and the sample was then cemented to a rigid polycarbonate registration frame (to be described in detail in Section 3.2.2). The frame holds the osteochondral samples, facilitates positioning during trypsinization, provides a rigid base for the mechanical measurements, and serves as a common coordinate reference frame for registering mechanical and MRI measurements of each sample.

To prepare the sample for mounting, a 1/8 inch drill bit was used to drill 10 to 20 shallow (3 to 5 mm deep) holes into the inferior (bottom) trabecular bone surface of the sample. A similar number of shallow, randomly-spaced holes were drilled into the base plate of the polycarbonate frame. (It was found in early tests that if the surface of the bone was not roughened by drilling, the bone would separate from the frame after repeated freeze-thaw cycles. No separations occurred in 10 samples *with* the drilling procedure). Devcon 5-minute epoxy (Devcon, Danvers, MA) was mixed and liberally applied to both the bone surface and the base plate, with care taken to ensure the epoxy resin permeated well into the drilled holes. The bone surface was then positioned over the center of the base plate of the registration frame, pressed to the base plate with firm finger pressure and held tightly for several seconds. Additional epoxy was applied to all the exposed bone surfaces of the sample to seal them and limit escape of blood or serum. The epoxy was permitted to set and cure for 10 to 15 minutes.

Human specimens

Human tibial plateaus were obtained from patients undergoing total knee replacement. These were performed at the Brigham and Women's Hospital (Boston, MA) and the West Roxbury Veterans Administration Hospital (West Roxbury, MA). All applicable guidelines for human studies and proper tissue handling were scrupulously followed, including obtaining project approval from MIT's Committee On the Use of Humans as Experimental Subjects (COUHES). All human tissue was handled in strict adherence to established BL-2 level guidelines for blood borne pathogen containment and decontamination, including use of appropriate protective garments and face shields (particularly during dissection, sawing and drilling of the samples), habitual application of work area disinfection procedures (70% ethanol or 10% bleach sprays and wipes) and autoclaving or chemical disinfection of all apparatus and tools coming into contact with human tissue and fluids contacting the tissue.

Surface areas of the plateau specimens showing visible heterogeneity but with minimal frank surface disruption (denuded bone, fissures, cuts, etc.) were selected and outlined by stippling with a fine-tipped India-ink marker (Pigma 0.8 mm, Pigma Micron, Sakura, Japan). These regions, rectangular and approximately 21 mm long by 15 mm wide, were then cut from the plateaus using a razor saw. The samples included subchondral bone of typically 4 mm to 9 mm thickness. The samples were mounted on acrylic registration plates with epoxy cement, following a similar protocol for the bovine samples described above. (The bottom trabecular bone surface of the human samples was typically only drilled with 10 or fewer very shallow holes to facilitate epoxy "grip" of the sample.) Exposed bone surfaces were also sealed with epoxy to minimize the release of serum proteases from the bone marrow. The samples were then equilibrated in 2 mM $Gd(DTPA)^{2-}$ as described in Section 5.1.1. In general, if the interval between MRI imaging and mechanical testing was under 24 hours, the samples were maintained at 4°C, otherwise they were frozen at –20°C.

Tissue storage

Some bovine and human samples were frozen and stored at –20°C (after wrapping in polyethylene film and Parafilm) prior to mechanical testing. All samples were frozen after initial testing. Several investigators have reported that freezing at –20°C does not affect the material properties of cartilage (Athanasiou, Rosenwasser, Buckwalter et al. 1991; Kempson, Spivey, Swanson et al. 1971; Maroudas, Bullough, Swanson et al. 1968). A few investigators have suggested that freezing *does* alter cartilage material properties (Black, Shadle, Parsons et al. 1979; Hori and Mockros 1976). The results of repeated testing on the specimens of the current study with intervening freezing supports the view that freezing –20°C at for periods of at least up to two months does not significantly alter cartilage mechanical properties in response to indentation (see Section 4.3.3.2).

3.1.2 Trypsinization of bovine samples

After the tibial hemi-plateau was affixed to the frame, a portion of the sample was immersed in a well-stirred, room-temperature solution of 2.5 mg/ml trypsin (Gibco BRL Life Technologies, Grand Island, NY) in Hank's solution, to which was added 1% v/v of an antibiotic/antimycotic solution containing penicillin G (10,000 units/ml), streptomycin sulfate (10 mg/ml) and amphotericin B (25 μg/ml) (Product #A7292, Sigma Aldrich, St. Louis, MO). The degree of GAG depletion was varied by adjusting the length of time the sample was immersed over a range of 2 to 12 hours. At the end of the degradation, the sample was removed from the trypsin solution and rinsed, first with Hank's solution for 30 minutes., then with bovine fetal calf serum for one hour to neutralize any remaining trypsin, then finally again with Hank's solution for 30 minutes.

3.2 Mechanical-MRI registration/calibration system

3.2.1 Objectives

As noted above, one of the primary objectives of this research was to develop a method to accurately register physical locations on the surface of an osteochondral sample with regions in a dGEMRIC $T1_{Gd}$ or GAG image. This requires that both the position of the mechanical indenter and the coordinate measurements in MR image-space can be referenced to a common origin or set of fiducial markers. The approach of the current work was to create a set of markers, fixed in position with respect to the sample, which can be both touched with the indenter and visualized in the MRI scan. These markers were created in a frame or baseplate to which the sample was rigidly affixed.

This frame or baseplate was also designed to provide three additional functions:

1) Supporting the sample for handling and providing a means of rigidly fixing the sample to the base of the hydration tank/translation stage system during mechanical testing.
2) Simplification of alignment of the sample in the bore of the RF coil during MR imaging, and the improvement of alignment repeatability.
3) A source of known, calibrated spatial position reference markers to allow spatial nonlinearities in the MR imaging system to be assessed and, if deemed necessary, corrected.

3.2.2 Registration frame/plate design, development and fabrication: four versions, final version

Figure 3-1 illustrates a registration frame designed so as to position marker holes in three dimensions around an entire bovine tibial plateau. The frame is fabricated out of polycarbonate and holes are drilled in the base plate and at the top of each of the four cylindrical posts (Figure 3-2a). The post heights and hole positions were dimensioned to a tolerance of +/- .001 inch (+/- .025 mm). Prior to imaging, these holes were filled with 1 mM Gd(DTPA)$^{2-}$ solution, providing distinctly visible markers in the MR images. If the field of view of a 3D MR study is chosen so as to include the marker holes in the volume, the location of any point on the sample can then be referenced to one or more marker hole locations. To permit registration of these positions with mechanical test loci on the sample, the indenter is first located at one of the marker holes and then displaced to the desired location on the sample. Each marker hole has a diameter of 1.2 mm, equal to 2/3 the diameter of the hemispherical indenter tip. This permits seating of the indenter tip into a marker hole, providing a fixed origin reference point for the indenter: test loci on the cartilage surface may then be specified as x, y and z displacements of the indenter from one of the marker holes (Figure 3-2b).

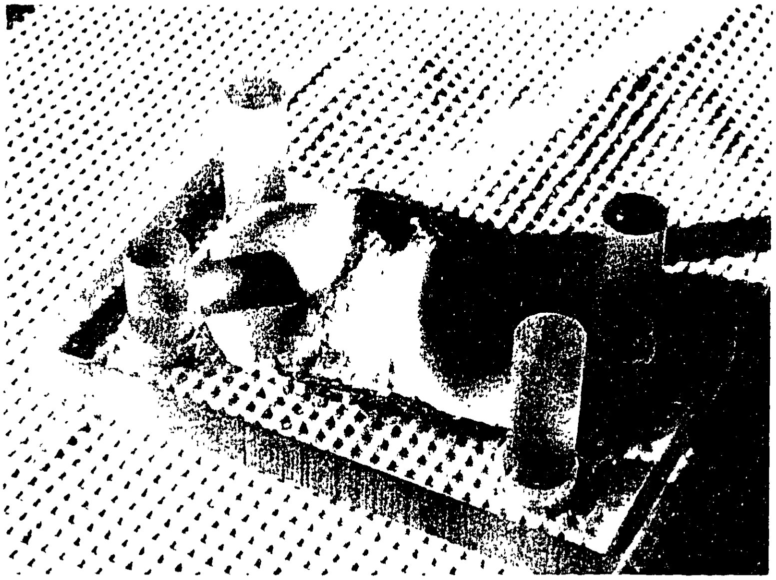

Figure 3-1 Version 1 registration frame, consisting of a rectangular polycarbonate base and four cylindrical polycarbonate posts. Marker holes, filled with Gd(DTPA)$^{2-}$ solution prior to imaging, are machined in the base and tops of the posts. The posts heights and hole positions are machined to +- .001 in. (.025 mm) tolerances. Markers are positioned in three-dimensions around the sample. asymmetric post arrangement aids identification of sample orientation (left-right, etc.) on MR scans. The size of this frame, while large enough to permit mounting of an entire bovine tibial plateau, limited its use to the largest RF coils on the Bruker Biospec 2T MR imager

Figure 3-2e-f shows the manner in which the registration frame also serves to position the sample in the bore of the RF coil employed for imaging. The baseplate of the frame is dimensioned so as to position the articular surface at approximately the center of the smallest coil employed for imaging studies. For use with a larger coil, a sample positioner was fabricated, again serving to center the sample's surface in the coil, and also facilitating position and orientation adjustments of the sample.

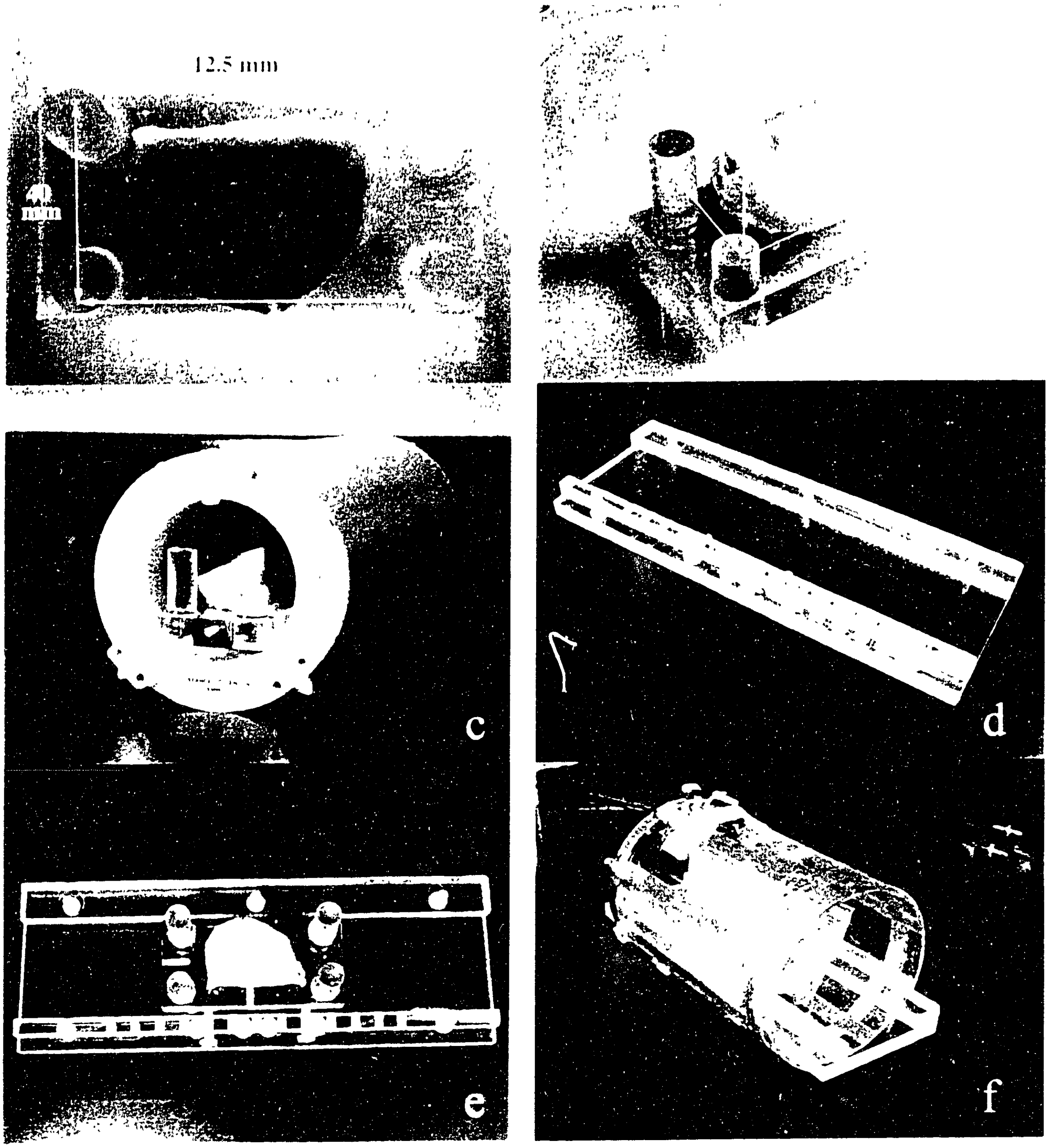

Figure 3-2 Version 2 registration frame and frame positioning system. **(a)** Frame geometry and marker hole placement. **(b)** Origin of a 3D coordinate system is defined with respect to the top marker of the shorter post. **(c)** Baseplate width is machined so as to position surface of typical sample near center (most linear region) of 7 cm RF coil. **(d)** Sample positioner fabricated to hold sample in larger, custom-built RF coil. **(e)** Frame secured in central channel of positioner by nylon screws. **(f)** Positioner (with wrapped sample secured in place) positioned in RF coil. Extension of positioner beyond mouth of RF coil facilitates access for sample position adjustment (rotation and longitudinal position).

Version 3 of the registration frame (Figure 3-3) was similar in dimension to version 2 but included additional vertical posts to place additional markers closer to the sample surface. The goal was to position registration markers as close to the areas of the sample surface which would be tested. Since dimensional distortions and nonlinearities in the MR images were observed (presumably due to field inhomogeneities) minimizing the distance between registration markers and test sites on the articular surface would presumably minimize registration errors due to these distortions. Also, the distortions typically increase away from the center of the field of view of the MR images; positioning the registration markers closer to the center of the sample positions them in a region of greater field linearity and lower geometric distortion.

For human tissue studies, a small-bore 8.45T Bruker DRX imager was used with a 1 inch inner-diameter RF probe. This necessitated a much smaller registration plate. Figure 3-4 shows the solution employed: a 42 mm long by 22 mm wide custom-machined acrylic plate with a central matrix of 1.2 mm diameter marker holes spaced on a rectilinear 3 mm grid. The plate and holes were fabricated on a CNC milling machine yielding an inter-hole spacing tolerance of +/- .025 mm (+/- .001 in.). The marker holes were

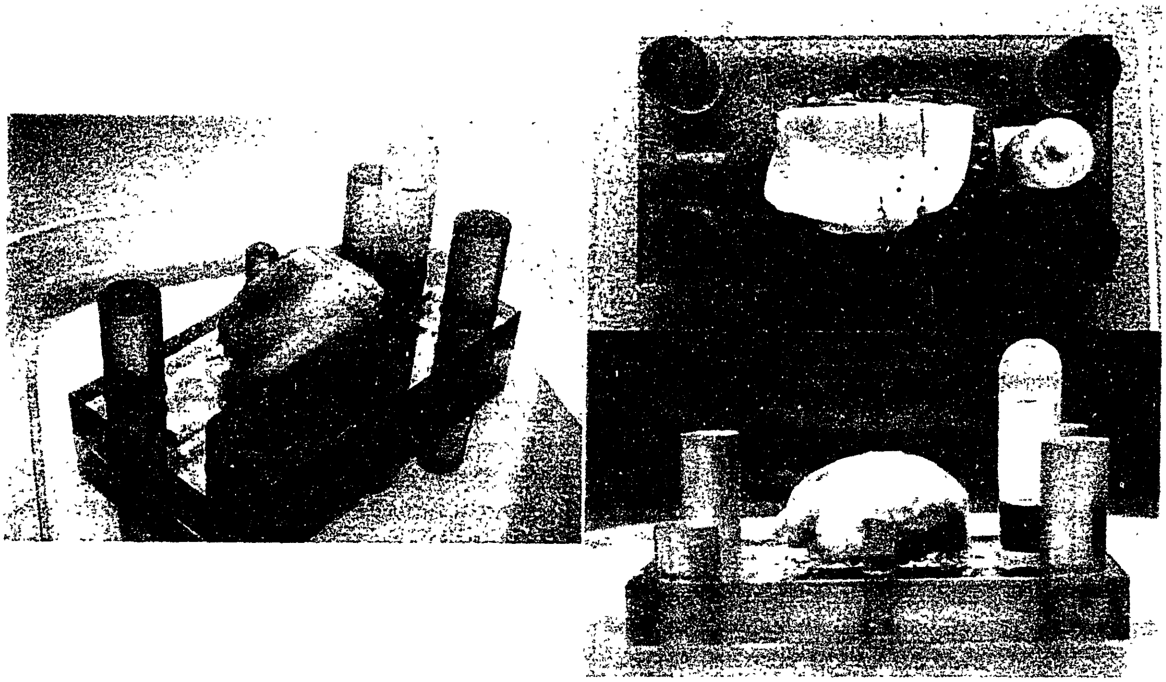

Figure 3-3 Version 3 registration frame with bovine hemi-plateau mounted in place. India-ink lines delineate boundaries of a multi-level trypsinization experiment; dots indicate loci of mechanical testing. The orange-capped vial is filled with 1 mM $Gd(DTPA)^{2-}$ solution and serves as a calibrated concentration reference for T1 imaging.

filled with agarose gel containing 2 mM $Gd(DTPA)^{2-}$; this gel proved to be stable to routine handling, immersion and freezing[6]. A tuberculin syringe with a 26 $^1/_2$ gauge needle (scored and cut flush to create a flat tip) was used to inject hot Gd-agar gel into each hole. The plate was cooled at 4 °C for 30 min., and a single-edged razor blade was used to cut the gel flush with the plate surface and remove the excess. The result was a cylinder of Gd-agar gel in each marker hole. The plate was then examined at 4X (Olympus BH-2 microscope) to ensure all holes were filled by the gel (Figure 3-4d).

A 22 mm by 15 mm rectangular cover plate was cut from a polystyrene patria dish, and the top surface was roughened with 150 grit silicon carbide abrasive paper. The cover plate was cemented over the central area of the marker hole matrix (Figure 3-4b) using solvent cement (Plastruct Plastic Weld, Plastruct Inc., City of Industry, CA). Each human osteochondral sample was cut into a rectangular block of approximately 22 mm long by 15 mm wide by 1 cm high. The bone surface was dried with gauze and then fastened with epoxy to the top, roughened surface of the cover plate. This fixed the osteochondral samples directly above the matrix of marker holes (Figure 3-4c). MRI slices could then be positioned perpendicular to the plate and passing through rows or columns of the marker hole matrix: test loci were then defined as locations on the cartilage surface directly above the marker holes (additional test loci were also defined directly above the midpoints between marker holes).

Additional holes in the registration plate were located close to the periphery of the plate and not covered by the sample. This allowed accessibility to touch contact with the indenter tip (Figure 3-8).

---

[6] The gel was formulated by combining 0.2 ml Magnevist and 1 g of agarose powder with sufficient Hank's solution to bring the total volume to 50 ml. The solution was then brought to a boil and allowed to cool slightly before injecting into the registration holes.

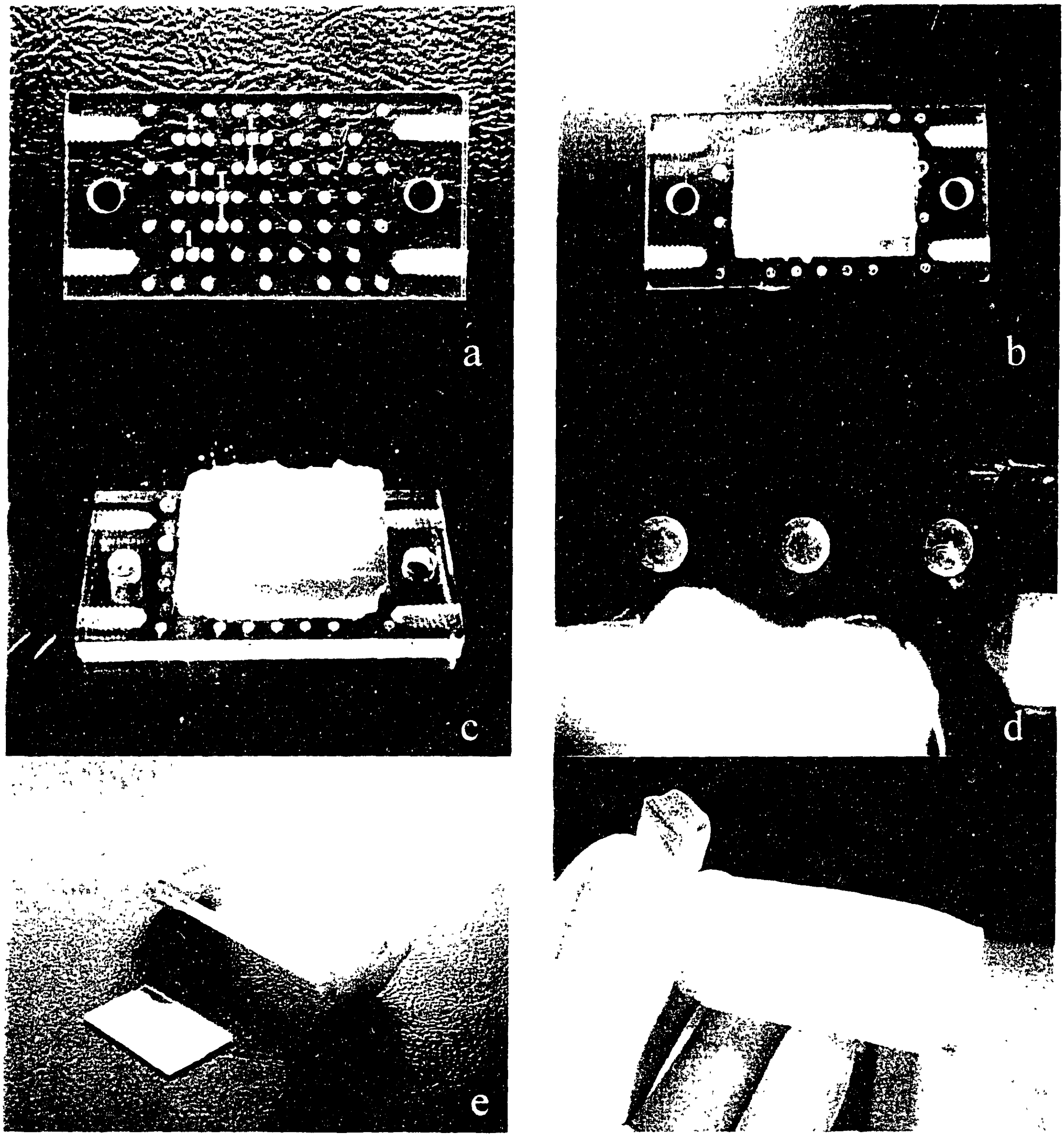

Figure 3-4 Version 4 registration plate. **(a)** Plate prior to mounting cover plate or sample. The marker holes of the central 5 rows of the matrix are beneath the sample (excepting the extreme left and right columns). The hole pattern of these five rows has the binary numbers 1 through 5 encoded by placing extra holes, representing "ones", between the regularly-spaced holes (the binary pattern is read right-to-left). This allows unambiguous identification of slice number and orientation in the MR scans. **(b)** Marker holes have been filled with 2mM Gd(DTPA)^{2} agarose gel, and cover plate has been attached. **(c)** Human tibial plateau sample cut and mounted to top of cover plate with epoxy. **(d)** Closeup of marker holes showing gel. **(e)** Two nylon disks can be attached at each end of plate, providing centering of the sample in the 1 inch i.d. RF probe used for imaging. **(f)** A latex wrap preserves sample hydration and permits safe handling of specimen. Centering disks are machined so that, with the latex wrap in place, a friction fit is maintained in the RF probe.

3.3 Indenter and positioning of test loci

3.3.1 Indenter

In situ indentation was performed with a rigid, nonporous, hemispherically tipped indenter with a diameter of 1.5 mm. The indenter was machined from aluminum; the shaft of the indenter was threaded to match the 1/4-28 interior thread of the load cells. The indenter size and geometry was chosen to match the tip of a standard blunt arthroscopic probe (Acufex Model 010001, Smith & Nephew, Inc., Andover, MA).

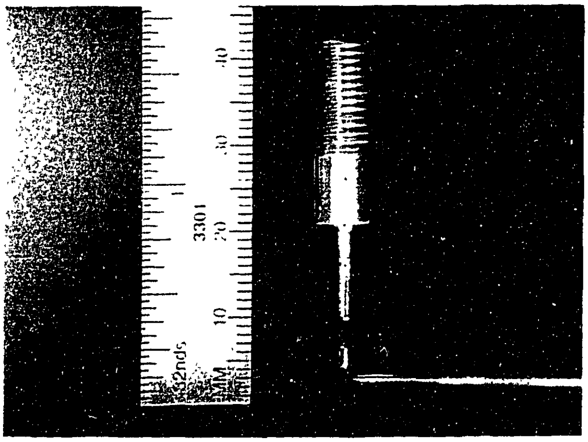

Figure 3-5 Machined indenter (above) and end of standard blunt arthroscopic probe.

3.3.2 Positioning apparatus and techniques

Targeting of the probe tip to a desired test locus on the surface of a sample was performed in one of two ways. For the bovine samples and human sample HT1, ink-dot targeting was employed. For all remaining human samples (mounted on the version 4 registration plate), more accurate, calibrated positioning was achieved by employment of tip-to-marker-hole alignment and quantitative displacement offsets using a micrometer-driven two-axis linear translation stage. In all cases testing was performed at room temperature with the samples fully immersed in Hank's solution.

Ink-dot targeting

Target points on the cartilage surface were marked with spots of India ink applied with a 0.8 mm tip diameter permanent marker (Pigma Micron; Sakura, Japan). India ink marks did not diffuse appreciably and remained in place during prolonged immersion and after repeated freeze-thaw cycles. Targeting was achieved by using the translation stage to position a marked location beneath the indenter tip while viewing the position of the tip relative to the mark from two roughly orthogonal directions.

Displacement-offset targeting

Prior to testing, the registration plate was secured to the bottom of a hydration

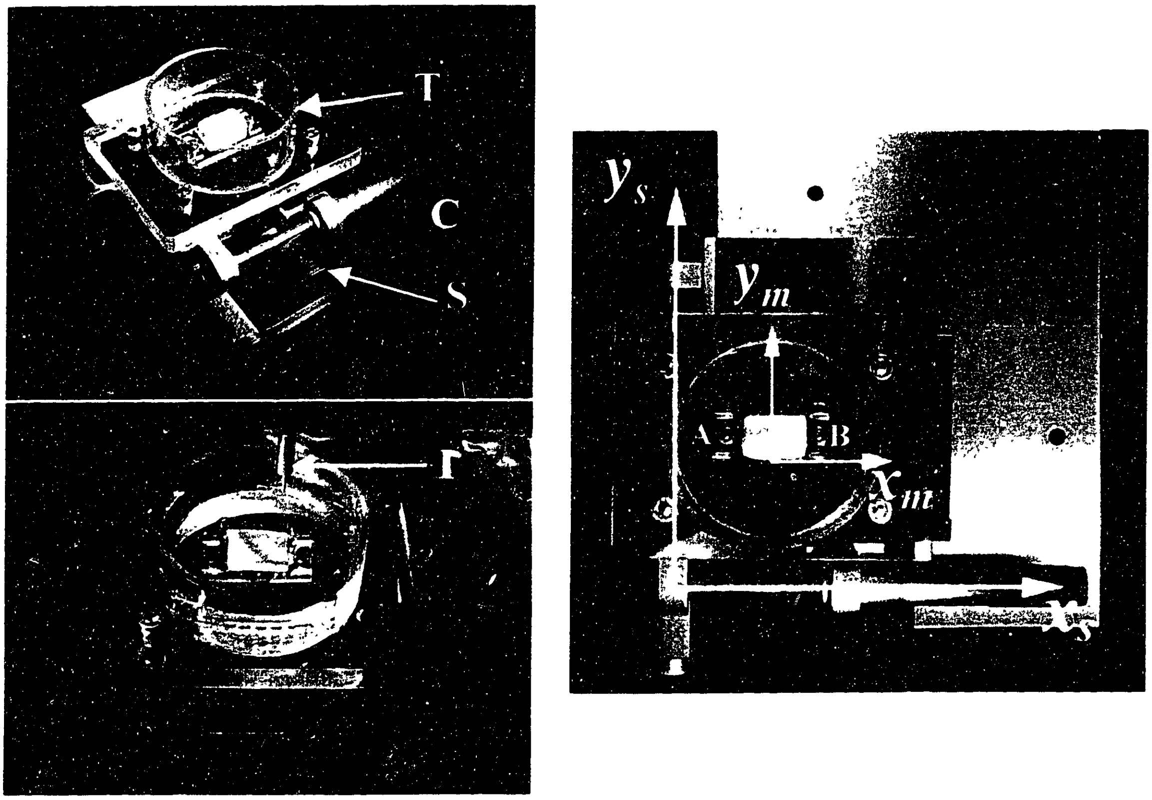

Figure 3-6 Sample positioning apparatus. **(Top left)** Registration frame (with sample) affixed to the bottom of the acrylic/polycarbonate hydration tank **T**, which is secured to a micrometer-driven two-axis (x-y) translation stage **S**. An aluminum coupling plate **C** attaches the stage to the top of the stationary table of the compression testing apparatus. **(Right)** Two screws (A and B) pass through closely-toleranced holes in the registration plate, securing it to the base of the hydration tank. The holes in the registration plate are machined to be axis-aligned with the x_m axis of the marker hole matrix. The corresponding holes in the base of the hydration tank are machined to be axis-aligned with the x_s axis of the translation stage. Securing the registration plate to the tank base thus aligns the marker hole axes with the translation axes. **(Bottom left)** Positioning apparatus in place beneath indenter **I** on compression testing apparatus.

chamber affixed atop a micrometer-driven two-axis linear translation stage (Figure 3-6). The stage enabled each test locus to be precisely positioned beneath the indenter.

The registration plate defined 117 possible test locations: these are points on the surface of the sample directly above each marker hole in the central 5 by 7 matrix of holes or directly above the midpoints between the holes, as defined in Figure 3-7.

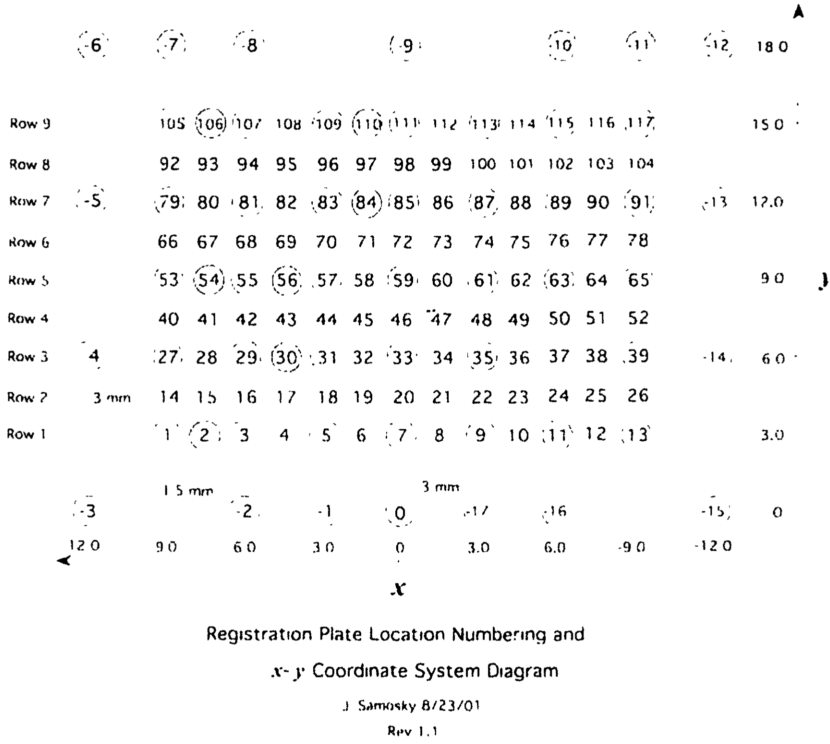

Figure 3-7 Test locus map for registration plate and coordinate definitions. Circles designate $Gd(DTPA)^{2-}$-agar-filled hole locations on the acrylic registration plate. 117 test loci are defined on a rectilinear grid with 1.5 mm spacing. Test loci are labeled with positive integers. Holes on the periphery of the sample permit localization of the indenter tip to a chosen mechanical origin marker hole (typically marker hole #0).

To accurately position a chosen test locus beneath the indenter, a two-step procedure was followed:

(1) *Mechanical origin definition.* A *mechanical origin marker hole* was defined by locating the indenter tip to one of the exposed holes along the periphery of the sample (the holes numbered with 0 or negative integers in Figure 3-7). Typi-

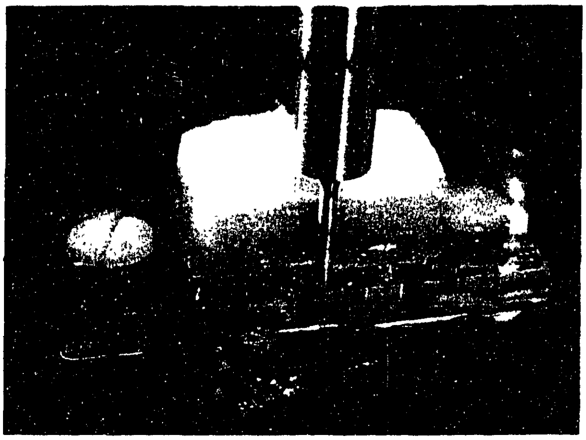

Figure 3-8 Indenter located to mechanical origin marker hole.

cally, the near-edge midpoint marker hole #0 was selected. Tip-to-hole locating was accomplished by the following iterative procedure:

(i) The indenter was lowered until it was just above the surface of the registration plate. The x and y micrometers were adjusted to bring the selected origin marker hole beneath the indenter by visual inspection.

(ii) The indenter was lowered until a load was noted, indicating contact of some portion of the hemispherical indenter tip with the edge of the targeted hole. The x and y positions x_1 and y_1 were recorded.

(iii) The x and y micrometers were adjusted in the direction that reduced the load, indicating that the hole was being more closely centered on the indenter tip. Displacement was continued in the same direction until an increase in load was noted, indicating indenter contact with the opposite edge of the marker hole. The x and y positions x_2 and y_2 at the point where the load just began to increase were recorded.

(iv) The estimate of the center position (x_0, y_0) was calculated from:

$$x_0 = (x_1 + x_2)/2 \qquad y_0 = (y_1 + y_2)/2$$

(v) Steps (ii) through (iv) were iteratively repeated until the indenter tip was centered within the chosen origin marker hole to within a tolerance of +/- 10 µm. (Figure 3-8)

(vi) The final values of x_0 and y_0 were calculated and recorded. x_0 and y_0 now define the *mechanical origin position.*

(2) *Displacement to a test locus.* The indenter was raised and the desired test locus was moved beneath the indenter by displacing the sample the appropriate offsets in x and y. For example, to reach locus #63, the x and y micrometers would be set to (x_0 – 6.0 mm) and (y_0 + 9.0 mm), respectively.

Note that step (1), mechanical origin definition, is performed just once per experiment. All subsequent test locus positioning requires only dialing in the appropriate *x* and *y* displacements. Also note that because the axes of the rectilinear marker hole matrix are aligned with the axes of translation (Figure 3-6) displacement-offset targeting can be achieved with translations only–rotation of the sample relative to the indenter is not required.

3.4 Results: accuracy and repeatability of positioning and registration

3.4.1 Accuracy of marker hole localization

The accuracy with which the indenter can be positioned above a desired target marker hole is dependent on factors including the following:

1) *The accuracy of the x-y positions of the marker holes in the registration plate (relative to the origin hole).* The indenter is positioned by first locating the indenter to the origin hole and then applying a specified displacement to reach a position above any other hole. Therefore the *relative* accuracy of the hole positions with respect to the origin hole is a determinant of positioning accuracy, and is determined primarily by the accuracy of the tools used to machine the plate–in this case, a Bridgeport computer numerical control (CNC) vertical milling machine[7]. In particular, the accuracy of the positions at which the holes are drilled (with respect to each other) is determined by the milling machine's x axis (table slide) and y axis (saddle slide) encoders, and potential deflection of the drill bit and its holder.

---

[7] Variation in plate dimensions due to temperature and coefficient of thermal expansion, are considered negligible, since the plate was machined at room temperature and was employed at room temperature, with only a few degrees of potential temperature variation.

The precision of the milling machine encoders was 0.01 mm (10 μm). Accuracy specifications for the encoders were unavailable. Drill bit deflection was assumed negligible, since the bit was chucked so that only approximately 5 mm was exposed (giving a low diameter/shaft-length aspect ratio of 4.2) and the acrylic plate was quite soft relative to the bit.

2) *The accuracy with which the indenter can be located to (i.e., centered on) the origin marker hole.* This is determined by the sphericity of the indenter tip and circularity of the marker holes, and the accuracy with which the indenter tip is nestled into the marker hole during the marker hole locating procedure. In particular, the amount of available travel in *x* and *y* at the end of the procedure (the available clearance between the indenter tip and the marker hole edges) places an upper bound on the error between tip center and hole center (assuming tip sphericity and hole circularity).

   In the present work, we did not quantitatively measure indenter tip sphericity or marker hole circularity, although both were assessed through qualitative direct visual examination as well as examination under a 10X microscope, both of which revealed no obvious deviations from sphericity or circularity.

   The precision of locating the indenter tip to the origin marker hole was assessed experimentally through repeat measurement of the *x* and *y* position of the origin marker (following the procedure described in Section 3.3.2). A tolerance within +/- 30 μm was obtained between initial and repeat measurements.

3) *The displacement accuracy of the x-y translation stage and the alignment of the rectilinear array of marker holes with the axes of translation.* The stage translational positioning accuracy is determined by the accuracy of the positioning micrometers and the perpendicularity of the two linear (*x* and *y*) stages. The alignment accuracy of plate and stage is principally determined by (A) the play (clearance) between the two screws used to affix the plate to the base of the hydration

tank and the two mounting holes in the plate and (B) the play of the four screws used to affix the hydration tank base to the translation stage.

The *x* and *y* axis micrometer drives have a precision of 1 μm. Perpendicularity of the stages is not an adjustable parameter, and is not specified by the manufacturer. Alignment accuracy was not assessed independently, but was measured as part of total accuracy, discussed below.

4) *Operator care and consistency and repeatability of the indenter-marker-hole colocation protocol.*

   Again, assessment of these parameters will be described below.

To assess overall targeting accuracy and repeatability, four series of experiments were performed:

A) After locating the indenter to the origin hole (#0), the indenter was located to marker holes number -3, -6, -12 and –15 for the registration plates of samples HT3A and HT11A. These holes are the exposed "corner" holes at the periphery of the registration plate, farthest from the origin (see Figure 3-7). The procedure was repeated a second time for HT3A. The *x* and *y* displacements from the origin to each test hole were determined and compared to the nominal values (again, see Figure 3-7).

   The results are presented in Table 3-1. The overall average error is about 50 μm +/– 40 μm in both *x* and *y*. The overall maximum errors were +119 μm and –108 μm. It should be noted that these represent worst case results, as the marker holes tested were maximally far from the origin, thus maximizing error due to mis-alignment of the registration plate with the *x-y* translation stage axes (accuracy determinant #3 above).

	Average absolute error +/- standard deviation (mm)		**Maximum + and – errors (mm)**	
Sample	**x**	**y**	**x**	**y**
HT3A trial 1	.062 +/– .044	.040 +/– .037	+.030 –.108	+.093 –.003
HT3A trial 2	.055 +/– .037	.066 +/– .045	+.020 –.092	+.119 –.014
HT11A	.027 +/– .019	.059 +/- .041	+.053 –.008	+.104 – .010
overall	**.050 +/– .037**	**.054 +/- .039**	**+.053 –.108**	**+.119 –.014**

Table 3-1 Accuracy test for displacements from origin hole to other marker holes.

B) Two additional operators[8] (other than the author) located the indenter to the origin and to marker holes -3, -6, -12 and –15 of sample HT3A. The *x* and *y* displacements from the origin to each test hole were determined and compared to the values obtained by the author. The results are presented in Table 3-2.

	Average absolute error from operator J.S. +/- standard deviation (mm)		**Maximum + and – errors (mm)**	
	x	**y**	**x**	**y**
Operator R.O.	.016 +/– .013	.019 +/– .015	+.004 –.033	+.007 –.017
Operator A.W.	.012 +/– .005	.011 +/- .009	+NA[§] –.018	+.022 –.014

Table 3-2 Interoperator repeatability of marker hole locating with indenter. § Not Applicable: all errors in this trial were negative.

Repeatability in all cases is within 20 μm on average, with maximum differences of +22 μm, –33 μm.

The results of experimental series A confirm that the *average* error in locating the indenter above a marker hole is well under one voxel at the minimum voxel size in the MRI scans employed in the present work (voxel dimension of 100 μm) and

---

[8] Rachel A. Oppenheimer and Ashley A. Williams.

maximum errors are on the order of one voxel. The results of experimental series B indicate that accuracy determinant #2 above (the accuracy of centering the indenter on a marker hole) is on the order of +/– 20 µm, and that a high degree of interoperator repeatability is obtained when following the protocol established for indenter-marker-hole localization.

C) An implicit overall test of indenter positioning accuracy and reproducibility is provided by the tests of cartilage surface localization repeatability presented in Section 4.3.2. Detailed discussion of these experiments will be presented in the section, but in brief, surface profiles were measured for sets of colinear loci on two different samples. These profiles were then measured a second time from 1 to 10 hours later. In all cases (Figure 4-9 and Figure 4-10) the repeat profiles were, on average, within 9 to 24 µm of the initial measurements. Since the surface varied in height as much as 400 µm between test loci (e.g., loci 33A and 33 on sample HT6A, Figure 4-10), the low variance between repeated measurements of the surface location indicates a high degree of indenter positioning repeatability.

D) A second overall test of indenter positioning accuracy is provided by repeated testing of the load response at loci with intervening repositioning of the indenter. As will be discussed in more detail in Section 4.3.3, reproducibility of load measurements (with inter-trial intervals on the order of hours) was +/- 5%. This indicates a high degree of functional repeatability in the positioning system.

In summary, the apparatus, methodology and protocols developed to accurately position the indenter with respect to the registration plate marker holes result in an overall accuracy within 100 µm (one voxel), interoperator repeatability within 20 µm (1/5 voxel) and excellent functional performance in reproducibly determining both cartilage surface profiles and load responses to indentation.

3.4.2 Accuracy of visualization of marker holes on MRI scans

The positions of the centers of the marker holes could be reproducibly determined to within +/– 1 voxel in the MRI scans. The deviation between the perpendicular line drawn from a marker hole to the cartilage above it and the row of pixels passing through the center of the marker hole was estimated to be 1 voxel or less. (The ROI for $T1_{Gd}$ or [GAG] averaging was centered on the row of pixels passing through the center of a marker hole.) Therefore, in the worst case, the ROI defined in the cartilage above a marker hole and the "true ROI" for that marker hole would be offset by 2 voxels or less.

Combining this error with the maximum indenter positioning error discussed in the previous section (roughly 100 μm) leads to a total worst-case registration accuracy of 3 voxels or 300 μm. Typical accuracy is estimated at half that amount, or 150 μm.

Chapter 4

Mechanical testing

This chapter presents the mechanical testing apparatus, protocols and experimental procedures used to test cartilage stiffness using *in situ* indentation. Our goal was to measure focal stiffness at an array of locations on each sample, using an indentation test roughly analogous to the short-duration probing of an articular surface by a surgeon using a hand probe. The sample positioning system and registration plate described in the previous chapter provided a means to accurately target test loci with respect to fixed markers. This chapter describes the mechanical tests performed at these test loci to obtain indices of cartilage stiffness which could then be correlated with the MRI-based indices of GAG content to be described in Chapter 5.

4.1 Mechanical testing apparatus

Indentation testing of articular cartilage specimens was performed using a custom-built compression testing apparatus (Figure 4-1) (which can also serve as a mechanical spectrometer for sinusoidal compression testing) (Z Development, Cambridge, MA). This apparatus consists of a lower, stationary platform (supporting the translation stage and hydration tank) and an upper, motor-driven platen. Load cells (Sensotec, Columbus, OH) are mounted in the movable platen and allow measurement of force with a resolution of 0.1 g over an approximately 500 g range. The indenter (described in Section 3.3.1) was vertically oriented and rigidly fixed beneath a load cell directly above the translation stage. Computer-controlled vertical displacements were applied via a microstepping mo-

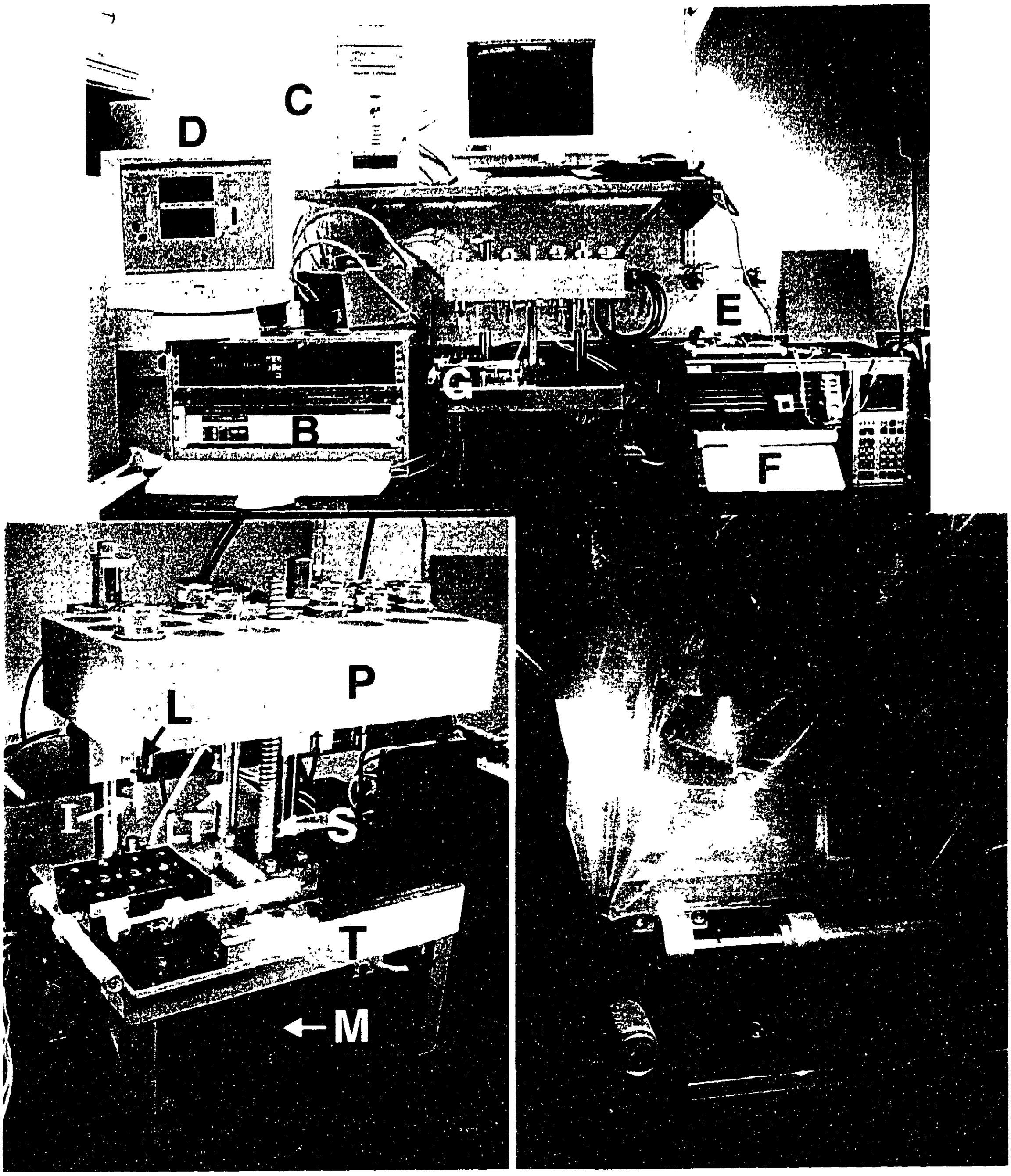

Figure 4-1 **(Top)** Experimental set-up for performing mechanical testing of osteochondral samples: **A**: Compression test apparatus (mechanical spectrometer) **B**: Control and readout electronics **C**: Computer running LabView software **D**: Display with graphical control and acquisition interface **E**: Custom-built quadrature-to-analog signal converter (used to provide an analog displacement signal to the strip chart recorder) **F**: Strip chart recorder **G**: Sample positioning stage **(Bottom left)** Compression test apparatus: **P**: Movable upper platen **T**: Stationary table **M**: Stepping motor **S**: Drive screw **LT**: Linear displacement transducer **I**: Indenter **L**: Load cell **(Bottom right)** An experiment in progress. Sample is immersed in a hydration tank which is fixed to the translation stage. Polyethylene sheeting provides protection from contact with human sample and fluid. For more detail on the sample positioning system, please see **Section 3.3.2.**

tor (Compumotor, Rohnert Park, CA) coupled to a screw drive (1 turn = 5 mm vertical displacement). Software program modules (LabView, National Instruments Corp., Austin, TX) were created to automate the control of the indenter displacement profiles and continuously record the resulting load and displacement as functions of time. Indenter vertical position was measured by means of a magnetic incremental linear encoder with position accuracy of 1 μm and a total measurement range of 52.202 mm. (Digital Gauging Probe; Sony Magnescale, Orange, CA). While running experiments, the apparatus and operator were shielded from contact with human tissue and fluids by a 1 mil (25.4 μm) thick polyethylene sheet which completely surrounded the hydration tank (Figure 4-1 bottom right)The control and data acquisition computer (e-Machines eTower 300k, 300MHz AMD-K6 processor, running Windows 98) was interfaced to the load cell amplifiers, displacement transducer and microstepping motor via serial port connections. The LabView modules proved unable to sample the analog load cell signal through the serial port interface at a rate above 4 Hz. This was clearly unacceptable for reliably recording the peaks of pulse waveforms with rise times on the order of 1 second or less (or the peaks of sinusoidal load signals on the order of 1Hz). To overcome this limitation, a strip chart recorder was used to record the load and displacement signals in parallel with the computer interface. (This was also done to provide redundancy of data recording and a convenient paper roll format for the experimental data.) All load and displacement measurements in the current study were made by means of linear measurement of peaks or other waveform features directly on the paper chart recordings (C-Thru Ruler Company, Bloomfield CT). Early experiments utilized a Linseis model L6514 4-channel recorder (–3dB point of 2.5 Hz and a specified accuracy of +/- 0.35%); later experiments, including all human tissue experiments, employed a Linseis model L2200 4-channel recorder (–3dB point of 2 Hz, +/- 0.25% DC accuracy, +/- 1% AC accuracy) (Linseis GmbH, Selb, Germany).

In order to enhance measurement accuracy, the frequency response of each strip-chart recorder was measured using an HP 33120A function generator (Hewlett-Packard, Palo Alto, CA) as a variable-frequency sine source. For experiments employing pulse or sine frequencies above 0.5 Hz, the measured frequency responses curves were used to correct the measured data for the frequency rolloff of the recorder. (The data on strip-chart recorder frequency response is documented in Appendix D.)

The analog load signal for strip-chart recorder input was obtained directly from the load cell signal conditioner electronics. The signal is 10 mV per gram of load. (Based on observation of this signal with a digital oscilloscope, it was observed that the signal appears to be obtained from the output of a sample-and-hold circuit, with a sample rate of roughly 11 Hz. This results in a stair-stepped appearance of the analog output signal, although with the frequency response of the strip-chart recorders and the typical chart speeds used, this stair-stepping was insignificant and typically unnoticeable.)

The Sony Magnescale linear displacement transducer produces an A/B quadrature output signal. Each quadrature signal transition corresponds to 0.5 μm of linear displacement. The strip chart recorder requires an analog input; therefore, the quadrature signal needed to be converted to an analog signal proportional to displacement. A custom quadrature-to-analog (Q/A) signal converter circuit was therefore designed and built[9]. The quadrature signal was first converted to an incremental count value by an HP HCTL-2020 quadrature decoder/counter. The counter output fed an analog devices AD660 16-bit digital-to-analog converter. The Q/A converter included circuitry for digital timing, reset (zeroing) and analog output calibration as well as a power supply and LED status monitors on the counter output lines. The Q/A converter output is set to a full-scale range of 0 to 10.0 volts, which corresponds to a linear displacement range of 32.768 mm (i.e., 2^{16} quadrature signal transitions from the Magnescale output at 0.5 μm per transition). A 1 mm displacement therefore corresponds to a signal change in the Q/A output of 305.2 mV. The Q/A converter analog output had demonstrated performance of +/- 0.33 mV absolute accuracy (equivalent to +/- 1.1 μm displacement) and +/- 0.3% linearity.

---

[9] Informally dubbed by fellow lab members the "JoeTron2000".

4.2 Indentation testing protocols

4.2.1 Development/rationale

All mechanical tests performed were controlled-displacement experiments. Preliminary work performed on bovine specimens examined step, sinusoid and pulse tests as different ways of interrogating cartilage stiffness. The pulse test, in particular, was examined as a means of quickly, simply, and reproducibly eliciting a short-term compressive response, with parameters (time course, indenter geometry) roughly analogous to the type of indentation applied by a surgical probe during *in vivo* examination. Comparisons were made between the results of pulse, step, and sinusoidal steady-state tests for selected series of loci on three human specimens. These comparisons were made to learn if major differences were exhibited in the different measures of cartilage stiffness assessed by the three methods (i.e., static equilibrium stiffness, dynamic steady-state stiffness, and short-term stiffness for the step, sinusoid and pulse tests, respectively).

In general, displacement amplitudes for all tests were chosen so as to keep estimated peak stresses under 4MPa, a value toward the lower end of the physiologic stress range (peak physiological contact pressure in the human femoropatellar joint has been estimated at 3 to 18 MPa, with compressive strain of 13% or greater). Displacement amplitudes were also constrained to keep the load responses below the load cell measurement limit of nominally 500 g.

4.2.2 Surface localization procedure

Once a point on the cartilage surface was identified for testing, it was positioned beneath the indenter tip via adjustment of the x-y translation stage. A critical first procedure is to position the indenter tip at the surface of the sample, since all subsequent displacements will be measured relative to this reference point. The vertical (z) position of the indenter tip when it is just contacting the uncompressed cartilage surface is termed the *zero-point*, and the procedure for localizing the tip to the surface is termed *surface localization.*

To localize the surface, the indenter was lowered under manual control until it was within approximately 2 mm of the surface. A LabView control module was then run

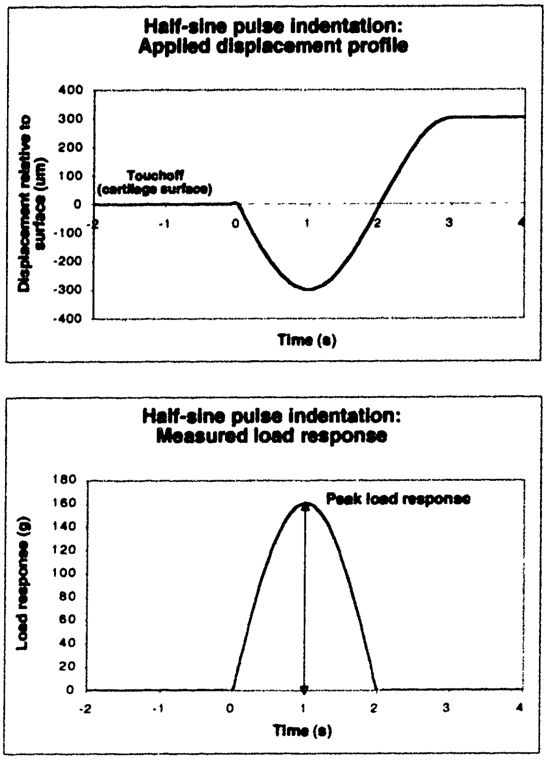

Figure 4-2 Half-sine pulse indentation protocol: **(top)** Applied displacement. **(bottom)** Measured load response. The peak load response is used as a measure of the short-term compressive stiffness of the cartilage.

which lowered the indenter at a rate of 10 μm/second while monitoring the load. When the load increased above a preset threshold (nominally 1.0 g), the indentation was immediately stopped and the indenter was then raised until a load of 0 grams was measured. Noise in the load measurement system was typically ≤ 0.1 g.

Experiments examining the repeatability/consistency of the surface localization procedure are presented in Section 4.3.2.

4.2.3 Half-sinusoid pulse indentation testing

The half-sine pulse indentation protocol consisted of the following:

(1) The sample was translated in *x* and *y* in order to locate a test site beneath the indenter. Test sites were defined as loci on the cartilage surface centered above the marker holes in the registration plate or centered above the midpoint between adjacent holes.

(2) The indenter was lowered until contact with the cartilage surface was established (indicated by a nominal 1 g tare load).

(3) A single half-sine pulse displacement of 300 μm amplitude at 0.25 Hz was applied.

(4) The resulting load response was continuously recorded and the peak load was measured (Figure 4-2).

The indentation parameters were chosen so as to limit peak loads (in general) to under 500 g. The stress distribution beneath a hemisphere displaced a finite distance into a finite-thickness layer is not uniform (nor even analytically tractable), so a peak load cannot easily be translated into an equivalent peak stress. However we note that the Hertz solution ($r = \sqrt{Rd}$) for the contact radius r of a sphere (of radius R) displaced a distance d into an infinite elastic half space provides a reasonable lower estimate for the contact area. For our parameters, r equals 0.47 mm, giving an area of surface contact between indenter and cartilage of 0.80 mm^2. Using this area, a peak load of 100 g then corresponds with an approximate average peak stress of 1.2 MPa. (If the simpler assumption is made that the entire area of the indenter tip below the pre-indentation surface level is in contact with the tissue, the area of contact is 1.41 mm2. This gives an average peak stress of 0.70 MPa for a 100 g peak load.)

4.2.4 Steady-state sinusoidal indentation testing

This test assesses the dynamic stiffness of the cartilage over a range of frequencies. The response to varying preloads and strain amplitudes may also be examined.

First, the zero-point is set at the cartilage surface as described above. Then a ramp displacement lowers the indenter to a specified initial offset depth D. A sinusoidal displacement waveform with frequency f_1 and peak amplitude A is then applied. (The resulting sinusoidal displacement profile thus varies between a depth of D and $D+2A$). The sinusoidal displacement is applied for between 2 and 4 minutes (determined by observing the time required for the load response to reach equilibrium for a given frequency of excitation). The indenter is then returned to the initial offset depth D and held for a period of time sufficient for the tissue to reach equilibrium (nominally 1.5 min.). Another sinusoidal displacement profile is then applied with a different frequency f_2. The procedure may be repeated for additional stimulus frequencies.

For human sample studies, a 15% prestrain was employed (i.e., $D = 0.15t$, where t is cartilage thickness at the test locus), with A = 10 μm, and typical frequencies of f_1 = 0.1 Hz and f_2 = .02 Hz.

The steady-state load amplitude is measured as the peak-to-peak amplitude during the last cycle of each test, yielding the parameter $L_{pp,ss}$ (load, peak-to-peak, steady state). (A measure of cartilage dynamic stiffness may then be computed as the ratio of steady-state peak-to-peak load to applied peak-to-peak displacement amplitude: $L_{pp,ss}/2A$.)

4.2.5 Step displacement

This test assesses the static equilibrium stiffness at multiple strain levels.

First, the zero-point was set at the cartilage surface as described above. Then, a series of step displacements was made, with each step having a specified incremental height. Each level of the resulting "descending stairstep" profile is held for a period of time sufficient for stress-relaxation to occur in the cartilage, typically 2 to 5.5 minutes, a duration empirically determined to result in recovery of the load to an approximately flat asymptote. (Larger total strains required a longer time to reach equilibrium: at 15% total strain, the hold time was 5.5 minutes.)

We note that dynamic stiffness information can also be extracted from the experimentally observed stress-relaxation response curves. We only used the equilibrium stiffness data in the present work.

4.2.6 Multiple-function ("Full Monty") displacement protocol for pulse, step and sinusoidal steady-state tests

As described in section 4.2.1, pulse, step and sinusoidal steady-state displacement protocols were applied to selected series of locations to compare the different load responses. For these experiments, a multiple displacement function protocol was developed (colloquially dubbed "The Full Monty Protocol"). At each test location, the following indentation tests were applied:

- Fixed-amplitude pulse test (peak load measured)
- Fixed-strain pulse test (peak load measured)
- Fixed-amplitude step tests (with peak and steady-state loads measured)
- Fixed-strain step test (steady-state load measured)

- Sinusoidal steady-state tests at two frequencies (peak-to-peak steady-state load measured)

The specific protocol employed will now be described. The pulse, step and sinusoidal steady-state protocols described in the preceding three sections were applied sequentially according to the following protocol while the resulting load response was continuously recorded:

(1) Surface localization of the indenter was established.

(2) A 200 μm half-sine pulse indentation (0.25 Hz) was applied; the peak load was measured.

(3) A 10% strain half-sine pulse indentation (0.25 Hz) was applied; the peak load was measured. The displacement magnitude equal to 10% strain was calculated based on prior measurement of cartilage thickness from MRI studies, described in Section 0)

(4) A 100 μm step indentation was applied (with a displacement rate of 25 m/s) and held for 2 minutes. The transient peak load and equilibrium load (after stress-relaxation had occurred) were measured.

(5) A second 100 μm step indentation was applied (bringing total indentation to 200 μm) and held for 3 minutes. The transient peak load and equilibrium load were measured.

(6) The total indentation was increased to 15% strain (again, based on prior measurement of cartilage thickness from MRI studies). To reach 15% strain, the indenter was displaced from the 200 μm level to 15% strain over a one-minute interval. Early attempts to achieve 15% strain via a rapid step resulted in loads substantially exceeding the nominal load-cell limit (500 g). Displacement was held at 15% strain for 5 minutes, at which point the equilibrium load was measured.

(7) Using the previous 15% displacement as a baseline preload, a 20 μm amplitude peak-to-peak (p-p) sinusoidal displacement was applied at 0.1 Hz for 2 minutes. The p-p amplitude of the last cycle of the resulting load response was measured. This provided a measure of the cartilage dynamic stiffness at 15% preload and 0.1 Hz.

(8) Approximately 2 minutes of rest was allowed following the first sinusoidal excitation. Then 2.5 minutes of a 20 μm amplitude sinusoidal displacement at .02 Hz were applied; again, the p-p amplitude of the last cycle of the resulting load response was measured.

The detailed parameters of this displacement protocol are schematically depicted in Figure 4-3. Actual recordings of the displacement profiles and resulting load responses from a representative experiment (Sample HT11A, location #56) are presented in Figure 4-4.

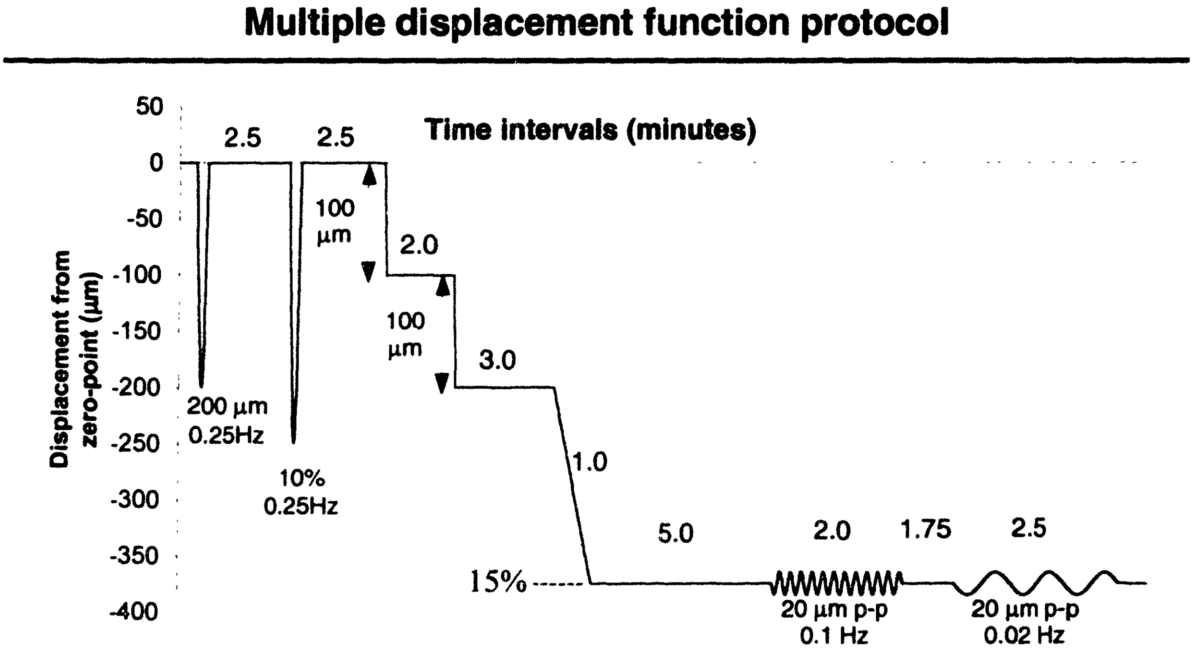

Figure 4-3 A fixed-amplitude pulse, a fixed-strain pulse, two fixed-amplitude steps, one fixed-strain step and two sinusoidal steady-state displacements are applied sequentially at each test locus in the multiple displacement function experiment. Numbers without units are time intervals in minutes. Example displacement amplitudes shown are for a test locus with cartilage thickness of 2.5 mm, the median thickness of locations tested. Note that the time scale for the half-sine pulses and sine waveforms has been slightly expanded for clarity.

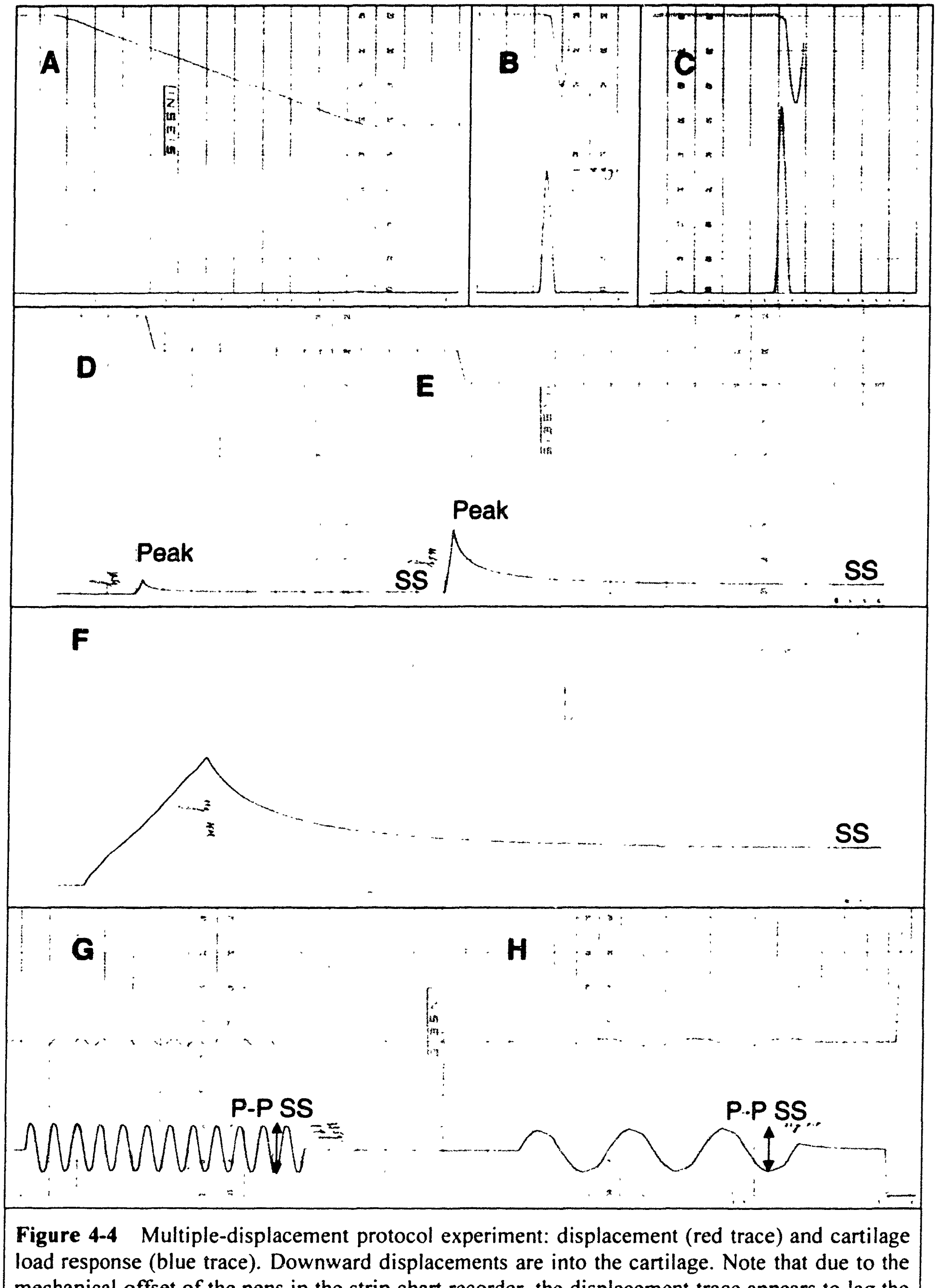

Figure 4-4 Multiple-displacement protocol experiment: displacement (red trace) and cartilage load response (blue trace). Downward displacements are into the cartilage. Note that due to the mechanical offset of the pens in the strip chart recorder, the displacement trace appears to lag the load trace by 1/2 horizontal unit. SS = steady-state. See text for full description.

In Figure 4-4, the following applied displacements and measured load responses are demonstrated (displacements are graphed in red, load responses in blue):

- **(A)** Surface localization. A 10 μm/s ramp displacement is applied until a 1 g load is measured. The displacement value at the end of the ramp is defined as the zero-point displacement (i.e., the cartilage surface).
- **(B)** 200 μm half-sine pulse displacement and resulting load response. (Note that the baseline pen position for zero-point displacement has been moved upwards from the position in graph **A**.)
- **(C)** 10% strain half-sine pulse displacement and resulting load response. The cartilage thickness at this location was 2.4 mm, yielding a 10% strain value of 240 μm.
- **(D)** 100 μm step displacement. Peak and steady-state (SS) (i.e., equilibrium) load values are indicated.
- **(E)** Second 100 μm step displacement (200 μm total displacement). Peak and steady-state (SS) load values are again indicated.
- **(F)** Ramp displacement to 15% strain level (for 2.4 mm thickness, 15% strain = 360 μm). Steady-state load value is indicated.
- **(G)** 0.1 Hz, 20 μm peak-to-peak sinusoidal displacement, superimposed on 15% pre-strain. Peak-to-peak steady-state load value is measured.
- **(H)** 0.02 Hz, 20 μm peak-to-peak sinusoidal displacement, superimposed on 15% pre-strain. Peak-to-peak steady-state load value is measured.

4.3 Results

4.3.1 Correlations between different tests of stiffness

The multiple-displacement protocol described in the previous section was run at a series of locations on each of three human samples. The protocol defines 9 separate load responses: (1) peak load during 200 μm half-sine pulse, (2) peak load during 10% strain half-sine pulse, (3) peak load after 100 μm step, (4) steady-state load after 100 μm step, (5) peak load after 200 μm (total displacement) step, (6) steady-state load after 200 μm step, (7) steady-state load after 15% strain step, (8) peak-to-peak steady-state load after

0.1 Hz, 20 μm p-p sinusoid, and (9) peak-to-peak steady-state load after 0.02 Hz, 20 μm p-p sinusoid. The load response to 300 μm fixed pulse indentation (generally run separately from the multiple-function protocol) defines a tenth load response profile per sample.

To facilitate comparison of the results of the tests, the series of 10 load response profiles across all tested locations are graphed in Figure 4-5, Figure 4-6 and Figure 4-8. In order to quantify the similarity or difference between the responses, the linear correlations between each pair of load response profiles were calculated, and the resulting pair-wise Pearson correlation coefficients are presented in Table 4-2 and Table 4-3. Finally, the dynamic range of each profile was calculated and the load response dynamic ranges are compared for each series in Table 4-4. The dynamic range was defined as the ratio of the maximum to the minimum load response within the series of locations on one sample.

Comparison of load response profiles

All of the indentation tests on human sample HT3A showed qualitatively similar variation across a series of 11 colinear locations spaced 1.5 mm apart (Figure 4-5). Correlations between 8 of the 9 multiple-function protocol tests and the 300 μm pulse test were between 0.99 and 0.87. The 100 μm step steady-state response showed a lower correlation of r = 0.63. Nine of the ten tests showed a broad local minimum in stiffness between loci 85 through 89. (The 100 μm step steady-state test showed a less pronounced minimum at loci 84 and 85.) An interesting but subtle feature is that all three (100 μm, 200 μm, 15%) step equilibrium loads had in common a slight increase at location 87. For the other 7 tests, locus 87 was the global minimum value (or the next-to-minimum value, in the case of the sinusoidal tests).

Figure 4-6 presents the results of the test series on human sample HT11A. The top graph presents the results for all the *transient* load responses: the 200 μm, 300 μm and 10% strain pulse tests, and the 100 μm step and 200 μm step peak loads. All transient responses show a qualitatively similar variation across the 9 loci, with generally increasing stiffness seen between loci 54 and 61. The bottom graph presents the results for the *steady-state* load responses: the 100 μm, 200 μm and 15% step equilibrium loads and the peak-to-peak steady-state loads for the 0.1 Hz and 0.02 Hz sinusoidal displacement tests.

The 15% equilibrium load profile and both sinusoidal steady-state load profiles show a distinctly different morphology from the transient load profiles. Specifically, the stiffness peaks between loci 56 and 58 and falls off to either side of these loci.

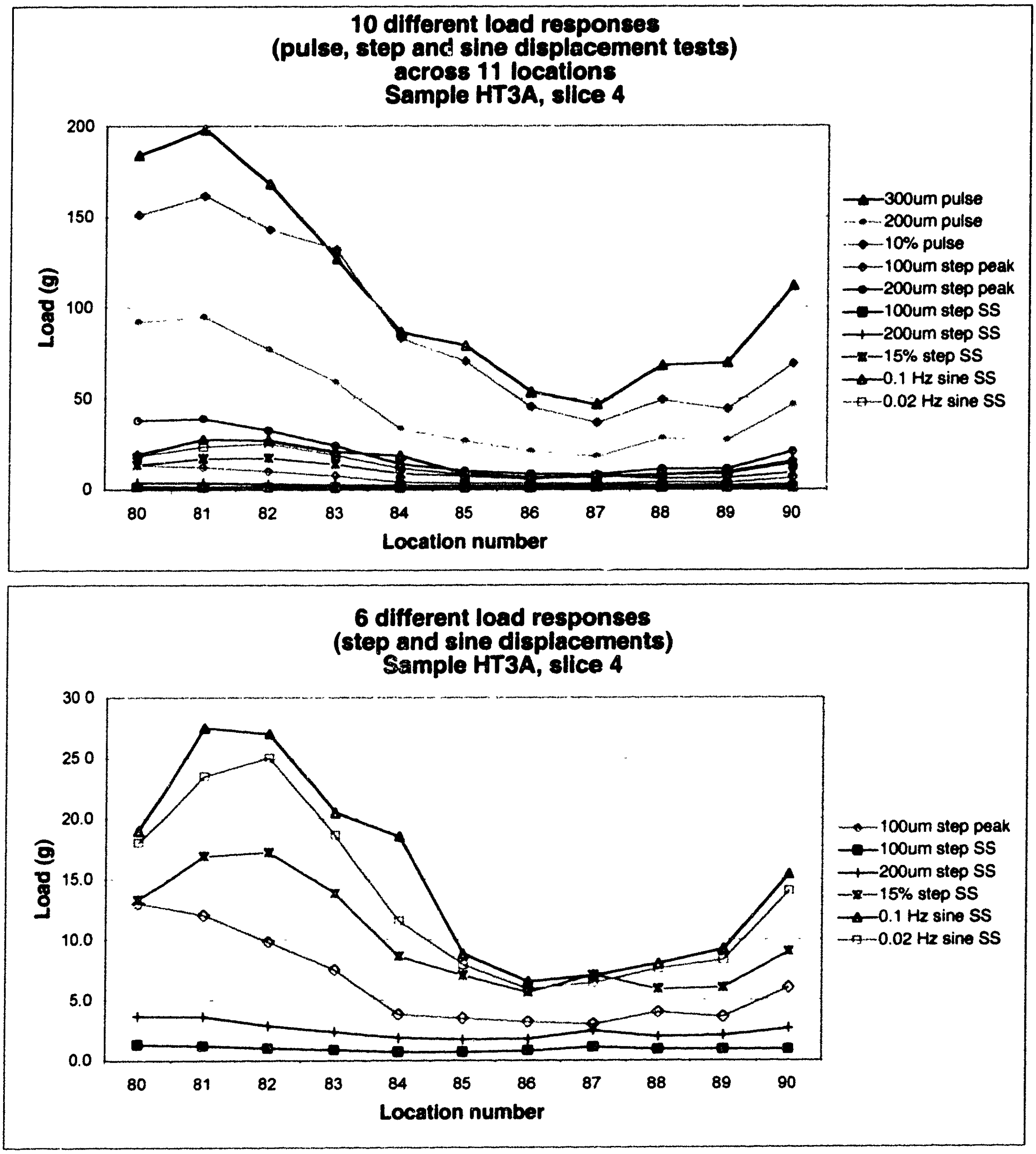

Figure 4-5 Comparison of 10 different load response profiles across 11 colinear locations (1.5 mm spacing) on sample HT3A. **(Top)** The peak responses to pulse and step displacements show similar variation across the 11 loci. **(Bottom)** The lower 6 profiles from the top graph are plotted separately with a rescaled *y* axis. All load responses show high correlation to the response to 300 μm pulse indentation (correlations range from 0.99 to 0.87) except for the 100 μm step steady-state response, which shows a moderate correlation of r = 0.63.

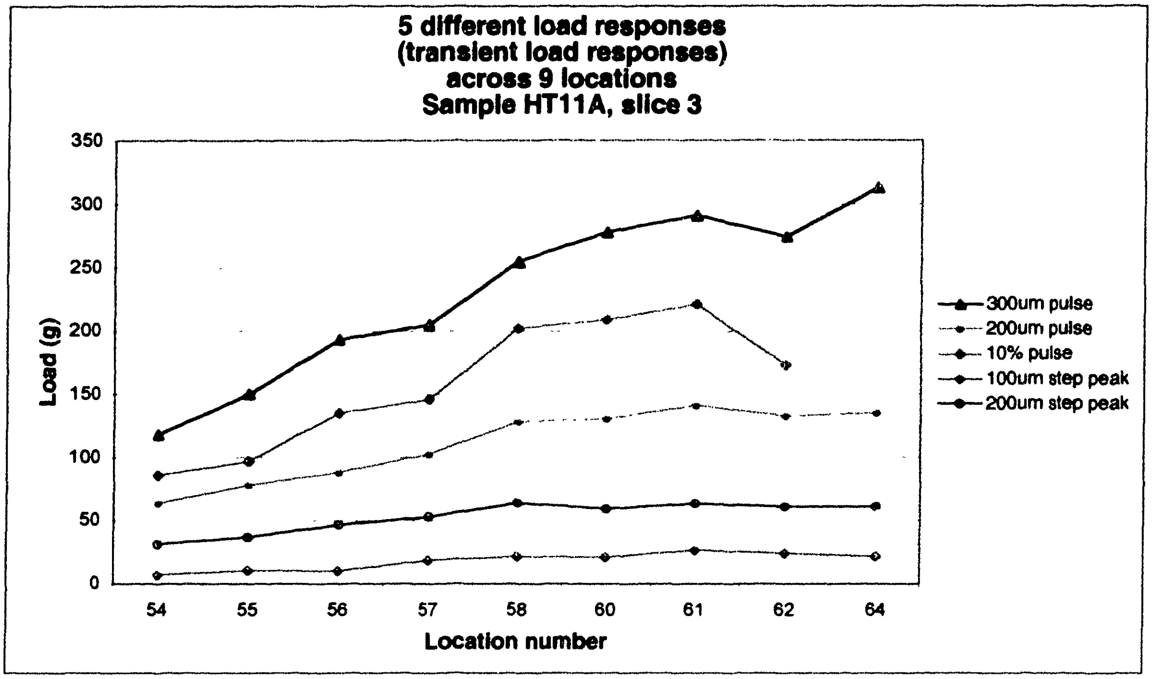

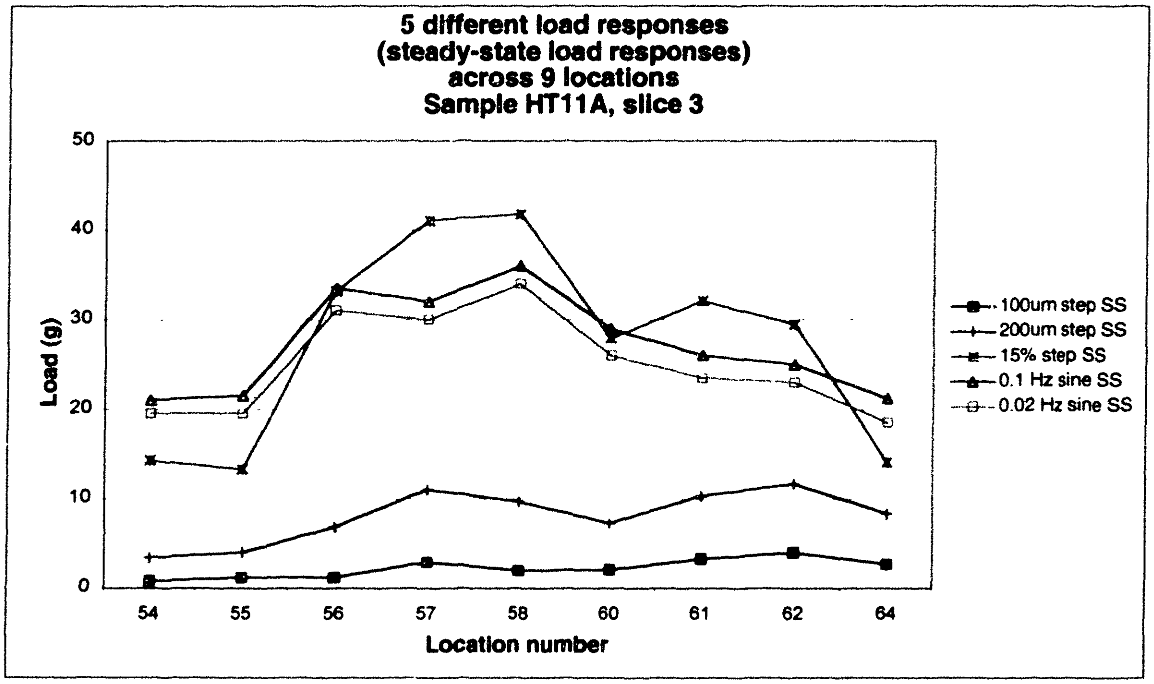

Figure 4-6 Comparison of 10 different load response profiles across 9 colinear locations on sample HT11A. **(Top)** The 5 transient load responses all show a similar variation across the 9 loci. **(Bottom)** The 100 μm and 200 μm equilibrium responses (bottom two traces) show qualitatively approximately similar variation to the transient responses. The 15% strain equilibrium response and the two sinusoidal steady-state responses (with 15% preload), however, show a different response pattern from the other profiles.

All five transient load profiles increase (or, for the 200 μm step peak, is approximately constant) from loci 58 to 61. All three load responses with 15% static strain (equilibrium and the two sinusoidal tests) decrease from loci 58 to 61. For this sample, thickness at loci 58, 60 and 61 was constant at 2.5 mm, so the difference between transient and 15% strain responses cannot be ascribed to thickness variation. A reasonable hypothesis is that the observed difference may reflect a different profile of cartilage GAG composition at shallower vs. greater depth in the sample. To examine this hypothesis, the locally averaged $T1_{Gd}$ profiles (indicative of GAG content) were computed across the test loci with ROI depths of 400 μm (shallow) and 800 μm (deep). The shallow and deep $T1_{Gd}$ profiles were then compared with the 200 μm pulse load profile and the 15% strain equilibrium profile.

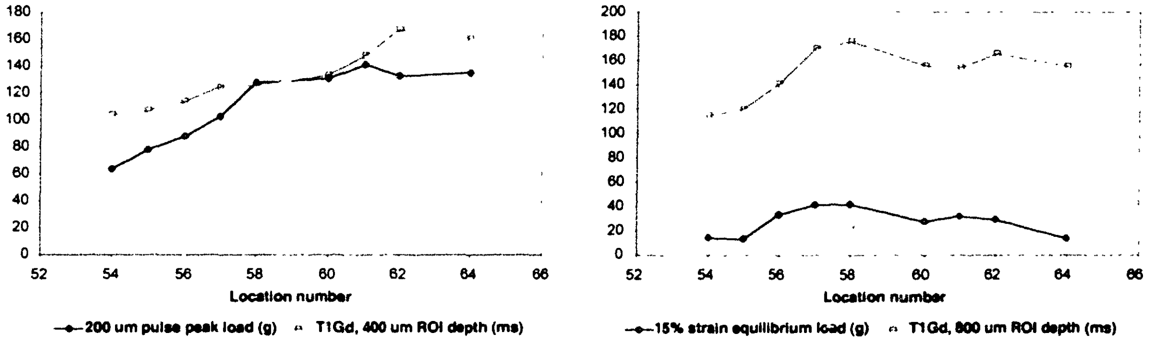

Figure 4-7 **(Left)** 200 μm pulse peak load shows similar variation to profile of $T1_{Gd}$ averaged to 400 μm depth ($r = 0.86$). **(Right)** 15% strain (375 μm indentation) equilibrium response shows similar variation to 800 μm depth-averaged $T1_{Gd}$($r = 0.77$). By comparison, the 15% strain equilibrium response shows no correlation to the 400 μm depth $T1_{Gd}$ profile ($r = 0.09$). (Sample HT11A).

The results are shown in Figure 4-7. Note that for both the 200 μm pulse load profile and the shallow $T1_{Gd}$ profile, an increase is seen from locus 58 to 61. For both the 15% strain equilibrium response profile and the deep $T1_{Gd}$ profile, a decrease occurs from locus 58 to 61. Furthermore, overall the 15% strain equilibrium response is uncorrelated with the shallow $T1_{Gd}$ profile ($r = 0.09$), but it is highly correlated with the deep $T1_{Gd}$ profile ($r = 0.77$). This supports the hypothesis that the 15% strain load responses are being influenced by a deeper region of the articular surface with a different stiffness profile than the more superficial region. (This result, although limited by small sample size, also suggests the power of the present methodology to closely colocalize mechanical and GAG measurements, allowing patterns of relationship between the two to be elucidated.)

Finally, the results for 14 loci examined on sample HT8A are presented in Figure 4-8. The loci were scattered, and so a wide variation of load response is demonstrated. In general, all transient load responses as well as the sinusoidal steady-state responses show similar patterns of variation. The three step-equilibrium responses show somewhat less variation and appear to have a more compressed dynamic range compared to the other responses.

Quantitative comparison of correlations among the load responses

To permit a quantitative comparison of the correlations (or lack thereof) between the different load responses, correlation tables were computed for each series. Table 4-1 provides a schematic map of the organization of the tables.

The tests are grouped into three categories: transient response tests, step-equilibrium response tests and sinusoidal steady-state response tests. Regions of the table are then defined that group the correlations between these categories.

The correlation results for samples HT3A, HT11A and HT8A are presented in Table 4-2 and Table 4-3.

The following general characteristics are evident:

(1) Correlations among the five transient tests (300 μm pulse, 200 μm pulse, 10% strain pulse, 100 μm step peak load, and 200 μm step peak load) were uniformly very high, with $0.81 \leq r \leq 1.00$ across all tests on the three samples (and all but two of the transient–transient correlations ≥ 0.91). This suggests that all of these displacement-response tests are interrogating similar cartilage characteristics and behavior.

(2) The correlation between the two different frequency sinusoidal tests are uniformly very high across the three samples, with $0.97 \leq r \leq 1.00$.

(3) The 100 μm step equilibrium load is generally only weakly to moderately correlated to the other tests. This test elicited extremely low-magnitude loads, typically less than 2 g and in all cases ≤ 4 g (and with comparatively low dynamic range for samples HT3A and HT8A–see next section).

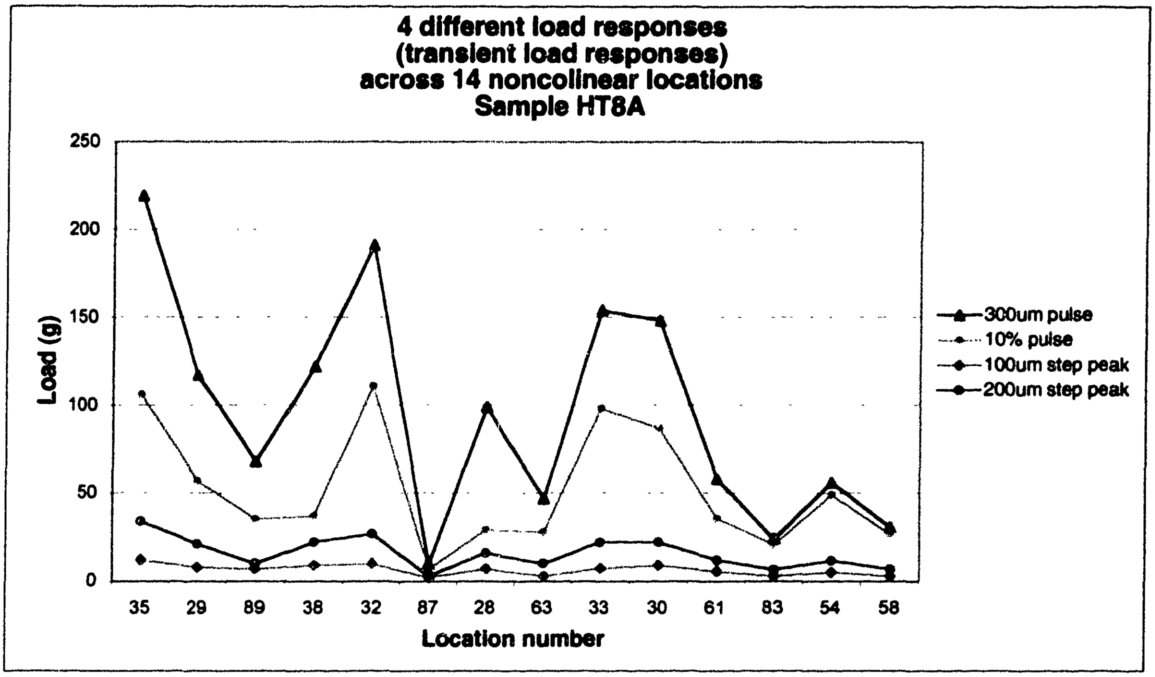

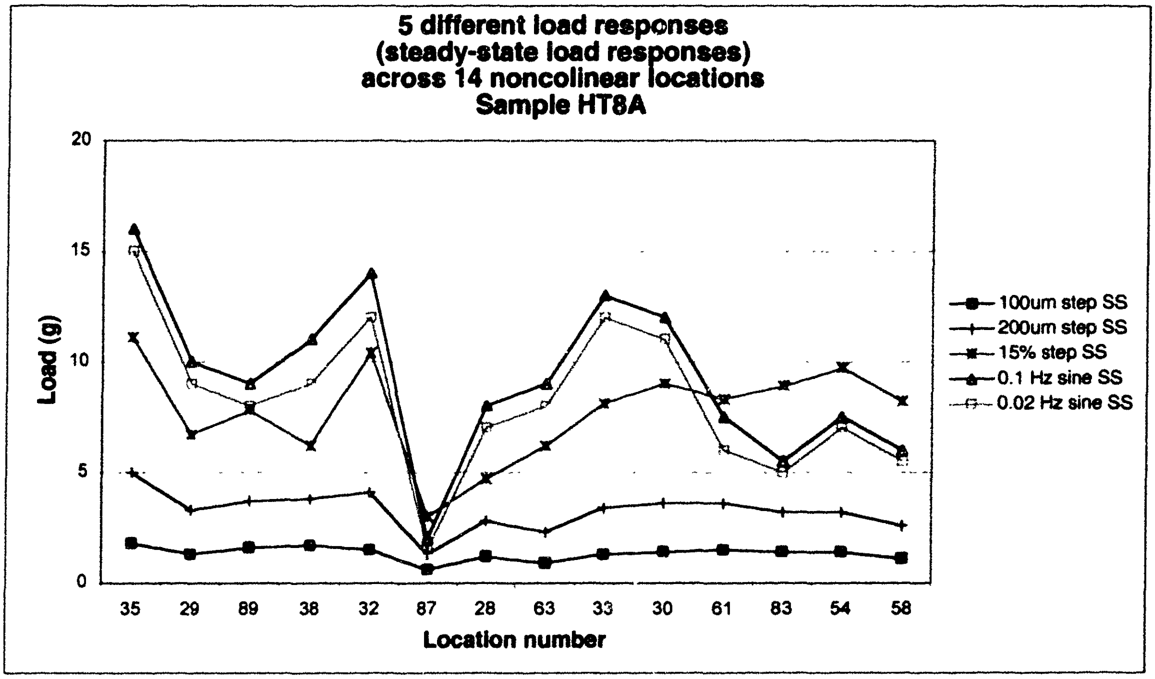

Figure 4-8 Comparison of 9 different load response profiles across 14 scattered locations on sample HT8A (the 200 μm pulse test was not performed on this sample). **(Top)** The 4 transient load responses all show a similar variation across the 14 loci. **(Bottom)** The sinusoidal steady-state responses (top two traces) show qualitatively similar variation to the transient responses. The 15% strain equilibrium response shows a generally similar profile, but the 100 μm and 200 μm equilibrium responses show less variation across the loci. All three equilibrium responses exhibit a smaller dynamic range than the other responses.

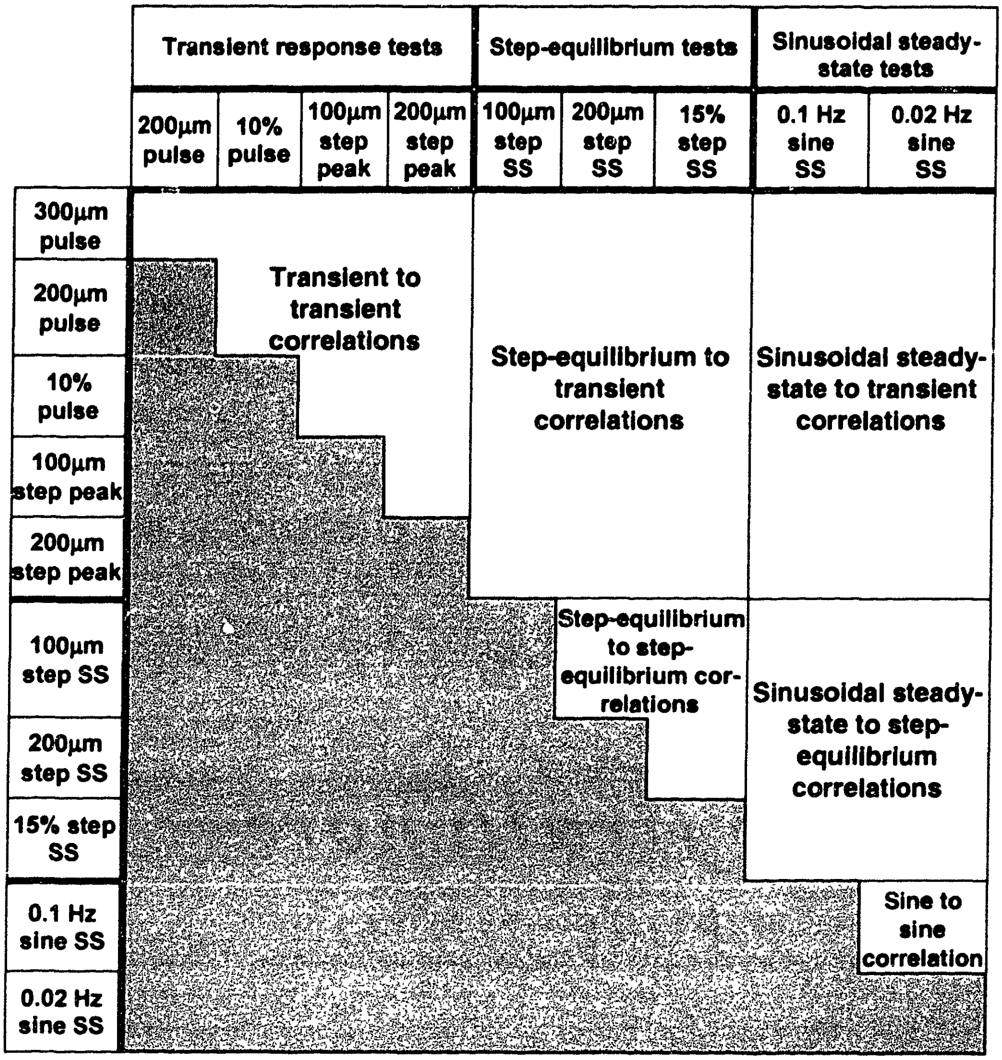

Table 4-1 Descriptive map of the indentation test correlation matrix. Three groups of indentation tests are defined: transient response tests (pulse and peak load responses), step-equilibrium tests and sinusoidal steady-state tests. The correlations of the 10 indentation tests to each other are then partitioned into the 6 combinations of these groups: (1) correlations of transient responses to transient responses, (2) step-equilibrium responses to transients, (3) sinusoidal steady-state to transients, (4) step-equilibrium responses to step-equilibrium responses, (5) sinusoidal steady-state responses to step-equilibrium responses and, lastly, (6) the correlation between the two sinusoidal steady state responses.

(4) The majority of the other tests are generally moderately to strongly correlated ($0.5 \leq r \leq 1.0$) across the three samples, with the notable exception of the correlations of the 15% step equilibrium response and both sinusoidal steady-state responses to all other responses for sample HT11A. Examination of the HT11A correlation matrix (Table 4-2 bottom) reveals a prominent "block" of weak correlations in the upper right of the matrix, reflecting the weak correlations of the three measurements made at 15% strain to all other

Sample HT3A

	Transients				Step-equilibrium responses			Sinusoidal steady-state	
	200μm pulse	10% pulse	100μm step peak	200μm step peak	100μm step SS	200μm step SS	15% step SS	0.1 Hz sine SS	0.02 Hz sine SS
300μm pulse	0.99	0.96	0.98	0.99	0.63	0.87	0.93	0.90	0.94
200μm pulse		0.96	0.99	1.00	0.69	0.90	0.92	0.88	0.93
10% pulse			0.93	0.95	0.52	0.78	0.95	0.92	0.94
100μm step peak				0.99	0.75	0.92	0.89	0.82	0.88
200μm step peak					0.70	0.91	0.93	0.88	0.93
100μm step SS						0.91	0.54	0.39	0.49
200μm step SS							0.78	0.70	0.76
15% step SS								0.95	0.98
0.1 Hz sine SS									0.97
0.02 Hz sine SS									

Sample HT11A

	Transients				Step-equilibrium responses			Sinusoidal steady-state	
	200μm pulse	10% pulse	100μm step peak	200μm step peak	100μm step SS	200μm step SS	15% step SS	0.1 Hz sine SS	0.02 Hz sine SS
300μm pulse	0.98	0.97	0.92	0.95	0.75	0.71	0.28	0.14	0.09
200μm pulse		0.97	0.97	0.97	0.79	0.77	0.37	0.20	0.15
10% pulse			0.91	0.95	0.64	0.71	0.65	0.48	0.44
100μm step peak				0.95	0.88	0.84	0.43	0.18	0.14
200μm step peak					0.77	0.85	0.55	0.40	0.35
100μm step SS						0.90	0.37	0.02	0.01
200μm step SS							0.71	0.44	0.43
15% step SS								0.91	0.91
0.1 Hz sine SS									1.00
0.02 Hz sine SS									

Table 4-2 Correlation matrices for multiple indentation tests, Samples HT3A and HT11A. Correlations color-coded. tan: $r \geq 0.8$, blue: $0.8 > r \geq 0.5$, red: $r < 0.5$.

Sample HT8A

	Transients			Step-equilibrium responses			Sinusoidal steady-state	
	10% pulse	100µm step peak	200µm step peak	100µm step SS	200µm step SS	15% step SS	0.1 Hz sine SS	0.02 Hz sine SS
300µm pulse	0.92	0.95	0.99	0.61	0.78	0.51	0.95	0.94
10% pulse		0.81	0.88	0.52	0.72	0.68	0.90	0.91
100µm step peak			0.95	0.75	0.86	0.48	0.90	0.88
200µm step peak				0.65	0.80	0.51	0.94	0.93
100µm step SS					0.95	0.70	0.67	0.65
200µm step SS						0.78	0.83	0.82
15% step SS							0.61	0.64
0.1 Hz sine SS								0.99
0.02 Hz sine SS								

Table 4-3 Correlation matrices for multiple indentation tests, Sample HT8A.

measurements. Conversely, the correlations of the 15% strain measurements among themselves are uniformly very strong (0.91 < r < 1.0) As discussed above, these phenomena appear to be related to the particular depth-dependent GAG distribution in this sample, with the deeper tests interrogating a different cartilage stiffness distribution than the shallower tests.

Dynamic range of load response measurements

The dynamic range of each indentation test was calculated for each sample as the ratio of maximum to minimum load response for the series of tests performed on the sample. The average load was also calculated for each test for each sample. The results are tabulated in Table 4-4.

All three pulse tests displayed comparable dynamic ranges across the three samples. For samples HT3A and HT8A, the transient responses exhibited higher dynamic ranges (by roughly twice or more) than the step-equilibrium responses. For HT11A, transient and step-equilibrium dynamic ranges were comparable (note that the dynamic range figure of 5.0 for the 100 µm step equilibrium load for HT11A is sensitive to the extremely low minimum load of 0.8 g encountered in the sample series, a load value even below the threshold used for surface detection. Using the next-to-minimum load value of 1.2 g yields a dynamic range of 3.3, comparable to the transient dynamic range values.) The dynamic range of the sinusoidal steady-state responses was typically within the range of the transient responses (slightly lower for sample HT11A).

The average loads exhibit the expected trends: in all cases, average load for a test increases with magnitude of displacement. Average loads for sinusoidal steady-state testing at 0.1 Hz were in all cases slightly higher than at 0.02 Hz, reflecting the expected increase in dynamic stiffness at higher frequency.

Also notable are the extremely low average loads for the 100 μm step equilibrium response (≤ 2.2 g) and the order of magnitude higher loads for the pulse responses compared to comparable-displacement equilibrium responses (e.g., average loads of 108 g, 96 g and 231 g for the 300 μm pulse response for HT3A, HT8A and HT11A respectively, compared to average loads of 10 g, 7.7 g and 27 g for the 15% strain equilibrium response.)

		Transients					**Step-equilibrium responses**			**Sinusoidal steady-state**	
		300μm pulse	**200μm pulse**	**10% pulse**	**100μm step peak**	**200μm step peak**	**100μm step SS**	**200μm step SS**	**15% step SS**	**0.1 Hz sine SS**	**0.02 Hz sine SS**
Dynamic Range	**HT3A**	4.3	5.3	4.4	4.3	4.6	1.9	2.1	3.1	4.2	4.2
	HT8A	22	–	15.9	6.0	11	3.0	3.8	3.7	8.0	10
	HT11A	2.7	2.2	2.6	3.7	2.1	5.0	3.4	3.1	1.7	1.8
Average load	**HT3A**	108	48	90	6.3	20	0.9	2.5	10	15	13
	HT8A	96	–	52	6.5	16	1.3	3.3	7.7	9.3	8.3
	HT11A	231	111	159	18	53	2.2	8.0	27	27	25

Table 4-4 Dynamic range and average load for each of ten indentation tests performed on series of loci on three human samples.

4.3.2 Accuracy and reproducibility of surface localization

Accurate surface localization (zero-point establishment) is a precondition for consistent and repeatable indentation measurements. It is also a prerequisite for meaningful long-term repeat studies (to examine whether changes occur in the sample due to treatments such as freezing, refrigeration and room temperature exposure). For a sample which shows a substantial gradient in the height of the surface near a locus, reproducibility of surface localization at a test site after moving then repositioning the sample to its original location also serves as an implicit confirmation of the accuracy of the mechanical positioning system.

The short-term reproducibility of the surface localization procedure was examined in several experiments according to the following procedure. A series of loci were selected for testing. Each locus was positioned beneath the indenter and the *z*-axis surface position (zero-point) was recorded after running the surface localization procedure. A series of pulse, step, and sinusoidal steady-state indentation tests was then run at the locus. The sample was then translated to position a new test locus beneath the indenter. This process was continued until all loci had been tested. At the conclusion of the series of tests, the sample was translated so as to reposition the first locus tested beneath the indenter. The surface localization procedure was then run a second time at each locus (repeating the order of initial testing) and the zero-point value again recorded. In summary, at each test location *L*, surface localization was performed followed by indentation tests, a rest period occurred while the sample was moved and other loci were tested, then the sample was moved to reposition *L* beneath the indenter again and a second surface localization was performed.

The results of three such experimental studies are illustrated in Figure 4-9 for two series of tests on sample HT3A (21 loci total) and in Figure 4-10 for two series of tests on sample HT6A (25 loci total). The first series (Figure 4-9 top) shows surface profiles derived from initial and repeat surface localization runs at 11 locations on HT3A with inter-trial intervals of from 1 to 6 hours. An average difference of –9.0 µm was obtained between initial and repeat surface determinations. The second series (Figure 4-9 bottom) shows initial and repeat surface localizations at another 10 locations on HT3A at intervals from 10.6 to 3.3 hours. An average absolute deviation of 12.1 µm was obtained. Two more experimental series examined touch-off repeatability at 12 loci on HT6A with a fixed inter-trial interval of 2.2 hours and at an additional 13 locations with a fixed inter-trial interval of 2.0 hours. Average deviations of -24.0 µm and –18.4 µm, respectively, were obtained between surface determinations in the two series.

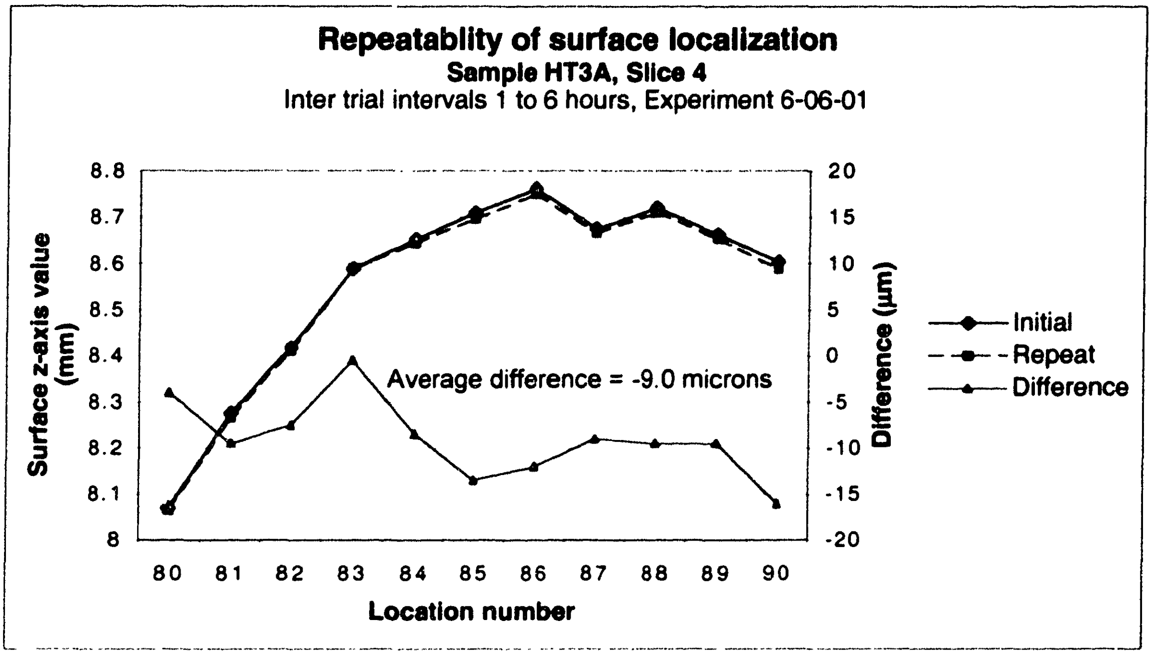

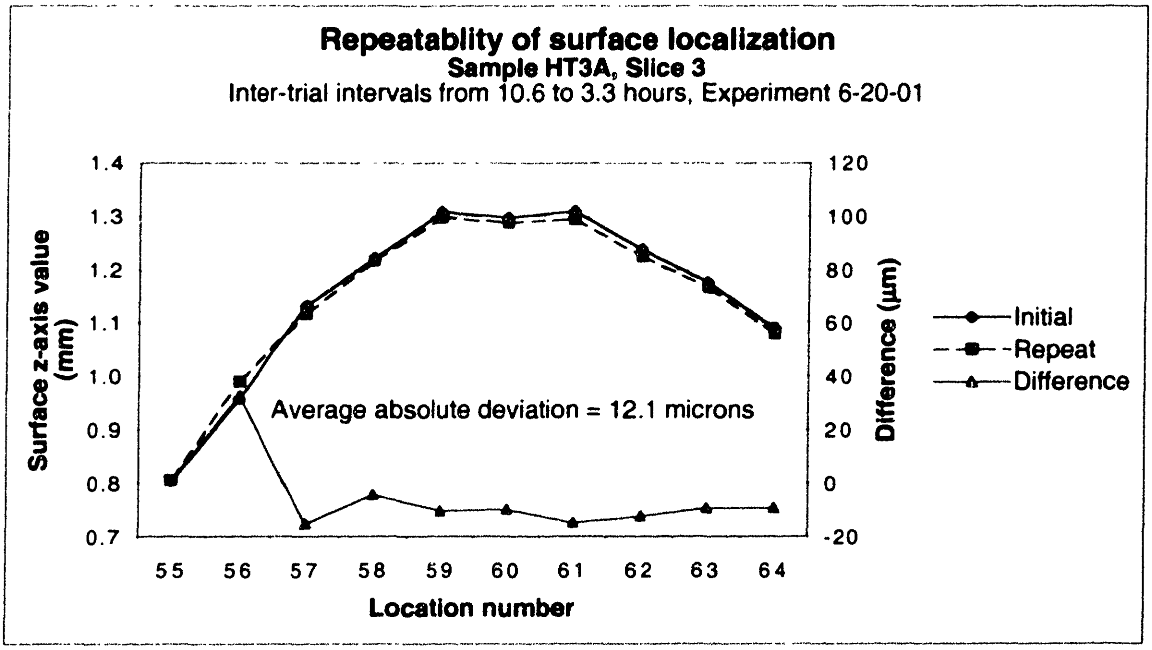

Figure 4-9 Repeatability of surface localization for series of 11 loci (top) and 10 loci (bottom) on sample HT3A, with inter-trial intervals on the order of hours. The solid blue curve indicates the zero-point value of the cartilage surface on performing initial surface localization. The dashed red curve shows the zero-point value on repeat testing (after executing indentation tests at each locus with movement of the sample.) The lower green curve shows the difference, in µm, between the initial and repeat surface localizations.

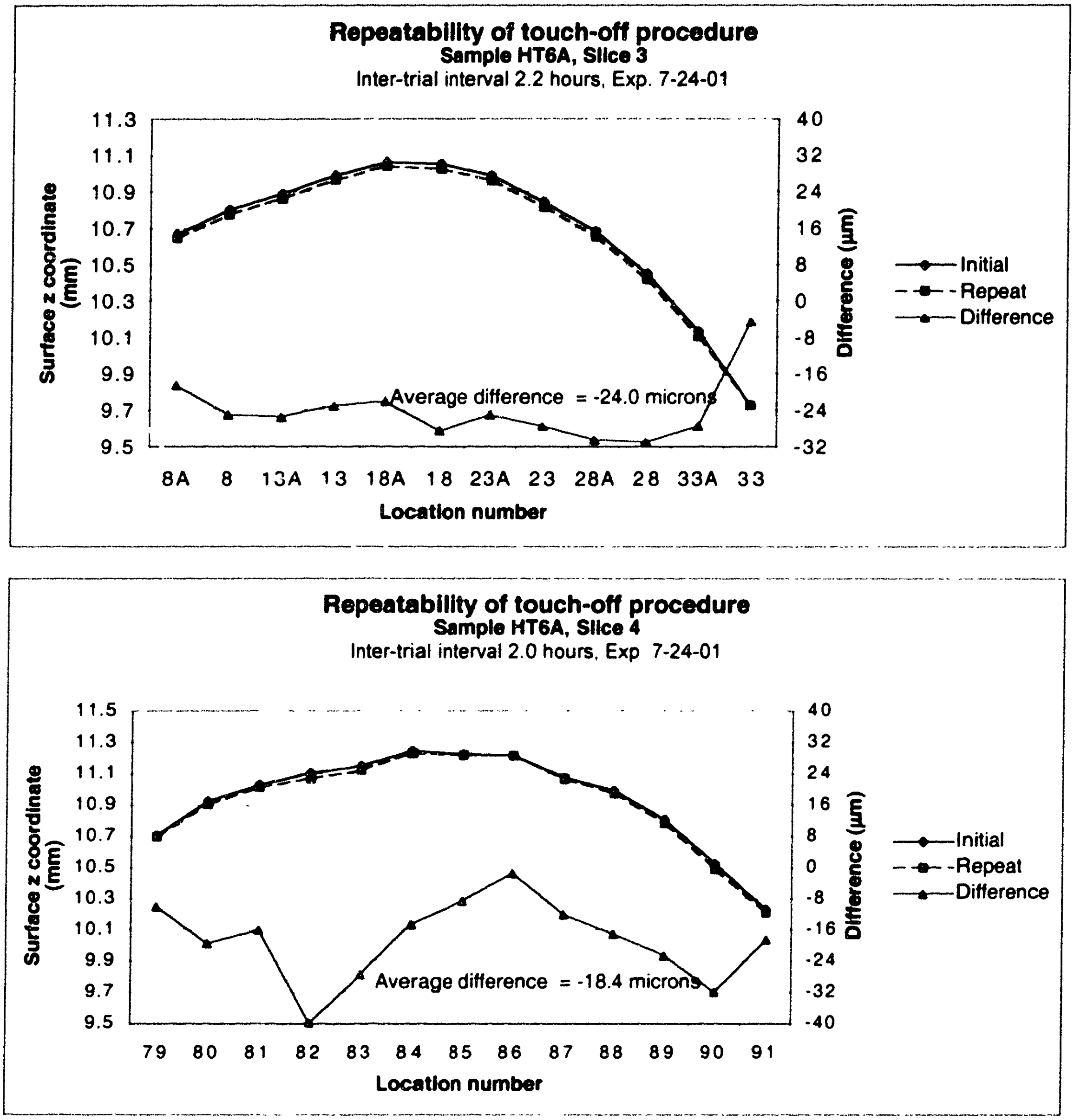

Figure 4-10 Repeatability of surface localization for series of 12 loci (top) and 13 loci (bottom) on sample HT6A, with inter-trial intervals near 2 hours. The lower green curve shows the difference between the initial and repeat surface localizations, which averaged –24 µm and –18.4 µm for the two series.

The results of the four series (46 loci total) indicated that the articular surface could be repeatedly localized using the present methodology to within 16 µm on average over all locations examined. This average deviation between repeat surface localizations is less than 1% of the median cartilage thickness, and is equal to 5.3% of the amplitude (300 µm) used for pulse indentation testing.

Long-term surface localization reproducibility and the stability of articular surface morphology

An examination was made of the reproducibility of surface location measurements with a three-month interval between trials. This served to (a) test the accuracy of the sample positioning system with complete removal and replacement of the hydration tank and registration frame, and (b) examine whether the sample surface morphology changed appreciably over the course of the experiments due to, for example, local swelling of the articular surface.

The surface locations of 13 test loci on sample HT3A were determined initially, and then again at a three month interval. Because the *z*-axis measurement system of the mechanical testing system gives relative rather than absolute vertical position, one location (locus #9) was chosen as a zero-reference for comparing the height of the surface in initial and repeat surface location measurements (Figure 4-11). During the three-month interval, the sample was subjected to three imaging studies, three mechanical testing studies, and at least four freeze-thaw cycles. Over the three months, it was exposed to cumulative room-temperature exposure of over 24 hours, the majority of this in hydration in Hank's balanced salt solution (with 2 mM $Gd(DTPA)^{2-}$ and 1% v/v penicillin/streptomycin/amphotericin).

The result, shown in Figure 4-11, demonstrated that the average absolute deviation between the two surface determinations across the loci was 19 μm, which is less than 1% of the mean thickness of the loci tested (2.2 mm). This was comparable to the deviations observed in the short-term surface-localization reproducibility studies described in the preceding section (hours between tests, 16 μm average deviation, equal to <1% of mean thickness of test loci).

These studies demonstrate that the surface localization procedure is capable of both short-term and long-term reproducibility of under 20 μm on average, that the surface can be repeatedly localized to within 1% of cartilage thickness, and that the articular surface differential morphology does not change appreciably over the course of months of testing and sample storage using the protocols of this study. (Note that because surface localization measurements were relative, not absolute, these studies would not be sensitive to a uniform, global rise of the cartilage surface occurring over the three month interval.)

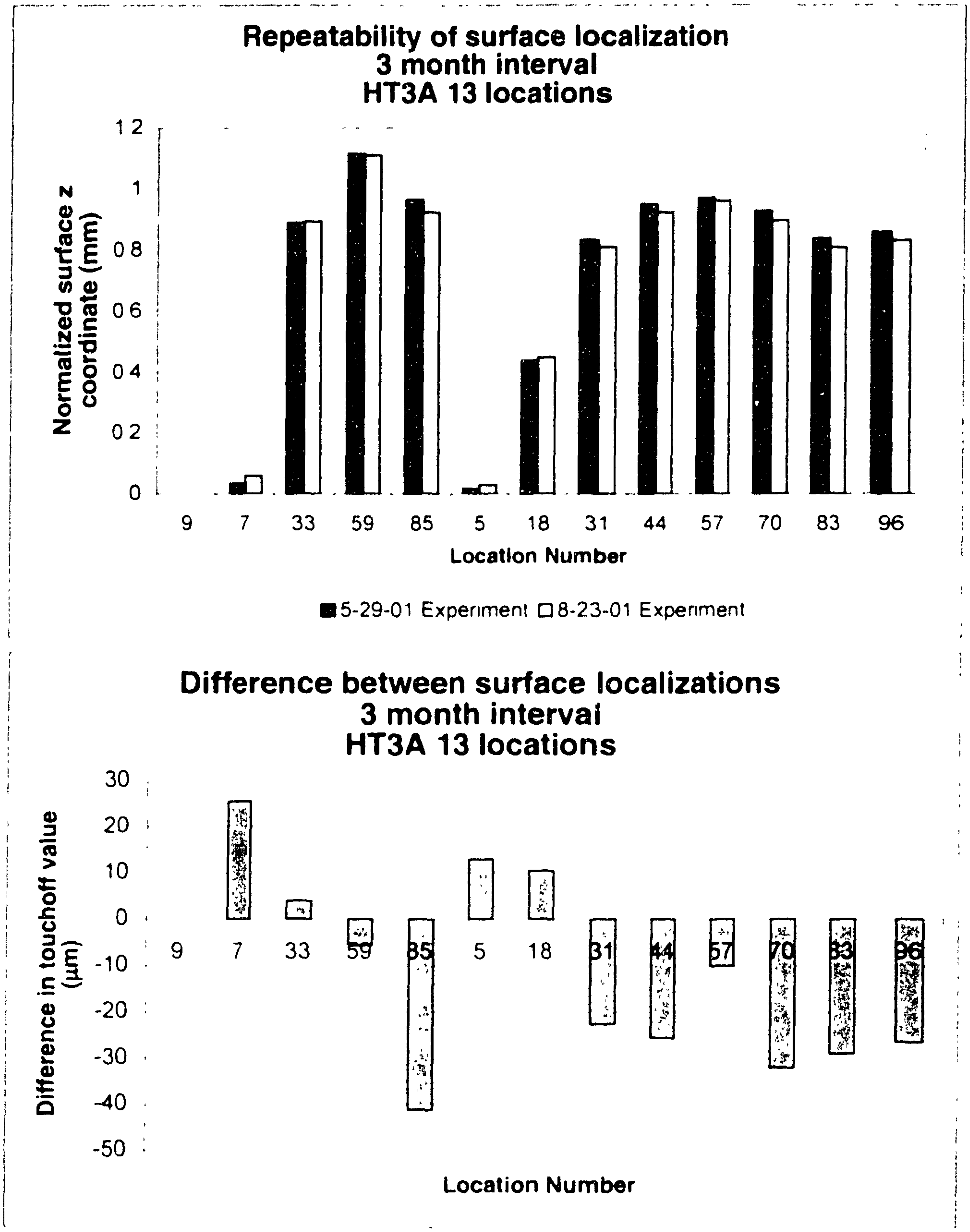

Figure 4-11 Long-term reproducibility of surface localization. The z-axis location of the surface was determined for 13 locations on sample HT3A at a 3 month interval. **(Top)** Comparison of surface z coordinate on initial and repeat measurements. All measurements are referenced to location 9. **(Bottom)** The difference between the two measurements. Average absolute deviation = 19 µm.

4.3.3 Temporal and spatial reproducibility of mechanical measurements

The sample positioning technique and pulse indentation protocol demonstrated a high degree of experimental reproducibility. Short term (inter-trial interval of hours) reproducibility of load measurements was, on average, within +/- 5%. Long term reproducibility was examined by repeating tests at intervals up to 10 weeks. (Samples were stored frozen at –20°C between tests). With long-term repeat testing, the average absolute deviation among repeated tests at a given locus was under 10%.

4.3.3.1 Repeated tests at the same location over short time intervals

The short-term reproducibility of measured load responses serves as an implicit confirmation of the accuracy of indenter-sample positioning. Longer-term reproducibility confirms that biomechanical properties are stable during the time course of the experiments, and with extended exposure to room temperature, and refrigeration and freeze-thaw cycles.

Figure 4-12 shows the results of examining short-time reproducibility of 10 different load response measurements run at two different loci on human sample HT3A. The multiple-function protocol set of 10 displacement protocols was run twice at each of the two test loci. The inter-trial interval was 6 hours for locus 13 (top) and 4 hours, 45 min. for locus 23 (bottom). All measurements varied by $\leq +4.7\%$, -2.2% between trials (with the exception of locus 23, 200 μm pulse, which varied +9.3%).

More extensive examination of short-term reproducibility for the fixed-amplitude 300 μm half-sine pulse test is demonstrated in Figure 4-13 for 26 locations (13 on each of two slices) tested on sample HT6A, with an inter-trial interval of approximately two hours. A very close inter-trial correspondence is seen at each locus, with an average absolute deviation between trials of 5.0% (+/- 5.3% standard deviation).

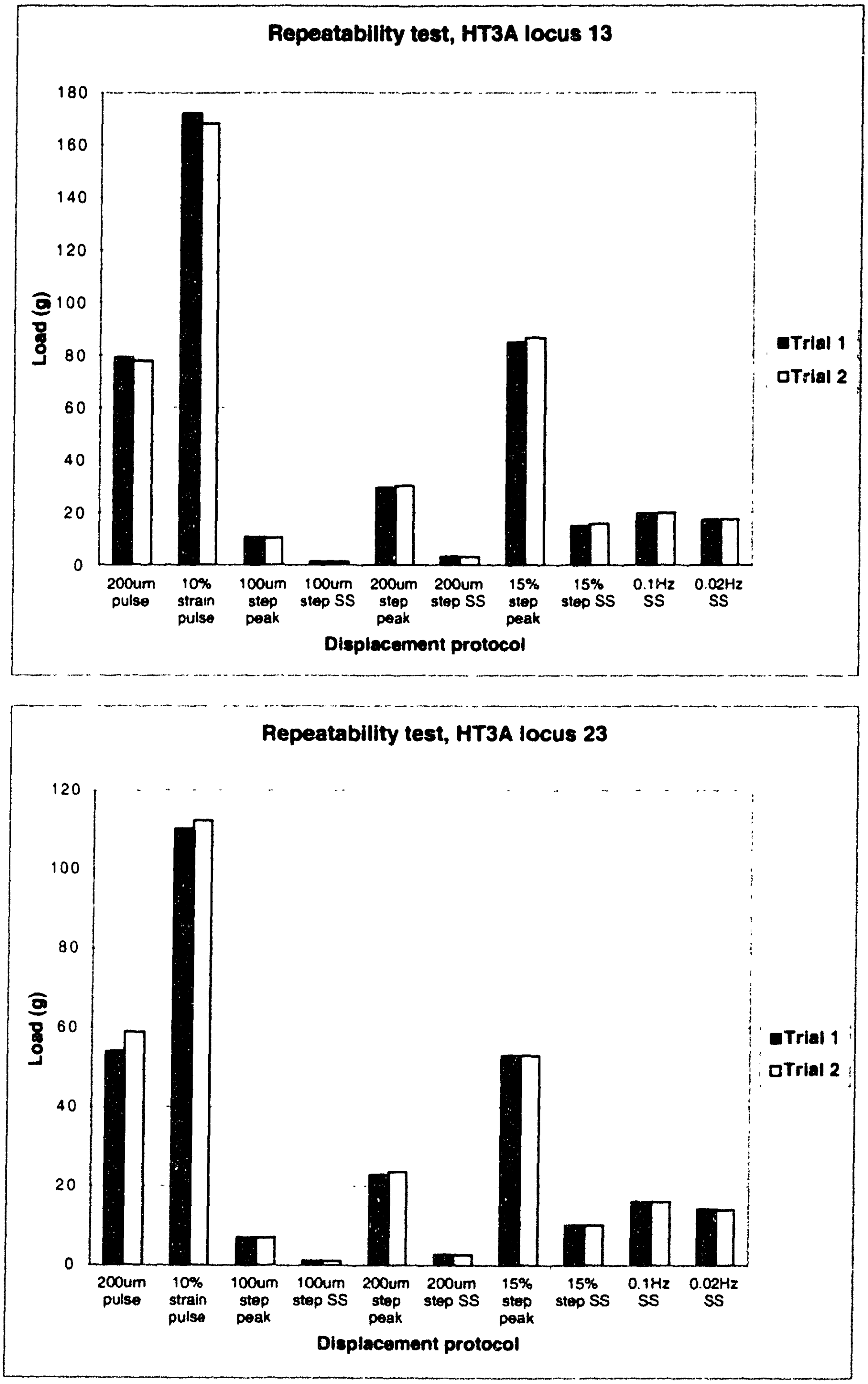

Figure 4-12 Examination of short-term reproducibility of load response measurements. Trial 2 was performed 6 hours after trial 1 for locus 13 (top) and 4 h 45 min after trial 1 for locus 23 (bottom). All repeat measurements were within 5%, except for locus 23, 200 μm pulse, which varied +9.3%.

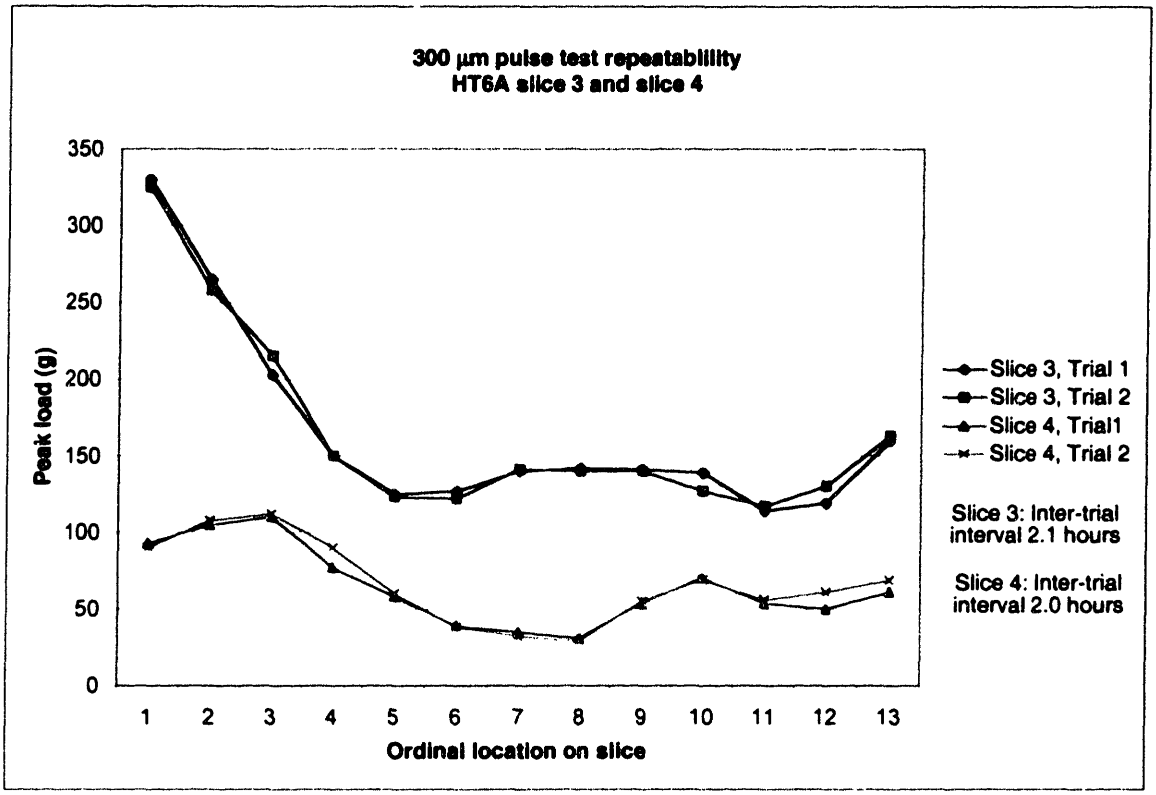

Figure 4-13 Test of short-term (2 hour) reproducibility of 300 µm half-sine pulse test load response. Over the 26 locations tested, the average absolute deviation was 5.0% (+/- 5.3% sd) between trials.

4.3.3.2 Repeated tests at the same location over longer time intervals and by different operators

Long-term reproducibility was examined for the 300 µm half-sine pulse protocol by repeat measurements at multiple locations over time intervals up to 10 weeks.

Three sets of load response measurements were made over a period of two months on sample HT3A, with an interval of approximately 3 weeks between trials one and two, and an interval of approximately 9 weeks between trials two and three. In addition, to test the repeatability of the mechanical measurement system and experimental protocol when the mechanical test methodology was employed by different operators, the third trial was run by a separate team of investigators, without the presence of the author.

The results are presented in Figure 4-14. Good repeatability was demonstrated even at 12 weeks between trials and with different operators employing the protocol. Across the 11 loci tested, the results of the three trials were on average within +/- 7.6%.

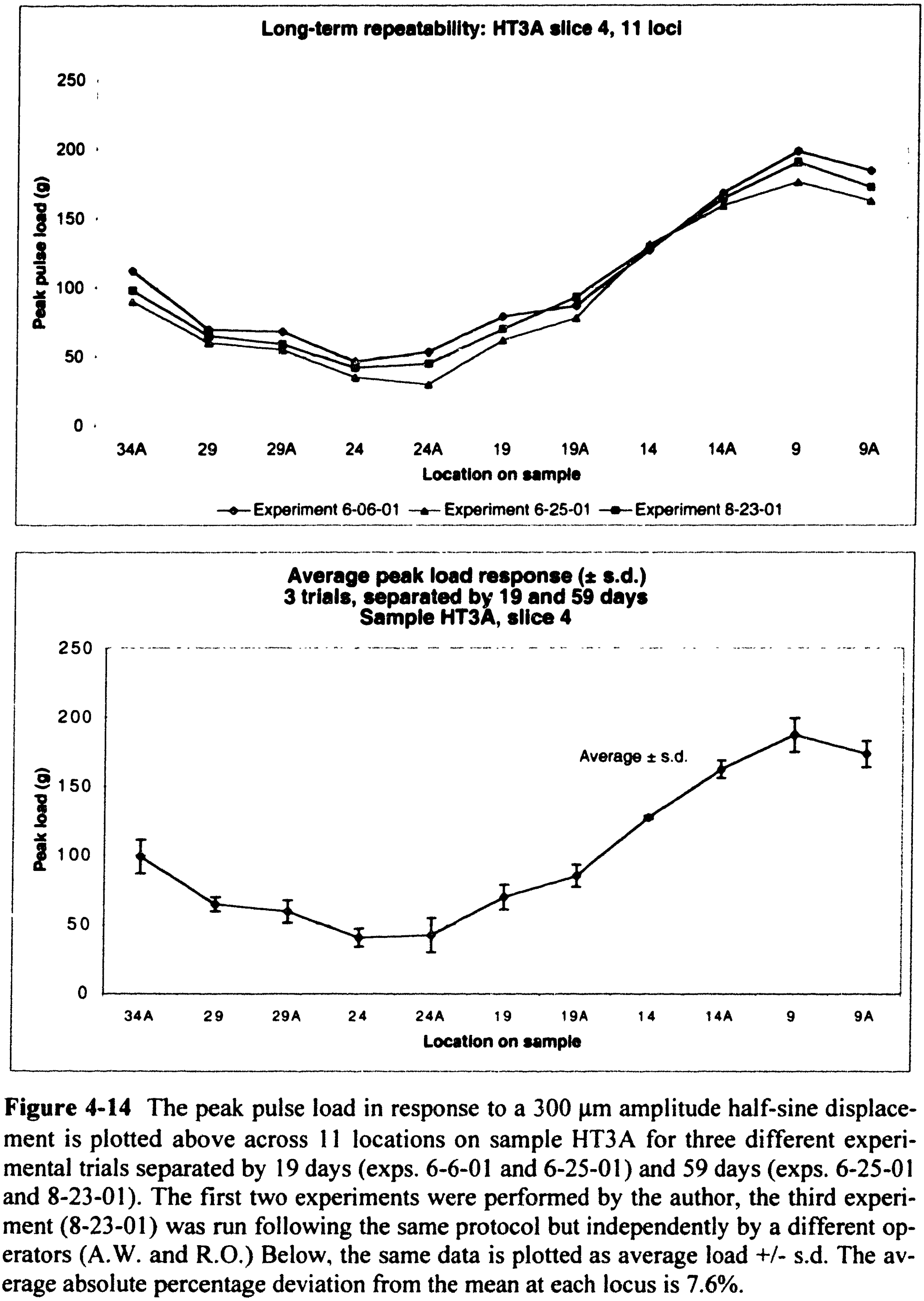

Figure 4-14 The peak pulse load in response to a 300 μm amplitude half-sine displacement is plotted above across 11 locations on sample HT3A for three different experimental trials separated by 19 days (exps. 6-6-01 and 6-25-01) and 59 days (exps. 6-25-01 and 8-23-01). The first two experiments were performed by the author, the third experiment (8-23-01) was run following the same protocol but independently by a different operators (A.W. and R.O.) Below, the same data is plotted as average load +/- s.d. The average absolute percentage deviation from the mean at each locus is 7.6%.

4.3.4 Summary of accuracy and reproducibility results

The key findings of the tests of accuracy and reproducibility of the mechanical positioning system and indentation test methodology are summarized here:

- With intertrial intervals of between 1 and 6 hours, the surface of the cartilage could be repeatedly localized to within 16 μm on average (average across four experimental series, 46 loci total). This accuracy between initial and repeat trials is < 1% of the median cartilage thickness and equal to 5% of the indentation amplitude employed.
- With a three-month interval between trials, the surface location could be reproducibly found with an average absolute deviation of 19 μm (13 loci tested).
- The maximum deviation between initial and repeat measurements of surface positions across all experiments performed (59 loci tested) was 41 μm.
- Load response measurements showed +/- 5% average reproducibility with intertrial intervals of 2 to 6 hours. This degree of reproducibility was maintained for 10 different displacement protocols examined (pulses, steps and steady-state sinusoids).
- Over a period of three months and with different operators performing the tests, load response measurements showed average reproducibility of +/- 8%.
- Overall, the studies presented in Section 4.3.2 and 4.3.3 demonstrate that the surface localization procedure is capable of both short-term and long-term average reproducibility of under 20 μm, that the load response (with multiple displacement protocols) shows +/- 5% average reproducibility with short inter-trial intervals and +/- 8% average reproducibility with inter-trial intervals of up to three months and with different operators performing the tests. The studies further demonstrate that the mechanical behavior of the cartilage and the articular surface shape does not change appreciably over the course of months of testing and with intervening freezing, freeze-thaw cycles, immersion, and cumulative exposure to room temperature of up to 24 hours.

Chapter 5

MR Imaging and Image Analysis

5.1 MRI experiments

5.1.1 $Gd(DTPA)^{2-}$ equilibration

Prior to imaging, samples were equilibrated for a minimum of 12 hours in well-stirred $Gd(DTPA)^{2-}$ (Magnevist; Berlex Laboratories, Wayne, NJ) in Hank's Balanced Salt Solution[10] (HBSS, 1X; Invitrogen Life Technologies, Carlsbad, CA) at 4°C, to which was also added 1% v/v of an antibiotic/antimycotic solution containing penicillin G (10,000 units/ml), streptomycin sulfate (10 mg/ml) and amphotericin B (25 μg/ml) (Product #A7292, Sigma Aldrich, St. Louis, MO) to retard bacterial and fungal growth[11]

Bovine samples, imaged at 2 T were equilibrated in 1 mM $Gd(DTPA)^{2-}$. Human samples, imaged at 8.4 T, were equilibrated in 2 mM $Gd(DTPA)^{2-}$. (Cartilage T1 increases with increasing field strength. The time to perform an inversion recovery imaging experiment increases with T1, since total recovery time increases. To keep experiment time manageable, 2 mM $Gd(DTPA)^{2-}$ equilibrate was employed for experiments at 8.45 T.) The volume of equilibrate was chosen to be approximately 100 times the tissue

---

[10] Components: KCl 5.33 mM, KH_2PO_4 0.44 mM, $NaHCO_3$ 4.0 mM, NaCl 138.0 mM, Na_2HPO_4 0.3 mM, glucose 5.6 mM.

[11] 1 liter of 1 mM $Gd(DTPA)^{2-}$ solution with 1% P/S/A is formulated by combining 2 ml Magnevist and 10 ml reconstituted P/S/A solution then adding sufficient Hank's solution to bring the total volume to 1 liter. For a 2 mM $Gd(DTPA)^{2-}$ solution, 4 ml Magnevist would be employed.

volume, which was estimated by weighing the sample and assuming a tissue density of approximately 1g/ml.

5.1.2 Sample preparation and positioning for imaging

Prior to imaging, samples were removed from the equilibration solution and the cartilage surface was lightly blotted to remove excess solution with gauze or tissue. The sample was then wrapped in polyethylene film or two layers of latex to preserve hydration during the imaging experiment. (For the human samples, careful wrapping in triple-tested pathogen-impermeable latex sheaths (Trojan® non-lubricated condom, Carter-Wallace, Inc., New York) was also done to prevent potential exposure of personnel to pathogens and to prevent contamination of the MR apparatus.)

The technique used for sample positioning and alignment depended on the RF coil employed:

(1) For bovine samples imaged in the 7 cm Bruker volume coil (used in the Biospec 2 T imager) the version 2 registration frame, by design, centered the sample in the coil and aligned the marker holes with the longitudinal axis of the imager bore (see Figure 3-2c).

(2) For bovine samples imaged in the 15 cm custom coil, the registration frame was first mounted in the frame positioner (Figure 3-2e) and the positioner was then inserted into the coil: this centered and aligned the sample (Figure 3-2f).

(3) For human samples imaged in the 1 inch coil (used in the 8.45 T Bruker DRX imager) the nylon positioning disks attached to the version 4 registration plate (Figure 3-4e,f) centered the sample within the coil and provided a friction-fit to the inside of the RF coil, thus aligning the plate with the longitudinal axis. Linear end-to-end centering within the coil was achieved by use of a set of acrylic spacers of varying heights. (Once a spacer was determined to center a particular sample, it could be employed for future imaging of that sample, guaranteeing quick and reproducible centering in the field of view.)

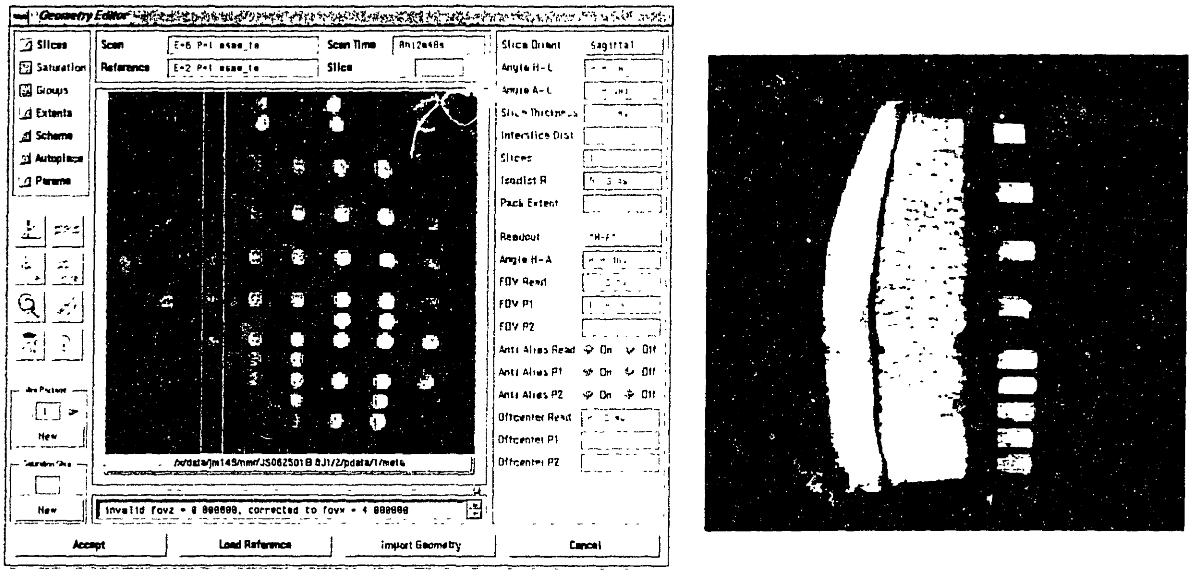

Scan: E-6 P-1 esae_te
Scan Time: 0h12m48s
Reference: E-2 P-1 esae_te
Slice
Slice Orient: Sagittal
Angle H-L
Angle A-L
Slice Thickness
Interslice Dist
Slices
Isodist R
Pack Extent
Readout: "H-F"
Angle H-A
FOV Read
FOV P1
FOV P2
Anti Alias Read: ○ On ✓ Off
Anti Alias P1: ○ On ○ Off
Anti Alias P2: ○ On ○ Off
Offcenter Read
Offcenter P1
Offcenter P2

/x/data/jm145/nmr/JS062501B.0J1/2/pdata/1/meta

```
invalid fovz = 0 000000, corrected to fovx = 4 000000
```

Figure 5-1 (left) Slice positioning for imaging of human samples mounted on the version 4 registration plate. A coronal proton-density image through the plane of the registration plate displays the Gd(DTPA)^{2} agar filled marker holes. A five-slice sagittal IR study is then specified as shown by aligning the slices perpendicular to and centered on rows of marker holes. (Note that the slices are specified so that the study slice numbers (1 through 5, left to right; slice number 1 is highlighted with a bolder outline in the figure) match the marker-hole matrix slice numbers, binary-encoded in the marker hole pattern, as defined in Figure 3-4a. This assures unambiguous matching of MRI images to physical sections in the sample.) **(right)** Resulting sagittal section (here, slice number 3). The cartilage surface is toward the left, and the MR-lucent marker holes are clearly defined toward the right.

5.1.3 Slice positioning by use of registration plate markers

For the human sample studies using the version 4 registration plate, MRI slices were oriented perpendicular to the registration plate by specifying the slices with respect to a localizer scan which passed through the plane of the registration plate. The slice positions were centered on rows or columns of the marker hole matrix in the registration plate (Figure 5-1, left). Each slice therefore included both a set of marker holes and an overlying section of the sample (Figure 5-1, right). Typically, 5 slices were imaged per sample, with each including 11 test loci.

5.1.4 MRI scan protocols

Bovine samples

Samples were typically imaged at 2T in a 300 mm bore imager (Bruker BioSpec, Bruker NMR, Billerica, MA) with either a 7 cm diameter RF coil (Bruker) or a larger, custom-built 12 cm diameter coil (courtesy of Dr. Carl Winalski, Brigham and Women's Hospital, Boston, MA). Multislice 2D and 3D scan protocols were employed, utilizing both saturation recovery (SR) and inversion recovery (IR) sequences with from 5 to 9 delays ranging up to 2000 ms. Imaging at 2T was performed after equilibration of the sample in 1 mM Gd(DTPA)$^{2-}$.

Human samples

Samples were typically imaged at 8.45T (Bruker Avance DRX 360; Bruker NMR, Billerica, MA) at 25°C using an inversion recovery sequence with 9 delays between 20 ms and 1000 ms and TR of 1200 ms or 1500 ms. A matrix size of 256 by 256 and field of view of 2.56 cm by 2.56 cm yielded in-plane resolution of 100 µm. (Sample HT3A, thinner than the others, was imaged with a matrix of 256 by 128 and FOV 2.56 cm by 1.28 cm.) Slice thickness was 1.5 mm (equal to the indenter diameter.) Typically, 2 excitations were acquired and averaged. With these parameters, total imaging experiment time was approximately 3 hours.

5.2 T1$_{Gd}$ map computation from IR scans

T1$_{Gd}$ maps were computed from the inversion recovery image sequences by estimating the parameters ρ_1, ρ_2 and T_1 of the theoretical biexponential signal recovery function at each pixel position:

$$s(\rho_1,\rho_2,T_1,TI,TR) = \left| \rho_1(1-2\rho_2 e^{(-TI/T_1)} + e^{(-TR/T_1)}) \right|$$

where:

$s(\rho_1,\rho_2,T_1)$ is the measured MRI signal intensity

(i.e., the pixel intensity in the IR image)

T_1 is the spin-lattice relaxation time which we wish to estimate

ρ_1 and ρ_2 are parameters related to signal magnitude

TI is the inversion time used for the image (i.e., delay time)

TR is the repeat time used for the image (a constant for all images in a given study)

For an inversion recovery study with *n* inversion delays (*TI*'s), we obtain *n* images per slice, one for each specified *TI*. For each pixel position *P* in a given slice, we therefore obtain *n* measured values of *s*, one for each *TI*. The values of *s* and *TI* are theoretically related by the biexponential recovery function above. We therefore define the error function for pixel position *P* as:

$$error = \sum_{i=1}^{n}\left(s_i - \left|\rho_1(1-2\rho_2 e^{(-TI_i/T_1)} + e^{(-TR/T_1)})\right|\right)^2$$

We then seek the values of ρ_1, ρ_2 and T_1 that minimize the above error. This was performed independently for each pixel using an unconstrained nonlinear optimization routine utilizing a simplex search method coded in MATLAB. The result was, for each MRI slice, a quantitative per-pixel value for T1 in the Gd(DTPA)$^{2-}$ equilibrated cartilage.

5.3 [GAG] computation from $T1_{Gd}$

In selected cases, GAG concentration ([GAG]) maps were computed from the $T1_{Gd}$ maps. To perform this computation, two additional parameters are needed for each pixel: $T1_{tissue}$ (T1 in the absence of Gd(DTPA)$^{2-}$) and Gd(DTPA)$^{2-}$ relaxivity R. While it is possible to measure $T1_{tissue}$ directly by performing an IR or SR scan in the absence of Gd(DTPA)$^{2-}$, this was not done in the current study for three reasons: (1) it would have required additional exposure of the samples to the above-room-temperature environment of the MR scanner (and, in the absence of Gd(DTPA)$^{2-}$, the long T1 would necessitate a much longer scan time), (2) the computation of [GAG] is much less sensitive to variation in $T1_{tissue}$ than to variation in $T1_{Gd}$ (discussed further below) and (3) it would have been necessary to register the $T1_{tissue}$ images with the subsequent dGEMRIC $T1_{Gd}$ images; any errors in registration would have introduced errors in the computation of [GAG].

In computing [GAG] for the human samples, which were imaged at 8.45T, the cartilage $T1_{tissue}$ was assumed to be uniformly equal to 1.7 s, and Gd(DTPA)$^{2-}$ relaxivity was taken as 4.5 (mM•sec)$^{-1}$. Both parameters were assumed invariant with respect to variation in cartilage GAG, collagen and water content. This is a reasonable assumption for $T1_{tissue}$, since for typical parameter values the computation of [GAG] is on the order of 50 times more sensitive to variations in $T1_{Gd}$ compared to $T1_{tissue}$. At 8.45T, R may range from 4.2 $(mM\bullet sec)^{-1}$ for severely GAG–depleted cartilage to 4.7 $(mM\bullet sec)^{-1}$ for intact cartilage. The assumption of constant R causes on the order of 10% error in calculating [GAG].

The details of the calculation of tissue glycosaminoglycan concentration are presented in the following.

First, tissue $Gd(DTPA)^{2-}$ concentration is calculated from the relationship:

$$[Gd(DTPA)^{2-}]_{tissue} = \frac{1}{R}\left(\frac{1}{T1_{Gd,tissue}} - \frac{1}{T1_{tissue}}\right)$$

where R is the relaxivity of the contrast agent in the tissue and $T1_{tissue}$ is the T1 of the tissue in the absence of $Gd(DTPA)^{2-}$. (Again, in the current work, T1 in the absence of $Gd(DTPA)^{2-}$ was not measured, rather a nominal value of 1.7 s was assumed.)

The tissue fixed charge density, FCD_{tissue}, is then computed from the concentration of $Gd(DTPA)^{2-}$ in the tissue according to the following relationship:

$$FCD_{tissue} = -2.0\,[Na^{+}]_{bath}\frac{[Gd(DTPA)^{2-}]_{tissue} - [Gd(DTPA)^{2-}]_{bath}}{\sqrt{([Gd(DTPA)^{2-}]_{tissue}[Gd(DTPA)^{2-}]_{bath})}}$$

where $[Na^{+}]_{bath}$ is the concentration of sodium in the equilibrating solution (equal to 0.142M for Hank's solution) and $[Gd(DTPA)^{2-}]_{bath}$ is the concentration of $Gd(DTPA)^{2-}$ in the equilibrating solution (1 mM or 2mM for the current experiments). The units of FCD_{tissue} are moles of charge per liter.

Tissue GAG concentration is then calculated with the assumptions of 2 moles of negative charge per mole of GAG and a molecular weight of 502.5 g/mole GAG:

$$[GAG] = \frac{FCD}{2}502.5\,g/mol$$

The units of [GAG] are grams per liter (or, equivalently, mg/ml).

The theoretical relationship between [GAG] and $T1_{Gd}$ is illustrated in Figure 5-2 for cartilage equilibrated in 2mM $Gd(DTPA)^{2-}$ and imaged at 8.45 T. (T1 in the absence of GAG assumed equal to 1.7 s, R assumed equal to 4.5 $(mM\bullet sec)^{-1}$.) The relationship is monotonic and nearly linear for the experimental parameters employed in this work and for the expected range of [GAG] in human articular cartilage.

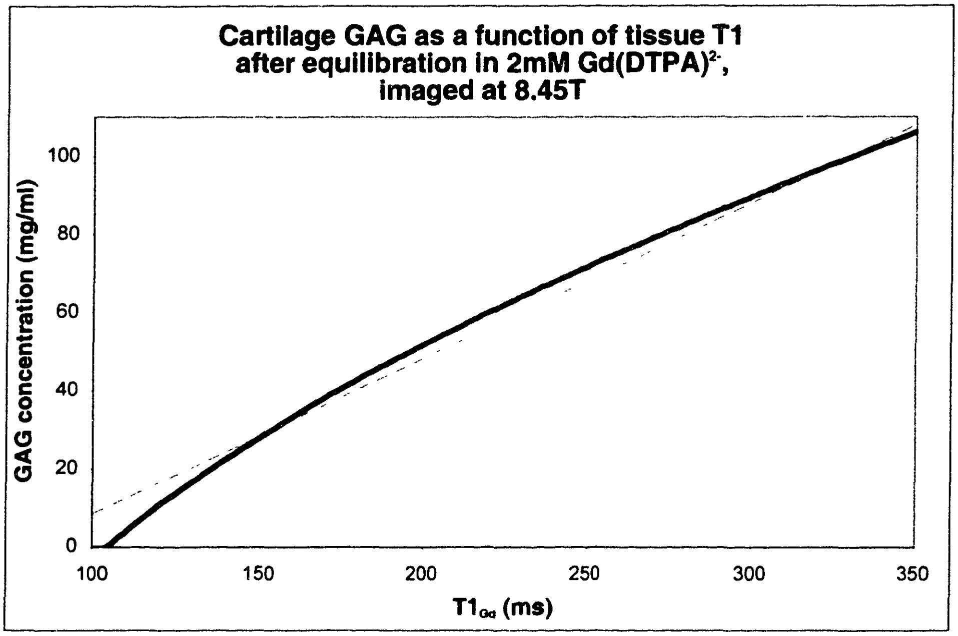

Figure 5-2 Theoretical relationship between tissue [GAG] and dGEMRIC-measured T1. For comparison, the dotted line is the best linear fit to the data.

Assumption of constant $T1_{tissue}$: sensitivity analysis

To examine the effect of the assumption of constant $T1_{tissue}$, the sensitivity of $[Gd(DTPA)^{2-}]_{tissue}$ to variation in $T1_{Gd}$ and $T1_{tissue}$ can be calculated:

Let

$$f(T1_{Gd},T1_{tissue}) = [Gd(DTPA)^{2-}]_{tissue} = \frac{1}{R}\left(\frac{1}{T1_{Gd,tissue}} - \frac{1}{T1_{tissue}}\right)$$

then the sensitivity of $[Gd(DTPA)^{2-}]_{tissue}$ to $T1_{Gd}$ is

$$\frac{\partial f}{\partial T1_{Gd}} = -\frac{1}{R(T1_{Gd})^2}$$

and the sensitivity of $[Gd(DTPA)^{2-}]_{tissue}$ to $T1_{tissue}$ is

$$\frac{\partial f}{\partial T1_{tissue}} = -\frac{1}{\mathrm{R}(T1_{tissue})^2}$$

Taking the ratio of the two sensitivities:

$$\frac{\dfrac{\partial f}{\partial T1_{Gd}}}{\dfrac{\partial f}{\partial T1_{tissue}}} = \left(\frac{T1_{tissue}}{T1_{Gd}}\right)^2$$

This ratio assumes its lowest value when $T1_{tissue}$ takes on its lowest expected value and $T1_{Gd}$ assumes its highest value. For 2mM $\mathrm{Gd(DTPA)}^{2-}$ and 8.5T, these values both occur for intact cartilage and are 1.5 s and 0.2435 s, respectively. Substituting in the above equation, we find that the minimum sensitivity ratio is 37.95. This implies that $[Gd(DTPA)^{2-}]_{tissue}$ is at least 38 times more sensitive to variation in $T1_{Gd}$ than to $T1_{tissue}$. Typically, $T1_{tissue}$ varies by +/-10% or less, whereas $T1_{Gd}$ varies by as much as +/- 50%. Hence, while the assumption of constant $T1_{tissue}$ will introduce some error into the computation of [GAG], the effect of $T1_{Gd}$ tissue *variation* on calculated [GAG] will be more than two orders of magnitude greater than the effect due to variation in $T1_{tissue}$.

5.4 Segmentation of cartilage surface

Prior to computing local $\mathrm{T1_{Gd}}$ averages, the cartilage surface in the $\mathrm{T1_{Gd}}$ maps needed to be segmented. It was especially important for this study that an accurate determination of the surface was made, since it was the $\mathrm{T1_{Gd}}$ in the pixels nearest the surface that was of most relevance to the examination of correlation with surface indentation. (The magnitude of the indentation was equal to 3 pixels.) Fortunately, since the specimens were imaged in air, a clean background-cartilage surface boundary was typically found. Intensity thresholding was therefore generally adequate to segment the cartilage surface. One-dimensional profiles of image signal intensity were examined in the brightest IR image (the final delay image) for a slice. These profiles ran from the background region into the cartilage. From the profile, an estimate of the background noise level was obtained, and then an intensity threshold was chosen so as to be slightly above the peak noise value observed.

5.5 Spatially-localized averaging of $T1_{Gd}$ or [GAG] at each test locus

At each locus on the cartilage surface where a mechanical measurement was to be made, the average $T1_{Gd}$ in a region of interest [ROI] beneath the locus was calculated (this is termed a *locally-averaged* $T1_{Gd}$ *value*).

5.5.1 Determination of position of test loci on MR images via registration markers

Marker hole center positions (in image-space coordinates) were measured in the images. The coordinates of the midpoints between marker holes were likewise measured. (The mechanical test loci were always chosen to be directly above the marker holes or the midpoints between marker holes.) Since the images were specified so as to be perpendicular to the registration plate, the center coordinates of the mechanical test loci (i.e., the coordinates where the tip of the indenter contacted the surface during mechanical testing) were directly above the marker holes or directly above the midpoints between the marker holes.

5.5.2 Region-of-interest (ROI) specification and $T1_{Gd}$ averaging within the ROI

Given the image-space coordinates of the mechanical test loci, a semiautomated algorithm was used to define ROIs in the cartilage beneath each test site. Each ROI was a rectangular region of cartilage, 1.5 mm wide (the diameter of the indenter), centered on the indentation loci, and extending from the surface of the cartilage to a specified depth. An average $T1_{Gd}$ value was then computed within the ROI for each test locus.

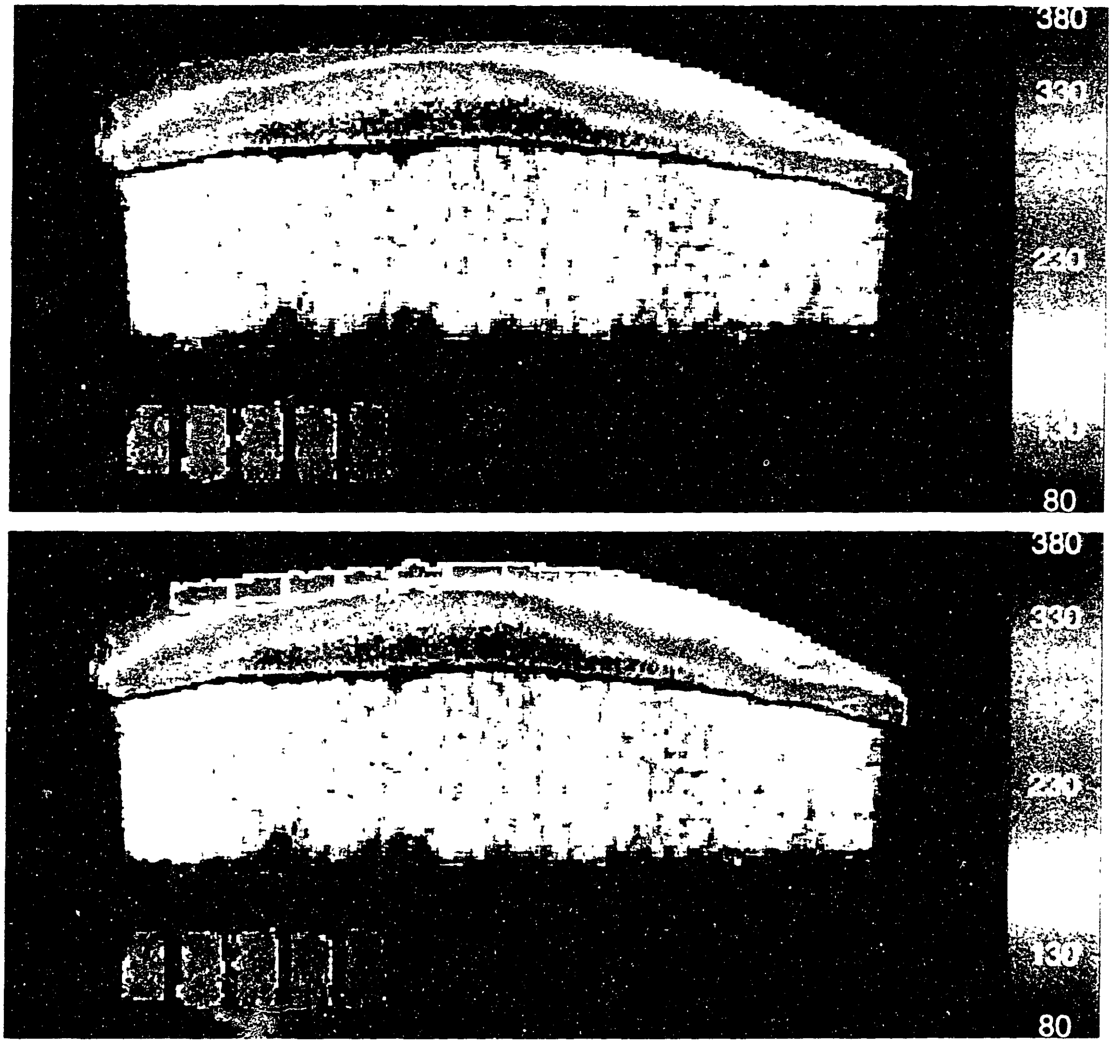

Figure 5-3 **(top)** T_{1Gd} map for sample HT 11A, slice 3. The cartilage is toward the top (bone is shown in grayscale.) Note the registration plate marker holes beneath the sample. The colorbar is calibrated in milliseconds. **(bottom)** A region of interest (ROI) has been defined in the cartilage at each site where indentation testing was performed (white outlines). The ROIs are located directly above marker holes or the midpoints between marker holes. Each ROI is 1.5 mm wide and extends from the surface to a specified depth (shown here is a depth of 600 μm). A locally-averaged T_{1Gd} value is calculated for each indentation site by averaging all pixels within the ROI at that site

5.6 Thickness measurements at test loci positions via measurements on MR images

Measurements of cartilage thickness were made at each indentation test location on the human samples. These data were acquired to support the examination of the potential effect of thickness on the measured load response, as described more fully in Section 6.1 and Section 7.5.

5.6.1 MRI scan parameters and thickness measurement technique

For initial studies on samples HT3A and HT6A, thickness was measured on the brightest image (i.e., the image with the longest delay time) of the inversion recovery sequence used to generate the T1 maps. Because these scans used a slice thickness of 1.5 mm, the effect of voxel partial-voluming was a concern. If the thickness of the cartilage changed significantly across the 1.5 mm thickness of the slice, the measured thickness would tend to be the maximum thickness of the cartilage within the slice, and average thickness beneath the indenter (the value of interest) would therefore tend to be overestimated. Visual examination of the anterior edge of the samples demonstrated significant thickness variation (Figure 5-4). Across all samples a common pattern was seen of thin-

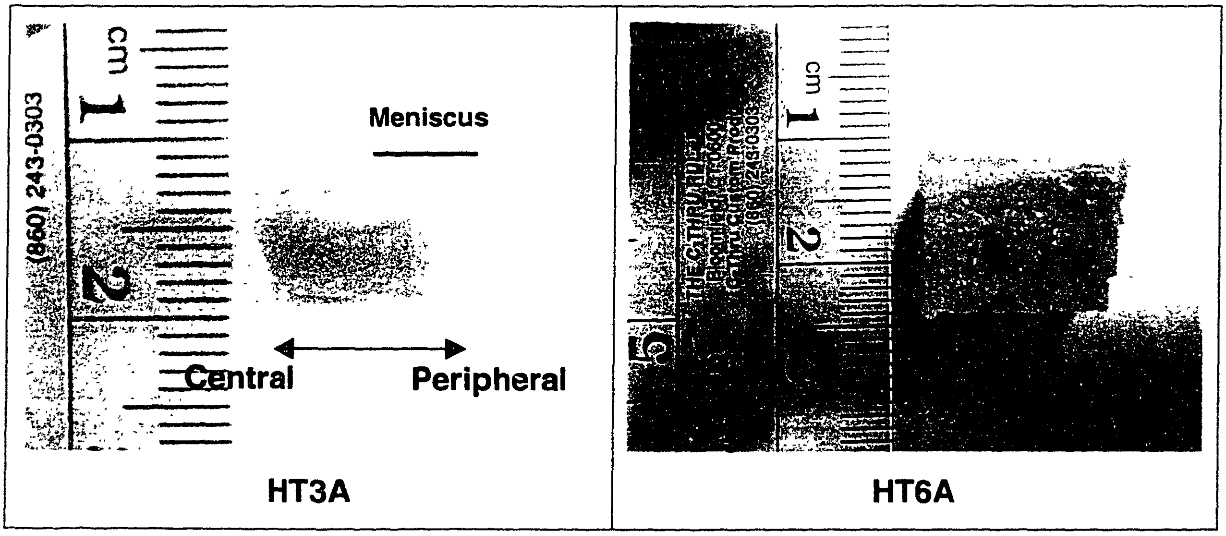

HT3A

HT6A

Figure 5-4 Thickness variation along peripheral-central axis of samples of human tibial plateau. Anterior views, with peripheral edge of sample (i.e., the edge covered by the meniscus *in vivo*) to the right. Approximate region covered by the meniscus is indicated for HT3A.

Scan ID	Sample	Slice Thickness (mm)	TE (ms)	TR (ms)
JS053001	HT3A	1.5	13.4	1500 (TI = 1000)
JS062501A	HT3A	0.25	13.4	1500
JS061501	HT6A	1.5	13.4	1200 (TI = 1000)
JS072301B	HT6A	0.25	22.6	2500
JS062501B	HT8A	0.25	13.4	1500
JS072701	HT11A	0.25	13.4	2000

Table 5-1 MRI scan parameters for studies to measure cartilage thickness.

ner cartilage toward the peripheral edge of the sample (the region covered by the meniscus *in vivo*) and a monotonic increase in thickness toward the central edge (the region not covered by the meniscus, and exposed to direct contact with the femoral condyle).

To examine the effect of MRI slice thickness on measurement of cartilage thickness, new MRI studies were performed on HT3A and HT6A with a slice thickness of 0.25 mm, and the thickness measured on the thinner scans was compared with the values obtained on the 1.5 mm thick scans. Based on the results (see the next section), thickness measurements for all subsequent studies were made only on 0.25 mm thick scans.

A multislice spin-echo protocol was employed for the 0.25 mm thick scans, with 100 μm by 100 μm pixel size. For each study, 5 sagittal slices were specified, centered on rows of registration plate marker holes as described in Section 5.1.3 and Figure 5-1. The scan parameters employed for each study are summarized in Table 5-1.

Measurements of thickness were made using the Paravision software system (version 1.1.5 or version 2.1, Bruker NMR, Billerica, MA). Using the geometry tool module, lines were drawn from the surface of the cartilage to the edge of the dark region defining the cortical bone (Figure 5-5). The lines were perpendicular to the plane of the registration plate, and aligned with the midpoints of the marker holes and the midpoints between marker holes (these positions define the locations at which indentation tests were performed).

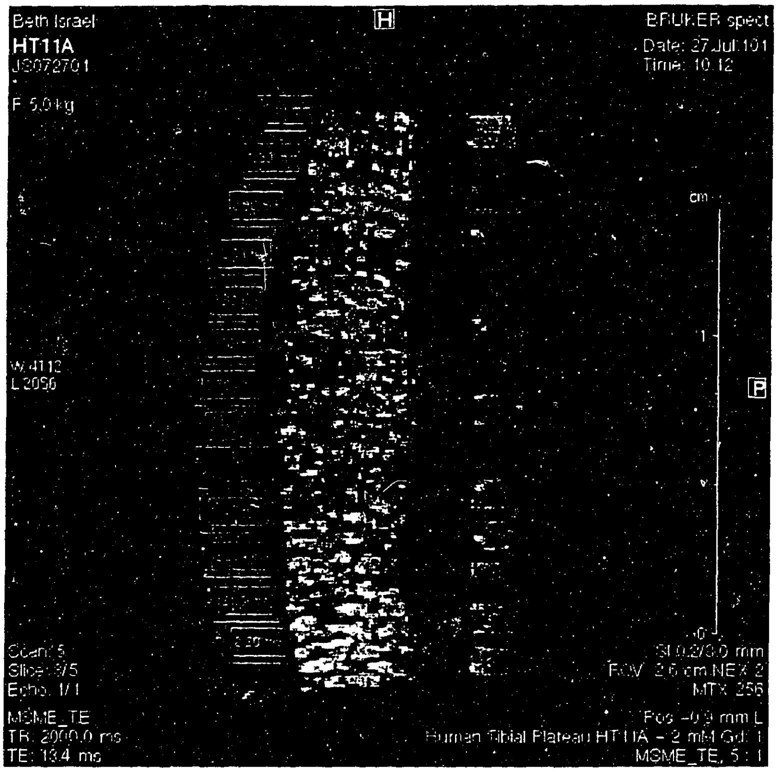

Figure 5-5 Example of cartilage thickness measurements made on human sample HT11A. Scan slice thickness is 0.25 mm, in-plane resolution is 0.1 mm

5.6.2 Comparison of results from scan protocols with 0.25 mm and 1.5 mm slice thickness

The results of comparing thickness measurements made on 0.25 mm and 1.5 mm thick scans confirmed that the 1.5 mm thick scans tended to overestimate thickness, especially for the thinnest cartilage in the peripheral region of the sample, presumably due to partial volume error. Figure 5-6 compares thickness profiles for four slices through sample HT3A. Note that the discrepancy between the measurements is largest for the more peripheral slices (slices 1 and 2). The more central slices (slices 3 and 4) are in a region with a lower peripherocentral thickness gradient; as expected, the measurements made on the 0.25 mm and 1.5 mm scans show less disparity in this region.

Overall, the average difference between thickness as measured on 0.25 mm scans relative to 1.5 mm scans was -17% for HT3A and -8% for HT6A. The differences in the thinnest slices, however, were as high as -52% and -33% for HT3A and HT6A, respectively. For subsequent work, thickness measurements in the thinnest regions are the most critical, therefore the 0.25 mm thick scan protocol, assumed less prone to partial-volume error, was used for all subsequent thickness measurements.

5.6.3 Results: Thickness measurements

Comprehensive thickness data from all studies of all samples are tabulated in Appendix A. For the three samples analyzed for the possible effect of thickness on stiffness–$\mathrm{T1_{Gd}}$ correlation (HT3A, HT6A, HT11A; see section 7.5), the median thickness was

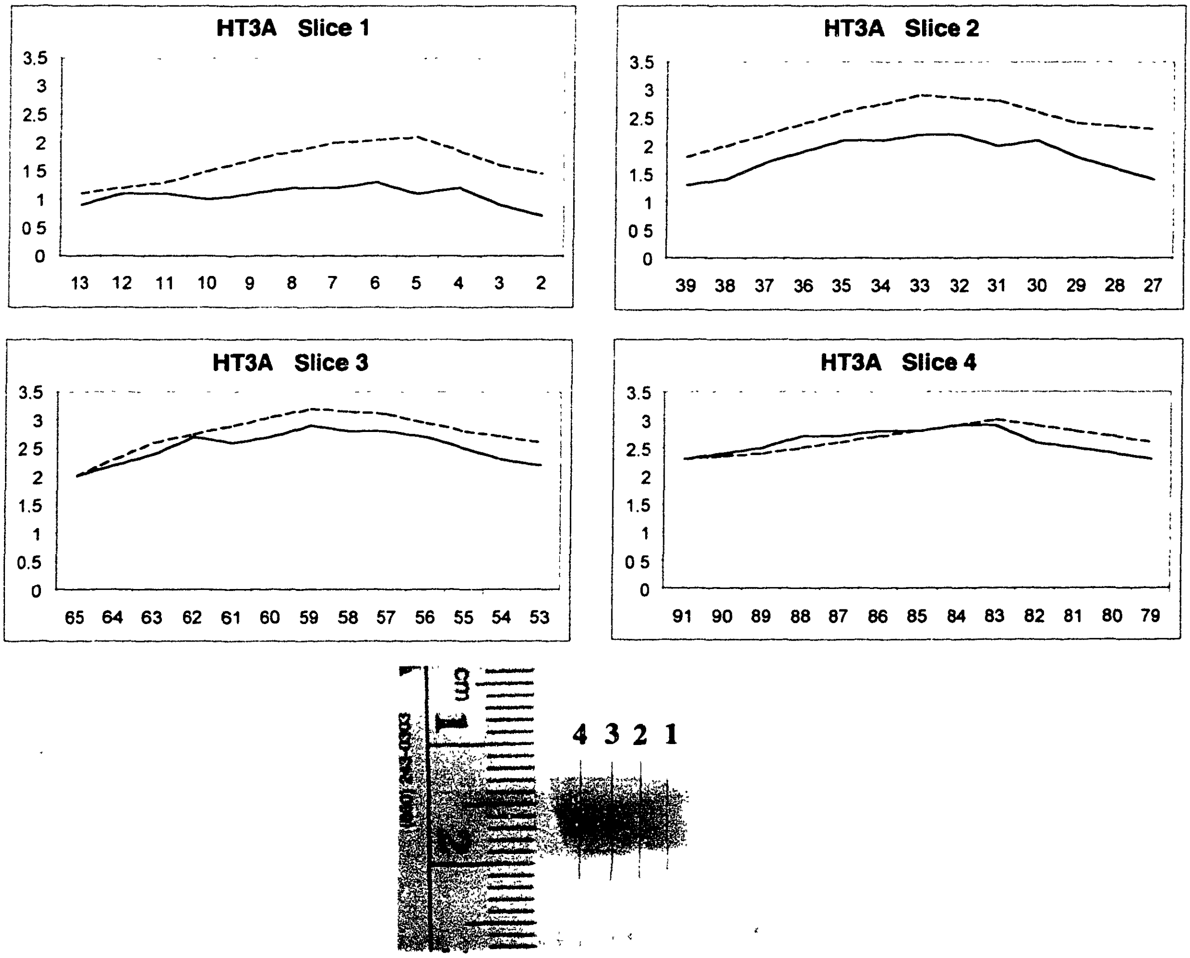

Figure 5-6 Comparison of thickness profiles measured on 1.5 mm thick MRI scans (dotted lines) and 0.25 mm thick MRI scans (solid lines). Positions of the four slices relative to the sample are shown in the lower illustration.

2.5 mm, with a range of 1.4 mm to 4.2 mm. The distribution of cartilage thickness over the 119 test loci on these samples is presented in the histogram of Figure 5-7. (All thickness measurements here and used in all subsequent analyses were made on 0.25 mm thick MRI scans.)

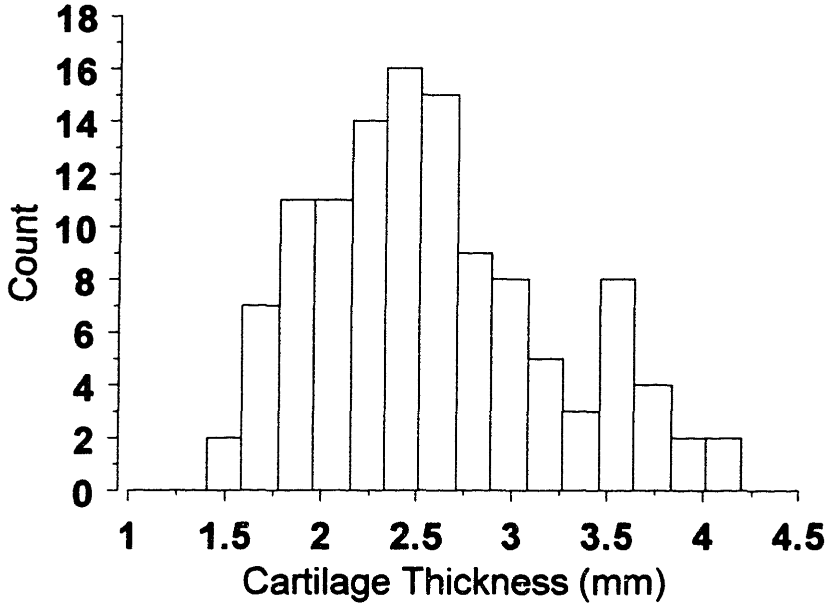

Figure 5-7 Distribution of cartilage thickness across 119 test loci. Median thickness is 2.5 mm; range is 1.4 mm to 4.2 mm. Cartilage thickness was measured at each test locus on MRI scans through the center of the loci with 0.25 mm slice thickness. Measurements were made from the surface of the cartilage to the superficial boundary of the cortical bone.

Chapter 6

Finite Element Modeling

6.1 Thickness as a potentially confounding independent variable

Variation in thickness is expected to influence the measured load response, with the effect becoming more prominent for very thin cartilage. Considering the limiting cases for a compliant layer on a rigid substrate, as thickness $t \rightarrow 0^+$, indentation into the subchondral bone would occur, manifesting as extremely high measured stiffness; as $t \rightarrow \infty$, we asymptotically approach the behavior of a compliant infinite half-space. For a given finite indenter diameter a, we expect variation in load response due to thickness to be related to the indenter-layer aspect ratio a/t. For a sufficiently small value of a/t, we expect the indentation behavior to become less variant with respect to increasing t and approach the behavior limit of an infinite half space.[12] The question of interest is whether, for a given indenter size and geometry, a cartilage thickness value t_0 can be identified such that for all $t > t_0$, the load is approximately independent of t (i.e., the layer thickness is effectively infinite). The specimens in the current study exhibited a range of cartilage thickness from 1.4 mm to 4.2 mm (Figure 5-7). To determine to what degree thickness varia-

---

[12] This phenomenon has been investigated experimentally as well as theoretically. Waters, for example, examined the indentation of thin rubber sheets by steel balls and determined that for lubricated contact, when the ratio t/a_t of rubber thickness t to area of ball contact a_t is greater than 5, estimates of the rubber stiffness (Young's modulus) from indentation measurements will be within 5% of the true value. (Waters 1965)

tion might be influence the load response variation we observed, and to examine means of excluding thickness as a confounding influence, a finite-element simulation was performed to ascertain the expected dependency of load response on thickness.

The author commissioned the finite element (FE) modeling to the expert care of Anna Galea of Harvard University's Biorobotics Laboratory (under the direction of Dr. Robert Howe). Ms. Galea has recently developed a model for the analysis of indentation of an elastic layer. The author provided the specifications and parameters for the current model, and Ms. Galea very generously created the model geometries and ran the FE computations. The validation, interpretation and analysis of the results were performed by the author, who is responsible for their application to the current work and conclusions thereby drawn.

6.2 Models (isotropic, linearly elastic, boundary conditions, contact conditions), parameters (E, v, thickness), results

To model the load response of a cartilage layer to a 300 μm, 0.25 Hz indentation by a spherical indenter, the greatly simplifying assumption was made that the cartilage behaves like a single phase, linearly elastic solid. This assumption may be justified on the basis of the short time scale of the indentation test (an assumption which was experimentally verified for the indentation protocol employed in the current work; see Section 6.4). The poroviscoelastic behavior of cartilage is due to water movement (and, secondarily, to intrinsic viscoelasticity of the matrix). When forces are applied rapidly and then removed, there is insufficient time for significant fluid flow to occur. In much of the analytical and experimental work on poroviscoelastic models, attention has been focused on time scales of load application in the range of seconds to tens of minutes. The instantaneous response, in the absence of appreciable fluid flow, is approximately elastic rather than viscoelastic: prior work has shown that, theoretically, at $t = 0^+$, the linear biphasic model behaves like an incompressible (i.e., Poisson ratio $\nu = 0.5$) single-phase elastic solid (Mak, Lai and Mow 1987), and, experimentally, that for short-time compressive loads cartilage likewise behaves approximately the same as an incompressible, single-phase elastic solid (Armstrong, Lai and Mow 1984). Eberhardt et al. (1990) examined the

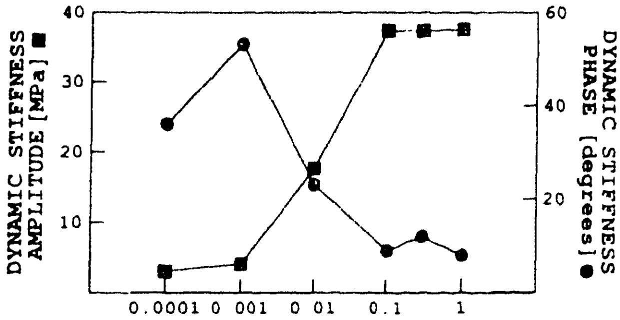

Figure 6-1 Amplitude (squares) and phase (circles) of bovine cartilage dynamic stiffness as compression frequency is varied. Below 0.1 Hz, significant water flow occurs and the dynamic stiffness falls dramatically. From (Sah, Kim, Doong et al. 1989)

justification for the use of linear elastic models at short time scales by comparing the behavior of three different cartilage models–biphasic poroviscoelastic, viscoelastic and elastic–for times from 0 to 200 ms after load application. They found that, for an unconfined compression experiment, the difference between the stress predicted by the linear elastic model and the biphasic poroviscoelastic model of Armstrong et. al (1984) was under 1% at 200 ms. They concluded that for loading times under 200 ms, cartilage can be considered an elastic material.[13] Oscillatory unconfined compression studies performed by Sah et al. also support the assumption of elastic behavior at short time scales (Sah, Kim, Doong et al. 1989). Figure 6-1 shows a graph of the measured dynamic stiffness of cartilage as a function of the frequency of cyclic loading. The stiffness remains relatively constant for loading frequencies from 1 Hz to 0.1 Hz, then falls precipitously for lower frequencies. This suggests that appreciable fluid flow does not occur with cyclic load application above 0.1 Hz for the specimen geometry employed in the study.

In our finite element analysis, we modeled the indentation of an isotropic linearly elastic layer by a rigid hemispherical indenter (diameter Ø = 1.5 mm, depth of indentation = 300 μm). The model geometry was created using FEMAP (Finite Element Modeling and Postprocessing, version 8.0a, Structural Dynamics Research Corp., Exton, PA) and the finite element computations were performed in Abaqus version 5.8 (Hibbitt, Karlsson & Sorensen, Inc., Pawtucket, RI). The elastic layer was constructed using 4-node axisymmetric elements (Abaqus type CAX4). The bottom nodes of the layer were rigidly

---

[13] Eberhardt et al. further note that "specific time dependencies will change for different material geometries and test conditions, but this should not be of major significance, nor will it change the basic conclusions."

fixed. The stiff hemisphere was displaced into the elastic layer with a frictionless contact condition and the resulting static stress and strain in the layer were computed using a finite-displacement, nonlinear solution method. The total vertical force exerted by the layer on the indenter was then computed (using FEMAP) as the layer thickness was varied between 0.75 mm and 10.0 mm.

Figure 6-2 shows an example graphical result of one of the finite element models with a layer thickness of 2 mm. The actual model employed axisymmetric elements, and hence the model mesh needed to be defined only for one half-slice through the axis of symmetry, as detailed in Figure 6-3.

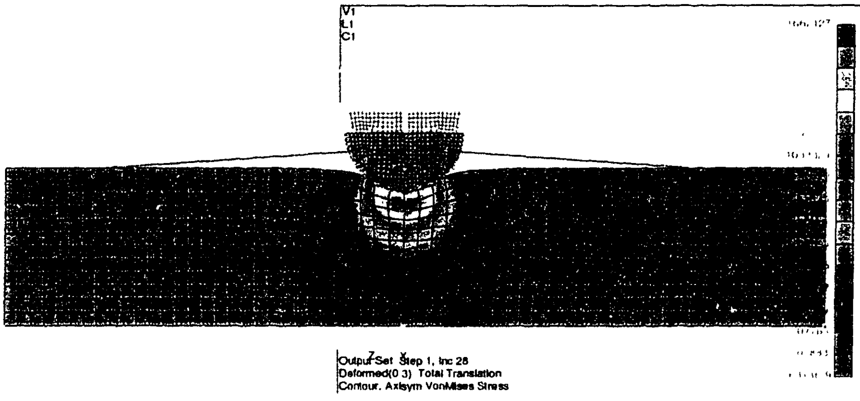

Figure 6-2 Axisymmetric graphical result of finite element analysis of 300 μm indentation of a 2 mm thick linearly elastic layer on a rigid substrate by a 1.5 mm diameter rigid hemispherical indenter with a frictionless interface. The colormap displays VonMises stress. The element edge dimension in the layer is 167 μm.

Details of the mesh undergoing deformation are presented in Figure 6-4. VonMises stress maps for layer thicknesses of 0.75 mm, 2.5 mm and 5.0 mm are presented in Figure 6-5.

A significant result of the analyses of Figure 6-2 and Figure 6-5 is the effect of thickness on peak stress (the stress indicated by the highest level of the colorbar): the models predict peak VonMises stress of 3.2, 1.7, 1.6 and 1.5 MPa for layer thicknesses of 0.75, 2.0, 2.5 and 5.0 mm, respectively. There is a dramatic increase in stress for the thinnest layer, but less than 11% difference in peak stress between the 2.0 mm and 5.0 mm layers, suggesting that the cartilage mechanical response for this experiment is relatively insensitive to thickness variation when thickness ≥ 2.0 mm. (This will be explored in further detail below.)

Details of the stress maps of Figure 6-5, presented in Figure 6-6, reveal that for the range of thicknesses examined, the majority of stress occurs in a volume of material beneath the indenter with a depth between approximately 600 μm and 750 μm. This is significant for the selection of the region in the MRI data over which averaging of $T1_{Gd}$ (or [GAG]) is performed, since, for a meaningful correlation between stiffness and tissue $T1_{Gd}$ to be made, we want the region to match the volume of cartilage undergoing stress from the indenter. The results of the FE modeling suggest that, for the region to contain the highest 50% of the stress due to the indentation, an appropriate depth for the region would be roughly 600 μm to 750 μm.

A final series of result images is presented in Figure 6-7, which shows stress distributions for three models with the same thickness (2.5 mm) but varying elastic modulus E (2 MPa, 4.425 MPa and 8.85 MPa). The results demonstrate that, as expected for a linearly elastic material, the magnitude of the stress is proportional to the elastic modulus (for example, the peak VonMises stresses of 0.72 MPa, 1.60 MPa and 3.20 MPa are directly proportional to the respective moduli of 2 MPa, 4.425 MPa and 8.85 MPa), but the pattern of stress distribution is invariant with changing modulus (assuming the material is homogeneous).

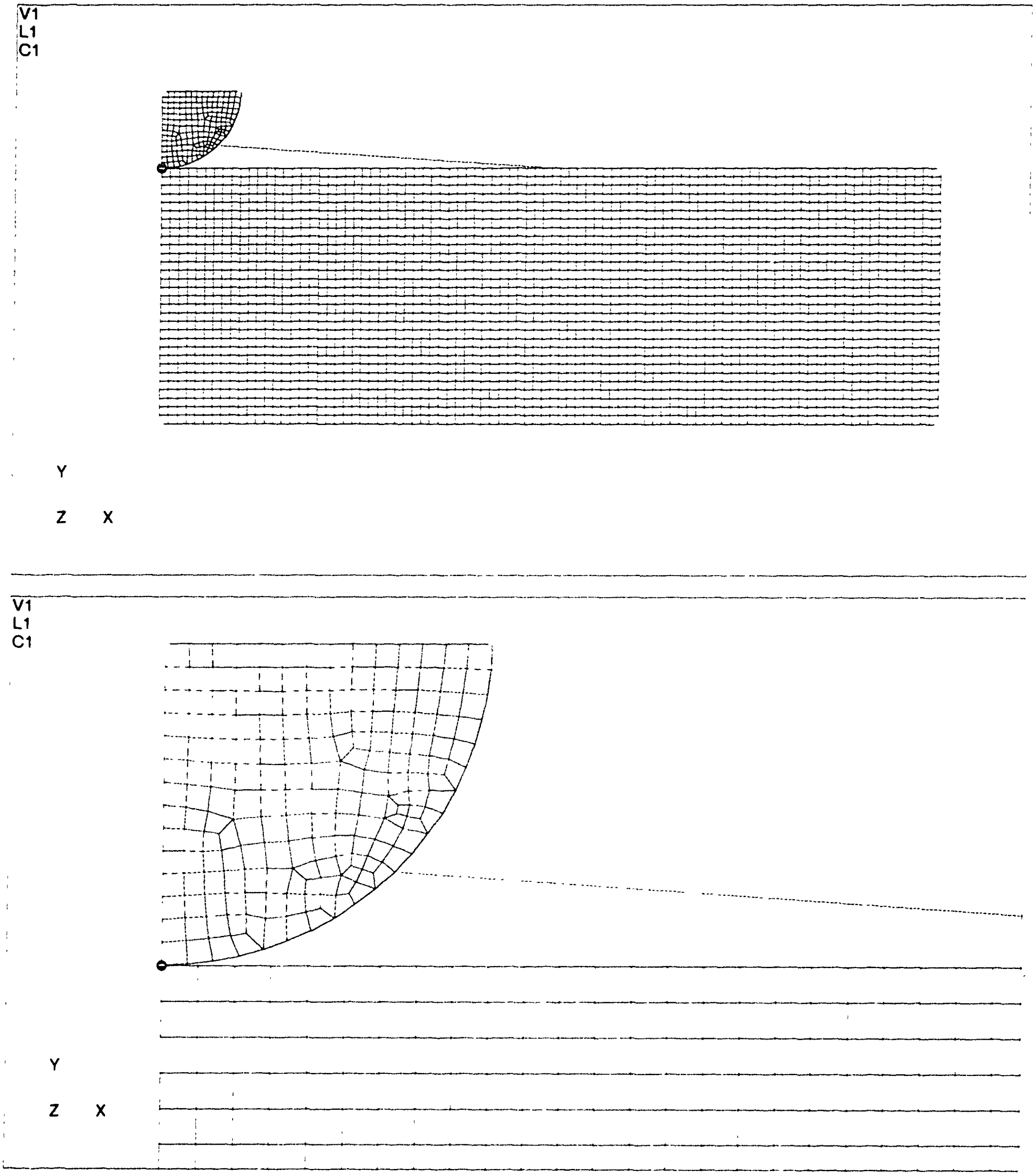

Figure 6-3 **(top)** Mesh designed for finite element model. (Note that the oblique line running from indenter to surface is an artifact of the axisymmetric mesh generation software.) **(bottom)** Detail view of indenter and layer surface, showing mesh structure on surface and within the rigid hemispherical indenter. Surface nodes on the indenter are spaced evenly along a quarter-circle arc.

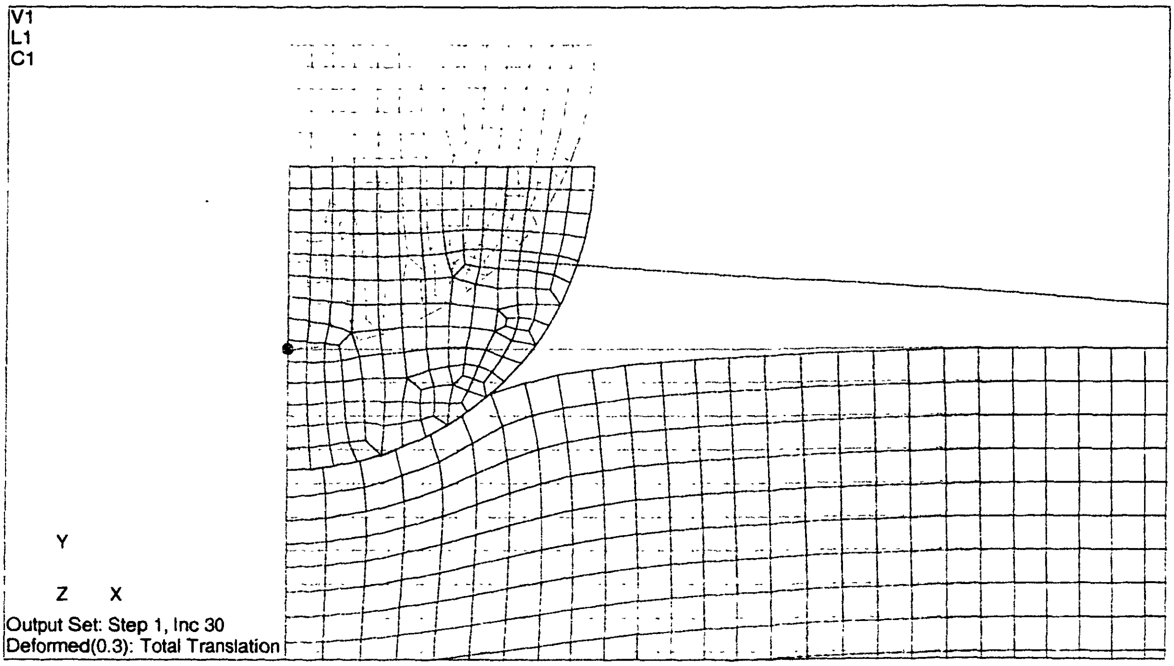

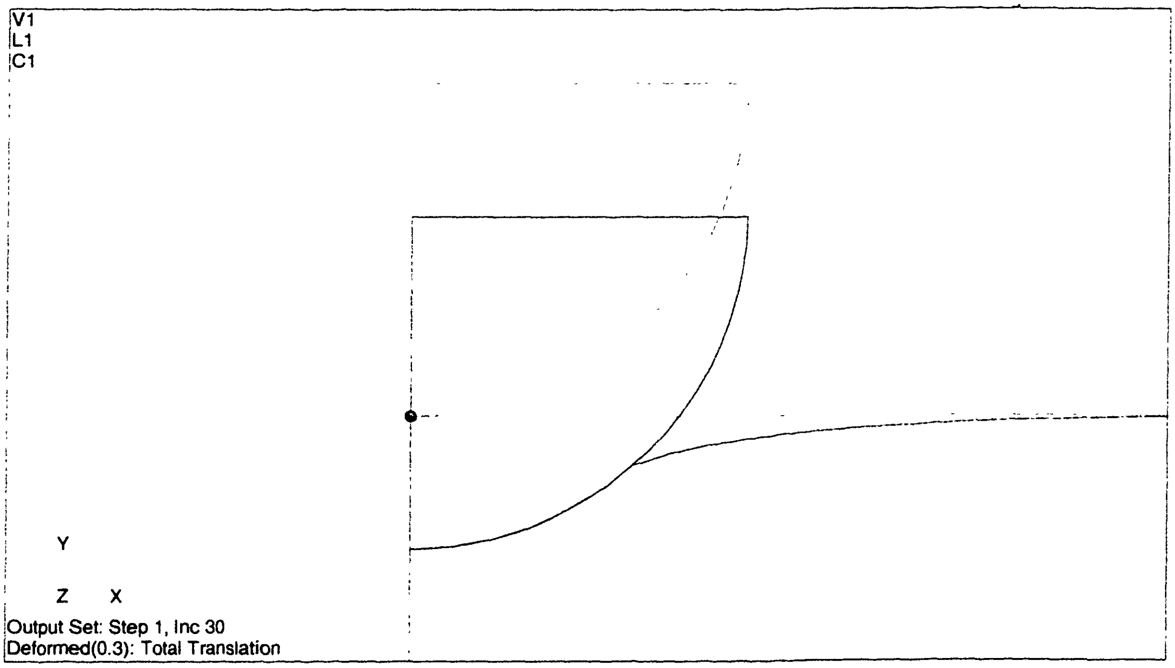

Figure 6-4 **(top)** Detail of mesh deformation with 300 μm displacement of the indenter. **(bottom)** Detail of surface deformation and contact area between indenter and layer surface after indentation.

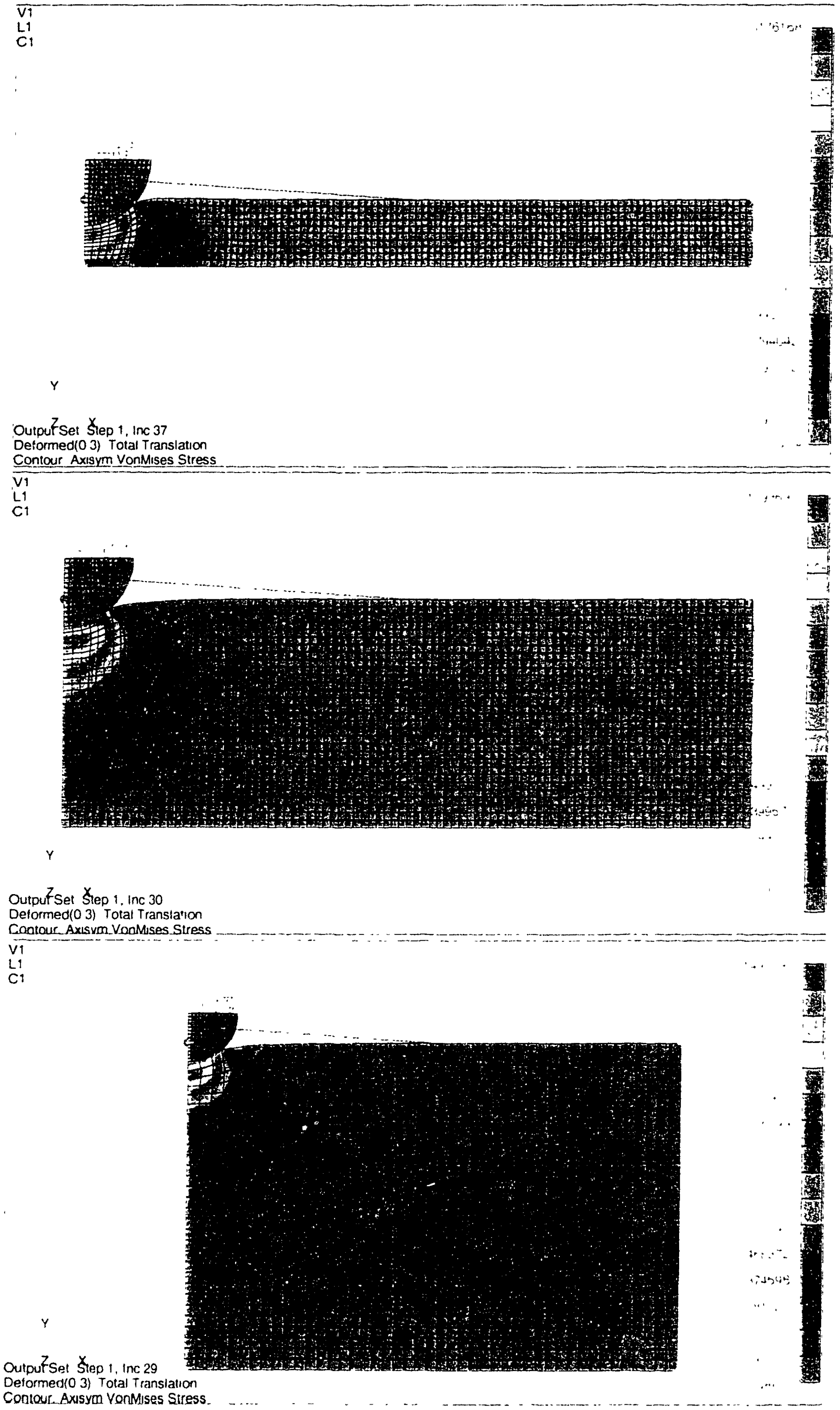

Figure 6-5 VonMises stress maps for finite element models with elastic modulus E = 4.425 MPa, a nominal value for normal cartilage. Layer thickness is 0.75 mm (top), 2.5 mm (middle) and 5.0 mm (bottom). Layer element size is 75 μm (top), 83 μm (middle) and 167 μm (bottom).

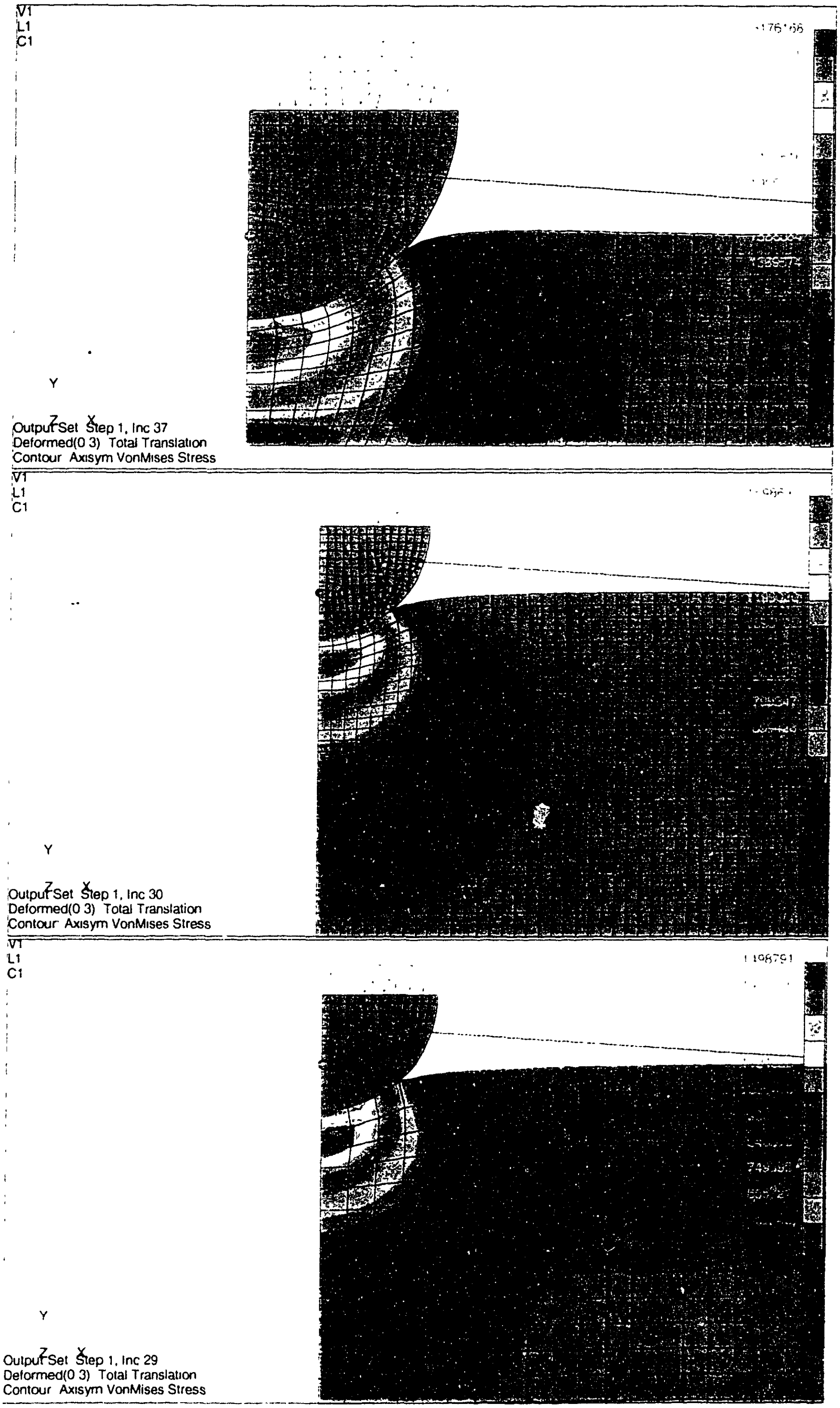

Figure 6-6 Details of VonMises stress maps shown in Figure 6-5. The upper 50th percentile of VonMises stress (green to red on the Colormap) occurs in a volume beneath the indenter with approximate depth of 8 elements = 600 μm (top, 0.75 mm layer thickness), 9 elements = 750 μm (middle, 2.5 mm layer thickness) and 4 elements = 670 μm (bottom, 5.0 mm layer thickness).

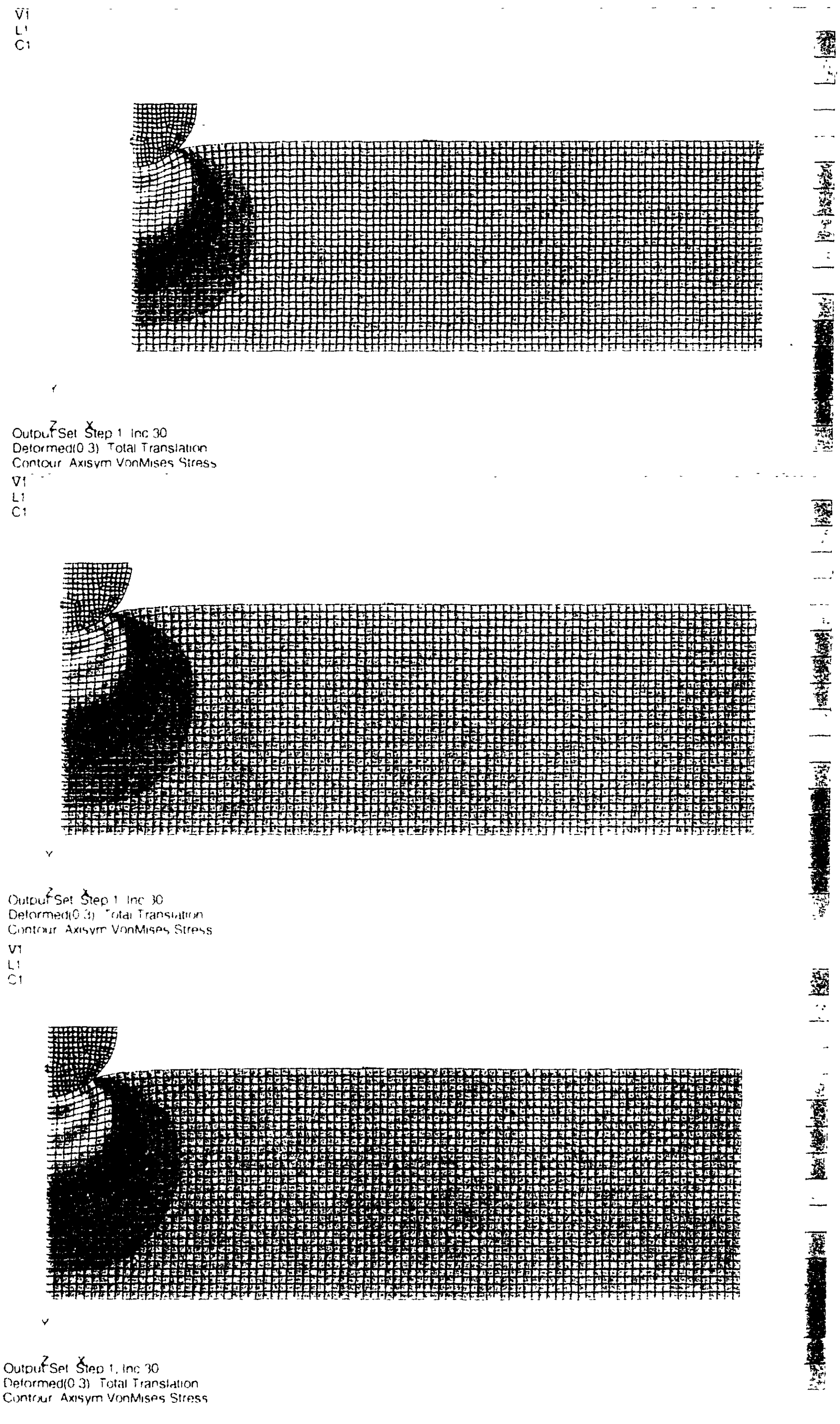

Figure 6-7 Constant thickness layer and varying elastic modulus E: VonMises stress maps for indentation of 2.5 mm thick layer with F = 2 MPa (top), 4.425 MPa (middle) and 8.85 MPa (bottom). The stress magnitude scales exactly proportionally to E, but the pattern of stress distribution is independent of E.

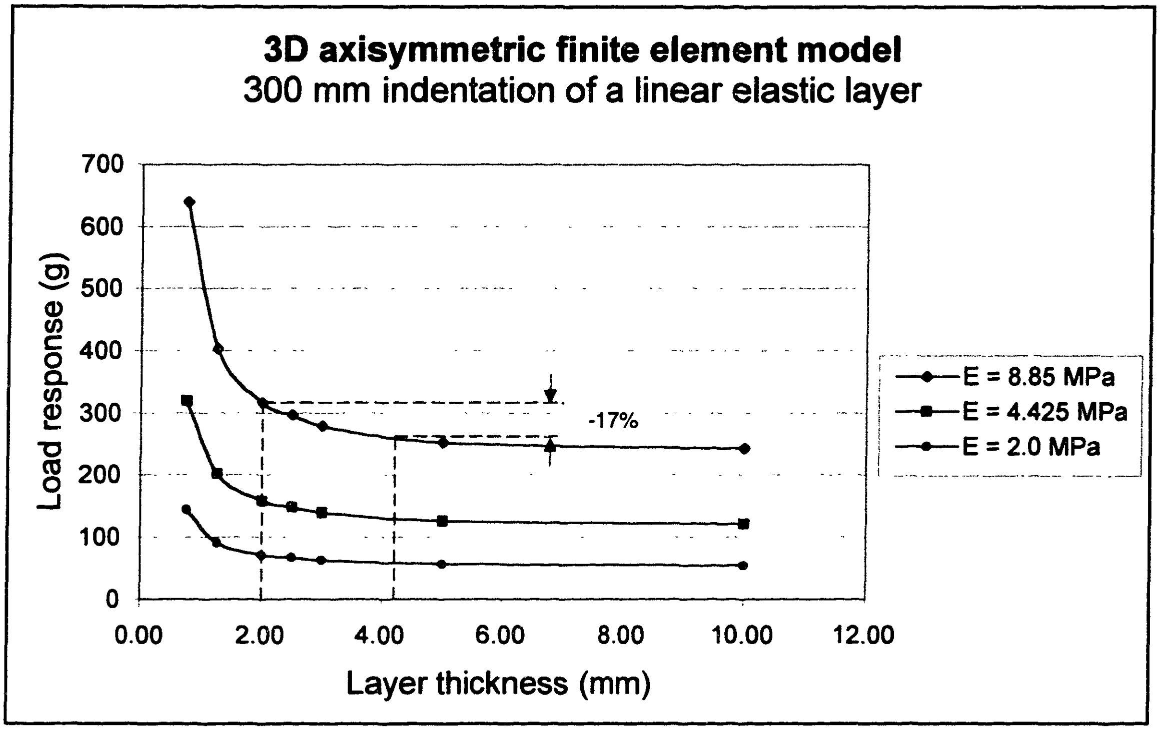

Figure 6-8 Predicted variation in load response with variation in layer thickness for a linearly elastic layer indented to a depth of 300 μm by a 1.5 mm diameter rigid hemisphere. Poisson's ratio ν = 0.499. The load changes by 17% between 2.0 mm and 4.2 mm independent of the value of Young's modulus E.

Figure 6-8 shows curves of load vs. thickness computed from the model results. Curves are shown for three specified nominal values of elastic modulus. The value E = 4.425 MPa was chosen as a nominal value for normal cartilage from previously reported work (Eberhardt, Keer, Lewis et al. 1990). Poisson's ratio ν was set equal to 0.499 to model the instantaneous, incompressible material behavior of cartilage predicted by linear biphasic theory (Armstrong, Lai and Mow 1984).

The salient features of the analysis are (1) the rapid increase in load as layer thickness decreases, especially in the region below approximately 2.0 mm, and (2) for a given elastic modulus, the ratio of loads at any two selected values of thickness is independent of the elastic modulus magnitude.

We used these results in our analysis of the correlation between load response and locally-averaged $T1_{Gd}$ to control for the potential confounding effect of thickness variation. Between 2.0 mm and 4.2 mm the predicted load response changes by less than 20%

due to thickness effects alone. We therefore reanalyzed the correlations between load and locally-averaged $T1_{Gd}$, including only those loci on each sample with a cartilage thickness greater than or equal to 2.0 mm. The results of this analysis will be presented and discussed in Section 7.5, but, in brief, we found that load remained correlated to $T1_{Gd}$ when examining only those test loci with thickness $\geq$ 2.0 mm, and therefore thickness variation alone does not contribute significantly the observed variation of load with $T1_{Gd}$. (We note that Lyrra, Jurvelin, Pitkänen, et al. (1995) also examined the theoretical dependency of load response on elastic layer thickness for an indentation paradigm very similar to that used in this thesis: they employed a 1.3 mm diameter, cylindrical plane-ended indenter with 300 μm displacement. They concluded that indenter force is nearly independent of cartilage thickness for thickness greater than 2 mm. Their analysis was, however, based on the analytical mathematical model of Hayes, Keer, Herrmann and Mockros (1972) which is strictly valid only for infinitesimal strains. 300 μm indentation corresponds to strains of 7.5% to 15% over the thickness range of 4 mm to 2 mm: strains of this magnitude are not infinitesimal, and hence FE modeling was adopted for the analysis in this thesis.)

6.3 Validation of FE model: comparison to Hertz analysis, comparison to empirical results

To validate the model, three tests and examinations were made.

First, when the node density was increased by a factor of 10, the computed indenter force changed less than 3%. This demonstrated that the FE model was converging appropriately and that an appropriate resolution for the model had been chosen. (This test was performed by Anna Galea; the remaining validation studies were performed by the author.)

Second, since over a century ago Heinrich Hertz developed an analytical solution for the indentation of a sphere into an infinitely thick elastic layer (Hertz 1895a; Hertz 1895b), we compared the load predicted by the FE model for the thickest layer modeled (10 mm) with the Hertz solution for the indentation of an infinite half-space by a rigid sphere with frictionless contact conditions (Timoshenko and Goodier 1970). Hertz found that, for two spheres with radii R_1 and R_2 in frictionless contact, the relationship between displacement d and compressive force F is:

$$d = \left(\frac{9\pi^2 F (k_1 + k_2)^2 (R_1 + R_2)}{16 R_1 R_2} \right)^{1/3}$$

$$k_1 = \frac{1 - \nu_1^2}{\pi E_1} \qquad k_2 = \frac{1 - \nu_2^2}{\pi E_2}$$

where E_1 and E_2 are the elastic moduli and ν_1 and ν_2 are the Poisson's ratios of the two spheres, respectively.

To analyze the case of a rigid hemisphere with radius R indenting a semi-infinite half-space of cartilage with modulus E and $\nu = 0.5$, we set $R_1 = R$, $R_2 \rightarrow \infty$ (the half-space "radius"), $E_1 \rightarrow \infty$, $E_2 = E$, and $\nu_1 = \nu_2 = 0.5$. Substituting into the above expressions and rearranging, we can solve for the force F in terms of the displacement, cartilage elastic modulus and indenter radius:

$$F = \sqrt{\frac{256}{81} d^3 E^2 R}$$

Substituting $d = 300 \cdot 10^{-6}$ m, $E = 4.425 \cdot 10^6$ Pa and $R = 0.75 \cdot 10^{-3}$ m into the above expression yields a force F of 1.119 N (114 g). The finite element model exhibits asymptotic behavior at 10.0 mm thickness (Figure 6-8) and predicts a force of 1.190 N (121 g). The FE solution differs by 6.3% from the analytical solution, which we considered as an acceptable validation of the FE result.

Finally, as an order-of-magnitude empirical sanity check, the general predicted load response of the model was compared to the actual empirically observed load responses observed during indentation testing experiments. The FE predicted load response of on the order of 150 to 200 g for "normal" cartilage compares favorably with the approximately 200 to 500 g range of load response observed in our 300 μm pulse indentation experiments for loci with visibly intact cartilage.

6.4 Experimental results to validate that 0.25 Hz pulses are in the "short-time elastic response region" of cartilage: multiple-frequency pulse tests

The 300 μm amplitude half-sine pulse displacements employed as the principal test of cartilage stiffness in the current work were run at a frequency of 0.25 Hz. The peak load was measured after one-quarter cycle, at the time of peak displacement (t = 1 second). The discussion of Section 6.2 indicated that "near t = 0" the response of cartilage is closely approximated by a single-phase linear elastic model. To validate our assumption of the appropriateness of a linear elastic model for a 0.25 Hz pulse indentation test, two sets of experiments were performed. First, half-sine pulse tests were performed at four locations (two submeniscal, two central) as the frequency of the pulses was varied over a two order of magnitude range from .01 Hz (rise time = 25 seconds) to 1 Hz (rise time = 0.24 seconds). This was done to determine where the response to the 0.25 Hz pulse would lie on the expected S-shaped response-vs.-frequency curve. The results (Figure 6-9) demonstrated that at frequencies lower than 0.25 Hz the load response monotonically decreased at each test location, indicating that at lower frequencies appreciable fluid flow was occurring with resulting poroviscoelastic behavior. Between 0.25 Hz and 1.0 Hz, a plateau occurred in the load response-vs.-frequency curves: the load response at 0.25 Hz was in all cases within 11% of the average load response between 0.5 Hz and 1 Hz. These results indicated that with 0.25 Hz half-sine pulses (with 300 μm amplitude and the specific indenter geometry employed) insignificant water flow occurred and hence the cartilage response could reasonably be considered to lie in the elastic regime.

Having verified for these loci that at 0.25 Hz the load response was near the "linear regime" plateau, a second set of experiments was performed at 8 locations (7 of them different from the four tested in the first set of experiments) selected as exhibiting a four-fold range of stiffness variation. In this second set of experiments, a comparison was made of the load responses to 0.25 Hz, 0.75 Hz and 1.25 Hz half-sine pulses.

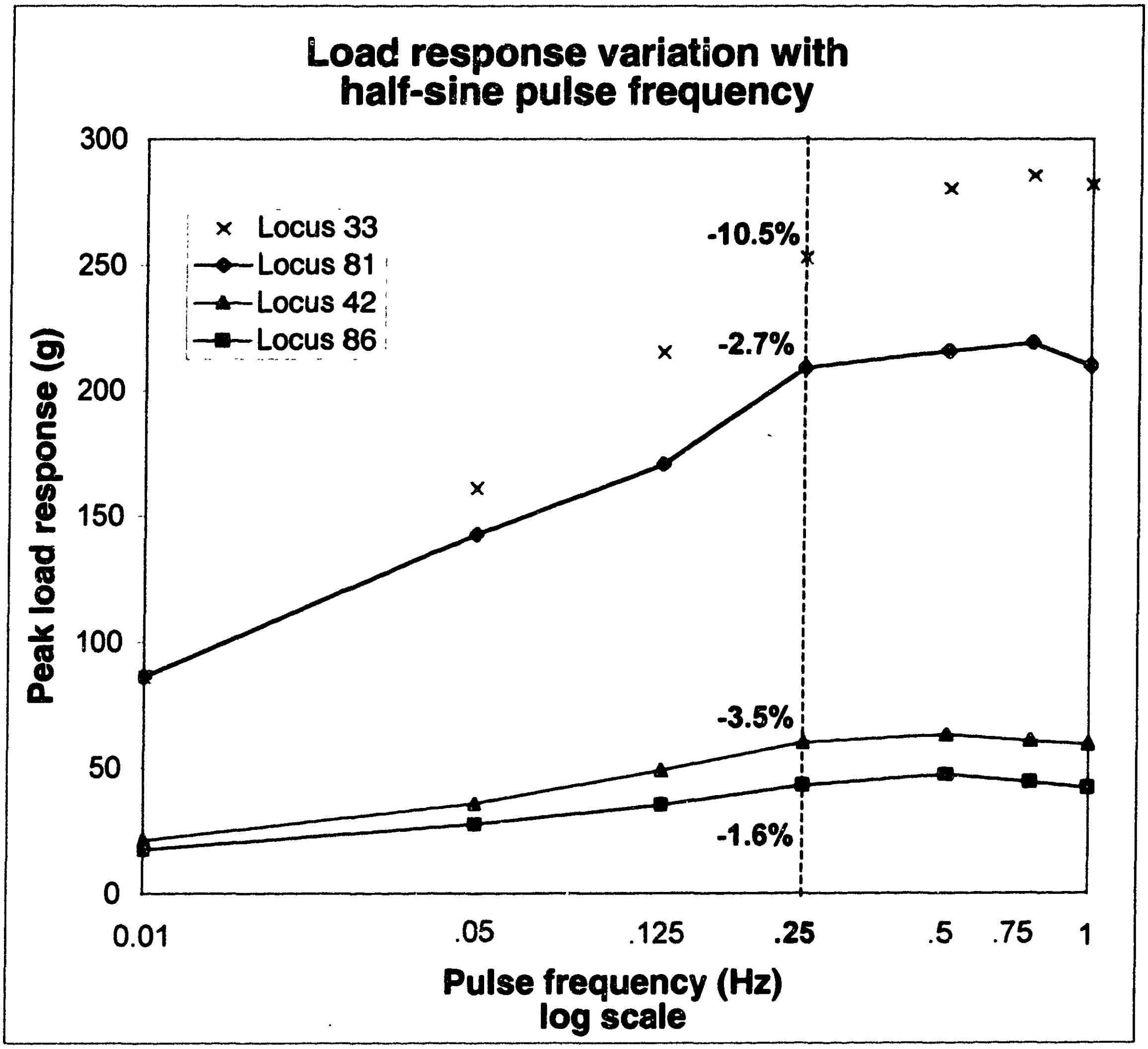

Figure 6-9 Variation in peak load response with half-sine pulse frequency. Four test locations were selected on sample HT3A: two submeniscal (loci 33 and 42) and two central (loci 81 and 86). In each region, one stiffer and one softer locus was selected. At each locus, pulse tests were performed at 7 different frequencies from .01 Hz to 1 Hz. At each locus, the load response curve exhibited a plateau at higher frequencies. The load response at 0.25 Hz was compared to the average of the load responses at 0.5 Hz, 0.75 Hz and 1.0 Hz: the percentage difference is indicated on the chart for each curve. In each case, the load response at 0.25 Hz varies by no more than 11% from the average load response at the higher frequencies. This indicates that the 0.25 Hz pulse protocol (with the indentation geometry employed) is operating in or near the "instantaneous" response regime of the cartilage, a regime which is accurately modeled by linear elastic behavior. (Note that all load responses for frequencies ≥ 0.25 Hz have been corrected for the frequency response of the strip chart recorder using the data in Appendix C.)

The results of these experiments showed the average difference in load responses between half-sine pulse tests at 0.25 Hz, 0.75 Hz and 1.25 Hz to be well under 10% (Figure 6-10 and Figure 6-11) across all locations tested. This further confirms that, using the geometry and displacement amplitude of the current pulse-indentation protocol, at a load time of 1 second insignificant fluid flow has occurred. We therefore conclude that the pulse indentation we employed is operating in the sort-time ("instantaneous"), linear-elastic regime, and the use of a linear elastic model for the finite element analysis of the load response to 0.25 Hz pulse indentation is valid and appropriate.

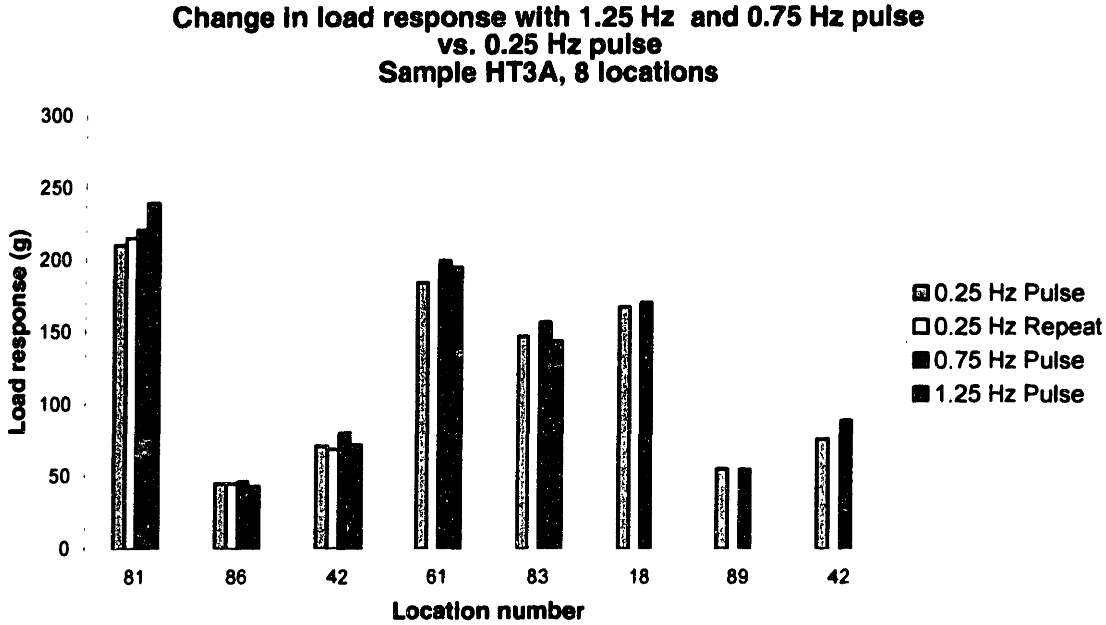

Figure 6-10 8 locations on HT3A were tested with 300 μm amplitude half-sine pulses at 0.25 Hz (1 s rise time) and 0.75 Hz (0.33 s rise time). 5 of the locations were also tested at 1.25 Hz (0.2 s rise time). (Loci 81, 86 and 42 were also tested a second time at 0.25 Hz to examine repeatability. All load responses have been corrected for the frequency response of the strip chart recorder using the data in Appendix C.)

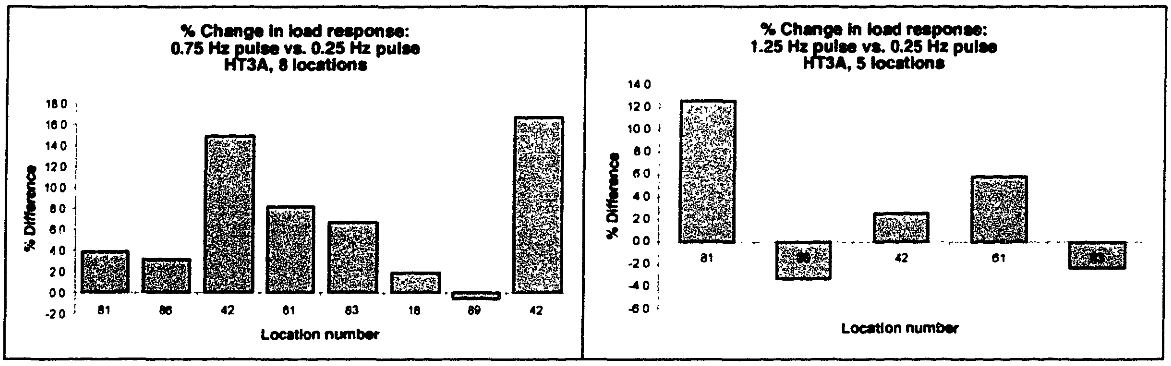

Figure 6-11 (Left) Percentage difference between load response to 0.75 Hz vs. 0.25 Hz half-sine pulse tests. Average difference = 6.8% +/- 6.2% s.d. **(Right)** Percentage difference, load response at 1.25 Hz vs. 0.25 Hz. Average = 3.1% +/- 6.5% s.d.

Chapter 7

Correlation of Load Response with $T1_{Gd}$ and GAG

In this chapter, the key pieces of the experimental work are brought together: we here examine the spatially-localized correlation between the mechanical stiffness measurements described in Chapter 4 and the dGEMRIC $T1_{Gd}$ (or GAG) data obtained using the methodology of Chapter 5. Early studies in both bovine and human tibial plateaux will be presented in which the registration of mechanical and MRI data was done via ink-spot targeting for mechanical tests, and hand measurement of the spot positions with respect to landmarks on the sample to derive ROIs in the MR images corresponding to the test loci. The results of the main studies employing the registration plate and quantitative positioning described in Chapter 3 will then be presented. The use of the registration-plate-based targeting, positioning and registration provided a calibrated, quantitative, less cumbersome, and more accurate methodology, permitting a much larger number of locations to be tested per sample and accurately colocalized to the MRI scans. The registration plate technique also enabled systematic, repeatable and comprehensive examination of the articular surface.

The correlation between stiffness and GAG content will be examined both qualitatively, by comparing profiles of stiffness (load response) variation and GAG variation, and quantitatively, by examining the overall correlation between load response and locally-averaged $T1_{Gd}$ for four different patients (130 test sites total). We will employ the results of the finite element analysis of Chapter 6 in an examination of the effect of ROI depth on the correlation between load response and $T1_{Gd}$. We will also apply the finite element analysis results to an examination of the possible effect of cartilage thickness as a confounding variable. Finally, we will examine possible differences in the stiffness-$T1_{Gd}$ correlation for two anatomically distinct regions of the tibial plateau

7.1 Bovine samples: normal and trypsinized

This section presents the results of stiffness and $T1_{Gd}$ measurements and correlations for a half-trypsinized bovine tibial plateau.

The plateau was prepared and trypsinized according to the procedure in Section 3.1.2. Six locations at which mechanical tests were performed were marked with India ink spots, 3 each in the trypsinized and non-trypsinized regions (Figure 7-1).

The sample was then equilibrated in 1mM Gd-DTPA^{2-} and imaged at 2T with a multislice inversion recovery sequence (9 TIs, range 17 to 2000 ms). Figure 7-3a (left) shows a proton density image of the sample (the final inversion delay image, TI = 2000ms). The articular cartilage surface is visible on the left edge of the image; the right edge is the cut bone, epoxied to the registration frame. The growth plate is also visible, running obliquely in the center of the image. Figure 7-3b (right) displays the $T1_{Gd}$ map computed from the 9 IR images. A difference in $T1_{Gd}$ of the cartilage is distinctly visible above and below the level of trypsinization (indicated by the "Tryp" line on the vertical axis.) The average cartilage $T1_{Gd}$ above this line (to a depth of 2 mm, or 4 pixels) is 277 ms (nontrypsinized region), and 182 ms below it (trypsinized, GAG-degraded region) (decrease of 34%) (see Figure 7-2). Figure 7-3b also shows the positions of six loci where indentation testing was conducted, with their positions relative to the trypsinization level indicated on the vertical axis.

Spatially-localized averaging of $T1_{Gd}$ was performed for each locus. In each case, the ROI over which averaging was performed was 1.5 mm (3 pixels) parallel to the surface by 1.0 mm (2 pixels) deep. (Topologically, each ROI was an 8-connected set of 6 pixels). The slice thickness was 2.0 mm.

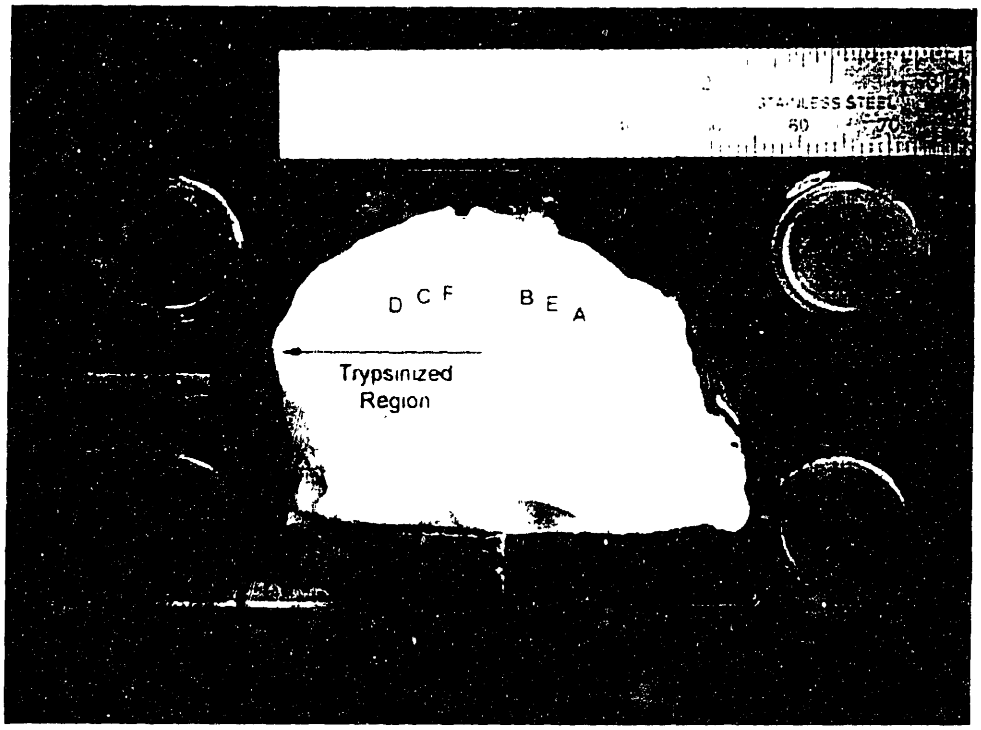

Figure 7-1 Half-trypsinized bovine hemi-plateau on registration frame. Note the increased translucency of the trypsinized region. At each of the six marked locations indentation testing was performed and locally averaged H_A was calculated.

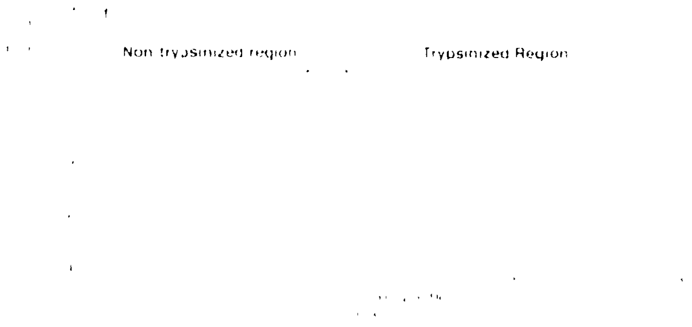

Figure 7-2 H_A profile through surface of half-trypsinized bovine tibial plateau. H_A decreases by 34%, on average, in the trypsinized region.

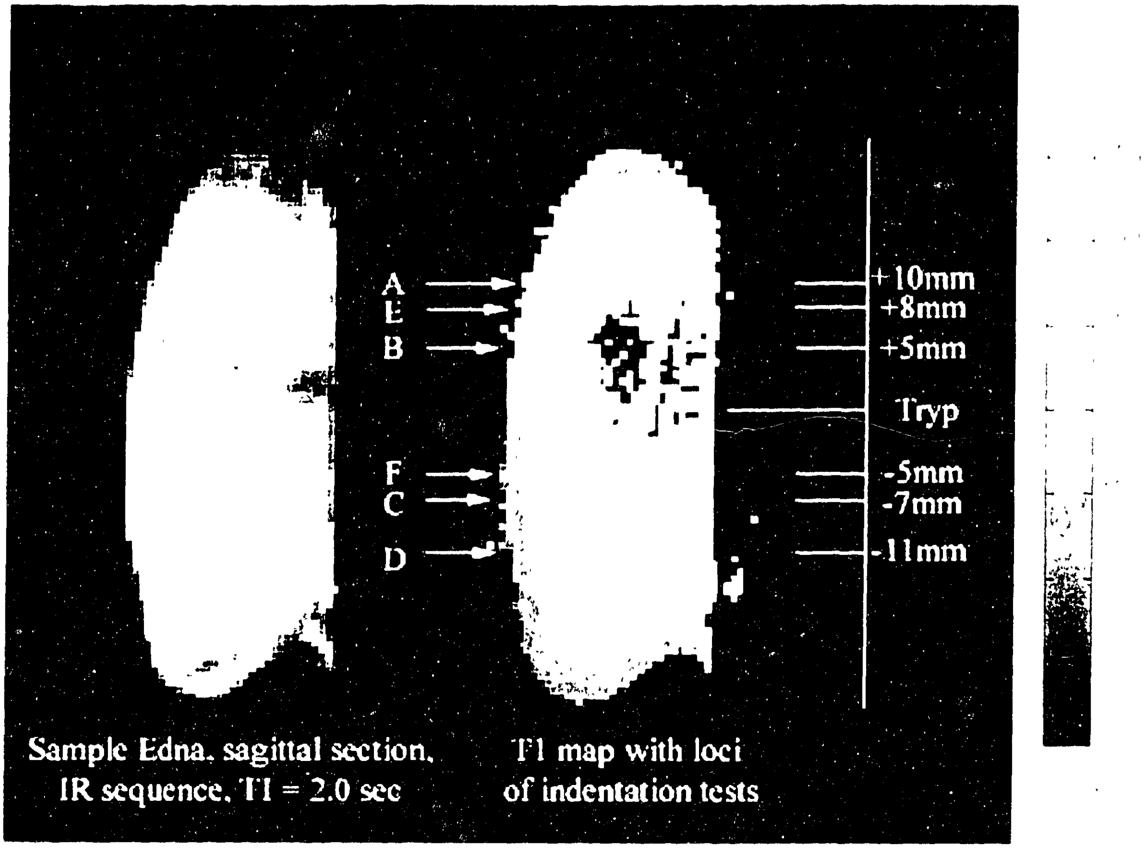

Figure 7.3 (a, left) [illegible] (b, right) [illegible]

[illegible]

Half-Sinusoid Pulse Testing of Partially-Trypsinized Bovine Sample
Amplitude = 200um, f = 0.1 Hz

	Peak load (g)					Average Peak Load (g)	Stiffness Index (kN/m)	Locally Averaged T1 (ms)
Non-trypsinized	Trial #1	Trial #2	Trial #3	Trial #4	Trial #5			
Location A	71	88	84	91	95	85.8	4.21	267
Location E	81	89	89	101	93	90.6	4.44	259
Location B	100	110	122	112	112	111.2	5.45	277
Trypsinized								
Location F	38	50	50	-	52	47.5	2.33	179
Location C	41	44	52	55	56	49.6	2.43	175
Location D	48	49	52	58	54	52.2	2.56	172

Table 7-1 Stiffness and T1 data for partially-trypsinized bovine tibial plateau. Each row reports data for one of the six test loci. **Average Peak Load** is the average peak load, taken across the five independent trials at each location.

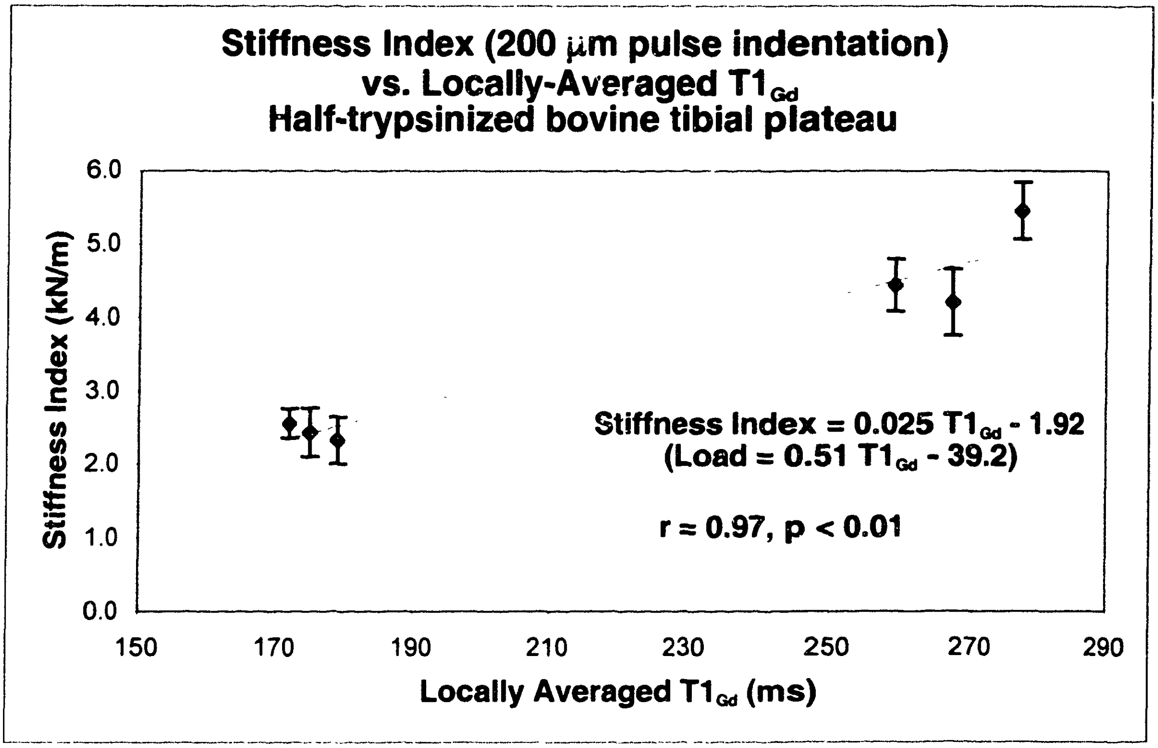

Figure 7-4 Correlation between Stiffness Index and $T1_{Gd}$ for six locations tested. The three loci with lower stiffness index and lower T1Gd values were in the trypsinized portion of the plateau.

7.2 Human sample: preliminary study

An initial study to examine stiffness-$T1_{Gd}$ correlation was performed on a sample of human tibial plateau without use of the registration plate (sample HT1, age of patient not known; sample dimensions 56 mm anterio-posterior, 25 mm medio-lateral). This sample had previously been imaged at 2T with an inversion recovery sequence after equilibration of the sample in 2 mM Gd-$DTPA^{2-}$. 8 inversion delays were specified over the range 17 to 400 ms. Pixel dimension was 200 μm, slice thickness was 2 mm.

$T1_{Gd}$ maps were computed from the IR scan data. Figure 7-5 displays the GAG maps computed from the $T1_{Gd}$ maps for 4 sections of the MRI study. 12 locations, labeled A through L, were selected for mechanical testing. The positions of the loci on the sample were established by measuring their positions relative to the edges of the sample in the MR images and then making similar measurements directly on the sample. Each locus was marked on the surface of the sample by spotting with an India ink marker, as was described previously for the bovine samples. Location H was destroyed during mechanical testing by a wayward LabView program leading to uncontrolled downward displacement, puncture of the sample and destruction of the indenter; hence, the cartilage load response at location H was not obtained.

Half-cycle sinusoid indentation testing was applied at each of the 12 loci to assess the stiffness at the loci. The pulses were specified with a frequency of 0.25 Hz (1 sec. rise time) and an amplitude of 200 μm. Targeting of the indenter tip to the test loci was achieved through visual inspection: the indenter was lowered toward an ink spot and the position of the tip relative to the spot was assessed by viewing from two roughly orthogonal directions. The indenter was iteratively lowered and the sample repositioned until the indenter tip was centered over the test locus.

Locally-averaged $T1_{Gd}$ values were computed by manual definition of ROIs in the $T1_{Gd}$ maps beneath the test sites (Figure 7-6). The ROIs were 1.4 mm wide and had a depth of either 400 μm (twice the indentation depth) or the full-thickness of the cartilage. Cartilage thickness was also determined for all loci by measurement on the $T1_{Gd}$ maps. Thickness ranged from 2.3 mm to 3.2 mm across the 12 loci.

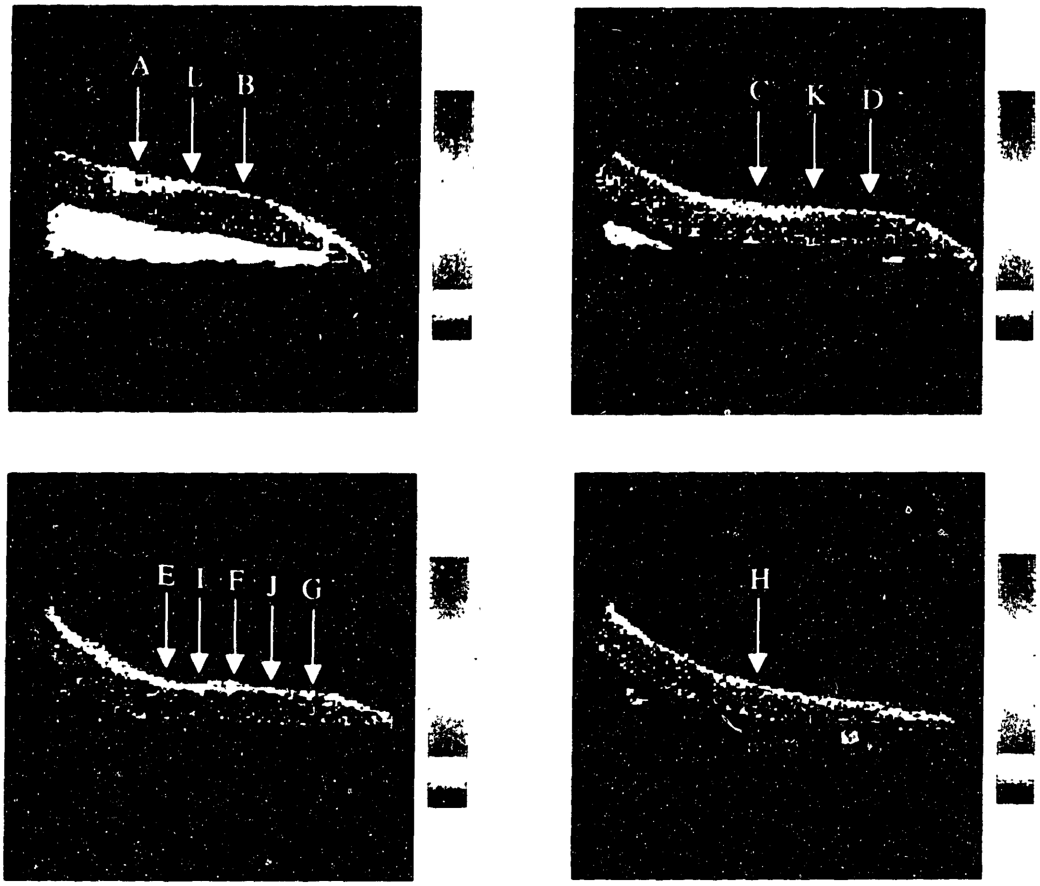

Figure 7-5 [GAG] maps derived from multislice IR study at 2T of portion of human tibial plateau. [Gd(DTPA)$^{2-}$] = 2 mM. Coronal sections, with peripheral region to the right. 2 mm slice thickness, pixel size 200 µm, FOV 2.56 cm. The loci at which pulse testing was performed are indicated. The colorbar indicates a GAG range of 0 to 80 mg/ml.

The result of analyzing the linear correlation between load response and T_{1Gd} is presented in Figure 7-7. A strong correlation ($r = 0.80$, $p < .002$) is exhibited between load response and T_{1Gd} for the 11 loci tested when the depth of T_{1Gd} averaging was 400 µm (twice the indentation depth). The slope of the load-T_{1Gd} linear regression line was 0.86.

When the same load response data were correlated to full-depth averaged T_{1Gd}, a moderate but still significant correlation ($r = 0.64$, $p = .017$) was obtained for this sample.

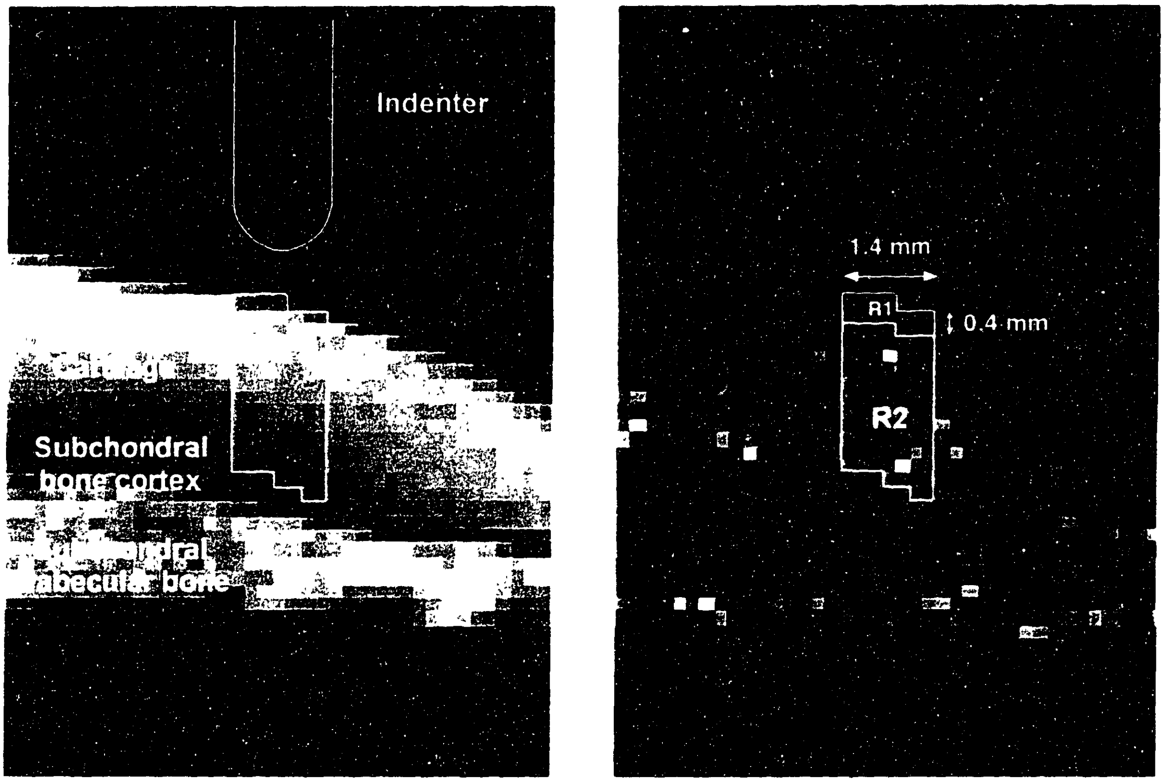

Figure 7-6 ROIs for $T1_{Gd}$ averaging. **(left)** A portion of the final delay image (TI = 400 ms) from the IR sequence near locus B. The calcified cortex of the subchondral bone is seen as a dark band interposed between the cartilage and deeper marrow-rich trabecular bone. A schematic depiction of the indenter geometry, drawn to scale, is also shown, and the cartilage beneath the footprint of the indenter is outlined. The displacement profile for indentation was a 200 μm half-sine pulse with frequency 0.25 Hz. **(right)** Shown in outline are the boundaries for the 400 μm depth and full-depth ROIs over which average $T1_{Gd}$ was computed. The 400 μm depth ROI is delineated by region R1. The full-depth ROI is the union of regions R1 and R2.

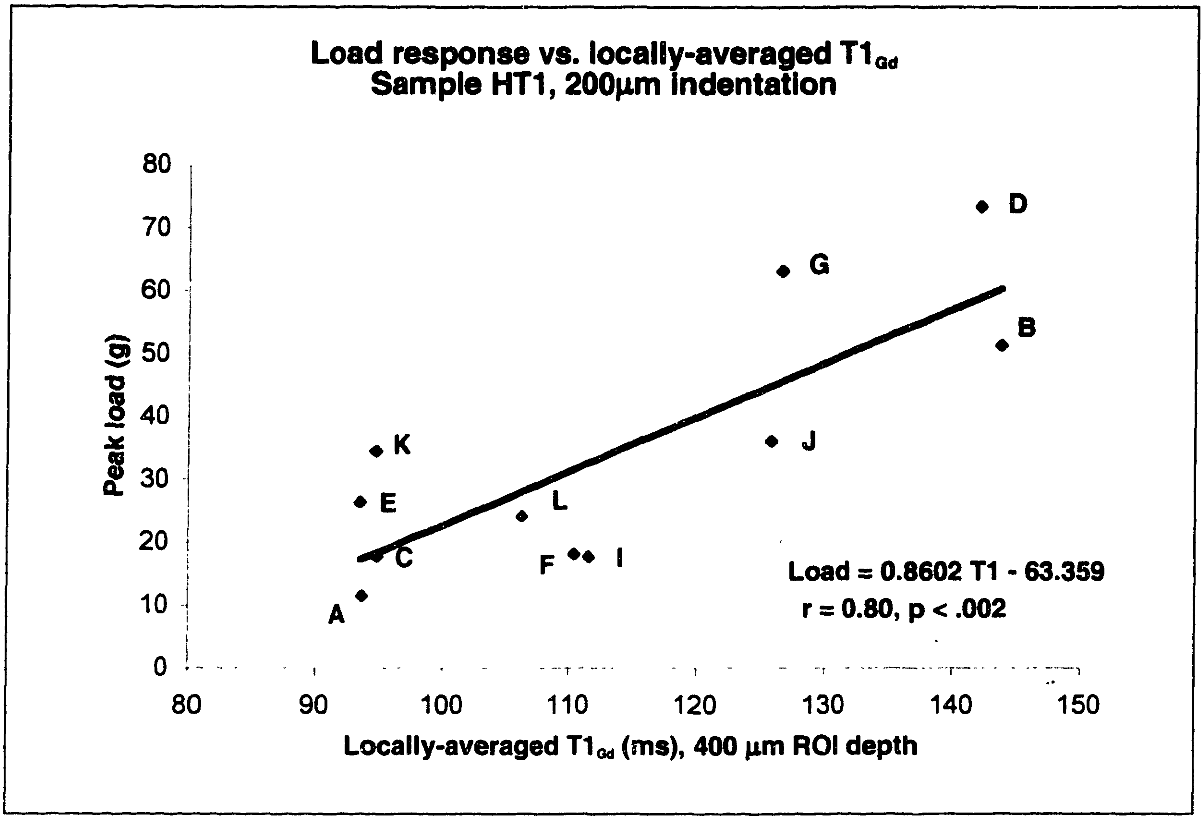

Figure 7-7 Correlation of peak load response with $T1_{Gd}$ averaged to 400 μm depth beneath the indenter for human tibial plateau sample HT1. Data labels correspond to the test locations indicated in Figure 7-5 (11 loci total).

7.3 Human sample results with registration plate and quantitative positioning

In this section, the results of experiments performed on human tibial plateau samples utilizing the mechanical-MRI registration plate are presented. These experiments resulted in the most precise colocalization of $T1_{Gd}$ to the indenter footprint. These experiments are also the most systematic exploration of the mechanical and MRI topography of the articular surfaces examined in this thesis.

7.3.1 Spatially-localized profiles of stiffness and [GAG] variation

Figure 7-8 shows three example [GAG] maps computed from corresponding T1 images from one sample (HT3A). Each map spans 11 loci spaced 1.5 mm apart. Indentation testing was performed at each locus (indicated by numbered arrows in Figure 7-8a). The three sections demonstrate three different patterns of [GAG] and stiffness variation: a focal area of deficit (Figure 7-8a), a region of relatively uniform [GAG] and stiffness (Figure 7-8b) and a region in which both [GAG] and stiffness increase from one end of the sample to the other (Figure 7-8c). In each case, a correlated pattern of load response variation and locally-averaged [GAG] variation is evident across the 11 colinear loci. In particular, the sensitivity of the test methodology to the presence of a focal lesion is demonstrated in Figure 7-8a. Here, a focal area of [GAG] depletion, evident in both the [GAG] map and the corresponding locally-averaged [GAG] profile, is associated with a correlated pattern of reduction in peak load response (Figure 7-8d).

7.3.2 Overall correlation of load response to locally-averaged $T1_{Gd}$

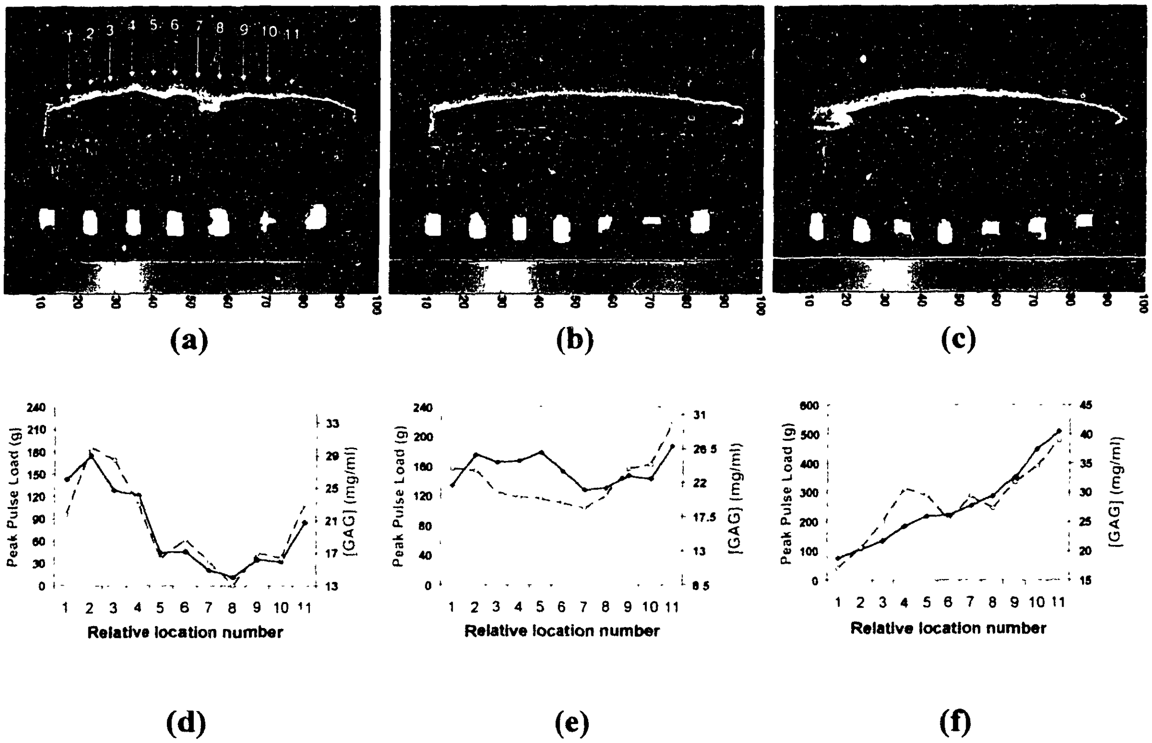

(a) (b) (c)

(d) (e) (f)

Figure 7-8 (a) (b) (c): [GAG] maps of three adjacent sections of human tibial plateau (sample HT3A): the cartilage surface is superior, the subchondral bone is inferior and displayed in gray-scale. Sections are separated by 3.0 mm. Colormap units are mg/ml. The numbered arrows in **(a)** show the positions of 11 loci where stiffness measurements were performed. (Similar sets of loci are defined for **(b)** and **(c)**.) MRI-lucent registration markers are visible beneath the samples. In **(a)**, an area of relative GAG depletion can be seen extending from locus 5 to locus 10. **(d) (e) (f):** Peak load responses (solid blue curves) and locally-averaged [GAG] values (dotted red curves, 600 μm depth ROIs) show similar variation across the 11 colinear locations in each slice. Especially noticeable are the focal reduction in both load response and [GAG] between loci 5 and 10 in **(d)**, the relatively smaller variation of both load response and [GAG] across most loci in **(e)**, and the approximately steady increase in both indices across the loci in **(f)**.

When data from all loci on each sample were pooled and the relationship between load and $T1_{Gd}$ was examined, the load response was found to be strongly correlated with locally-averaged $T1_{Gd}$ for each of the three patient samples (Figure 7-9), with Pearson correlation coefficients of 0.90, 0.69, and 0.81, respectively ($p < .0001$ for each). The slopes of the regression lines were similar: 7.75, 6.80 and 5.49 (g/ms). ANCOVA analysis of the homogeneity of the slopes indicated that they were not significantly different ($F = 1.188$, $p = .31$) from one another.

T1 ranged from 101 ms to 203 ms across all test loci. We note that for the protocol parameters employed (2mM $Gd(DTPA)^{2-}$, 8.45 T), a T1 range of 105 ms to 203 ms corresponds to a cartilage GAG concentration range of 0 mg/ml to 53 mg/ml. The range of GAG concentration in adult human articular cartilage has been previously reported to range from 60 mg/ml in normal cartilage to nearly 0 mg/ml in osteoarthritic cartilage.

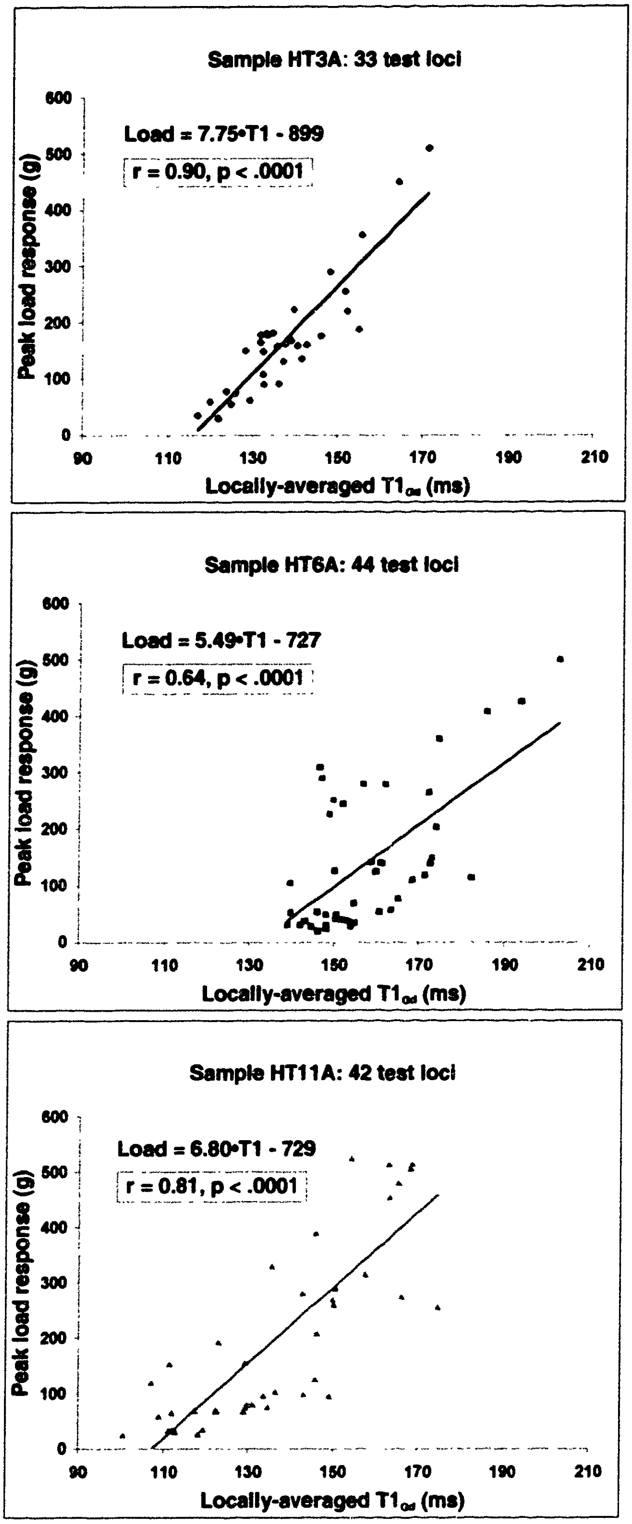

Figure 7-9 Peak load response at test loci is correlated with locally-averaged T1 at the loci for three different patient samples. Peak load was measured during application of a 300 μm amplitude, 0.25 Hz half-sine pulse indentation. T1 was measured at 8.45T with dGEMRIC after equilibration in 2mM Gd(DTPA)$^{2-}$. **(top)** HT3A, 62 y.o. female, lateral tibial plateau. **(middle)** HT6A, 78 y.o. male, lateral plateau. **(bottom)** HT11A, 81 y.o. female, lateral plateau. The slopes of the regression lines are not statistically significantly different (p = 0.31).

7.4 Variation in correlations with depth of ROI for $T1_{Gd}$ averaging

Locally-averaged $T1_{Gd}$ values were computed for ROI depths ranging from 100 μm to 1500 μm at each locus. For each sample, the correlation between load response and $T1_{Gd}$ across all loci was then examined as a function of ROI depth (Figure 7-10). The correlation coefficient generally exhibited a plateau or broad peak for ROI depths of 700 μm or less. We standardized the ROI depth for $T1_{Gd}$ averaging at 600 μm (equal to twice the indentation depth) for subsequent analyses.

A similar analysis was also made separately for the submeniscal and central regions of each sample; this will be described in detail in Section 7.6.

The correlation between load response and locally-averaged $T1_{Gd}$ as a function of depth of $T1_{Gd}$ averaging was also examined for the multiple displacement function protocols (pulse, step and sinusoidal) presented in Sections 4.2.6 and 4.3.1. Results of this analysis for all mechanical tests are presented in Figure 7-11 for three sets of colinear test locations: for sample HT3A, slice 4 (11 loci); sample HT3A, slice 3 (9 loci), and sample HT11A, slice 3 (9 loci). 10 different tests were performed at each test location on these

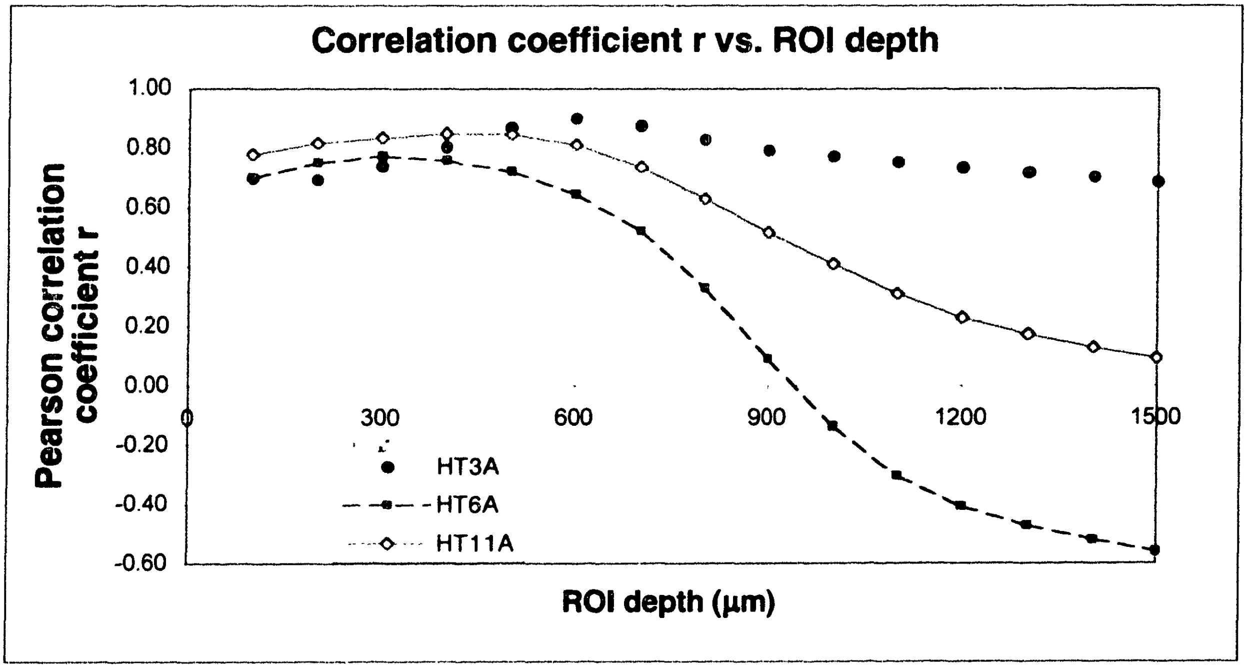

Figure 7-10 Variation in the correlation between load response and locally-averaged $T1_{Gd}$ as a function of the ROI depth (the depth of the domain over which $T1_{Gd}$ is averaged).

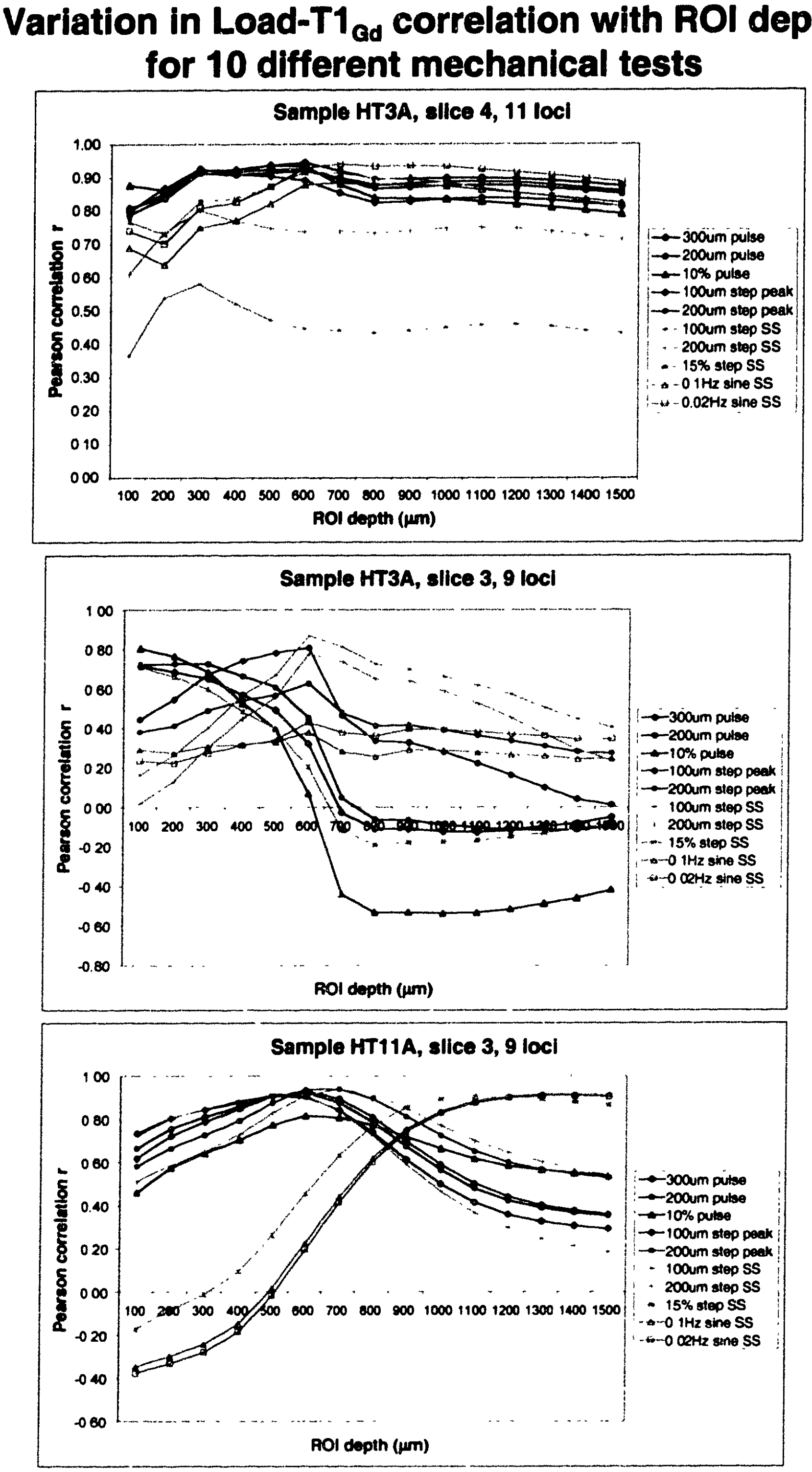

Figure 7-11 For 10 different mechanical tests, including pulse, step and sinusoidal displacements, the variation in the correlation between load response and locally-averaged $T1_{Gd}$ was examined as a function of the depth of the ROI over which $T1_{Gd}$ was averaged. SS = steady state load response. See Section 4.2.6 for a full description of the indentation testing protocols employed.

three slices (290 tests total for the 29 locations.) (A set of loci on sample HT8A was also tested with the multiple-displacement protocol: the mechanical data for this sample was presented in Section 4.3.1, but problems with the MRI study of this sample precluded its use for examining the correlations between load responses and $T1_{Gd}$.)

We will first describe some general features of these data, then examine one of the more interesting inferences they suggest: namely, that as indentation depth increases, deeper GAG content can influence the load response.

General trends in correlation for the different mechanical tests

The results across the three sets of loci show both similar and disparate features in the correlation profiles with respect to both type of test and depth of ROI. Although it is somewhat hard to generalize from these data (and the small sample size), several interesting features can be appreciated.

In Figures 7-13, 7-14 and 7-15, the correlation profiles are grouped into three categories by mechanical test characteristics: transient response tests, step-equilibrium tests and tests performed at 15% strain.

For sample HT3A, slice 4, all mechanical tests (except for the 100 μm step equilibrium test) exhibited a high correlation with $T1_{Gd}$ ($r > 0.60$) across all ROI depths examined from 100 μm to 1500 μm (Figure 7-11 top). (This is the same set of loci shown in Figure 7-8 (a) and (d) that demonstrate a focal area of GAG depletion.)

The 9 loci tested on slice 3 of the same sample (shown previously in Figure 7.8 (b) and (e)) show much more variability in load response-$T1_{Gd}$ correlation (Figure 7-11 middle). This set of data has a very restricted range of both load response and $T1_{Gd}$ however (see Figure 7-12), and therefore variability due to noise (i.e., load and MRI measurement variability) may obscure the load response–$T1_{Gd}$ correlations for this set of test locations.

All the transient responses[14] for HT3A slice 4 and HT11A slice 3 show very similar load response–$T1_{Gd}$ correlation profiles and correlation magnitudes (Figure 7-13 top, Figure 7-15 top). All the pulse responses for HT3A slice 3 show very similar correlation profiles (Figure 7-14 top). These results parallel the results reported in Section 4.3.1 which showed all transient tests to be highly correlated ($r \geq 0.81$) with each other.

---

[14] 200 μm and 300 μm fixed-displacement pulses, 10% strain pulse, 100 μm step peak response and 200 μm step peak response

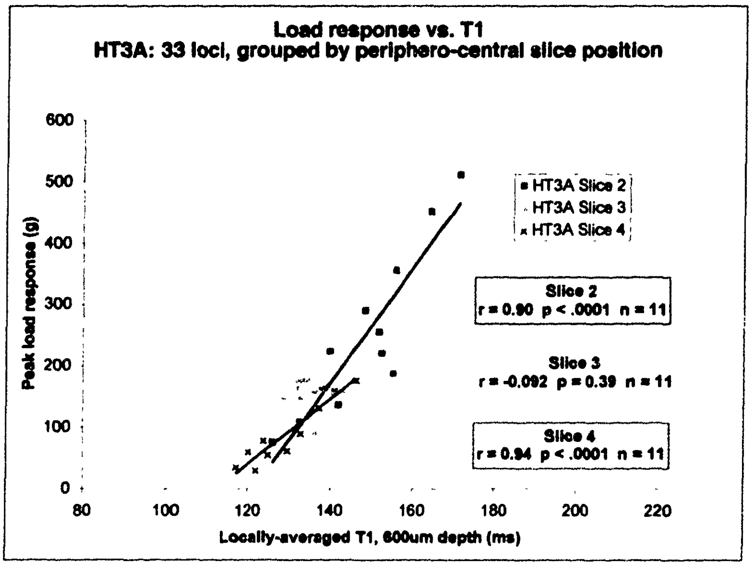

Figure 7-12 Load response and locally-averaged $T1_{Gd}$ data for sample HT3A, color-coded by slice. The slice 3 loci (yellow triangles) exhibited a small range of both load response and $T1_{Gd}$.

For HT3A slice 4 and HT11A slice 3, all three mechanical tests conducted at 15% strain showed very similar correlation profiles (Figure 7-13 bottom, Figure 7-15 bottom). HT3A slice 3 exhibited an anomalous disparity (Figure 7-14 bottom) among the "15% strain tests": the correlation profile for the 15% step equilibrium load response is markedly different than the 0.1 Hz and 0.02 Hz steady state load responses (which also used a 15% prestrain). There is no obvious explanation for this disparity.

Effect of deeper GAG content on deeper indentation

For sample HT11A, slice 3, all of the mechanical tests *except* those performed at 15% strain show very similar patterns of load response–$T1_{Gd}$ correlation with respect to ROI depth for $T1_{Gd}$ averaging (Figure 7-11 bottom). However load responses at 15% strain (the step-equilibrium response and the 0.1 Hz and 0.02 Hz dynamic responses) showed a *different* pattern of load response–$T1_{Gd}$ correlation with respect to depth. For these indentation profiles, the correlation rose from $r < 0$ for shallow ROIs to $r > 0.80$ for 1000 μm or greater ROI depth. For this sample, 15% strain is a deeper displacement (up to 375 μm) than any of the other tests. As was previously discussed for this set of test loci (see Figure 4-7 and related text) the observed higher correlation to $T1_{Gd}$ with greater ROI depth for the 15% strain tests may be indicative that the 15% strain load responses are

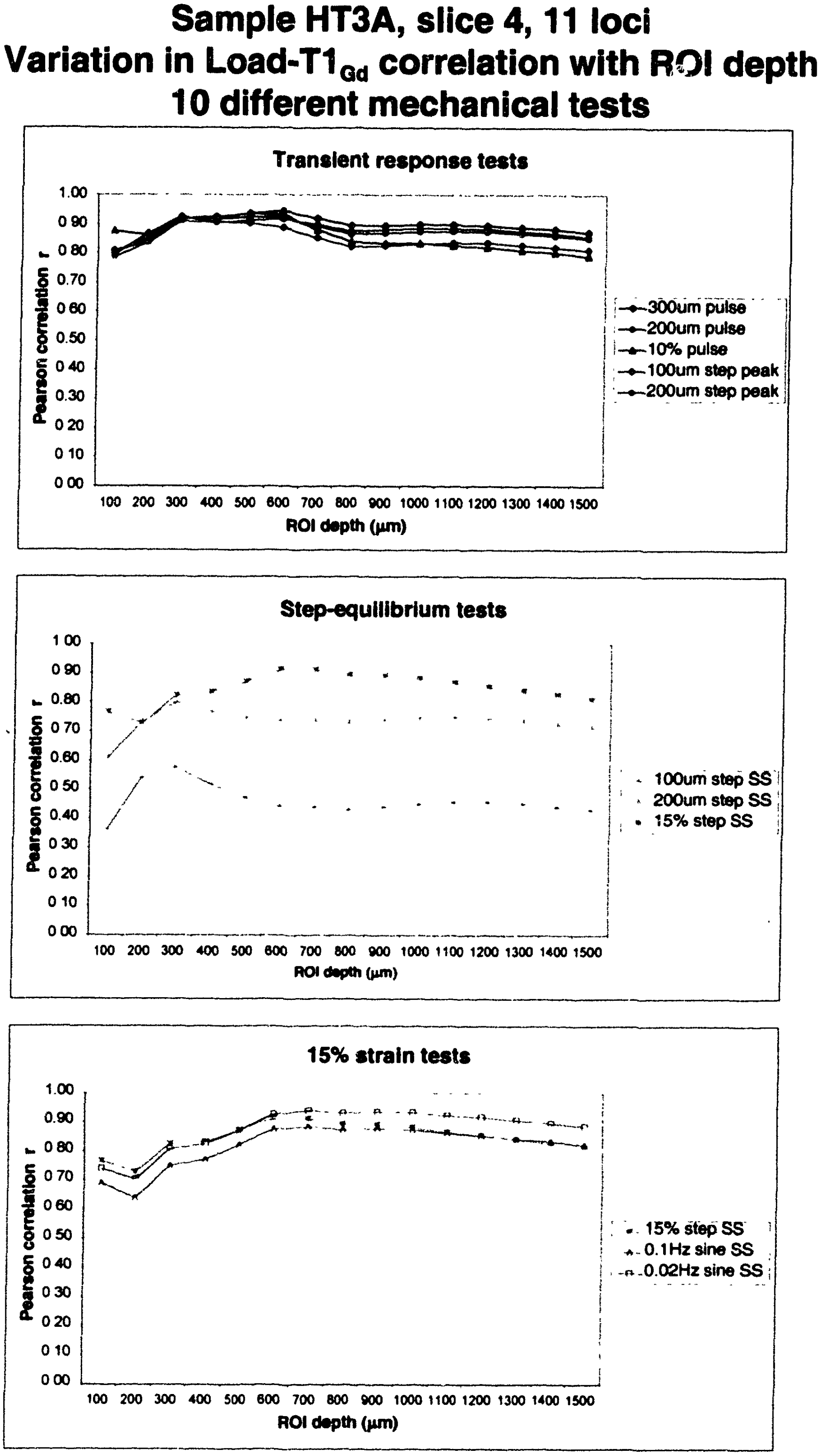

Figure 7-13 The correlation-vs.-depth profiles for sample HT3A, slice 4, plotted separately for the dynamic response tests (top), step-equilibrium tests (middle) and tests at 15% strain (bottom).

Sample HT3A, slice 3, 9 loci
Variation in Load-$T1_{Gd}$ correlation with ROI depth
10 different mechanical tests

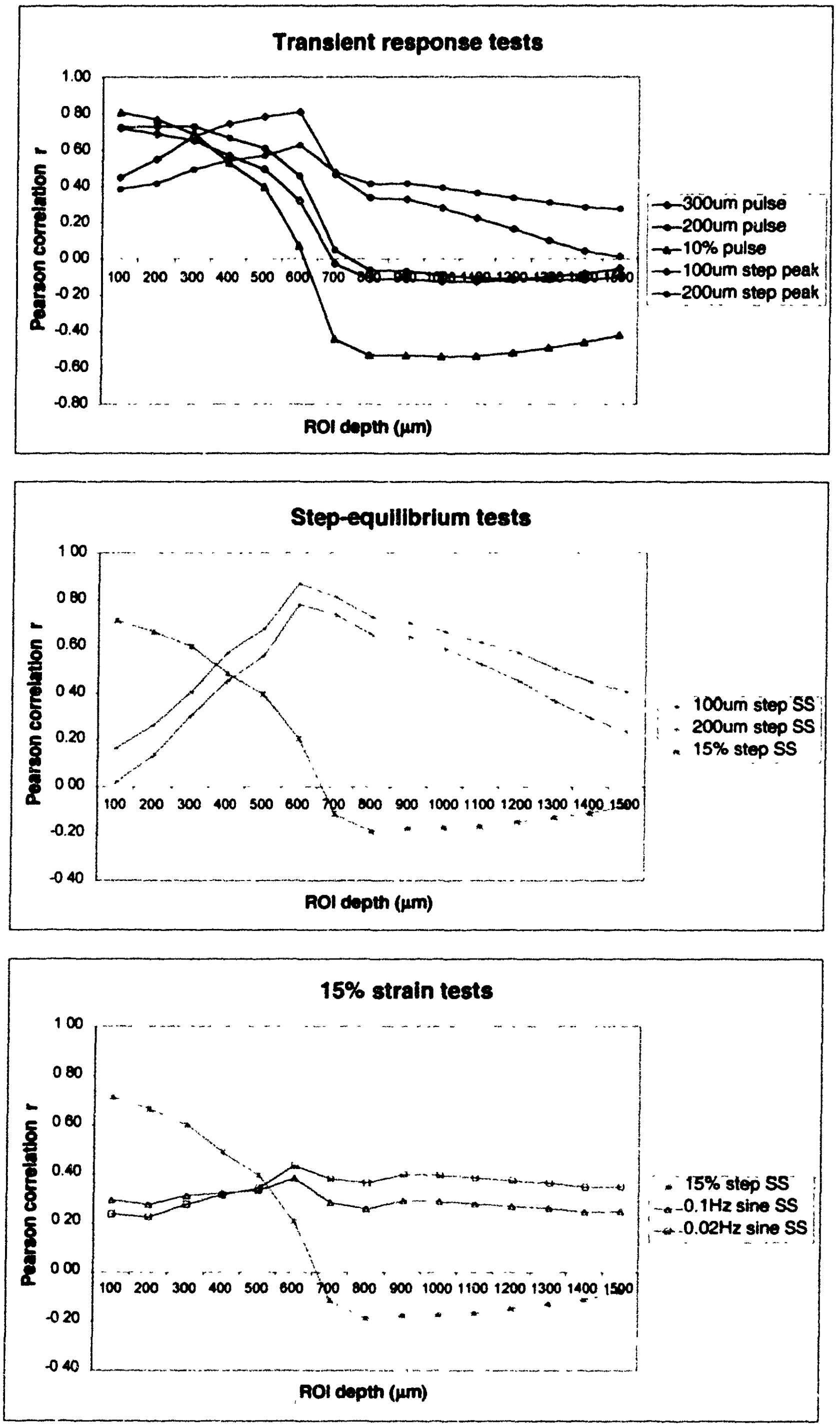

Figure 7-14 The correlation-vs.-depth profiles for sample HT3A, slice 3, plotted separately for the dynamic response tests (top), step-equilibrium tests (middle) and tests at 15% strain (bottom).

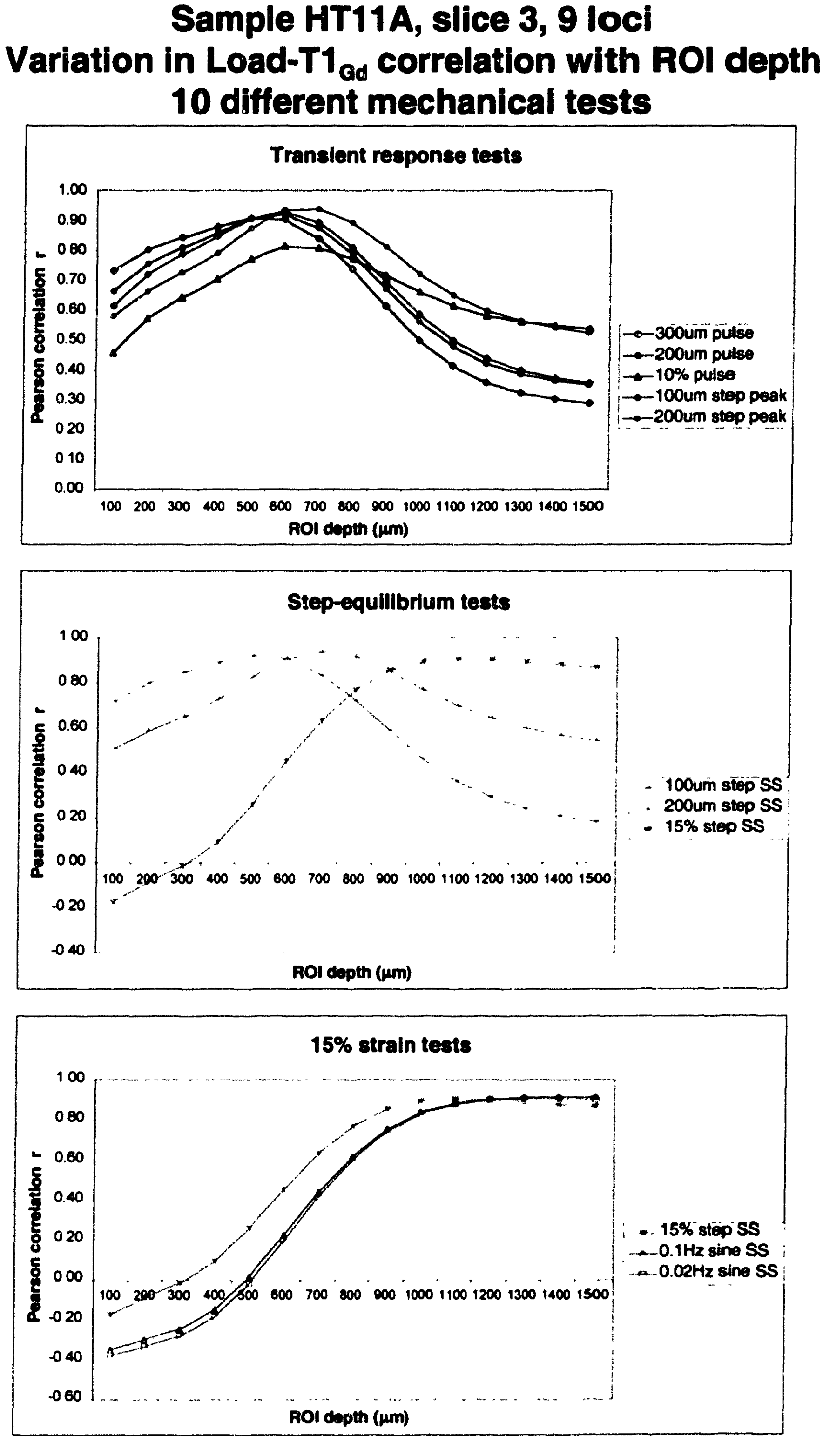

Figure 7-15 The correlation-vs.-depth profiles for sample HT11A, slice 3, plotted separately for the dynamic response tests (top), step-equilibrium tests (middle) and tests at 15% strain (bottom).

being influenced by a deeper region of the articular surface with a different stiffness (and GAG) profile than the more superficial region.

This difference between the shallower indentation tests and the 15% strain tests was *not* seen for sample HT3A slice 4. To examine why HT11A slice 3 showed a difference for the deeper tests and HT3A slice 4 did not, we generated $T1_{Gd}$ profiles for 5 different depths across each slice. $T1_{Gd}$ was averaged to a depth of 300, 600, 900, 1200, and 1500 μm at each test locus. These $T1_{Gd}$ profiles are displayed in Figure 7-16 (top) and Figure 7-17 (top) for HT3A slice 4 and HT11A slice 3, respectively. To make the *variation* in the profiles clearer (since it is the variation in the $T1_{Gd}$ profiles that will influence correlation with the load response profiles) we normalized each $T1_{Gd}$ profile to range between 0 and 1: these normalized profiles are presented in Figure 7-16 (middle) and Figure 7-17 (middle) for HT3A slice 4 and HT11A slice 3.

It is immediately apparent that HT3A slice 4 exhibits a remarkable uniformity in the shape of the $T1_{Gd}$ profiles irrespective of depth. This indicates that GAG content in this slice shows a similar pattern of variation independent of depth (for depths between 100 μm and 1500 μm). HT11A slice 3, however, shows a large change in the shape of the $T1_{Gd}$ profiles with depth. In particular, $T1_{Gd}$ increases markedly with depth near locations 57 to 58.

Since these profiles reflect GAG content, we can make the hypotheses that (a) HT3A slice 3 will *not* exhibit a difference in relative stiffness as indentation depth is increased (within limits) and (b) HT11A slice 4 *will* exhibit a difference in relative stiffness with deeper indentation. Specifically, we would expect that with deeper indentation, locations 57 to 58 would show a higher local stiffness, corresponding to the shape of the deeper $T1_{Gd}$ profiles.

To test these hypotheses, for each slice we examined the load response profile to a shallow indentation test (200 μm half-sine pulse indentation) and a deeper indentation test (15% step equilibrium). For the thicknesses of the loci on HT3A slice 4, 15% strain corresponds to an average indentation depth of 409 μm (450 μm maximum). For HT11A slice 3, 15% strain corresponds to an average indentation depth of 348 μm (375 μm maximum).

As shown in Figure 7-16 (bottom) and Figure 7-17 (bottom), the measured load responses confirm both the above hypotheses. For HT3A slice 4, the shallow and deep indentation responses are similar. For HT11A slice 3, with deeper indentation loci 57 to 58 show a higher load response relative to other loci. The shallow load response profile shows a clear similarity to the 300 μm depth $T1_{Gd}$ profile, while the deeper load response profile is similar to the deeper $T1_{Gd}$ profiles.

These data are limited and introduce the additional variable of comparing a short-time pulse load response to an equilibrium response. Still, the data are at least suggestive of a relationship between depth variation in GAG content and depth variation in stiffness (as indentation depth is varied). The data provide additional support for the hypothesis that GAG content local to the region stressed by the indenter is a determinant of indentation stiffness.

We also emphasize that it is the spatial resolution of the dGEMRIC technique and the close colocalization of mechanical tests to MRI ROIs (as provided by the registration methodology of this thesis) that enable these examinations to be made of the relationship between spatial patterns of GAG distribution and mechanical test parameters such as indentation depth.

Finally, we note that there is an additional suggestion in the data for sample HT11A slice 3 that correlation between load response and locally-averaged $T1_{Gd}$ may show sensitivity to the depth of the $T1_{Gd}$ averaging relative to the depth of indentation. For the step equilibrium responses for this sample (Figure 7-15 middle) the peak load-$T1_{Gd}$ correlation occurs at greater $T1_{Gd}$ ROI depths for deeper displacements: the peak correlation occurs near 500 μm, 700 μm and 1100 μm ROI depth for the 100 μm, 200 μm and 15% step equilibrium tests, respectively (15% strain corresponds to 348 μm average and 375 μm maximum displacement for the test loci in this set). This behavior again suggests that this sample may provide an example of cartilage for which deeper indentations are being influenced by a deeper region of the cartilage with a different stiffness and GAG profile than the superficial region.

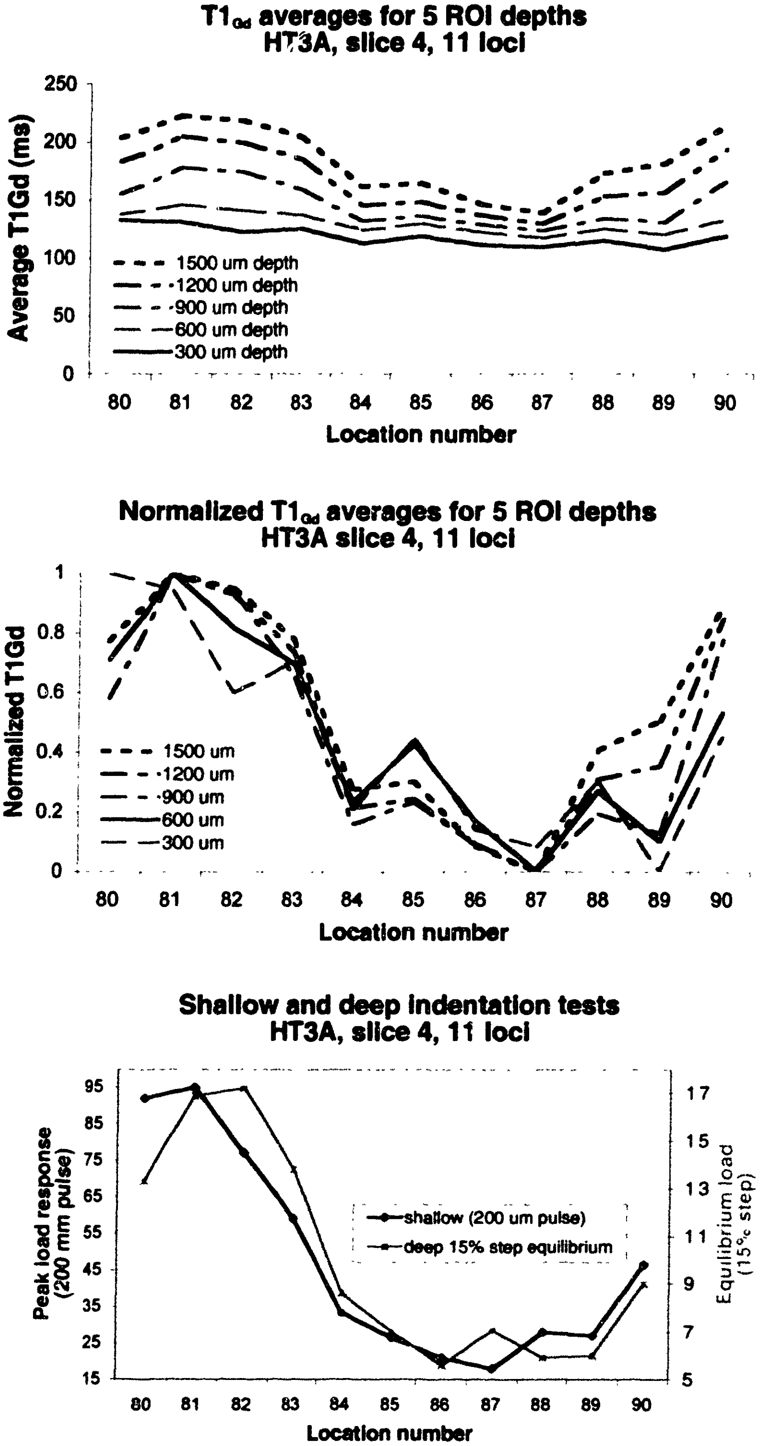

Figure 7-16 **(top)** $T1_{Gd}$ averages and **(middle)** normalized $T1_{Gd}$ averages for 5 different depths between 300 μm and 1500 μm for sample HT3A, slice 4. This slice exhibits similar $T1_{Gd}$ variation at all depths examined. **(bottom)** Profiles of load response for shallow and deeper indentation (15% strain = 409 μm average, 450 μm maximum). Both profiles are similar, and both are similar to the $T1_{Gd}$ profiles.

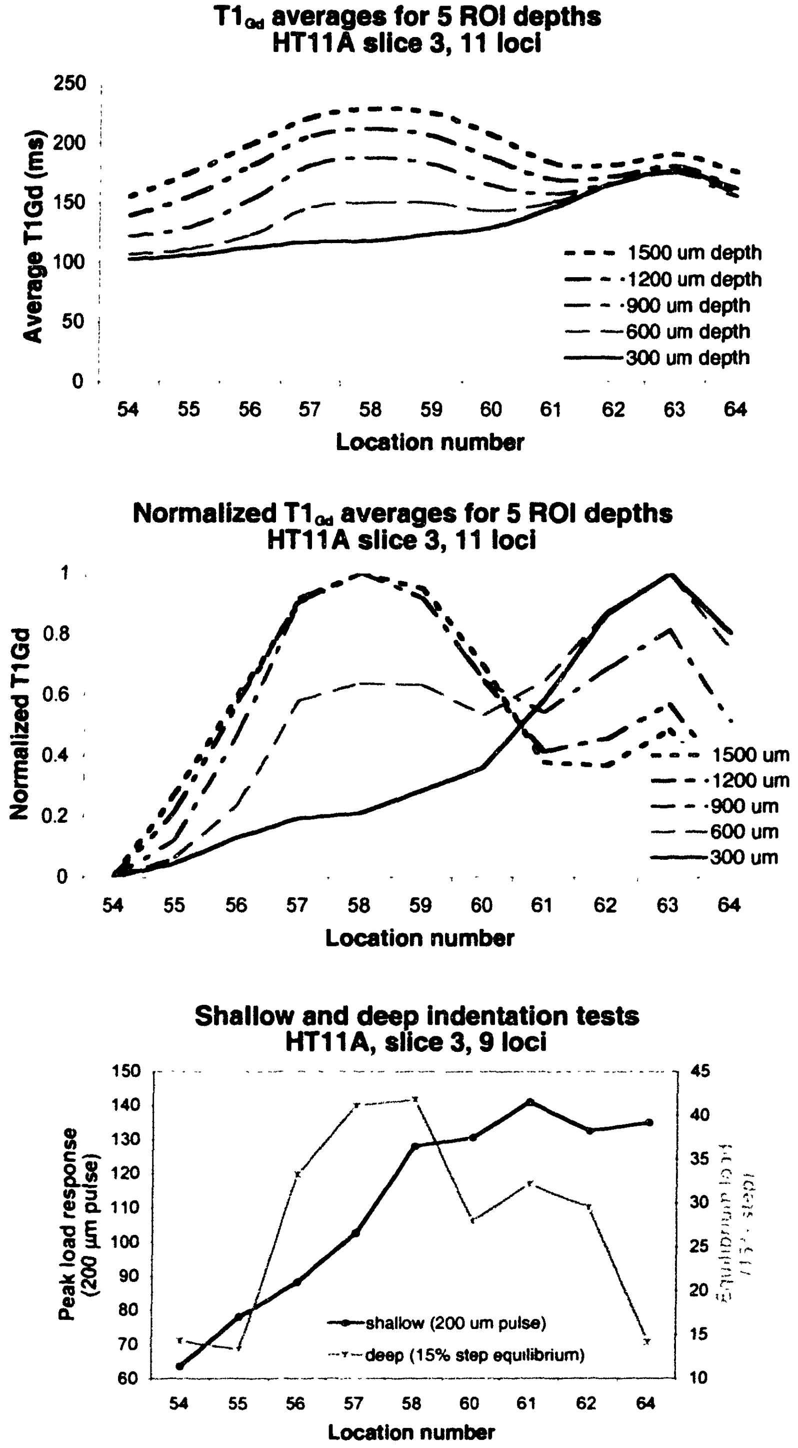

Figure 7-17 **(top)** T1$_{Gd}$ averages and **(middle)** normalized T1$_{Gd}$ averages for 5 different depths between 300 μm and 1500 μm for sample HT11A, slice 3. This slice exhibits much different T1$_{Gd}$ profiles as depth increases from 300 μm to 1500 μm. **(bottom)** Profiles of load response for shallow and deeper indentation (15% strain = 348 μm average, 375 μm maximum). The shallow indentation load profile is similar to the 300 μm T1$_{Gd}$ profile; the deeper indentation load profile is similar to the deeper T1$_{Gd}$ profiles. (Note that loci 59 and 63 were not mechanically tested.)

7.5 Analysis of thickness effects

The finite element results of the previous chapter indicated that, above 2 mm, variation in cartilage thickness would not significantly affect the indentation load response (with 300 μm indentation depth). To exclude thickness variation as a potential confounding variable, we reanalyzed the relationship between load response and $T1_{Gd}$ for only those loci with thickness ≥ 2.0 mm (Figure 7-18). The results demonstrated that strong correlations between load response and locally-averaged $T1_{Gd}$ were maintained for all three patient samples (97 loci total), with correlation coefficients of 0.81, 0.80, and 0.69 ($p < .0001$). Application of the Fisher r-to-z transformation revealed no statistically significant changes ($p > 0.17$ for all samples) in the Pearson correlation coefficient r for each sample between the case with all loci included and the case when only loci with thickness ≥ 2.0 mm were included.

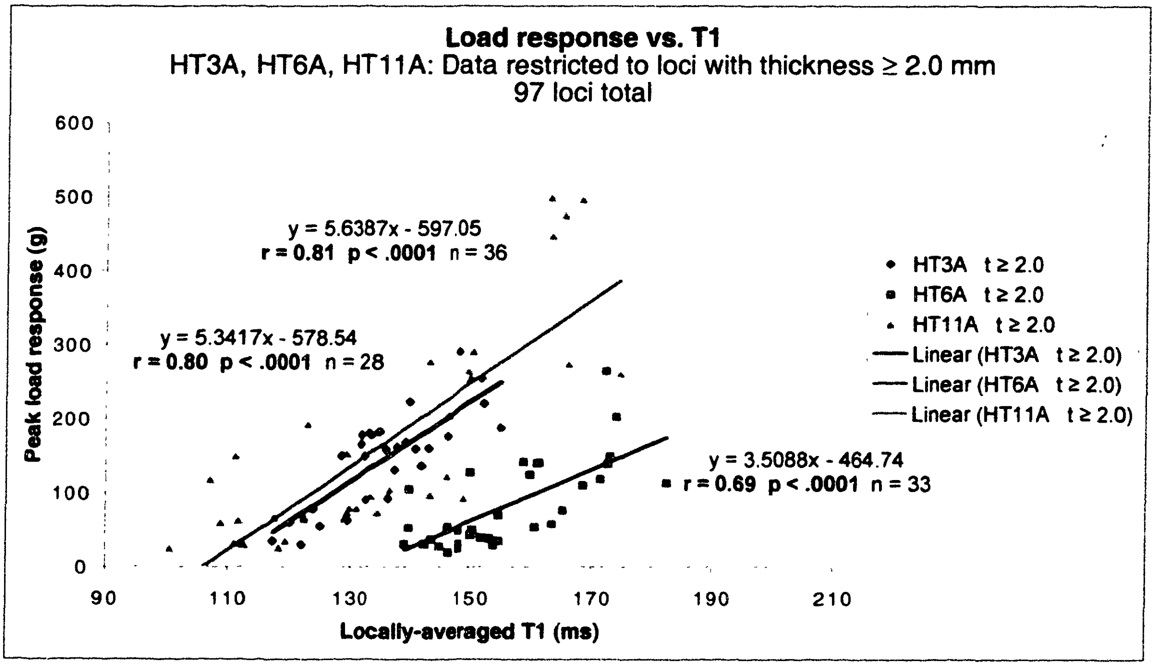

Figure 7-18 The correlation between peak load response and locally-averaged $T1_{Gd}$ is maintained after excluding all loci with cartilage thickness < 2.0 mm. There are no statistically significant changes in r values compared to Figure 7-9 ($p > 0.17$ for all samples).

7.6 Analysis of the effects of regional surface variation

The articular surface of the tibial plateau does not appear homogeneous to visual inspection. Typically, samples exhibited a smooth, glossy surface appearance in the more peripheral region which corresponds approximately with the area which is normally covered by the meniscus *in vivo* (Figure 7-19). In contrast, a roughened, textured and more translucent appearance was evident in the more central regions. In the intact joint, this is approximately the region exposed to direct contact with the femoral condyle.

In the present study, each sample exhibited this variation in appearance between the submeniscal and central regions, although to a varying degree (Figure 7-20). Significantly, the sample from the youngest patient (HT3A) exhibited the least visible differentiation between the two regions (HT3A was obtained from a 62 year old patient; samples HT6A and HT11A were obtained from patients of ages 78 and 81 years, respectively).

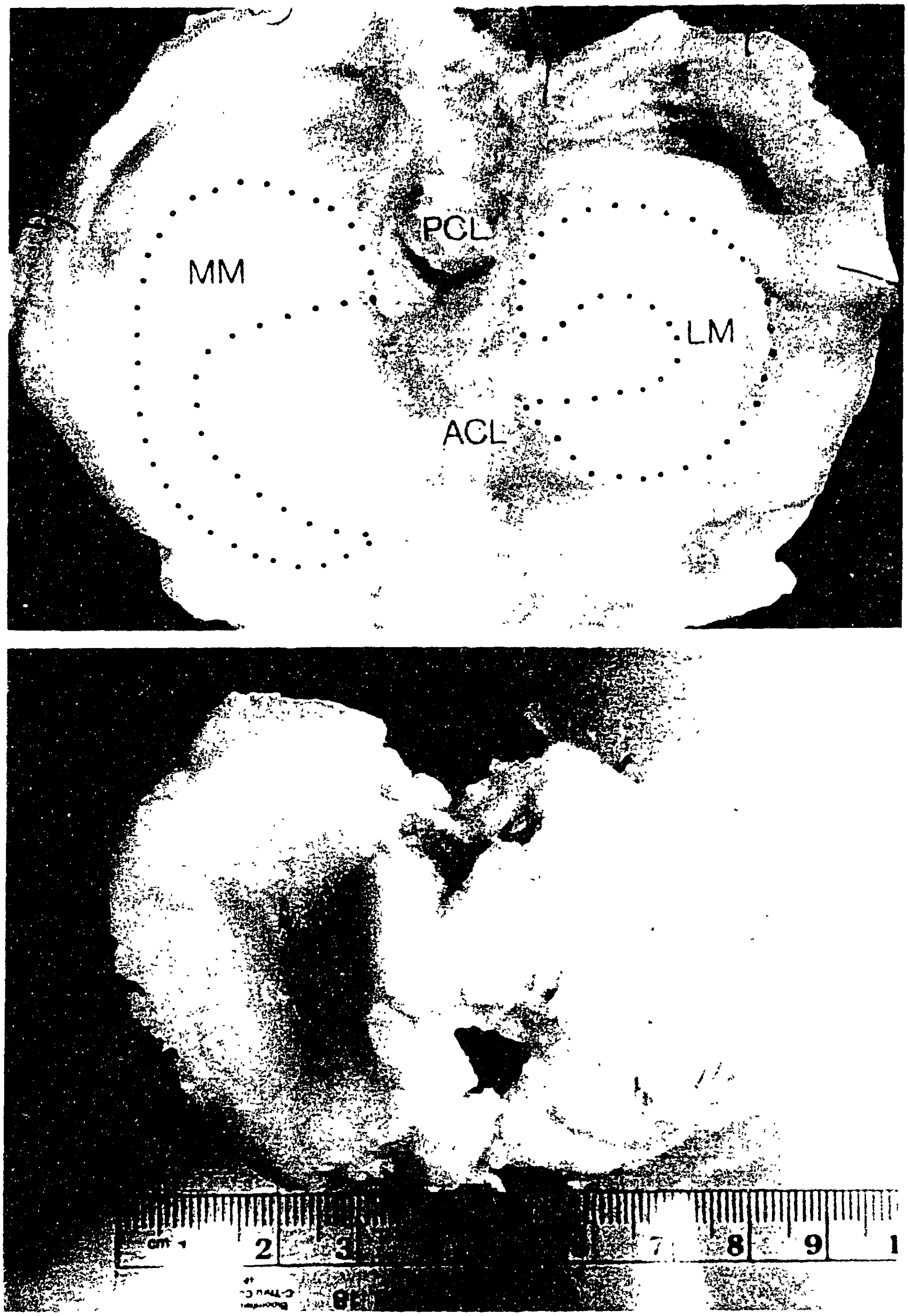

Figure 7-19 (top) Photograph of a human tibial plateau with menisci in place. MM = medical meniscus. LM = lateral meniscus. PCL = posterior cruciate ligament. ACL = anterior cruciate ligament. **(bottom)** Photograph of tibial plateau sample H16. On the right of the specimen India-ink stippling outlines the borders of sample H16A (examined in the current work). Note the smooth, glossy appearance of the submeniscal region (along the right edge of the specimen), and the more textured, translucent appearance of the more central region. (top photograph adapted from (Arnoczky, Dodds and Wickiewicz 1996))

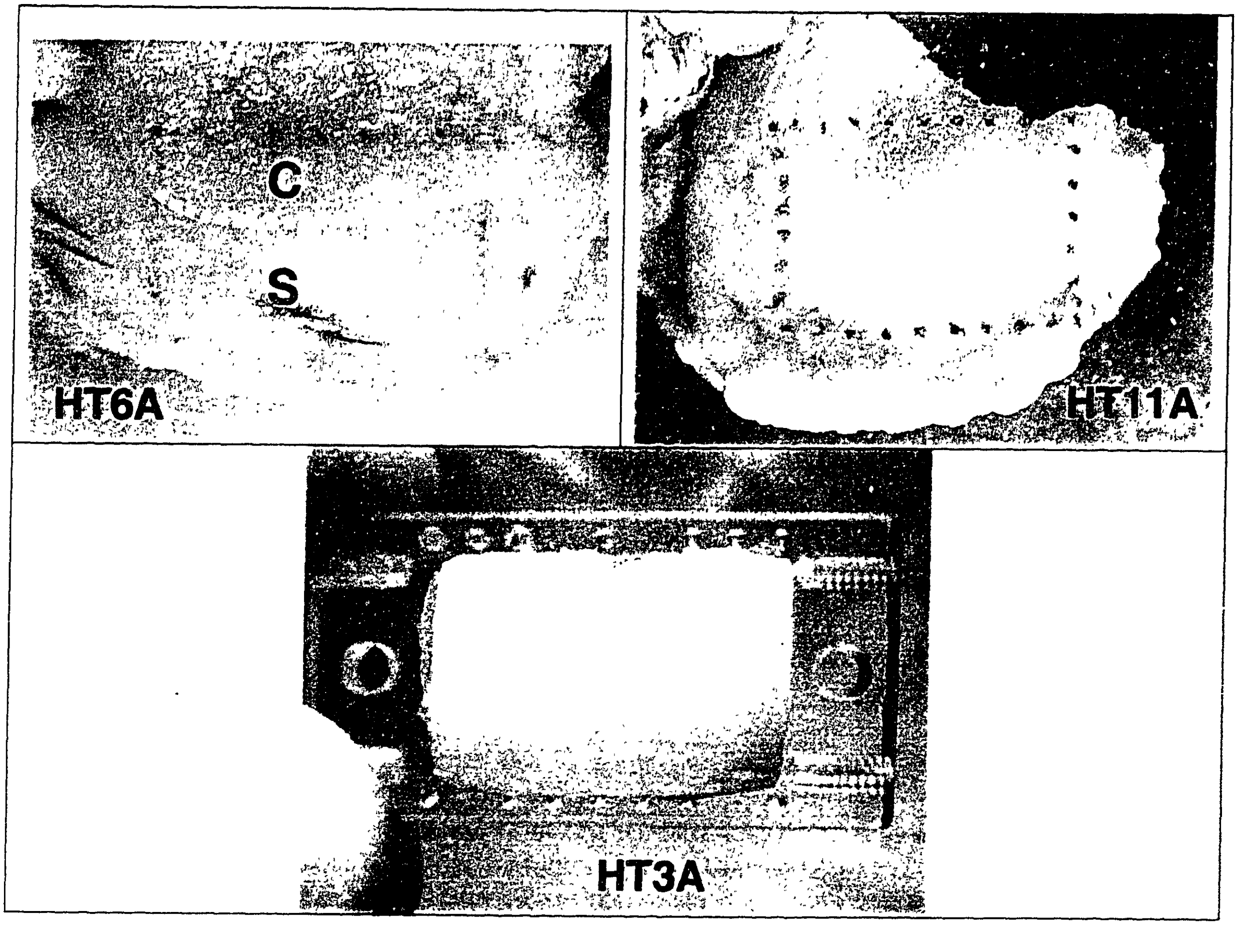

Figure 7-20 Heterogeneity of the surface properties of the articular cartilage of the tibial plateau. Each sample is oriented with the more peripheral region downward. Dotted India ink rectangular outlines delineate the boundary of the samples on the specimens which have not yet been cut. On HT6A, a line has been drawn indicating approximately the boundary between the submeniscal and central regions. The submeniscal region **S** appears generally smooth, glossy and grossly intact. The more central region **C** (normally in contact with the femoral condyle) appears to have a roughened, more textured surface. (Note that for sample HT6A, the area in the immediate vicinity of the surface fissures was excluded from mechanical testing and analysis.) HT6A and HT11A both exhibit fairly dramatic visual differences between the submeniscal and central regions. For HT3A, the distinction is less pronounced.

The evident variation in surface properties between these two regions suggested architectural changes which could influence the response to indentation. To examine this potential independent influence on indentation load response, we segregation the loci into submeniscal and central groups for each sample (Figure 7-21), and analyzed the correlation between load response and locally-averaged $T1_{Gd}$ separately for each group (Figure 7-22).

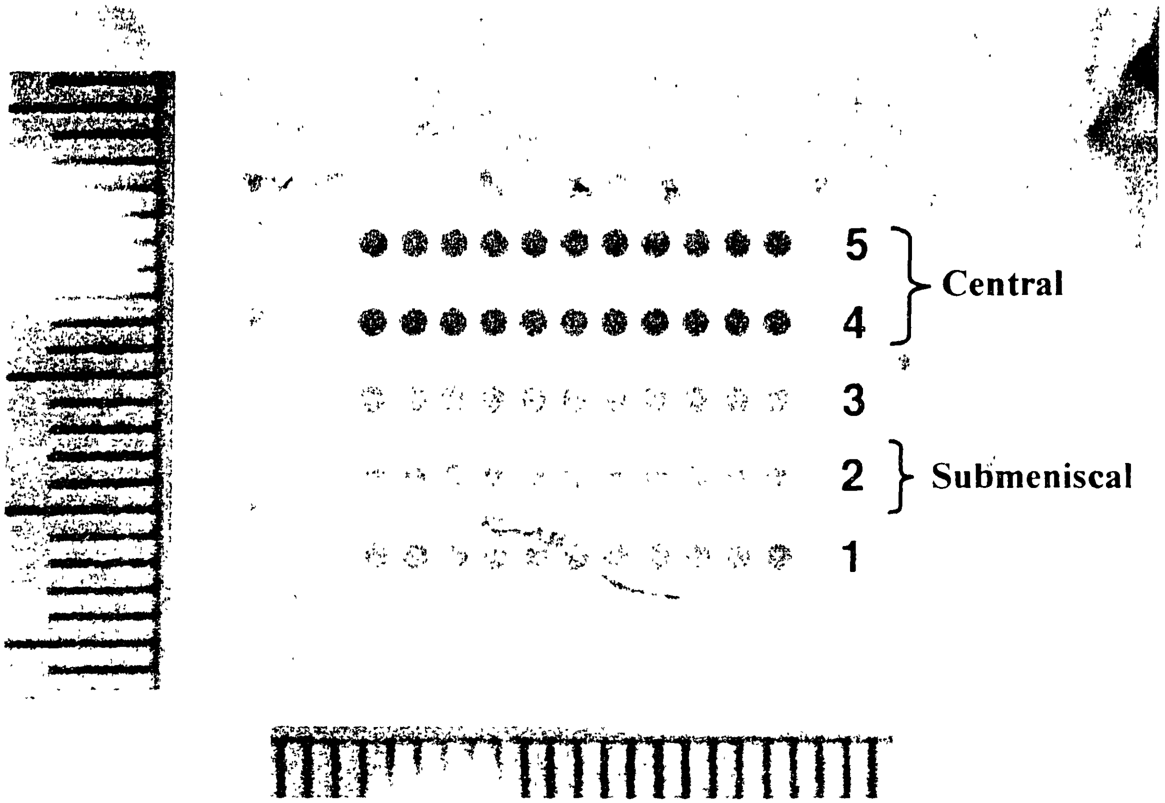

Figure 7-21 Partitioning of loci into a submeniscal set and a central set. For the sample shown (HT6A) all of the loci in row 1 were excluded due to the thinness of the cartilage and the presence of the clefts in the surface toward the middle of the row. The loci comprising row 2 were assigned to the **submeniscal** group. The loci in rows 4 and 5 were assigned to the **central** group. The loci in row 3, lying approximately on the boundary between the submeniscal and central regions, could not be unambiguously assigned to either group, and hence were excluded from the analysis.

In each of the samples, the central loci exhibit a lower average T_{1Gd} than the peripheral loci, and a dramatically lower average load response (Figure 7-22). Correlations between load response and T_{1Gd} were uniformly extremely strong in the peripheral region with $r = 0.97$, 0.90 and 0.94 ($p < .0001$) across the patient samples. Two of the samples (HT6A and HT11A) demonstrated a clear separation of load response characteristic between the peripheral and central regions, with much higher average load seen peripherally.

The load response T_{1Gd} data for HT3A do not appear to cluster into such distinct peripheral and central groups (although the highest loads are still seen peripherally). This appears consistent with the observation that the surface of HT3A appears to show less difference in surface appearance between the peripheral and central regions than the other specimens (Figure 7-20). It is again interesting to note that the patient whose knee yielded HT3A was significantly younger than the other two patients: 62 years old, compared to 78 years old (HT6A) and 81 years old (HT11A).

For HT3A, the difference in the slopes of the linear regression lines for the load-$T1_{Gd}$ relationship for the submeniscal (slope = 9.3) and central (slope = 5.3) regions did not quite reach statistical significance (p = .051). The differences in regression line slopes between regions for HT6A (submeniscal slope = 4.0, central slope =1.2) and HT11A (submeniscal slope = 5.3, central slope = 1.9) *were* statistically significantly different (p = .0012 for HT6A, p = .0002 for HT11A).

Relationship between load response–$T1_{Gd}$ correlation and ROI depth, partitioned by region

The strength of the correlation between load response and locally-averaged $T1_{Gd}$ as a function of the ROI depth employed for $T1_{Gd}$ averaging (see section 7.4) was reexamined separately for the submeniscal and central regions of each sample (Figure 7-23). Although somewhat different patterns of correlation with respect to depth are seen between samples and regions, the peak correlation in all cases occurs between 500 μm and 1000 μm, roughly two to three times the indentation depth. One region (the central region of HT6A) displayed negative correlation with increasing depth. Examination of the $T1_{Gd}$ map for this sample showed that in the central region, lower $T1_{Gd}$ superficially (and hence lower GAG superficially) tended to be associated with higher $T1_{Gd}$ deeper to the surface. The load response presumably reflected the GAG content in the more superficial region, i.e., the region interrogated by 300 μm indentation: averaging $T1_{Gd}$ to greater depths tended to include deeper GAG-rich regions (which presumably did not contribute as significantly to the variation in load response) and the correlation therefore reversed sign.

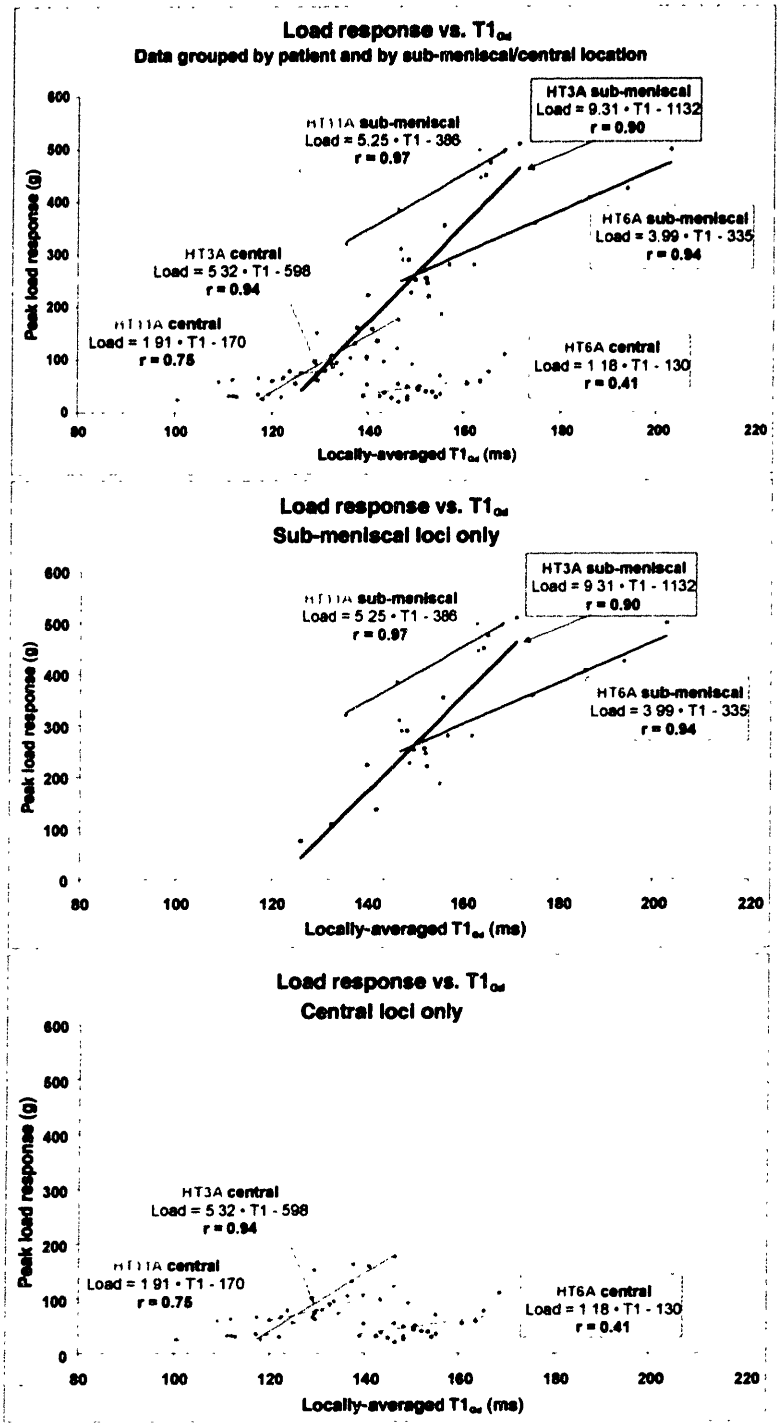

Figure 7-22 Data reanalyzed after partitioning into submeniscal **(middle)** and central **(bottom)** regions. The submeniscal loci exhibit uniformly high correlations between load response and locally-averaged T1$_{Gd}$. The central regions also exhibit significant correlations, but with more variability between samples. Samples HT6A and HT11A appear to show two distinct groups of load response-T1$_{Gd}$ relationship, based on submeniscal/central grouping. Sample HT3A, which exhibited the least frank variation in the appearance of the articular surface (and was from the youngest patient), does not exhibit a distinct separation between peripheral and central responses (p value for difference in submeniscal/central slopes equals .051, .0012 and ,0002 for HT3A, HT6A and HT11A, respectively).

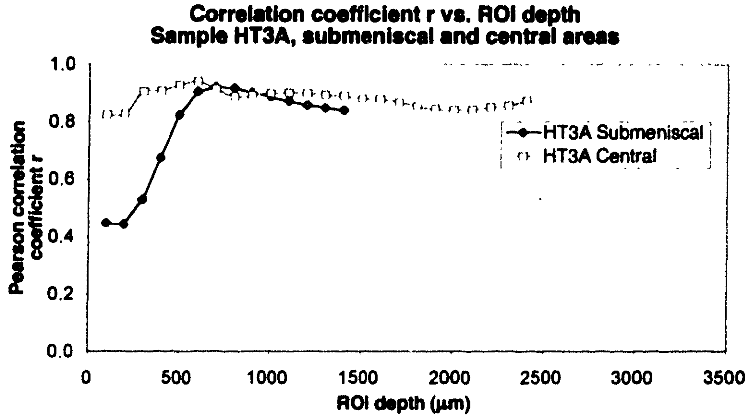

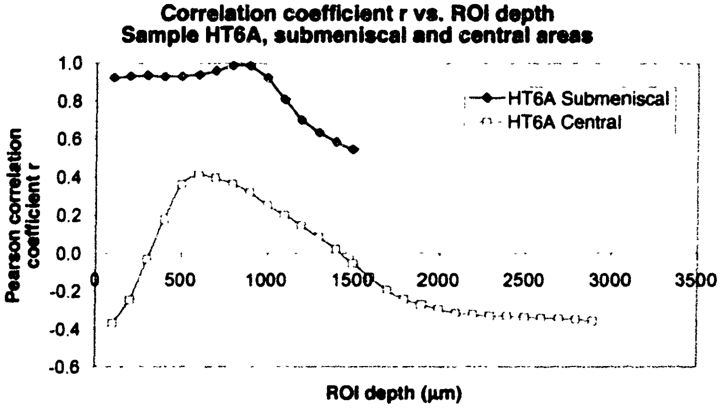

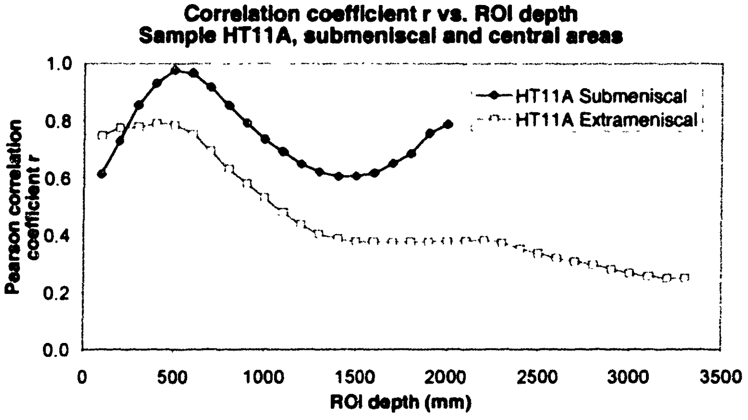

Figure 7-23 Variation in correlation between load response and locally-averaged $T1_{Gd}$ as a function of the depth of the ROI used for $T1_{Gd}$ averaging. (ROI width was constant at 1.5 mm). For each curve, the maximum depth examined is equal to the minimum depth of all test loci in that region (deeper averaging would have included subchondral bone for some loci).

Chapter 8

Discussion, Conclusions and Further Directions

8.1 Discussion

This study was conceived to determine if a noninvasive, nondestructive MRI-based method could be applied to estimate the stiffness of cartilage. Data acquired by an MRI-based imaging method were registered and correlated with the results of a test of stiffness (pulse indentation with a round-tipped indenter) intended to approximate the diagnostic probing of an articular surface by a surgeon.

To achieve close registration between the sites of indentation testing and the regions in which $T1_{Gd}$ was examined, we developed a methodology which permits *in situ* mechanical measurements and dGEMRIC-measured $T1_{Gd}$ (or GAG) values to be registered with submillimeter accuracy for test sites on an articular surface. This method utilizes a matrix of MR-lucent markers, fixed in location with respect to the sample, in conjunction with calibrated positioning of the sample for mechanical testing. The surface localization, pulse indentation and sample positioning protocols exhibited a high degree of repeatability (as did reproducibility with different operators and with long-term retesting). The measured load response was sensitive to focal deficits in cartilage mechanical integrity.

Correlation of load response and $T1_{Gd}$ (as an index of cartilage GAG)

The results of the correlation analysis demonstrated that the local compressive load response to short-time indentation is highly correlated with the colocal average $T1_{Gd}$ (and, consequently, GAG concentration) at the sites of indentation (Figure 7-7 and Figure 7-9).

To control for the potential confounding effect of cartilage thickness variation on load response, measurements of cartilage thickness were made at each test locus and the load–$T1_{Gd}$ data were reanalyzed for only those loci with cartilage thickness ≥ 2.0 mm. Based on a finite element model, variation of thickness ≥ 2.0 mm was predicted to cause less than 20% variation in load response. However we still observe a 500% or greater variation in load response and high correlations between load response and locally-averaged $T1_{Gd}$ for loci with thickness ≥ 2.0 mm. This indicates that the observed load-$T1_{Gd}$ correlation cannot be ascribed to a simple consequence of thickness variation, and supports the view that the variations in load response are a consequence of variations in the intrinsic mechanical properties of the cartilage, and that these variations are significantly related to glycosaminoglycan content.

Colocalization of GAG assessment to the site of indentation–the importance of registration and ROI selection

Finite element analysis indicated that, with 300 μm indentation, the upper 50th percentile of stress occurs in a volume with a depth between 600 μm and 750 μm (Figure 6-6). Empirically, we found the overall correlation between stiffness and locally averaged $T1_{Gd}$ exhibited a broad peak for ROI depths (the depth of the ROI over which $T1_{Gd}$ was averaged) in the range of 300 μm to 700 μm (Figure 7-10). The correlation decreased as ROI depth increased beyond 700 μm. This suggests the importance of the choice of the region over which GAG is assessed in studies of the relationship between indentation stiffness and GAG. In particular, it suggests that for a valid examination of the correlation between an indentation test and local GAG content, the region over which GAG is assayed must be representative of the GAG content in the region of cartilage actually subjected to compressive stress by the indentation.

In Figure 8-1, the illustration on the left schematically depicts the indenter used in the current study and the region (ROI) beneath the indenter over which $T1_{Gd}$ was averaged in order to compute a "locally-averaged $T1_{Gd}$" value. The ROI closely matches the region shown by the FE model to contain the highest stress (Figure 6-6) due to the indentation. In Section 2.4.1, we indicated that there are conflicting reports in the literature regarding whether short-time indentation response is correlated to GAG content. Figure 8-1 (right) shows the relation between indenter geometry and cartilage plug size used in the study by Franz, Hasler, Hagg et al. (2001) which found no correlation between indentation stiffness and proteoglycan content. In this study, the ratio of the area of the indenter footprint to the area of the cartilage plug extracted for biochemical analysis of proteoglycan was 21:1.

In another recent study (Bae, Temple, Rivard, et al. 2002), again comparing indentation response (using an instrumented hand-held probe) to biochemically assayed GAG content at the sites of indentation, the ratio of indenter footprint to plug area was 100:1. This study found only a weak correlation (that did not quite reach statistical significance)

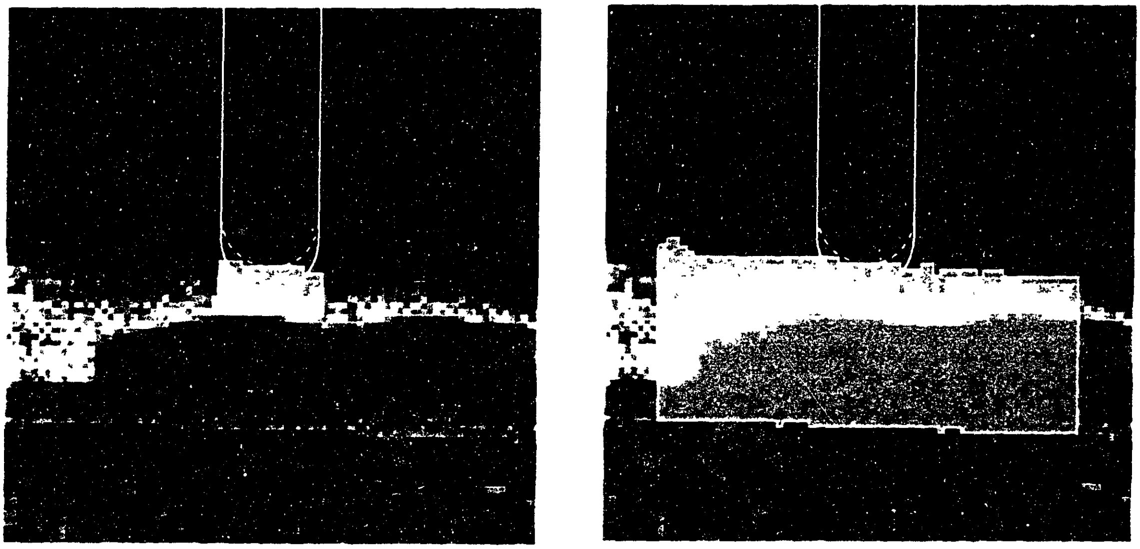

Figure 8-1 **(left)** Illustration, to scale, of the indenter geometry, indentation depth and region over which $T1_{Gd}$ was averaged in the main studies performed for this thesis. The position of the indenter as it just touches the surface is indicated with a dotted line; the solid outline represents the indenter after displacing 300 µm into the articular surface. (The image shown is an enlarged portion of the GAG map of Figure 7-8(a), approximately corresponding to relative location number 8.) The ROI used for $T1_{Gd}$ averaging is indicated by light gray shading: the depth shown is 600 µm. **(right)** Illustration, to scale, of the approximate relationship between indentation and the region assayed for proteoglycan content in the recent study of Franz, et al. (2001). This study found no correlation between cartilage indentation stiffness and proteoglycan content.

between stiffness and GAG (r = 0.24, p = 0.051).

A possible explanation for these results is that there was insufficient colocalization of GAG measurement to the region of indentation stress in these studies for a valid correlation to be obtained. Significantly, both of the studies cited above examined human knee articular surfaces exhibiting natural variation in cartilage integrity. As the results of the current study have shown, stiffness and GAG can vary significantly over a distance of only a few millimeters. As shown in Figure 8-2, load differences of greater than 70% were seen between adjacent test loci (spaced 1.5 mm apart) on samples HT3A, HT6A and HT11A (differences of over 150% in measured load were seen 1.5 mm apart on both HT3A and HT11A).

If a high degree of spatial variation in stiffness and GAG is present, it would be expected that a correlation between focal indentation stiffness and GAG might not be obtained if the regions of GAG assay were not closely matched to the sites of indentation. Essentially, if, as in the studies cited above, the region of GAG assay is much larger than the indenter footprint, the GAG assay may be averaging out local variation that the indenter detects.

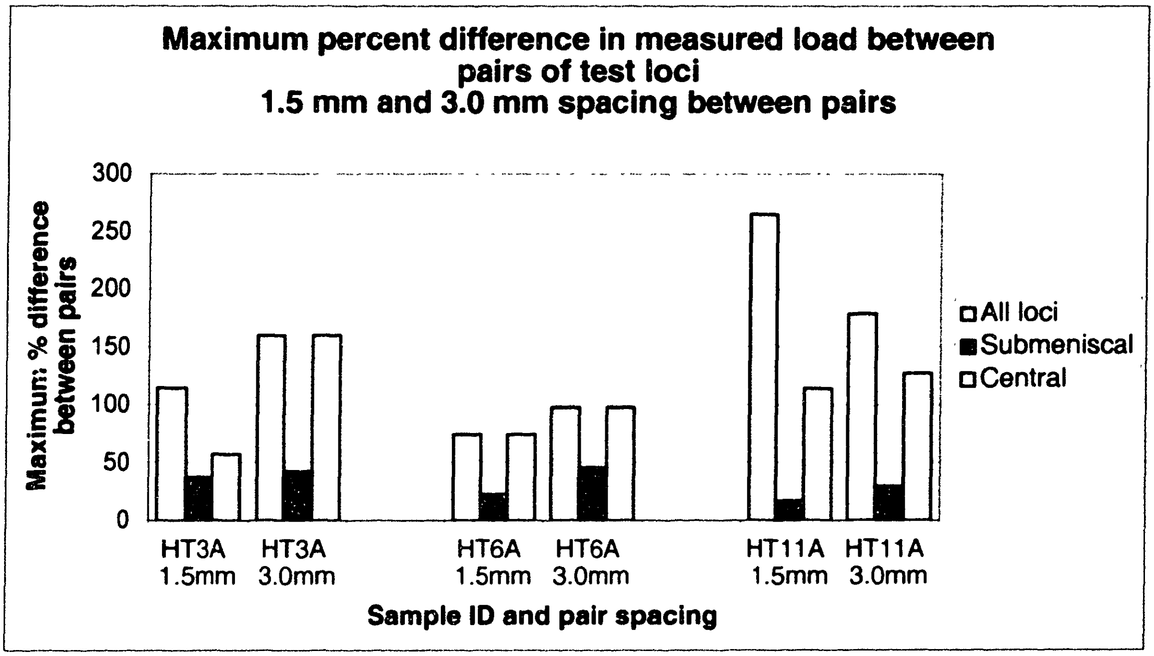

Figure 8-2 An examination of the spatial variability in stiffness for three samples of human tibial plateau. The difference in measured load response between pairs of loci 1.5 mm apart and 3.0 mm apart was determined for each sample. (Pairs were taken only from the same colinear row of loci). With 1.5 mm spacing, differences greater than 70% were observed for all samples.

We also note the study of Lyyra, Arokoski, Oksala et al. (1999) (again, described previously in Section 2.4.1) which *did* find focal indentation stiffness (measured with an instrumented hand-held probe) to decrease when GAG content decreased. In this study, the GAG content of bovine cartilage was interventionally modulated by degradation in trypsin or chondroitinase ABC. Enzymatic digestion typically creates spatially uniform reduction in GAG (see, for example, the $T1_{Gd}$ surface map of a half-trypsinized bovine sample from the present work shown in Figure 8-8). Therefore, it is a reasonable hypothesis that the GAG content in the regions of tissue assayed biochemically in this study was similar to the local GAG content at the indentation sites.

We suggest that some of the disparate findings regarding the relationship of short-time indentation stiffness and GAG content are explainable on the basis of whether the GAG measurements accurately represented the GAG content in the cartilage subjected to compressive stress by the indenter. The results of this thesis suggest that the combination of dGEMRIC GAG assessment and the mechanical-MRI registration technique employed herein offer a means to ensure that indentation measures of stiffness can be accurately colocalized with measures of GAG content. When such colocalization is achieved, the results of the current study indicate that focal indentation stiffness and GAG content are highly correlated.

Differences in the relationship between load response and $T1_{Gd}$ in the submeniscal and central regions of the tibial plateau

Although we observed high overall correlations between load response and $T1_{Gd}$, some samples displayed considerable dispersion in the data: i.e., a large range of load responses were observed for a small range of $T1_{Gd}$ (Figure 7-9 b,c). For example, for $T1_{Gd}$ in the range of 170 ms – 175 ms, we see a range of load responses for HT6A of approximately 100 g to 270 g. HT11A shows similar characteristics: for $T1_{Gd}$ approximately equal to 170 ms, two clusters of load responses are seen – one cluster near 500 g and the other near 270 g. This clustering in load response for a small range of $T1_{Gd}$ persisted for some samples and $T1_{Gd}$ ranges even after limiting thickness variation to $t \geq 2.0$ mm (Figure 7-18). This dispersion and clustering in the load–$T1_{Gd}$ data suggested that an additional variable or variables were influencing load response besides GAG content and cartilage thickness.

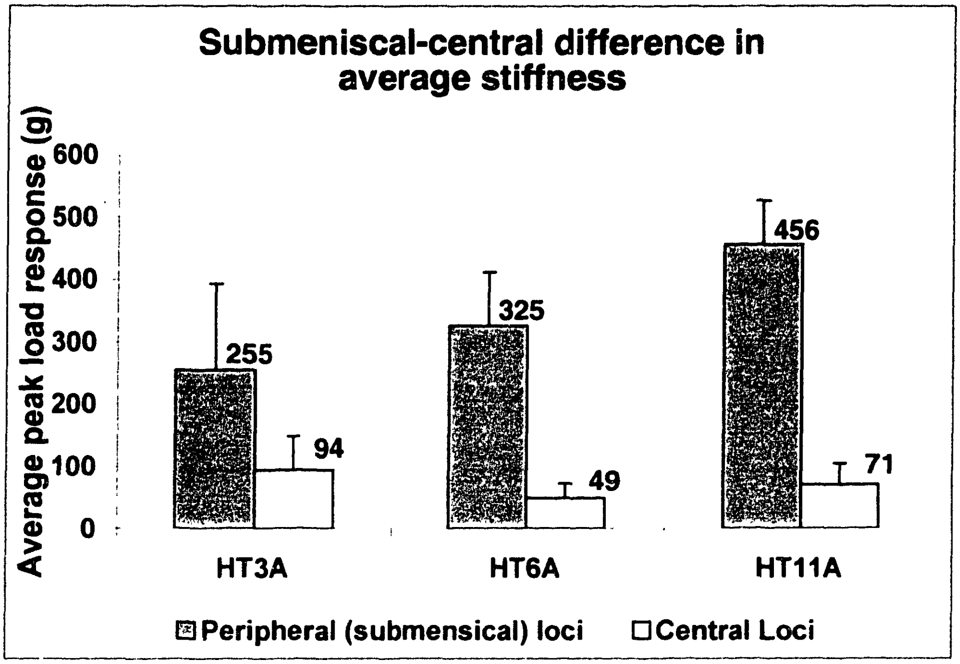

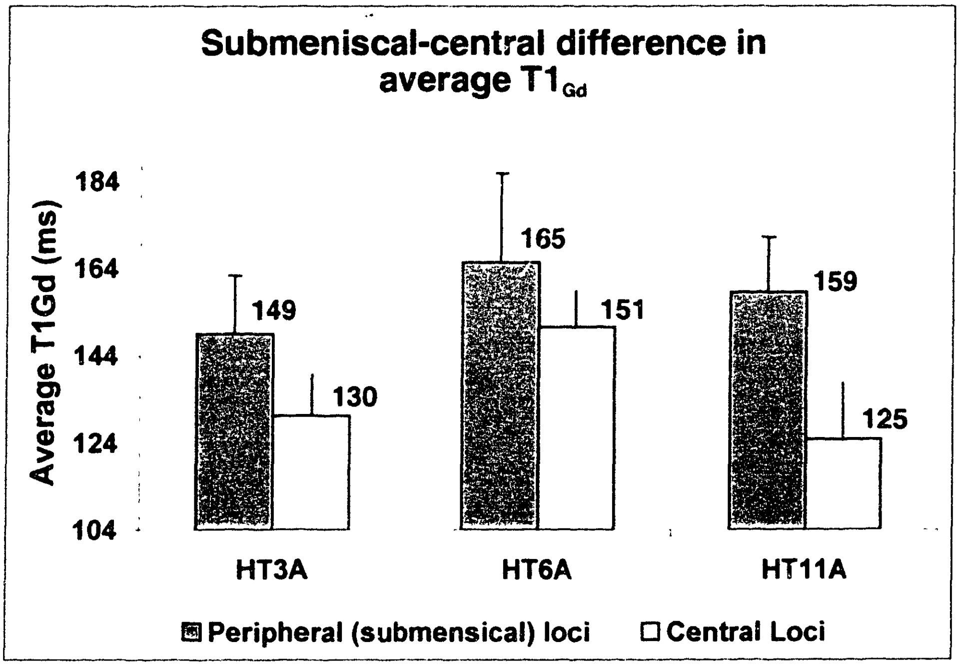

Figure 8-3 **(top)** The average load response of loci in the peripheral (submeniscal) region is 2.7 (HT3A) to 6.6 (HT6A) times higher than the average load response of loci in the central region. (Error bars indicate s.d.) **(bottom)** The average $T1_{Gd}$ is also higher in the submeniscal region ($p < .003$ for each sample), but the difference in $T1_{Gd}$ is insufficient to fully account for the difference in submeniscal/central load response for HT6A and HT11A (see text).

When the submeniscal region was evaluated separately, very high correlations between load and $T1_{Gd}$ were found (Figure 7-22). The average load response in the submeniscal region was also much higher ($p < .001$ for each sample) than in the central region (Figure 8-3 top).

While it is true that as a general pattern the submeniscal region is thinner than the central region, on the basis of the results of the finite element analysis the dramatic difference in average load response cannot be ascribed solely to submeniscal-central thickness difference. The predicted difference in load response due to the difference in average thickness between the submeniscal and central regions is 25% or less for all samples, whereas the difference in average load response between the submeniscal and central regions is between 170% (ratio of average loads between regions = 2.7) and 560% (ratio of average loads between regions = 6.6) (Figure 8-3 top). This data is summarized in Table 8-1.

		Average Thickness in Region (mm)	**FE Predicted Load for Average Thickness (Normalized)**	**Predicted % difference in stiffness due to thickness**	**Measured % difference in stiffness**
HT3A	submeniscal	1.9	3.22	**13%**	**170%**
	central	2.7	2.84		
HT6A	submeniscal	1.8	3.33	**25%**	**560%**
	central	3.6	2.66		
HT11A	submeniscal	1.8	3.33	**17%**	**540%**
	central	2.7	2.84		

Table 8-1 The difference in thickness between the submeniscal and central regions does not account for the difference in stiffness (load response to indentation) between the two regions.

Our findings are in agreement with the results of a recent study by Shepherd and Seedhom (Shepherd and Seedhom 1999) who examined the instantaneous compressive modulus at sites in the human hip, knee and ankle. They found a statistically significant difference in compressive modulus between the "covered" (submeniscal) and "direct" (central) regions of the tibial plateau in each of 10 joints tested. (The average ratio of the submeniscal modulus to the central modulus was 2.7, with a range of 1.5 to 3.6). A recent study by Appleyard, Swain, Khanna et al. (2001) found a similar pattern of variation in *dynamic* stiffness of sheep tibial plateaux using a handheld instrument. They found that the cartilage located beneath the menisci was 200% to 500% stiffer (dynamic shear modulus) than the central cartilage, although in this study only 9 locations were tested per hemi-plateau and the investigators did not report the difference in thickness between the submeniscal and central test locations.

As indicated in Figure 8-3 (bottom), average $T1_{Gd}$ (and therefore GAG) is higher in the submeniscal region compared to the central region. To examine whether the higher stiffness submeniscally could be accounted for solely on the basis of the higher average $T1_{Gd}$ submeniscally, an analysis of covariance was performed. In this analysis, the submeniscal and central load averages were first adjusted by the common slope of the load-$T1_{Gd}$ regression line, and then the difference between the adjusted average loads was tested using t statistics (this procedure is essentially a test to determine if the submeniscal and central load-$T1_{Gd}$ regression lines are significantly separated, i.e., whether their intercepts are significantly different; the details of this test are provided by Armitage and Berry (1987)). This analysis showed that for samples HT6A and HT11A there was a highly statistically significant difference ($p < .0001$) in load response between the submeniscal and central regions even after the difference in $T1_{Gd}$ between the two regions was taken into account. For HT3A there was *not* a statistically significant difference ($p = 0.71$) in load response between the submeniscal and central regions once the difference in $T1_{Gd}$ between the two regions was taken into account. This is a quantitative statistical verification of the qualitative observation (made in Section 7.6) that the load response data and load-$T1_{Gd}$ regression lines for HT3A do not appear to cluster into distinct submeniscal and central groups, whereas the load response data for HT6A and HT11A and the resulting load-$T1_{Gd}$ regression lines are clearly separated between the submeniscal and central regions (Figure 7-22). (We recall that HT3A was the sample from the youngest patient, and showed the least visible variation in surface appearance between the submeniscal and central regions.) The differences in statistics for the load-$T1_{Gd}$ regression analyses for the submeniscal and central regions for each sample are summarized in Table 8-2.

This analysis, in combination with the analysis of thickness presented above, indicate that for HT6A and HT11A some factor (or factors) in addition to GAG content and thickness variation is affecting indentation stiffness.

	Load-$T1_{Gd}$ Regression Line Slope			
	Submeniscal	**Central**	**p value for Δ between slopes**	**p value for Δ between average loads adjusted for Δ in average $T1_{Gd}$**
HT3A	9.3	5.3	.051	.71
HT6A	4.0	1.2	.0012	<.0001
HT11A	5.3	1.9	.0002	<.0001

Table 8-2 Summary of the statistical analyses of the relationships between load response and $T1_{Gd}$ in the submeniscal and central regions. (The regression line slope data have already been presented in Section 7.6.) The right column presents the p value for the difference in average load between the submeniscal and central regions after adjusting for the difference in average $T1_{Gd}$ between the two regions. HT6A and HT11A show statistically significant differences in the load-$T1_{Gd}$ relationship and average load (independent of $T1_{Gd}$) between the submeniscal and central regions; HT3A does not.

The visible difference in surface properties between peripheral and central regions suggests an alteration in surface architecture or composition in the central tibial plateau. In a prior study employing scanning electron microscopy, the central region of the tibial plateau in dog, rabbit and human showed distinct differences in collagen fiber arrangement compared to the peripheral, submeniscal zone (Clark 1991). The tangential zone was either nonexistent or very thin in the central region, comprising < 10% of cartilage thickness, compared to the peripheral region in which the tangential zone constituted up to 50% of the thickness. Splits between collagen fibers were seen in the central region. A thin, distinct, 5 μm thick surface layer (presumably the lamina splendens) was also seen in the periphery, but this layer was absent over the central cartilage which appeared "roughened and resembled the knap on a rug" (Clark 1991).

Cartilage is neither homogeneous nor isotropic; when examined histologically, it exhibits layers distinguished by collagen fibril content and orientation (among other characteristics) (Figure 8-4 left). Of particular note is the superficial layer, characterized by a dense network of collagen fibrils oriented tangentially to the surface. Focal indentation is a relatively complex mechanical stimulus which in theory evokes both tensile and compressive stresses (Figure 8-4 right). The superficial tangential tensile stiffness may create a “trampoline effect” (Cohen, Gardner and Ateshian 1993) which may greatly influence the indentation response, particularly for short loading times. The dependence of the short-term indentation response on cartilage collagen content has been demonstrated both theoretically and experimentally by numerous investigators (Lyyra, Arokoski, Oksala et al. 1999; Cohen, Gardner and Ateshian 1993; Bader, Kempson, Egan et al. 1992; Mizrahi, Maroudas, Lanir et al. 1986; Askew and Mow 1978). For example, in a study using similar indentation parameters to the current one (1 mm Ø plane-ended indenter, 300 µm displacement, with measurement of the mean load during the first second of indentation) Lyyra et al. found that superficial collagen derangement or depletion reduced measured stiffness, even when PG content was unchanged (Lyyra, Arokoski, Oksala et al. 1999). Hence it is plausible that the differences we observed in load response-$T1_{Gd}$ relationship between the peripheral and central areas may reflect alterations in collagen content, composition or organization. Such alterations may effect a superposed influence on load response independent of that due to variation in underlying PG content, and hence account for the increased dispersion of load response and data clustering we observed when both submeniscal and central loci were grouped together (Figure 7-9).

This hypothesis also suggests the attractive possibility that the use of MRI techniques to assess articular surface disruption (Grunder, Biesold, Wagner et al. 1998; Winalski, Aliabadi, Wright et al. 1993) or specifically collagen content or disruption (Nieminen, Töyräs, Laasanen et al. 2001; Nieminen, Toyras, Rieppo et al. 2000; Bageac, Gray, Zhang et al. 1999; Wagner, Werner and Grunder 1999; Xia 1998) – for example, mapping of the MRI parameter T2, which has shown sensitivity to collagen – might, in conjunction with dGEMRIC assessment of proteoglycan content, offer even more robust, tightly bound prediction of cartilage compressive load response and enable further enhanced noninvasive mapping of the mechanical stiffness of the articular surface. This is a clear direction for further research.

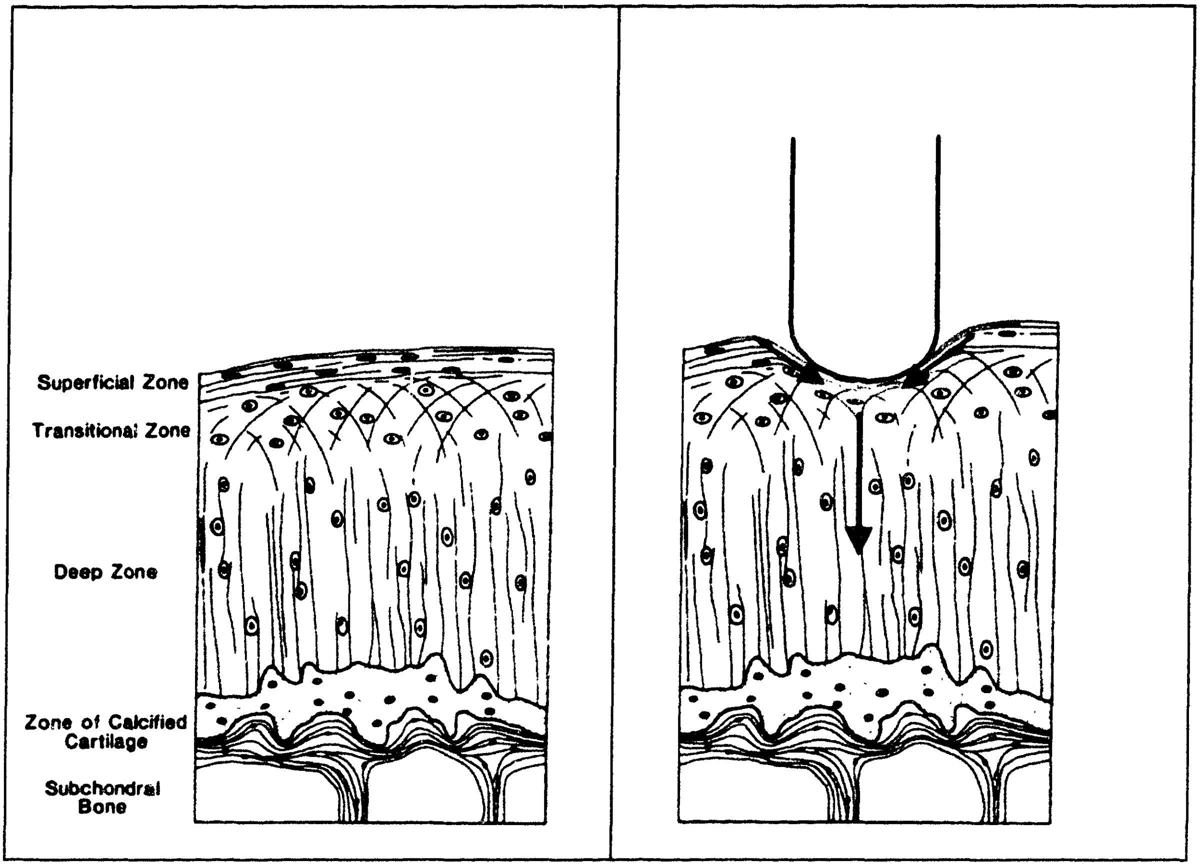

Figure 8-4 **(left)** Cartilage has a layered structure, with a superficial zone which is dense in tangential collagen fibers oriented parallel to the surface. **(right)** Focal indentation causes both tensile and compressive stresses in cartilage. In particular, tensile stresses occur in the collagen fibers near the articular surface (red arrows) while the region centered beneath the indenter is in compression. (Figure adapted and modified from (Bray, Frank and Miniaci 1996).)

8.2 Significance and applications

The current study demonstrates that locally-averaged $T1_{Gd}$ values, acquired through the application of the dGEMRIC methodology following $Gd(DTPA)^{2-}$ equilibration, are a significant predictor of the variability in the mechanical load response of an articular surface to focal compressive strain. The results expand on previous work by relating a non-invasively measured MRI parameter to a functional test of cartilage integrity, a test chosen to be roughly analogous to that routinely employed by surgeons. The current results thus relate the dGEMRIC measurement of $T1_{Gd}$ to cartilage mechanical response to indentation, the latter being similar to the mechanical assessment of cartilage during arthroscopic probing, which is a familiar and essential benchmark for surgeons' assessment of cartilage integrity.

Furthermore, to our knowledge, this is the first study in cartilage to closely localize a biochemical measure to the footprint of a small indenter (with dimensions similar to the hand probe used by surgeons), a capability made possible by the spatial resolution of dGEMRIC and the registration methodology employed. As indicated in the previous section, the results of this study may suggest an explanation for the disparate results reported in the literature concerning the relationship of short-time focal indentation stiffness to GAG content. Specifically, the present results suggest that the examination of the correlation between load response and GAG content in native tissue benefits from the close matching of the region within which GAG is assayed to the region of indentation.

In this section, we will briefly discuss three potential application areas of the results and implications of the current work: (1) preoperative planning and intraoperative guidance, (2) noninvasive cartilage mechanical parameter acquisition for surgical simulation and (3) basic research in the relationship between cartilage biochemistry and its mechanical properties. For each, we will also indicate pointers to future work, which will be described in the following section.

Enhancing preoperative evaluation of articular surface pathology and the creation of images for surgical guidance

An MRI-based imaging method to assess cartilage mechanical integrity promises several benefits vis-à-vis arthroscopic probing, namely: (1) it is noninvasive and does not require anesthesia, (2) it could potentially measure material properties throughout a 3D volume, thereby providing more comprehensive and higher-resolution information on the status of cartilage both across an articular surface and through its depth, (3) it is quantitative and (4) it is not limited by problems of access due to joint morphology.

Magnevist ($Gd(DTPA)^{2-}$) is an FDA approved and commonly used MRI contrast agent, and clinical dGEMRIC studies are currently in routine use for research. Application of the results of the current work to the clinical setting, however, must take account of several challenges. First is the question of resolution. The relatively high resolution scans employed in this study (100 μm pixel size, 1.5 mm slice thickness) required roughly 3 hours of scan time in a small-bore 8.45T research magnet. Current dGEMRIC clinical scans at 1.5T produce resolution on the order of 300 μm (with 2 mm slice thickness). Since the results of the current work tend to suggest that $T1_{Gd}$ measurement near the surface of the cartilage is most important for estimating the load response to surface indentation, current clinical scans offer only two to three voxels in the ROI depth range (600 μm to 900 μm) where the current work saw the highest correlation of $T1_{Gd}$ to indentation load response. Of course, the ROI depth range for maximum load-$T1_{Gd}$ correlation is very likely related to the depth of indentation employed (and hence the depth of the strain field in the tissue) as suggested by preliminary evidence in this study (see, for example, Figure 4-7 and associated discussion in Section 4.3.1.) A priori, it would seem unlikely that probing by hand would maintain a precisely constant depth of displacement. Therefore further investigation is indicated to determine the relationship between surgeons' clinical assessment of cartilage mechanical integrity and the depth and pattern of dGEMRIC-measured GAG content (this will be addressed in Section 8.3.1.) We do note, though, that smaller voxels sizes with equivalent signal-to-noise ratio and scan time can be achieved by going to higher field strength, and already 3T imagers are being employed for clinical investigational use. At 3T, pixel dimensions on the order of roughly 150 μm could be achieved in a reasonable scan time, approaching the resolution of the current study.

A second and related challenge is segmenting the cartilage surface in a clinical scan. In the current work, the samples were imaged in air so a relatively clean cartilage surface-background interface was obtained. Simple methods such as intensity thresholding proved adequate for segmenting the surface. In vivo, the cartilage surface is bathed in synovial fluid and cartilage surfaces are in close apposition to adjacent surfaces: for example, in the knee the cartilage surface of the tibial plateau is in close apposition with the cartilage surface of the femoral condyles and the fibrocartilagenous menisci. While good contrast is exhibited between cartilage and menisci, a distinct separation is not always evident between opposed cartilage surfaces. More advanced segmentation methods could be a key asset here, for example, methods incorporating shape-based priors (Kapur, Beardsley, Gibson et al. 1998; Kapur, Grimson, Kikinis et al. 1998) which utilize known articular surface morphology to aid the segmentation of the surface. Again, this is a clear direction for further investigation.

Given sufficient resolution and effective segmentation methods, however, the current study suggests that dGEMRIC (alone or in combination with other measures of cartilage biochemical content and structure) offers the potential to noninvasively map the mechanical characteristics of an articular surface.

As an example of this application, a topographic stiffness map of sample HT3A was compared to a $T1_{Gd}$ surface map of the same sample. The load response to pulse indentation was measured on HT3A at 104 locations on a 1.5 mm rectilinear grid (Figure 8-5). The load response data are presented as a color-coded topographic map in Figure 8-6 (top). The locally-averaged $T1_{Gd}$ data (600 μm ROI depth) obtained for this same sample are presented as a color-coded surface map in Figure 8-6 (bottom). Even with the relatively low-resolution of the $T1_{Gd}$ map, the overall pattern of $T1_{Gd}$ variation can be seen to be similar to the pattern of stiffness variation. Specific similarities between the two maps are described in the caption to Figure 8-6.

A map of articular surface stiffness could be used by surgeons prior to a procedure to quickly and comprehensively determine where pathology is indicated. The map could also guide them during procedures to quickly focus on suspect areas and could serve as an adjunct to probing in tightly constrained areas that are difficult to access. The map could be presented as a color-coded overlay on a 3D rendering of the articular surface, making it quickly comprehensible in an anatomically relevant way.

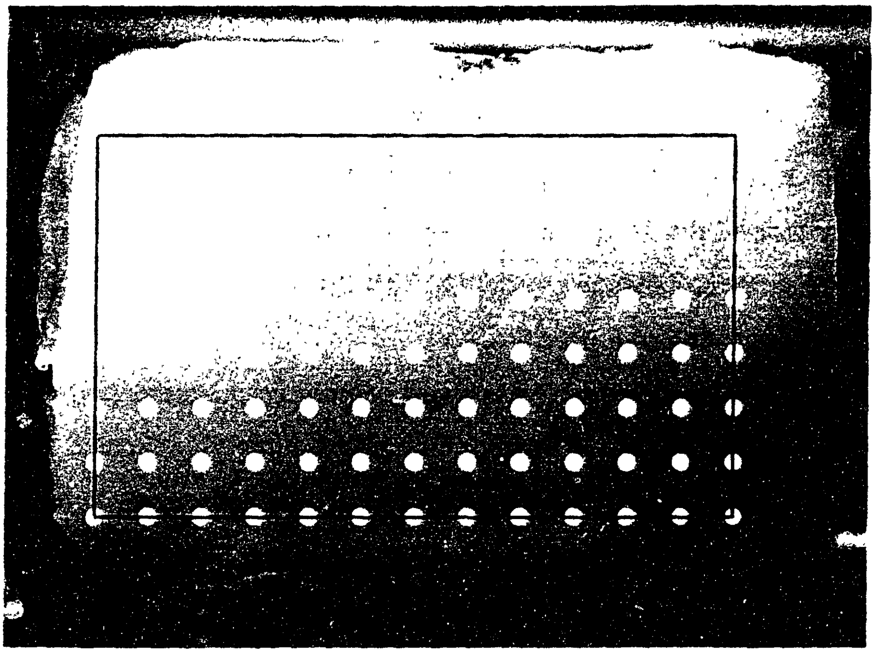

Figure 8-5 Photograph of articular surface of sample HT3A. The white dots indicate 104 locations tested to generate the topographic stiffness map shown in the top image of Figure 8-6.

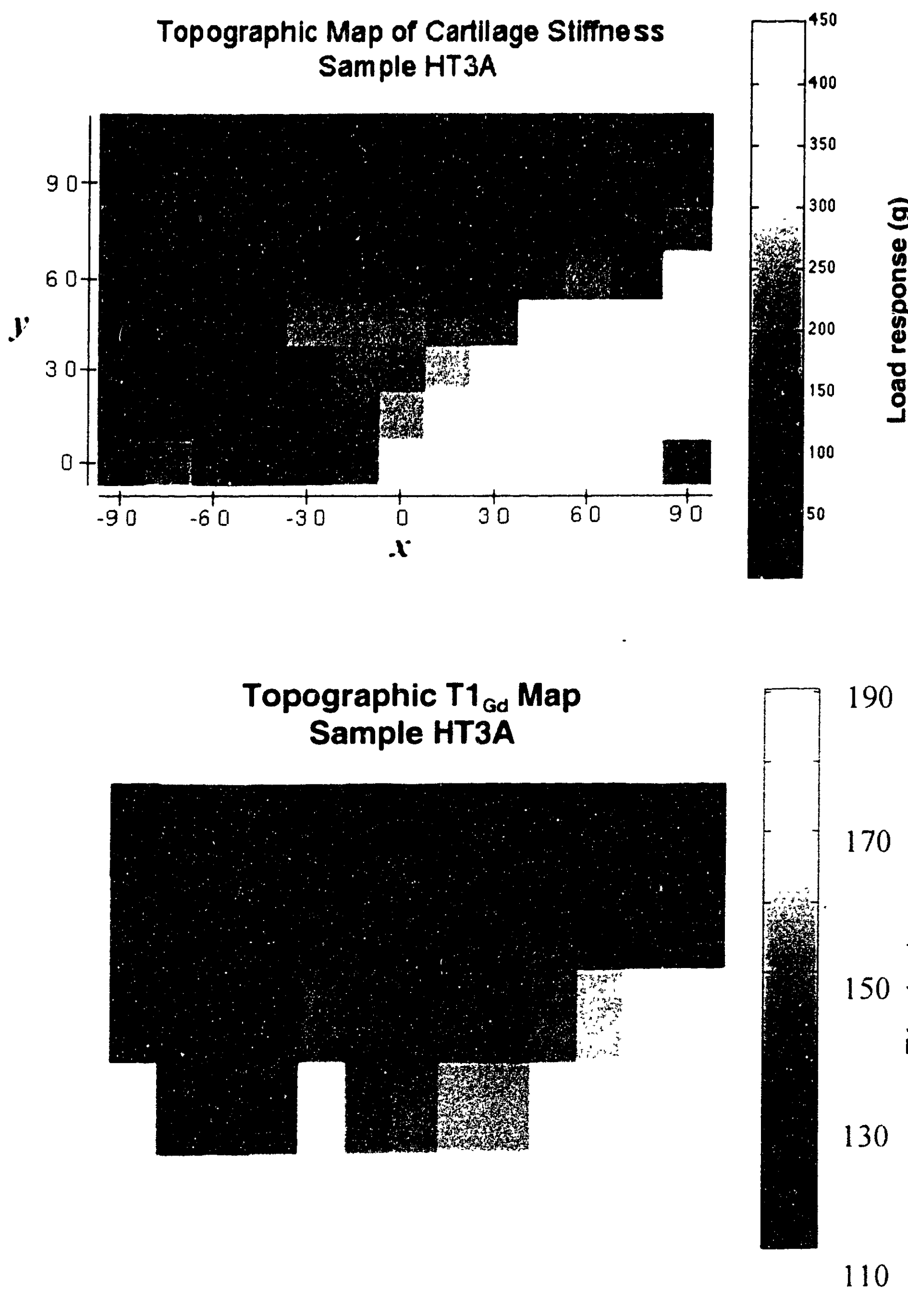

Figure 8-6 **(Top)** Topographic stiffness map for sample HT3A. Each map pixel represents a 1.5 mm by 1.5 mm area. The colorbar units are grams of peak load response (to 300 μm, 0.25 Hz half-sine pulse indentation). The four gray pixels in the lower right corner represent loci with loads exceeding the load cell range (> 500 g). **(Bottom)** MRI-acquired $T1_{Gd}$ map of the same specimen ($T1_{Gd}$ averaged to a depth of 600 μm). The $T1_{Gd}$ map shows generally similar spatial variation to the stiffness map: in particular, areas of softening seen at the top and left edge of the stiffness map correspond to areas of relatively lower T1 in the $T1_{Gd}$ map. Also, the cartilage is stiffest toward the lower right corner of the specimen and this area also exhibits the highest $T1_{Gd}$.

MRI methodologies may enable the creation of such a map noninvasively. As an example, a bovine tibial plateau was dGEMRIC imaged with a 3D protocol (1mM $Gd(DTPA)^{2-}$, 2T, 8 delays between 50 ms and 1500 ms, 10.24 cm by 5.12 cm by 5.12 cm FOV, 256 x 128 x 128 matrix, 400 μm isotropic voxels, 4 hours total scan time).[15] The surface of the sample was segmented (employing 3DSlicer, a program jointly developed by members of MIT's AI Lab and the Surgical Planning Laboratory at the Brigham and Women's Hospital, Boston) and rendered: the result is shown in three different views in Figure 8-7.

The plan view (Figure 8-7 bottom) can be compared with a plan photograph of the actual sample (Figure 8-8 top). Sample morphology is well represented in the surface renderings, including the notch in the edge of the sample made to indicate the level of trypsinization of the sample. (Prior to imaging, the left half of the sample was immersed for 8 hours in 2.5 mg/ml trypsin solution to degrade GAG content.)

A $T1_{Gd}$ map was computed from the 8 individual 3D data sets (one for each delay time) of the dGEMRIC scan. $T1_{Gd}$ values were averaged to a depth of 3 voxels (1.2 mm) and then mapped onto the surface of the sample. The result is shown in Figure 8-8, along with the photograph of the sample for comparison. The division between softened and normal cartilage is clearly displayed on the $T1_{Gd}$ surface map. Mechanical testing revealed that the roughly 20% decrease in average $T1_{Gd}$ between the two halves was correlated with a roughly 50% – 70% decrease in stiffness. The color-mapped T1Gd surface rendering this serves as a surrogate for a map of directly-measured mechanical integrity.

---

[15] Note that a 3D dGEMRIC study was attempted on sample HT3A but, as of the date of writing, unresolved problems with artifacts in the scan precluded its use for surface reconstruction and mapping.

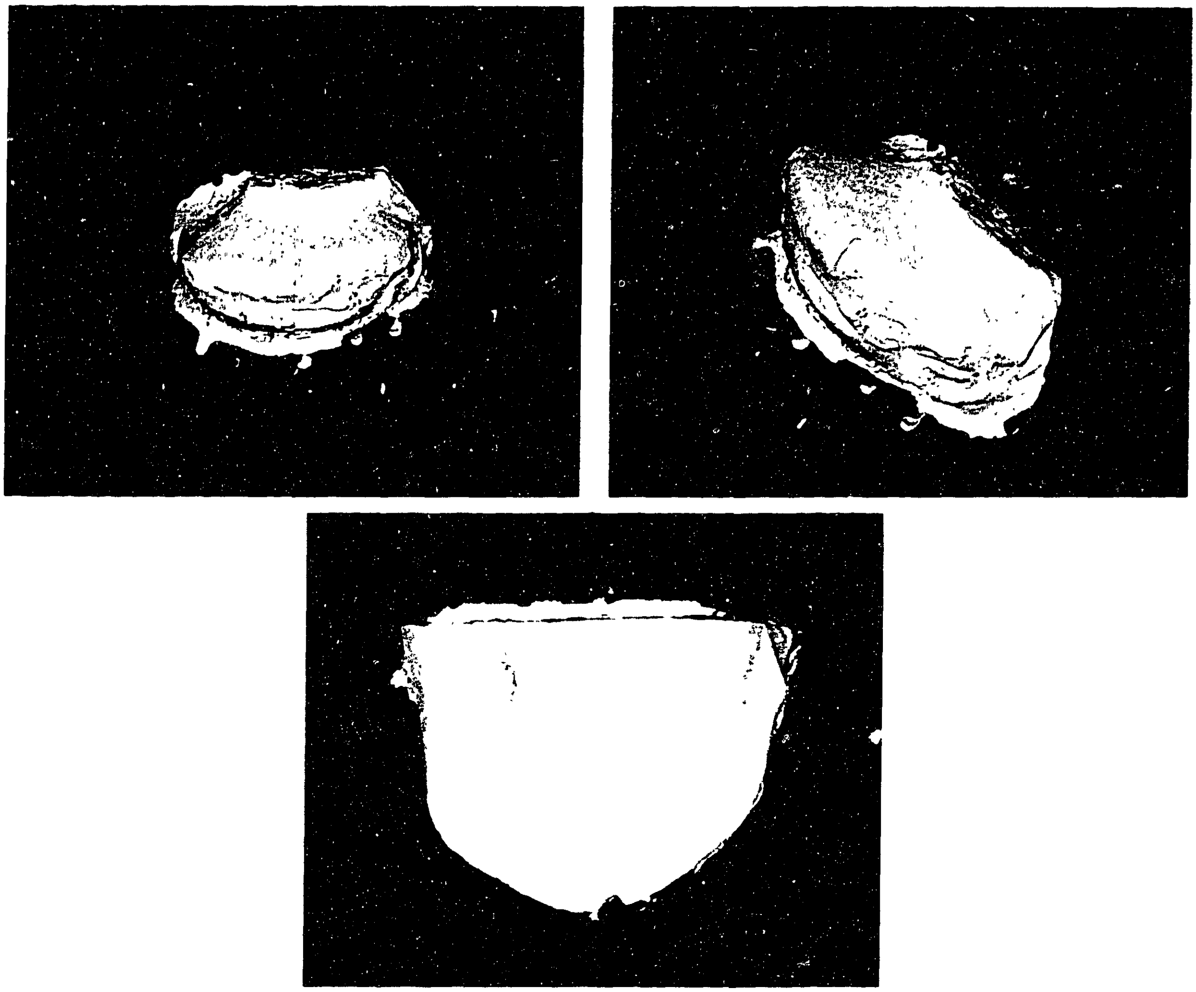

Figure 8-7 Segmented, surface-rendered views of a half-trypsinized bovine tibial plateau. The "spots" around the sample are the Gd(DTPA) filled registration marker holes in the registration frame (Version 2) attached to the sample (see Figure 3-2). (Top left) View looking at peripheral edge of sample, cartilage surface is on top. (Top right) Oblique view. (Bottom) Plan view, looking down at cartilage surface. Flat "mesa" area is cut bone (to reduce sample height). Note the notch in the peripheral edge of the sample: this is a scalpel cut made to demarcate the dividing line between the trypsinized and nontrypsinized halves of the sample.

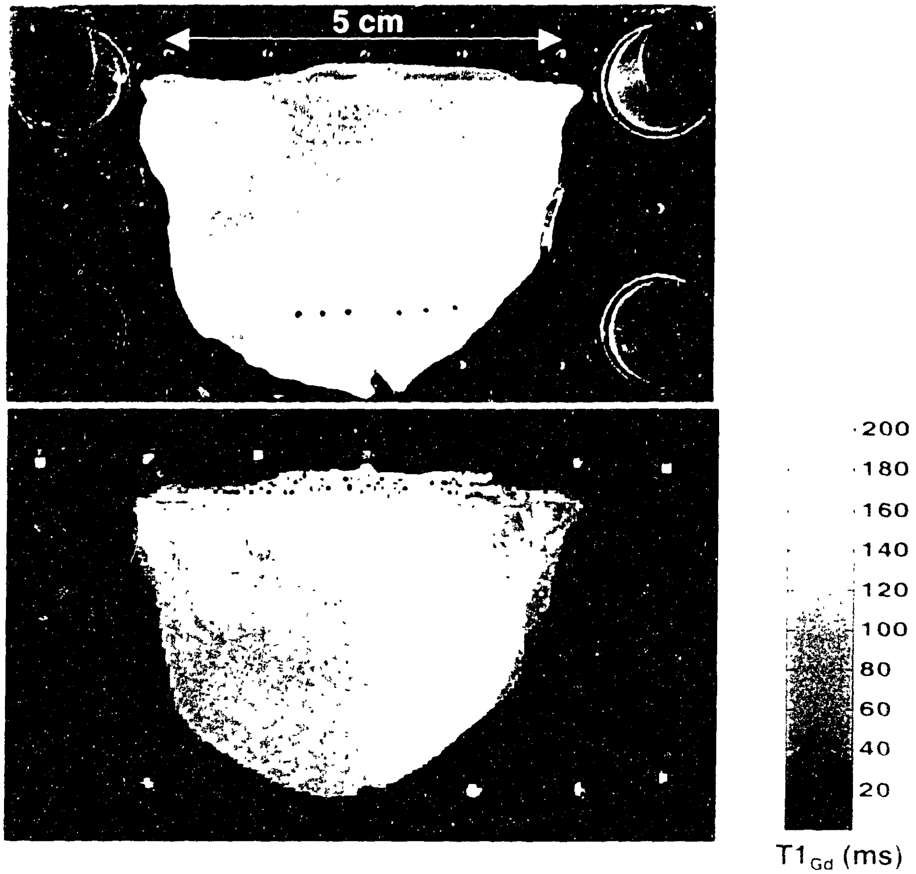

Figure 8-8 **(Top)** Plan view (from above) of bovine tibial plateau. The peripheral edge is oriented downward. The region to the left of the notch cut in the peripheral edge has been subjected to trypsin degradation. A slight darkening of the cartilage, indicative of increased translucency, is seen in the left vs. the right halves of the surface. **(Bottom)** Color map of $T1_{Gd}$ mapped onto the segmented surface (as shown in Figure 8-7). The GAG-depleted trypsinized area is clearly visualized, as is the distinct vertical separation between trypsinized and normal cartilage. Average $T1_{Gd}$ is approximately 150 ms in the normal region and 120 ms in the degraded region. Mechanical testing at the loci marked with ink spots revealed a 55% decrease in transient load response a 73% decrease in equilibrium load response in the degraded region.

The ability to apply a similar technique clinically would enable 3D renderings of articular surface integrity to be presented to surgeons. These "road maps" of pathology would have the morphological appearance of the actual joint surface, and therefore be readily and quickly comprehensible. The demonstrated correlation of the maps with mechanical indices of cartilage integrity could offer guidance to surgeons in familiar and functional terms, thereby offering the prospect of comprehensive, quantitative diagnosis, quicker, more efficient surgeries, and ultimately improved results for the patient. The quantitative nature of $T1_{Gd}$ maps could also permit effective longitudinal monitoring and assessment of the status of a patient's joint health, as well as offering a spatially comprehensive, noninvasive, quantitative means for assessing the efficacy of surgical or pharmacologic therapies.

Surgical simulation

As described in the first chapter, the initial motivation for this project arose from the desire for a means to noninvasively acquire cartilage material property data for incorporation into models of the articular surface in a surgical simulator.

Our understanding of the extraordinarily complex relationship between cartilage biochemical content and organization and its mechanical behavior has only recently reached a stage where FE models are able to accurately reproduce experimental results across different mechanical stimulus protocols (DiSilvestro and Suh 2001). Much work still needs to be done to elucidate the exact relationship between cartilage GAG and collagen content and architecture, in a fully anisotropic and heterogeneous model, and mechanical response to an arbitrary perturbation by an indenter of arbitrary geometry. Even were such a relationship known, a full 3D FE implementation of it for the complex geometry of an actual articular surface would almost certainly be sufficiently computationally expensive that it could not run fast enough for real-time surgical simulation, where visual frame update rates on the order of 30 Hz and haptic force-feedback update rates on the order of 1000 Hz are required.

An alternative approach is to experimentally determine a phenomenological (or multi-parametric statistical) relationship between indentation with a fixed geometry indenter and the resulting cartilage deformation and/or load response. Over a limited domain of indentation geometry, depth and rate (such as may obtain during arthroscopic hand probing) the data from studies such as the current one could potentially provide information on tissue response that would be applicable to a simplified model sufficiently accurate for task-specific perceptually-realistic simulation. For example, correlations between GAG content and load response to short-time indentation with an indenter similar to that employed during arthroscopic probing might provide parameters for a model of the specific task of probing a virtual articular surface in a simulator of arthroscopic surgery. Although task-specific, this could offer a much greater degree of realism than is currently available with, for example, plastic models. The ability to approximate actual patterns of softening as measured in actual patients would allow a greater range of tasks to be simulated and, potentially, a greater range of psychomotor skills to be developed which might then transfer from the simulated environment to the care of actual patients.

To assess how closely the results of the current work come to actual applicability for mechanical property measurement for surgical simulation, some idea is needed of the fidelity of stiffness measurement necessary to support perceptually realistic simulation of the probing of the articular surface. The issue is further complicated by the phenomenon of sensorimotor visual-haptic interactions in the perception of stiffness. Visual cues can have a significant effect on the perception of the stiffness of objects (Lécuyer, Burkhardt, Coquillart et al. 2001; Wu, Basdogan and Srinivasan 1999; Durfee, Hendrix, Cheng et al. 1997) to the extent that visual perception of deformation can dominate force-feedback sensation in perceiving which of two simulated objects is stiffer (Srinivasan, Beauregard and Brock 1996). Furthermore we are not aware of any studies to date that have been done directly addressing the issue of how accurately the response of a compliant object needs to be simulated (in either its visually perceived deformation response or its haptically perceived force-feedback behavior) in order to provide skills transfer in learning a task involving interaction with the object.

Nevertheless, to make some attempt at assessing applicability to haptic simulation, we examined prior work examining Weber fractions for assessing the stiffness of objects. A Weber fraction expresses the fractional change in a parameter to be just noticeable perceptually–a Weber fraction can also be referred to as a just noticeable difference (JND) if the JND is expressed as a fraction (or percentage change from an initial value). The JND for stiffness perception is relevant to assessing applicability of the load-$T1_{Gd}$ data to simulation in the following manner: suppose we wish to estimate a local cartilage stiffness value (for a simulator model of a cartilage surface) based on a measured $T1_{Gd}$ value. As Figure 7-9 shows, $T1_{Gd}$ is not a perfect predictor of load response: for a given $T1_{Gd}$, a range of load responses occurs. The variability (dispersion) of the load responses about the regression line can be regarded as error or noise in the estimation. However if the magnitude of this error is less than the JND for stiffness, it will not be a *perceivable* error, and hence would presumably not adversely affect the perceptual accuracy of a haptic simulation using the load-$T1_{Gd}$ data to estimate the spatial stiffness parameters for the model.

Jones and Hunter (1993; 1990) investigated the perception of stiffness and viscosity using a two-arm matching procedure in which subjects adjusted the stiffness or viscosity of a servomotor attached to one wrist until it was perceived to be the same as a second servomotor attached to the contralateral wrist. They reported Weber fractions of 0.23 and 0.34 for stiffness and viscosity, respectively. An early study of stiffness discrimination using a rigid surface interface between fingers and compliant objects found a JND for stiffness of 17% (Roland and Ladegaard-Pedersen 1977). Using a pinch-grasp experiment, Tan et al. (1995; 1992) found JNDs for compliance ranging from 8% to 99%, depending on the presence or absence of other cues such as terminal force or mechanical work (force integrated over displacement). An average viscosity JND of 12% (+/- 4% s.d., 6 subjects tested) was reported by Beauregard (1996) in a mechanical fingertip pinch-grasp paradigm.

None of these results are very generalizable. In particular, simulation of arthroscopic surgery involves estimating compliance by probing a surface by focal contact with a long tool with very small deflections of the surface. None of the above studies involved a similar experimental paradigm.

As an order-of-magnitude estimate based on the results of the above studies, we will postulate a benchmark JND range of 10% to 20% for stiffness discrimination.

To compare applicability of the current results to this benchmark, the load–$T1_{Gd}$ correlation data for HT3A, HT6A and HT11A were utilized (Figure 7-9). To compare the variability in load estimates made from $T1_{Gd}$ measurements with a benchmark JND, we computed the residuals for the load and $T1_{Gd}$ data presented in the graphs of Figure 7-9 (i.e., actual load – predicted load, where the predicted load is found from the regression line equation) and then expressed each residual as a percentage of the predicted load. We term these values the *residual fractions*, and they provide a measure of the error between actual load response and predicted load response as a fraction of the predicted value. The average and standard deviation of the absolute values of the residual fractions were then computed for each sample. Finally, the data for each sample were segregated into sub-

	HT3A	**HT6A**	**HT11A**
Overall	26 % +/- 17 % n = 33	66 % +/- 60 % n = 44	54 % +/- 68 % n = 39*
Submeniscal	19 % +/- 11 % n = 10*	8 % +/- 7 % n = 11	3 % +/- 3 % n = 7
Central	23 % +/- 16 % n = 11	26 % +/- 17 % n = 21*	20 % +/- 17 % n = 21*

Table 8-3 Residuals of load-T1$_{Gd}$ regression analyses, expressed as average absolute residual fractions +/- standard deviation. The sum of the n's for the submeniscal and central regions do not equal the overall n, since only those points that could be confidently partitioned between submeniscal and central regions were so assigned. * indicates that one outlying residual fraction was excluded from the total: this typically occurred when the predicted load was near zero, thus resulting in an uncharacteristically large value when the residual fraction (with the predicted load in the denominator) was calculated.

meniscal and central regions, and the average absolute residual fractions were computed for each region. The results are presented in Table 8-3.

The results, as expected, parallel the previously observed patterns of correlation. Overall, HT3A exhibits an average absolute residual fraction (AARF) of 26%, within the range of JNDs reported for stiffness perception. HT6A and HT11A exhibit overall higher AARFs and higher standard deviations. But in all cases, when the data for each sample are classified into submeniscal and central groups, AARFs of 26% or less are obtained. In the case of the submeniscal data, AARFs for all samples are under 20%, within our postulated benchmark range for JNDs for stiffness.

These results suggest that the accuracy with which dGEMRIC can estimate stiffness may approach the range of JNDs for stiffness perception, especially when variation in surface architecture/integrity is measurable and accounted for. This provides further motivation for exploring potential MRI-based methods of assessing collagen content, such as T2 imaging. Note that the results obtained here require only a binary assessment of surface integrity (which is reflected in the submeniscal/central grouping) and not a quantitative model relating collagen content to load response. For the purposes of parameter acquisition for haptic simulation, even a good/bad assessment of the surface or collagen content may yield accuracy in the range of JNDs for stiffness perception.

We note finally that JNDs are a fairly conservative benchmark for evaluating a methodology for parameter acquisition for simulation: they are smallest perceivable differences. The accuracy of parameter estimation needed to provide sufficiently perceptually realistic haptic behavior in a simulated model to provide effective learning and skills transfer may have less stringent bounds.

Basic studies of relationship of GAG and collagen to mechanical properties

The ability to colocalize GAG and the strain field due to indentation in an intact articular surface has numerous applications to our understanding of the basic mechanisms by which GAG supports the stiffness of cartilage and influences deformation behavior.

As was describe previously, FE methods have been developed for simulating the biphasic (poroelastic) material behavior of cartilage. Early models typically made assumptions of isotropy and homogeneity. Recent work has just begun to explore anisotropic and inhomogeneous models, incorporating, for example, gradients of GAG and collagen distribution or the influence of the collagen-rich surface zone on indentation response via its high tensile modulus in the transverse direction (Korhonen, Wong, Arokoski et al. 2002).

The methodology developed in this work could be applied to such modeling efforts. For example, maps of GAG distribution derived from dGEMRIC imaging, colocal thickness measurements, and colocal mechanical response measurements could all be applied to validating a hypothetical FE model of the effect of spatially-localized GAG distribution on indentation response. dGEMRIC could provide an essentially per-node value for GAG distribution as well as the geometry (thickness, surface morphology) of the cartilage layer. Predictions made by the FE model could be validated against the experimentally measured load responses which have been registered and colocalized with the GAG maps. Such a paradigm would potentially provide a powerful tool for advancing the state of the art in modeling cartilage structure and function. The same mechanical-MRI registration methodology developed in the current work could also be applied to T2 imaging, or other MR-based measures sensitive to collagen content.

8.3 Future work, further investigations

8.3.1 Position-tracked force-measuring probe design and experiments

Near the heart of the current research is the question: what are surgeons actually assessing when they probe an articular surface? What are the parameters of the forces and displacements they apply, and what do they see and feel in response? Are their assessments primarily visual or proprioceptive? How does the evaluation of cartilage integrity via hand probing compare with quantitative mechanical testing or biochemical content?

To begin to address these issues, substantial preliminary work was done on the construction of an instrumented surgical probe that could be used *ex vivo* to examine an articular surface. This probe allows the force applied to the tip of the probe to be measured. The position and orientation of the probe is also measured, allowing the position of the probe tip relative to a sample to be quantitated.

This apparatus is intended to support three separate experiments:

(1) *Measurement of surgical gestures during probing*

Very little is currently known quantitatively about the mechanical stimulus applied to the articular surface during traditional arthroscopic probing. The ability to measure force profiles (i.e., force and position as functions of time) as a surgeon examines an articular surface in vitro would provide at least baseline data on the magnitude and rate of loading during probing. This would help us to better relate what is being assessed during surgical probing to other, well-characterized *in vitro* tests of cartilage mechanical behavior.

(2) *Examination of the correlation between hand-probe assessment of cartilage integrity mechanical indentation testing, and between hand-probe assessment and dGEMRIC-measured GAG content (or other MRI indices of cartilage composition and structure.*

In this experiment, a surgeon would hand-probe a sample (such as a human tibial plateau) using the instrumented probe under arthroscopic visualization *in vitro* (Figure 8-12). The sample would be mounted to a registration frame. Using the in-

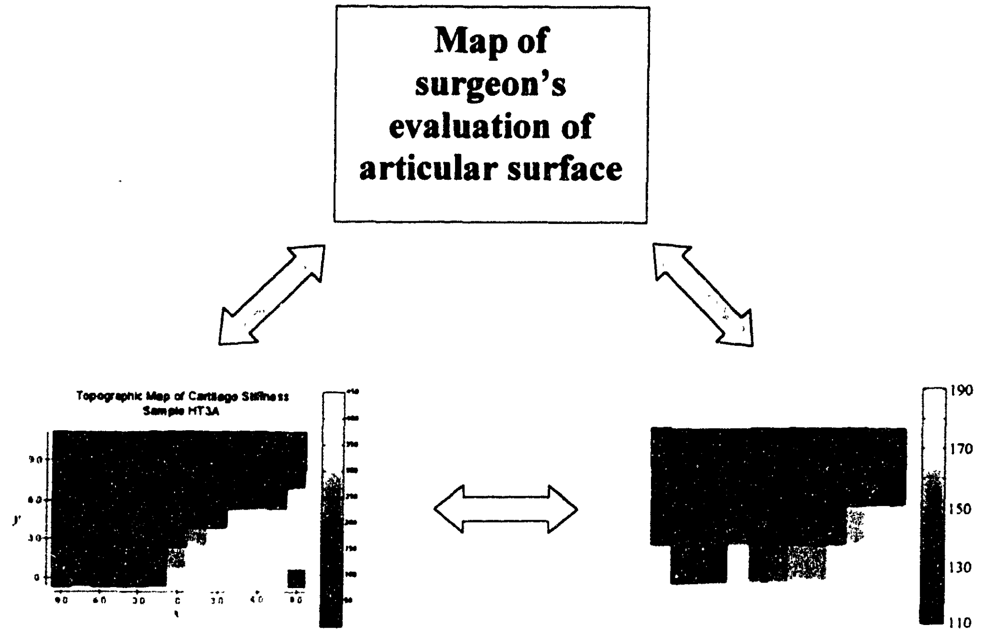

Quantitative stiffness map

$T1_{Gd}$ map

Figure 8-9 Use of the instrumented, position-tracked surgical probe would permit a map of a surgeon's clinical evaluation of an articular surface (top) to be compared to quantitative stiffness maps (obtained by indentation testing such as described in this thesis) and MRI-parameter maps (such as a dGEMRIC $T1_{Gd}$ map). The comparison between MRI-parameter maps and the surgeon's evaluation would be particularly important for providing a basis for a surgeon to interpret the MRI-derived map in a familiar and clinically-relevant manner.

strumented probe to examine the articular surface, the surgeon would provide a running assessment of locations where he or she observed clinically significant findings (softening, varying degrees of chondromalacia, etc.) Since the position of the probe is tracked and the sample is rigidly fixed within the array of marker holes in the registration frame, the probe tip can be calibrated to the marker hole positions and hence its position can be quantitatively calibrated to the sample. Areas determined to have significant pathology can then be tested mechanically. The entire sample would also be dGEMRIC imaged (and/or imaged to examine other potentially relevant MRI parameters such as T2). This would enable, for the first time, an examination of the relationship of what is perceived via clinical probing to quantitative indentation testing and MRI assessment of GAG (Figure 8-9).

(3) *Surgical simulator validation*

After data on force trajectories and surgeons' gestures are obtained via the experiment outlined in (1), the sample can be dGEMRIC imaged and the resulting GAG data employed in the creation of a virtual model of the sample's articular surface. Typically, a simulator employs a standard probe attached at the tip to a haptic device which, as the model is probed virtually, generated the required force-feedback to create a perceptually realistic experience of "feeling" real tissue. In order to validate the total input-output response of the simulator, the *instrumented* probe can be attached to the haptic device so that the actual output forces (and trajectories) occurring during use of the simulator can be quantified. This could then be compared with the previously measured forces and trajectories obtained from the real sample (the same one scanned to generate the simulator model). This would allow, to the best of our knowledge, the first methodology for quantifying the global haptic system fidelity of a simulator, by comparison of simulated haptic output to the actual forces and gestures employed while probing real tissue.

The remainder of this section will provide a brief overview of work already done to build the tracked, instrumented surgical probe.

Construction of prototype foil strain-gaged probe

In order to determine the type and optimize the placement of strain gages to be used in the instrumented probe, an analysis was first made of the expected strain the shaft of a standard arthroscopic surgical probe (Acufex model 010001, Smith and Nephew, Andover, MA) would experience in response to typical loads during probing of an articular surface. This analysis is presented in Appendix D.

A prototype probe was then constructed utilizing foil strain gages (Vishay Measurements Group model EA-06-031DE-350) and bondable terminals (Measurements Group model CPF 25C). Strain gages were placed at two locations along the shaft of the prototype probe (Figure 8-10). At each location, an axial pair of gages was affixed with cyanoacrylate above and below the probe shaft and wired to two arms of a Wheatstone bridge in a half-bridge configuration. Probe linearity was tested by hanging weights on the probe tip and measuring the output of the bridge. Linearity was confirmed to be +/-5%, with sufficient signal from the strain gage pair nearest the probe handle to enable measurements in the range of 50 – 100 g.

Specification and construction of silicon strain-gaged probe

Using the data obtained from testing with the prototype probe, a more sensitive probe was specified using silicon strain gages (silicon strain gages have greater than 10x the gage factor of standard foil gages). The design was forwarded to California Cybernetics (La Crescenta, CA) for construction. The final system consists of the strain-gaged instrumented probe; an electronics package that provides bridge excitation and preamplification of the strain gage signals and also houses an analog-to-optical converter; and an interface board that resides in a PC and communicates control signals for bridge excitation levels, as well as providing an optical interface for input of the preamplified signals (Figure 8-11).

Position and orientation tracking of the probe

To enable the position and orientation of the probe to be tracked, a Phantom haptic interface (SensAble Technologies Inc., Woburn, MA) was adapted for use with the probe. A coupler was designed to rigidly affix the back end of the probe handle to the encoder gimbal of the Phantom. The Phantom arm was appropriately counterweighted to compensate for the mass of the probe. Software and interfaces were attached to the host PC so that six degrees of positional freedom (translation and rotation) could be continuously recorded. Software was designed to translate Phantom coordinate space values to the coordinate space of the registration frame employed with the cartilage samples. Coupled with a probe-registration plate calibration routine, this will permit the coordinate system to be registered with the coordinate frame of the sample.

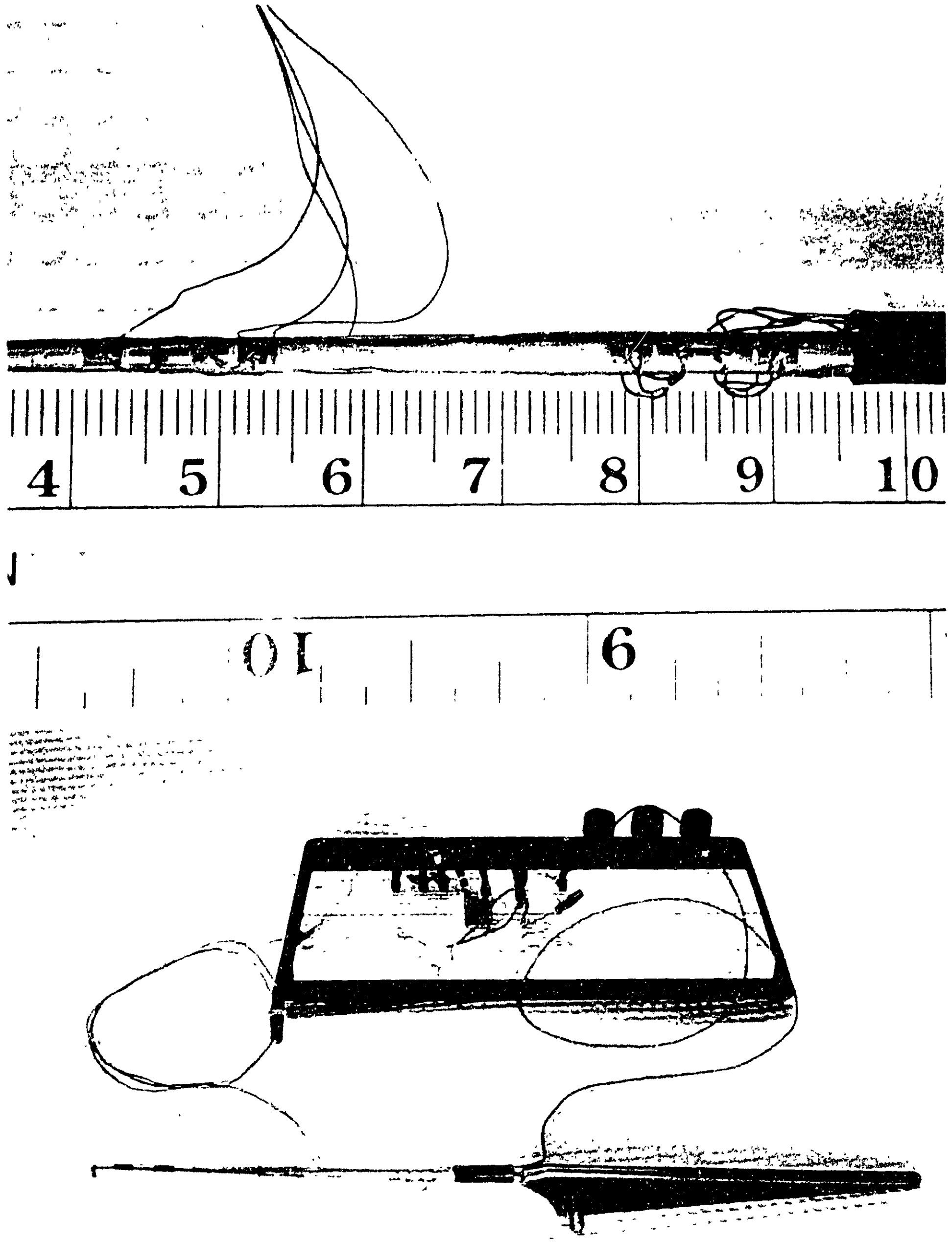

Figure 8-10 **(Top)** Detail of foil strain gage placement on probe shaft. Only one gage is visible at each location–a second gage is directly opposite each visible gage on the far side of the probe. **(Bottom)** Probe wired to half-bridge circuit (passive electronics).

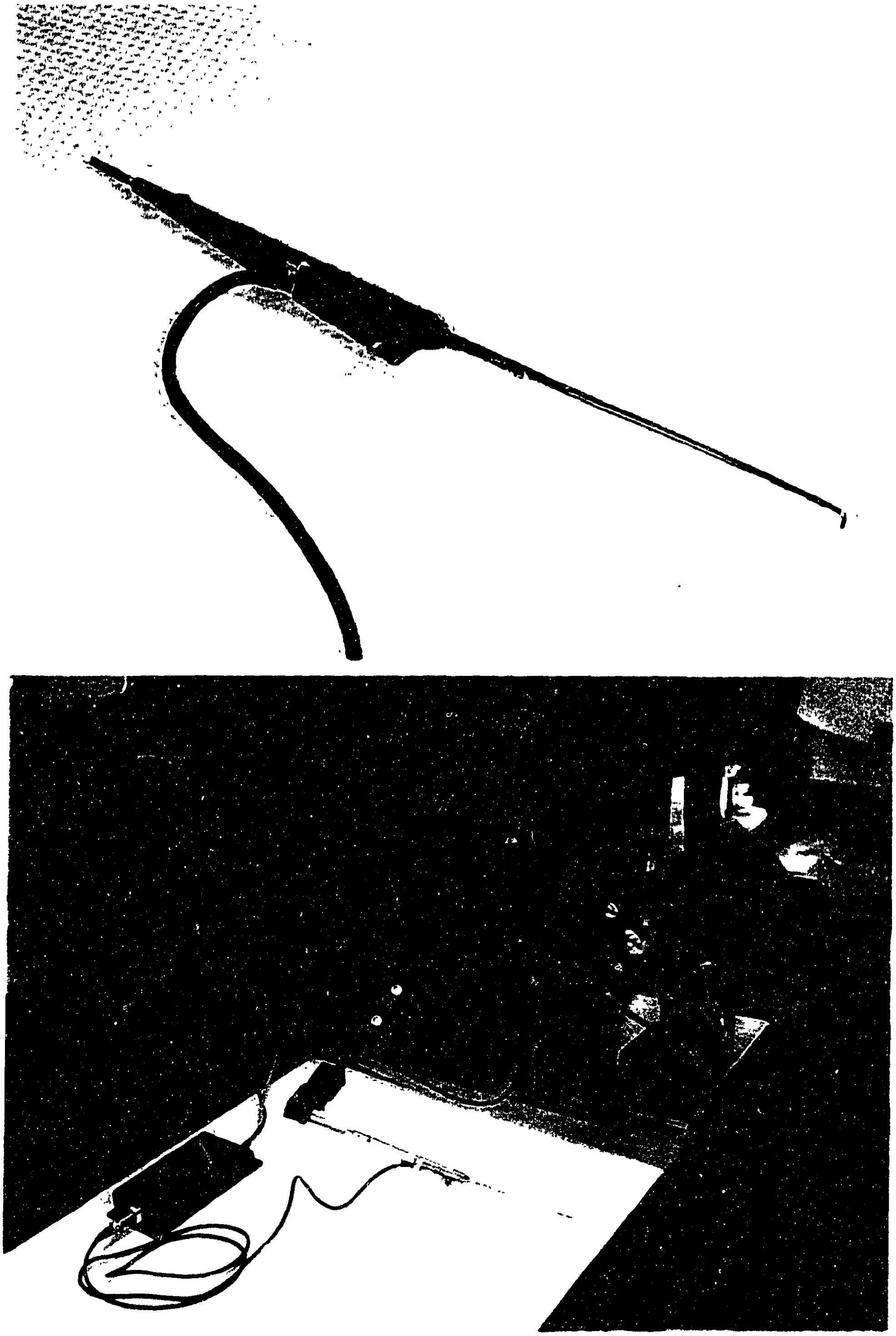

Figure 8-11 **(Top)** Final force-measuring probe with silicon strain gages. Two axes of force are measured (4 gages total). **(Bottom)** Probe attached to Phantom haptic interface, used in this application for position and orientation measurement only.

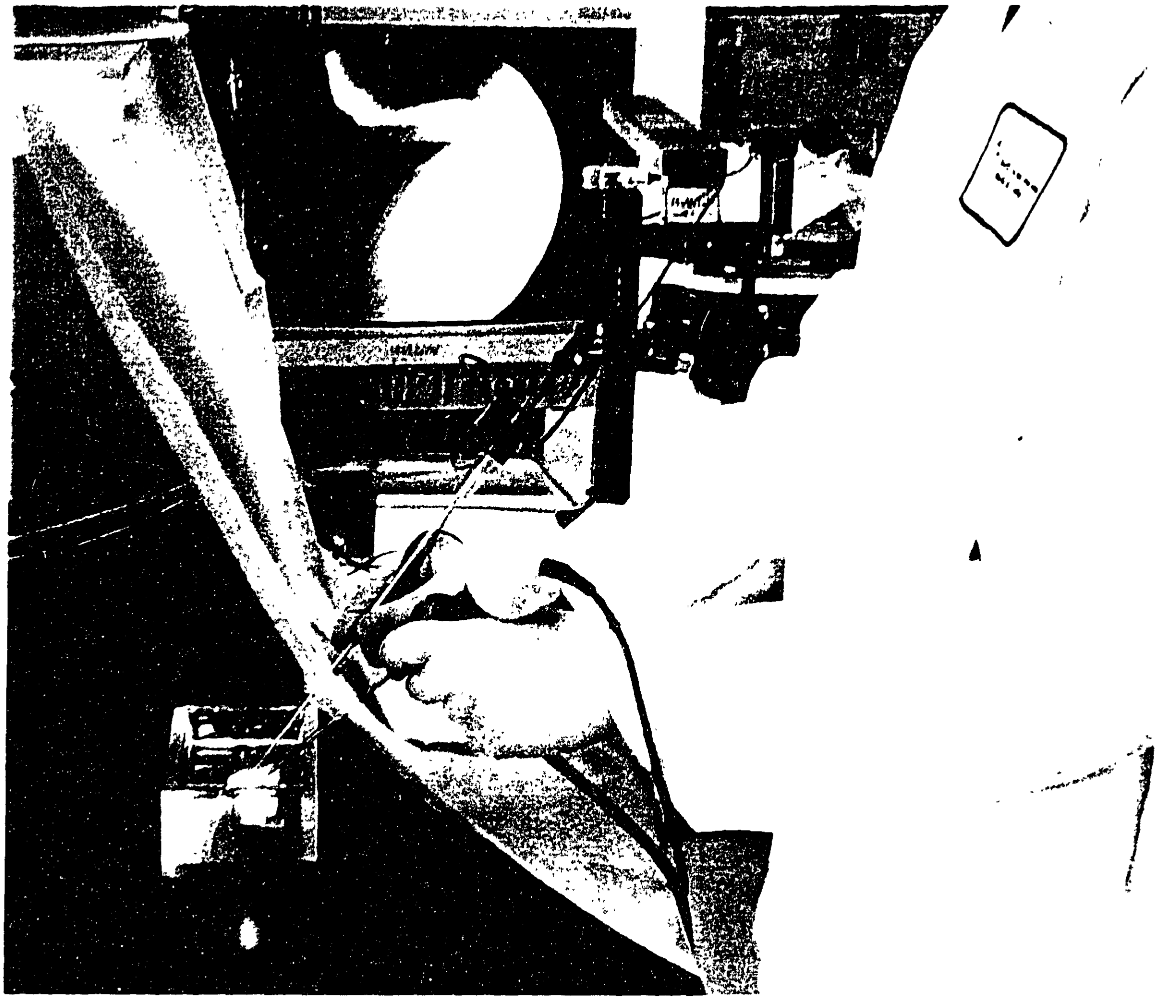

Figure 8-12 Use of the instrumented probe to measure the gestures a surgeon employs when probing an articular surface. An arthroscopic camera system was obtained (via generous loan from Smith and Nephew Corporation) and set up to permit the visual and proprioceptive sensoria of the OR to be approximated as closely as possible in the *in vitro* setting. The arthroscopic camera is being held in the operator's left hand; the instrumented probe, attached to the arm of the position-tracking Phantom, is being held in the right hand and used to examine the articular surface of a tibial plateau specimen mounted to a registration frame and immersed in Hanks solution. The tip of the probe can be seen in contact with the articular surface on the arthroscope monitor in the background.

8.3.2 Studies of surface integrity and collagen content

The partitioning of test loci into submeniscal or central regions in the current work was done by means of very coarse estimation, and many points were excluded from the partitioning analysis because they were near the boundary between the two regions and could not be definitively assigned to one or the other. Other methods for assessing surface integrity, such as India ink staining, could provide more definite partitioning, particularly in boundary cases.

More significantly, future work to determine in greater detail what differences exist between the submeniscal and central areas would deepen our understanding of why the areas can exhibit such distinctly different load-GAG relationships. Interesting questions abound: is the difference between submeniscal and central regions limited to the surface, or are there changes in composition and architecture throughout the depth that might influence indentation response independently of GAG content? Are there differences in collagen content, arrangement or both? Can we at least detect, and perhaps even quantify, collagen content and arrangement noninvasively by examining T2? Is collagen alteration an unambiguous indicator of surface disruption? Are there architectural or ultrastructural differences (independent of simply GAG or collagen concentration) that influence the mechanical behavior?

The correlation of our load response measurements with histological measures of ultrastructure and collagen content would be helpful in addressing some of these issues. After dGEMRIC imaging and mechanical testing, sections could be made through the samples along rows of marker holes. Although this is obviously a destructive procedure, it would allow histologic analyses could to be correlated with mechanical test results in a spatially-localized way.

As indicated in Section 2.4.2, there is evidence that the MRI parameter T2 shows sensitivity to collagen in cartilage. A fruitful line of future investigation may therefore be to examine whether combining both dGEMRIC T1 maps (providing GAG information) and T2 maps (providing collagen information) may result in even more robust estimates of cartilage indentation stiffness.

8.3.3 Clinical studies correlating *in vivo* imaging with either *in vivo* or *ex vivo* mechanical testing

As mentioned above, directions for research to move this methodology toward clinical application include potential improvements in clinical dGEMRIC scan resolution by moving to higher field strengths and the development of effective registration methods for cartilage surfaces in clinical scans.

The question of key relevance to the surgeon is whether a noninvasive clinical imaging methodology can provide information similar to what he or she can detect with a probe. The fundamental question of whether surgeons' perceptions when probing an articular surface correlate with dGEMRIC $T1_{Gd}$ maps obtained from *in vivo* clinical scans is a clear next step for investigation. This question could be directly addressed via the following experiment. Patients about to undergo total joint replacement could be scanned prior to their procedure to obtain $T1_{Gd}$ maps of their joint surfaces *in vivo* at clinical resolution. Pieces of the removed tissue could then be examined *in vitro* by surgeons using the position-tracked, instrumented probe described in the previous section. The surgeons' evaluations could then be directly correlated with dGEMRIC maps of GAG distribution (and/or additional MR indices of collagen distribution), to determine whether and to what degree the noninvasive imaging methods can predict the surgeons' clinical assessments determined via direct hand probing. The removed articular surfaces could also be tested using the benchtop indentation apparatus employed in this thesis to test the correlation between quantitatively measured mechanical properties and GAG content observable at *clinical* resolution.

The availability of hand-held probes (Artscan, ACTAEON™) for *in vivo* testing of cartilage stiffness might also offer an alternative approach, so long as regions of interest identified on clinical dGEMRIC scans could be sufficiently correlated with the sites of indentation. Selection of regions showing minimal local spatial variation of GAG might be targeted, thereby attempting to avoid the problems already discussed with inadequate colocalization of GAG measurement to the indenter footprint.

8.3.4 Improved methodology: automated testing

The current experimental apparatus could relatively straightforwardly be extended to provide a much higher degree of automation of mechanical testing of the osteochondral specimens. Once a sample is mounted to the tank and stage and the origin marker is found, electromechanical actuators could be employed on each axis of the translation stage to automate sample positioning. A complete pattern of test loci and a complete series of tests at each locus could be run fully automatically, with sample positioning, surface localization at each test locus, application of displacement profiles and measurement of resulting load responses all performed without operator intervention. (One could, in moments of ambition, imagine a remote, web-based interface to the control computer, including a web cam set up to provide a view of the sample. Data could be automatically directed to a web server which would also receive control directives from a password-protected access site. Once the experiment was set up, it could be monitored and even changed as needed remotely, from the convenience of office or home. Appropriate safety measures could be implemented to, for example, automatically stop the actuators, reverse displacement and alert the supervisory operator if load, displacement or stage translations exceeded specified limits.)

Such an automated system would allow a large number of locations to be tested on many samples with high efficiency, repeatability, and reduction in error due to operator fatigue.

8.4 Summary

We have presented a methodology which permits mechanical measurements and dGEMRIC-measured T1 values to be registered with submillimeter accuracy for test sites on an *in situ* articular surface. The pulse indentation peak load response is a relatively rapid test, exhibits a high degree of repeatability and is sensitive to focal deficits in cartilage mechanical integrity.

The current study demonstrates that locally-averaged $T1_{Gd}$ values, acquired through the application of the dGEMRIC methodology following $Gd(DTPA)^{2-}$ administration, are a significant predictor of the variability in the mechanical load response of an intact articular surface to focal compressive strain. Cartilage load response and $T1_{Gd}$ were found to be highly correlated ($r = .80, .90, .64, .81$ ($p < .002$); 130 test locations total) for four different patient samples studied. The variation in load response and correlation with $T1_{Gd}$ were demonstrably not a simple consequence of the effect of thickness variation.

The submeniscal region of the tibial plateau articular surface exhibited higher load responses compared to the central region and a very high correlation between load response and $T1_{Gd}$. The central region also displayed correlation between load response and

$T1_{Gd}$, although the parameters of the relationship appeared to differ from the submeniscal region. The difference may reflect differences in surface architecture, collagen content or collagen organization which independently affect indentation load response.

The estimation of load response from $T1_{Gd}$ appears particularly robust for submeniscal regions with a visibly smooth, untextured surface. For a sample with minimal visual difference between the submeniscal and central areas (HT3A) nearly identical correlations were obtained overall ($r = 0.90$), submeniscally ($r = 0.90$) and centrally ($r = 0.94$). With regional variation taken into account, dGEMRIC $T1_{Gd}$ measurement may offer a feasible means of noninvasively estimating cartilage surface stiffness variation even in samples with surface heterogeneity.

The strong correlation of load response to 300 μm indentation with $T1_{Gd}$, averaged over an ROI with 600 μm depth, is consistent with a view that GAG content local to the region of cartilage subjected to compressive strain plays a role in the short-time compressive load response to indentation. At the same time, the differences in average load and load-$T1_{Gd}$ correlations seen in the peripheral versus central articular surface are consistent with previous work demonstrating that collagen also plays a major role in determining short-time compressive behavior. This is in accord with the view that focal indentation is a relatively complex mechanical stimulus which creates both compressive and tensile strains in cartilage, and hence may be affected by both GAG and collagen content.

The investigation of MRI-based methods of collagen assessment, such as T2 imaging, may provide a fruitful adjunct to the dGEMRIC assessment of GAG content for the more quantitative modeling and prediction of articular surface load response throughout the joint surface.

This preliminary work suggests the possibility of an attractive means of assessing cartilage functional integrity and relating structure to function via a nondestructive and noninvasive technique, one which could potentially provide functional topographic mapping of spatial and temporal changes of a joint surface *in vivo*. Such a method could potentially provide comprehensive and functionally-relevant pictures of cartilage integrity preoperatively and intraoperatively to aid surgeons in diagnosing and treating cartilage pathology, could provide tissue property data for simulators of arthroscopic surgery, and could contribute to analytical and computational modeling aimed at increasing our understanding of the basic mechanisms of cartilage structure and function.

Appendix A

Cartilage thickness data

Test locus comprehensive thickness data: HT3A, HT6A, HT8A, HT11A

247 locations total

Multiple measurements with MR slice thicknesses of 1.5 mm and 0.25 mm for loci on HT3A and HT6A. Scan parameters at top of each column given as **in-plane resolution (µm), slice thickness (mm)** Slice orientations are sagittal (aligned with rows of marker holes in the registration plate) unless otherwise indicated.

HT3A Thickness Measurements

HT3A Slice 1

Locus#	5/24/01 250µm,1.5mm Transverse	5/30/01 100µm,1.5mm Sagittal	5/30/01 Composite	5/30/01 200µm,1.5mm Sagittal	6/25/01 100µm, 0.25mm Sagittal
13	NA	1.1	1.10	1	0.9
12	1	1.2	1.10	1.2	1.1
11	1	1.3	1.15	1.2	1.1
10	1.125	1.5	1.31	1.4	1
9	1.25	1.7	1.48	1.6	1.1
8	1.375	1.85	1.61	1.8	1.2
7	1.5	2	1.75	1.8	1.2
6	1.375	2.05	1.71	1.6	1.3
5	1.25	2.1	1.68	2	1.1
4	1.25	1.85	1.55	1.8	1.2
3	1.25	1.6	1.43	1.4	0.9
2	1	1.45	1.23	1.2	0.7
1	0.75	1.3	1.03	1.2	NA

Notes: values in color were interpolated from the thickness measurement made at the two adjacent loci. All other values are directly measured. **Composite** value for a locus is the average of the transverse and sagittal thicknesses measured at the site.

HT3A Slice 2

Locus#	5/24/01 250µm,1.5mm Transverse	5/30/01 100µm,1.5mm Sagittal	5/30/01 Composite	5/30/01 200µm,1.5mm Sagittal	6/25/01 100µm, 0.25mm Sagittal
39	1.5	1.8	1.65	1.8	1.3
38	1.75	2	1.88	1.8	1.4
37	2	2.2	2.10	2.2	1.7
36	2.125	2.4	2.26	2.4	1.9
35	2.25	2.6	2.43	2.6	2.1
34	2.375	2.75	2.56	2.6	2.1
33	2.5	2.9	2.70	2.8	2.2
32	2.5	2.85	2.68	2.8	2.2
31	2.5	2.8	2.65	2.6	2
30	2.5	2.6	2.55	2.6	2.1
29	2.5	2.4	2.45	2.4	1.8
28	2.125	2.35	2.24	2.2	1.6
27	1.75	2.3	2.03	2.2	1.4

HT3A Slice 3

Locus#	5/24/01 250µm,1.5mm Transverse	5/30/01 100µm,1.5mm Sagittal	5/30/01 Composite	5/30/01 200µm,1.5mm Sagittal	6/25/01 100µm, 0.25mm Sagittal	% difference between 6/25/01 and composite
65	2.25	2	2.13	2	2	-5.9
64	2.375	2.3	2.34	2.4	2.2	-5.9
63	2.5	2.6	2.55	2.6	2.4	-5.9
62	2.625	2.75	2.69	2.6	2.7	0.5
61	2.75	2.9	2.83	2.8	2.6	-8.0
60	2.875	3.05	2.96	3	2.7	-8.9
59	3	3.2	3.10	3.2	2.9	-6.5
58	3	3.15	3.08	3	2.8	-8.9
57	3	3.1	3.05	3	2.8	-8.2
56	2.875	2.95	2.91	3	2.7	-7.3
55	2.75	2.8	2.78	2.8	2.5	-9.9
54	2.625	2.7	2.66	2.8	2.3	-13.6
53	2.5	2.6	2.55	2.6	2.2	-13.7

HT3A data continues next page

HT3A Slice 4						
Locus#	5/24/01 250µm,1.5mm Transverse	5/30/01 100µm,1.5mm Sagittal	5/30/01 Composite	5/30/01 200µm,1.5mm Sagittal	6/25/01 100µm, 0.25mm Sagittal	% difference between 6/25/01 and composite
91	2.5	2.3	2.40	2.2	2.3	-4.2
90	2.5	2.35	2.43	2.4	2.4	-1.0
89	2.5	2.4	2.45	2.6	2.5	2.0
88	2.625	2.5	2.56	2.6	2.7	5.4
87	2.75	2.6	2.68	2.6	2.7	0.9
86	2.875	2.7	2.79	2.8	2.8	0.4
85	3	2.8	2.90	2.8	2.8	-3.4
84	3	2.9	2.95	2.8	2.9	-1.7
83	3	3	3.00	3	2.9	-3.3
82	2.875	2.9	2.89	2.8	2.6	-10.0
81	2.75	2.8	2.78	2.6	2.5	-9.9
80	2.625	2.7	2.66	2.8	2.4	-9.9
79	2.5	2.6	2.55	2.4	2.3	-9.8

HT6A Thickness Measurements

Slice 1			Slice 2			Slice 3		
Locus#	6/15/01 100µm, 1.5mm	7/23/01 100um, 0.25mm	Locus#	6/15/01 100µm, 1.5mm	7/23/01 100µm, 0.25mm	Locus#	6/15/01 100µm, 1.5mm	7/23/01 100µm, 0.25mm
13	1.4	1.3	**39**	1.4	1.3	**65**	2.3	2
12	1.4	1.3	**38**	1.6	1.5	**64**	2.6	2.3
11	1.3	1	**37**	1.8	1.6	**63**	2.8	2.6
10	1.3	1.1	**36**	2	1.7	**62**	3	2.6
9	1.4	1.5	**35**	2.3	1.9	**61**	3.1	2.8
8	1.7	1.5	**34**	2.2	1.9	**60**	3	2.8
7	1.9	1.6	**33**	2.3	1.9	**59**	3	2.7
6	1.7	1.5	**32**	2	1.9	**58**	3	2.3
5	1.7	1.5	**31**	2	1.9	**57**	2.7	2.4
4	1.7	1.2	**30**	1.9	1.7	**56**	2.7	2.3
3	1.5	1	**29**	1.9	1.7	**55**	2.5	2.1
2	1.3	0.9	**28**	1.7	1.6	**54**	2.1	2
1	1	1.2	**27**	1.6	1.4	**53**	2	1.7

HT6A data continues next page.

HT6A continued					
Slice 4			Slice 5		
Locus#	6/15/01 100µm, 1.5mm	7/23/01 100µm, 0.25mm	Locus#	6/15/01 100µm, 1.5mm	7/23/01 100µm, 0.25mm
91	3.2	2.7	117	3.1	3.4
90	3.4	3.1	116	3.3	3.6
89	3.3	3.4	115	3.6	3.8
88	3.6	3.6	114	3.8	4
87	3.8	3.8	113	3.7	4.2
86	4	3.6	112	3.8	3.8
85	3.9	3.5	111	3.9	4.2
84	3.8	3.7	110	3.8	3.9
83	3.6	3.4	109	3.7	3.6
82	3.4	3.2	108	3.7	3.6
81	3.1	3	107	3.6	3.6
80	3	2.9	106	3.5	3.5
79	2.9	2.5	105	3.3	3.3

HT8A Thickness Measurements

Slice 1		Slice 2		Slice 3		Slice 4		Slice 5	
Locus#	6/25/01 100µm, 0.25mm	Locus#	6/25/01 100µm, 0.25mm	Locus#	6/25/01 100µm, 0.25mm	Locus#	6/25/01 100µm, 0.25mm	Locus#	6/25/01 100µm, 0.25mm
13	0.6	39	1.3	65	1.8	91	1.9	117	1.6
12	1	38	1.7	64	2.1	90	2.2	116	1.4
11	1.1	37	1.9	63	2.3	89	2.2	115	1.6
10	1.3	36	2.2	62	2.3	88	2.3	114	2.5
9	1.4	35	2.2	61	2.4	87	2.4	113	2.6
8	1.4	34	2.4	60	2.5	86	2.4	112	2.8
7	1.5	33	2.5	59	2.7	85	2.5	111	2.8
6	1.5	32	2.4	58	2.8	84	2.9	110	2.9
5	1.4	31	2.4	57	2.7	83	2.8	109	3.1
4	1.3	30	2.4	56	3	82	3	108	3.1
3	1.1	29	2.2	55	2.9	81	3	107	3.2
2	0.9	28	1.8	54	2.8	80	3	106	3.2
1	0.8	27	1.7	53	2.6	79	2.8	105	3.1

HT11A Thickness Measurements

Slice 1		Slice 2		Slice 3		Slice 4		Slice 5	
Locus#	7/27/01 100µm, 0.25mm	Locus#	7/27/01 100µm, 0.25mm	Locus#	7/27/01 100µm, 0.25mm	Locus#	7/27/01 100µm, 0.25mm	Locus#	7/27/01 100µm, 0.25mm
13	1.2	39	0.8	65	1.3	91	2	117	2.2
12	0.8	38	1.1	64	1.8	90	2.3	116	2.3
11	0.7	37	1.4	63	2	89	2.7	115	2.6
10	0.7	36	1.7	62	2.3	88	2.8	114	3.1
9	1.1	35	1.8	61	2.5	87	3	113	3.2
8	1.1	34	1.9	60	2.5	86	3	112	3.3
7	1.2	33	2	59	2.5	85	2.8	111	3.2
6	1.2	32	2	58	2.5	84	2.8	110	3
5	1.1	31	2	57	2.4	83	2.6	109	2.7
4	1.1	30	2	56	2.4	82	2.5	108	2.4
3	1.1	29	1.8	55	2.2	81	2.5	107	2.2
2	1	28	1.8	54	2.3	80	2.6	106	2.3
1	1	27	1.4	53	2.2	79	2.7	105	2.4

Appendix B

Protocols employed

Bovine specimen preparation, trypsinization and Gd(DTPA)$^{2-}$ equilibration

Sample Preparation

Obtain a fresh, intact knee joint from a two-week old calf from a local research abattoir. Incise the capsule circumferentially, transect the anterior and posterior collateral ligaments and separate the joint, exposing the tibial plateau.. Dissect away as much soft tissue (ligament, capsule, fat) as possible, and clear the soft tissue (muscle, connective tissue) from the tibia. Mount the tibia vertically in a vise. Make a midsagittal saw cut, between the medial and lateral tibial eminences, to a depth of roughly 1 cm into the subchondral bone. Then make a transverse saw cut into the tibial bone, approximately parallel to the cartilage surface and at a depth of several millimeters below (distal to) the lateral edge of the plateau. This cut will intersect the first cut, yielding a hemi-plateau which includes the cartilage and several millimeters (approximately 5) of subchondral bone.

Liberally rinse the sample with Hank's balanced salt solution (HBSS, 1X; Invitrogen Life Technologies, Carlsbad, CA). Weigh the sample. Make linear measurements (width, length, height) and photograph the articular surface of the sample in plan view with a digital camera (macro mode, lens centered above sample, natural lighting or two-point incandescent illumination (no flash)). Horizontal and vertical rulers may be placed adjacent to the sample before photographing to calibrate linear measurement in the image.

The sample is then rigidly fixed to the base of a polycarbonate registration frame (the frame serves as both a sample holder and a coordinate reference frame for registering mechanical and MRI measurements of the sample.) Again, liberally rinse the bone surface of the sample with Hank's balanced salt solution, then dry with gauze. Using a 1/8 inch drill bit turned in a drill press at very low speed, drill 10 to 20 shallow (3 to 5 mm) holes into the distal bone surface of the sample (the side opposite the articular surface). Drill a similar number of holes into the base plate of the polycarbonate frame. Mix the two components of Devcon 5-minute epoxy (Devcon, Danvers, MA) thoroughly and liberally apply (a wooden popsicle stick works well) to both the bone surface and the base plate, taking care to ensure the epoxy resin permeates well into the drilled holes. Position the bone surface over the center of the base plate, and press it to the base plate with firm finger pressure, holding tightly for several seconds. Apply additional epoxy to any exposed bone surfaces, such as the surface exposed by the midsagittal cut. This seals the surfaces, helping to limit escape of serum which contains factors that can both degrade the cartilage and potently inactivate trypsin. Permit the epoxy to set and cure for 10 to 15 minutes. (The sample may be immersed in Hank's solution while the epoxy is curing.)

Trypsinization

Prepare the trypsin solution: add 20 ml deionized water to a stock bottle of powdered trypsin (Gibco BRL Life Technologies, Grand Island, NY), yielding a standard 25 mg/ml solution. Prepare a second bottle in the same way. Combine both and add 4 ml of reconstituted penicillin/streptomycin/amphotericin (P/S/A) antibiotic/antimycotic solution[16] (containing 10,000 units/ml penicillin G, 10 mg/ml streptomycin sulfate and 25 µg/ml amphotericin B; product number A7292, Sigma Aldrich, St. Louis, MO). Finally, add 356 ml of Hank's solution to bring the total volume to 400 ml. The solution will now contain 2.5 mg/ml trypsin and 1% v/v P/S/A.

Attach a support plate to the end of the registration frame. Rinse the sample thoroughly in Hank's solution. Place into a 1 liter beaker with the support plate down. Add one or two small magnetic stir bars to the base of the beaker. Fill the beaker with 2.5 mg/ml trypsin solution to the desired height relative to the sample. A 100 ml bottle, filled with water and tightly capped, may be added to the beaker, resting on the support plate, to take up volume in the beaker and reduce the amount of trypsin solution needed to reach the desired height on the sample. A pipette should be used to add solution so as to

---

[16] Sigma product #A7292 is provided as a dehydrated powder. Before use, it is first reconstituted by adding 20 ml of sterile, deionized water to the product bottle. (A 50 ml size is also available.)

minimize splashing of the solution onto the nonimmersed cartilage surface. If desired, place a thermometer probe into the beaker, and record the start, end, minimum and maximum solution temperature during trypsinization. Cover the beaker with a watch glass or polyethylene film, place on magnetic stirrer and allow to digest for the desired time (typically 6 to 12 hours) at room temperature, with continuous stirring.

After the desired digestion time has elapsed, pour off the trypsin digestate and save for subsequent GAG assay. A series of three rinses will now be applied to remove and inactivate the trypsin. Fill the beaker with fresh Hank's (with 1% v/v P/S/A) to a level about 5 mm higher than the trypsin level. Allow to sit for 1/2 hour. Pour off and repeat the rinsing with fetal calf serum (FCS) for 1 hour. Pour off and repeat rinsing with Hank's for 2 hours.

Remove the sample from the beaker, detach the support plate from the registration frame, and rise the entire sample thoroughly with Hank's. The sample is now ready for equilibration in $Gd(DTPA)^{2-}$ solution and MR imaging.

$Gd(DTPA)^{2-}$ Equilibration

Prepare a volume of $Gd(DTPA)^{2-}$ in Hank's solution to the desired concentration (typically 1 mM for imaging at 2 T or 2 mM for imaging at 8.45 T), with 1% v/v P/S/A added. The total volume prepared should be equal to approximately 50 times the volume of the sample. (To a first approximation, the volume of the sample in ml can be estimated as equal to its weight in grams. A nominal 50 g sample would thus require 2.5 liters of $Gd(DTPA)^{2-}$ solution.) As an example: 1 liter of 1 mM $Gd(DTPA)^{2-}$ solution with 1% P/S/A is formulated by combining 2 ml Magnevist (Berlex Laboratories, Wayne, NJ) and 10 ml reconstituted P/S/A solution, then adding sufficient Hank's solution to bring the total volume to 1 liter. For a 2 mM $Gd(DTPA)^{2-}$ solution, 4 ml Magnevist would be employed.

Equilibrate the sample in the $Gd(DTPA)^{2-}$ solution for a minimum of 12 hours. Place the sample and frame off-center in a large, covered beaker or plastic tray atop the magnetic stirrer. Stir continually for the 12 hours and maintain at 4°C. At end of equilibration, save 50 ml of solution for later imaging to verify and calibrate $Gd(DTPA)^{2-}$ concentration and corresponding $T1_{Gd}$.

Protocol for Pulse-Indentation Mechanical Tests

Sample and equipment preparation

Please wear gloves *and* a lab coat when working with the human tissue any time it is not (a) wrapped in latex or (b) behind the plastic sheet drape during Pressmaster experiments.

Remove the cartilage sample from the MRI and as soon as possible cut off the latex wrap and immerse the sample in room temperature 2mM Gd solution. (Use surgical scissors to cut the latex—they'll need to be autoclaved afterwards)

Locate the following:
1) the circular hydration tank,
2) 2 small stainless-steel screws
3) 4 large stainless-steel screws

Turn on the Pressmaster, computer, Linseis chart recorder, JoeTron2000. Check that the chart recorder has paper.

Start up the following LabView modules:
- Simple Motion
- Touchoff
- Play Sine Motion

Clean the tip of the 1.5mm hemispherically-tipped indenter (make sure it isn't bent) with an alcohol wipe and then screw it into the load cell above the stage. Use a pliers with a layer of tape wrapped around the jaws to gently tighten the indenter until it is firmly in place. After tightening, press lightly against it from the side to make sure it is well-seated and doesn't wobble.

Cut a piece of 1mil plastic sheeting (drop cloth) about 3 by 4 feet or so. Drape over the x–y translation stage so the middle of the sheet is about over the middle of the stage.

Position the circular hydration tank on the lab bench so the cut corner is toward you (toward the left). Fasten the sample registration plate to the bottom of the circular hydration tank using the two smaller stainless steel screws. After screwing the screws in most of the way, but before tightening them, use a gloved finger to apply gentle pressure to the back edge of the registration plate, pulling it gently toward you and against both screws. Tighten the screws while maintaining this gentle forward pressure on the plate: this will help ensure the plate stays straight against the screws.

Place the hydration tank base, cut-corner still toward you, on the plastic sheet on the translation stage. Pull on the sheet to make sure there are no wrinkles or folds under the tank base. Use the 4 large screws to fasten the base to the stage (punch them right through the plastic). Use a technique similar to that used for fastening the registration plate to the tank base: screw in all 4 screws most of the way, and then apply gentle pressure to the back of the tank base to pull it forward, against the screws, as they are given their final tightening.

Mechanical origin location

Before filling the tank with fluid, determine the position of the origin marker hole (hole #0):

1) Tare the load cell so the Sensotec display shows 0 g.

2) Use Simple Motion (SM) to bring the indenter down close to the sample. Adjust the x and y micrometers to bring hole 0 under the indenter tip, looking alternately from the front and the side of the tank to visually gauge the position of the indenter.. Iteratively lower the indenter and adjust the micrometer position until the tip of the indenter is centered just above hole 0.

3) Set SM to 50 um displacement and a rate of 10 um/sec. Move down in 50 um increments until a load (hopefully, just a few grams) is seen on the Sensotec readout. Adjust x and y until no load is seen. Move down another 100 or so um.

4) Now increase and decrease x and record the x positions where the load just begins to increase (the position value should be read at the x position where the load reads 0 grams, but any further x motion would result in the load increasing). Take the average of these two positions and set the x micrometer to this value (this is the *average center position for x*). We'll call the *difference* between these two positions The Wiggle Range.

5) Repeat the above for y. Remember to set the y micrometer value to the average value.

6) Now set SM to 20 um displacement and a rate of 10 um/sec. Lower in 20 um increments until a load is just seen. Repeat steps 4 and 5.

7) Repeat step 6 until The Wiggle Range is less than 20 um.

8) Round the final average center positions for x and y to 2 decimal places (10 microns). Record these values and enter them in the cells in the Excel spreadsheet beneath x and y, respectively, under "Mechanical Origin Absolute Position".

9) Make sure the x and y micrometers are adjusted to the final average center positions. Then zero the Sony readout (z = 0).

10) Set SM to 10,000 μm or so (and 1000um/sec) and raise the indenter.

Pulse indentation testing

Pour 2mM Gd-in-Hank's solution into the tank so it covers the surface of the sample to a depth of a few millimeters.

Pull the plastic drape up and out of the way of the micrometers: tape it to the top of the Pressmaster.

→ Make sure the back of the drape doesn't contact the white load cell wire, or you'll see nonzero load changes as the Pressmaster is moved. It's good to cut a "window" out of the plastic around the load cell and wire.

Make sure the sample has hydrated in solution for a total of at least one hour after being removed from the magnet, and at least 30 minutes continuously before the first mechanical test is run.

Set Play Sine Motion with the following parameters:

Amplitude = 300um
Offset = 0um
Offset rate = 10um/sec
Frequency = 0.25Hz
Number of cycles = 0.75 (this will show up in the display as "0.8")

Test the locations on the surface along the rows, going from left to right. For each location number, get the x and y positions from the columns labeled "Absolute Position (mm)" on the Excel spreadsheet.

Start at the left end of each row (the lowest numbered location) and test every other locus, i.e., for the first row, test in the order 1, 3, 5, 7, 9, 11, 13. Then go back to the left end of the row and test the skipped locations: 2, 4, 6, 8, 10, 12.

→ Each "jump" in x will be 3mm.

Then go to row 2, starting with locus 14, and repeat testing with the same every-other pattern.

→ Each "jump" in y (between rows) will be 1.5mm.

Continue for the other rows.

At each location:

1) With the indenter above the surface, verify that 0g load is seen on the Sensotec readout: re-tare the load cell if it's not at 0g.
2) Run Touchoff.
3) When Touchoff finishes, record the touchoff value on the spreadsheet.
4) Write down the location number on the chart paper.
5) Start the strip-chart recorder.

6) Rezero the JoeTron2000.

7) Run Play Sine Motion.

   →Press Cancel, then Stop to get out of the error dialogs.

8) Stop the strip-chart recorder.

9) Read the height of the load pulse from the LabView load window (as well as possible) and enter on the spreadsheet under the "300um pulse peak (g, LabView) column. This is just so in case the pen goes off-scale (or, as sometimes happens, it gets stuck) we have a back-up load measurement. It's helpful to choose "display slider bar" under "display options" for the LabView Load window and then use the slider bar to position the last peak at the left of the window: this will cause the y scale to adjust to the height of the peak, making it easier to read the peak value.

Play Sine Motion should finish with the indenter about 300 μm above the cartilage surface. If the cartilage surface has a sufficiently high slope this may not be enough clearance for moving to the next location. Keep an eye on the Sensotec load readout when adjusting the translation stage micrometers: if you see the load nudge up at all, immediately reverse gears, then use SM to move the indenter up 500 μm or so. Then continue moving to the next location.

The Full Monty Protocol

Sample and equipment preparation

As always, to stay safe please wear gloves *and* a lab coat when working with human tissue any time it is not (a) wrapped in latex or (b) behind the plastic sheet drape during Pressmaster experiments.

Follow the same preparation steps outlined above in the Pulse Indentation Protocol.

Likewise, follow the procedure outlined above for mechanical origin location.

Full-Monty Mechanical Testing

Ensure sufficient solution is in the tank so it covers the surface of the sample to a depth of a few millimeters.

Pull the plastic drape up and out of the way of the micrometers: tape it to the top of the Pressmaster.

→ Check that the back of the drape doesn't contact the white load cell wire, or you'll see nonzero load changes as the Pressmaster is moved. It's good to cut a "window" out of the plastic around the load cell and wire.

Open the Excel Full Monty Testing file.

Position the lab timer in a convenient spot.

For each location to be tested, the protocol runs as follows:

(Note that in the steps below, any time it says to enter a time value in the spreadsheet, this is only if the actual time you perform a measurement or test is different than the "default" time values: the default values are already entered in the appropriate cells in the spreadsheet. All time values are relative to 0:00 at the start of the first pulse.)

Time	Action
	Position the stage at the desired location. Tare the load cell to 0 g. Enter a sequential experiment number and the starting time on the spreadsheet.
	Set Play Sine Motion with the parameters: **300 um** Amplitude (→ yes, 300. This is a change from the 250 we talked about yesterday) **0 um** Offset **10 um/sec** Offset Rate **0.25 Hz** Frequency

	0.75 Number of cycles
	Run Touchoff. When done rezero the JoeTron2000.
	Enter the touch-off z position in the spreadsheet.
0:00	Reset the timer to 0. Start the timer. Run the 300 um pulse.
	Enter the end z position in the spreadsheet. Also enter the "LabView" pulse peak height value.
	Use Simple Motion to move the indenter back to the original touch-off z. Start by setting it for the value "Delta Z" from the spreadsheet, with a velocity of about 10 um/sec. Then set the displacement to 2 um, and increment as needed until the adjusted z is within 2 um of the touch-off z. An easy way to know you've "just got it" is to lower in increments while watching the strip chart recorder: you've just got it when the displacement pen slides back to the left. Enter the Adjusted Z value in the spreadsheet.
	Change the Play Sine Motion Amplitude parameter to equal 10% of the location thickness (given in the spreadsheet.)
2:30	Run the 10% pulse. Enter the start time in the spreadsheet.
	Enter the end z position in the spreadsheet.
	As before, use Simple Motion to bring the indenter back to the original touch-off z. Enter the Adjusted Z value in the spreadsheet.
	Set the Simple Motion parameters for **100 um** displacement, **25 um/s** rate.
5:00	Run the first 100 um step. Enter the start time in the spreadsheet.
	Enter the end z value in the spreadsheet. Check that the Step Size computed by the spreadsheet is roughly 100 um.
7:00	Record the steady-state load in the spreadsheet: **read this directly from the Sensotec load readout**. Enter the read-time in the spreadsheet.
7:15	Run the second 100 um step (no parameter changes are needed). Enter the start time in the spreadsheet.
	Enter the end z value in the spreadsheet. Again, check that the Step Size computed by the spreadsheet is roughly 100 um.
	While you're waiting for the load to steady-state-icize, set Simple Motion with the following parameters: Displacement = **"Step size: 3rd step"** value from spreadsheet Rate = **"Ramp rate: 3rd step"** value from spreadsheet. **Note that the ramp rate should be entered to 2 decimal places.**

10:15	Record the steady-state load for the 2nd step in the spreadsheet, again reading this directly from the Sensotec load readout. Enter the read-time in the spreadsheet.
10:30	Run the third step (which ramps to a total 15% displacement).
	After the one-minute ramp, enter the end z into the spreadsheet. Check that the Excel-computed Total Offset (%) is about 15%.
	While waiting, this can be a good time to measure the five peak values (on the chart paper) obtained thus far: the two pulses, the two fixed-steps and the 3rd step. Also while waiting, this can be a good time to set the Play Sine Motion parameters to: **10 um** Amplitude **0 um** Offset **10 um/sec** Offset Rate **0.1 Hz** Frequency **12** Number of cycles
16:30	Record the steady-state load for the 3rd step in the spreadsheet, again reading this directly from the Sensotec load readout. Enter the read-time in the spreadsheet.
16:45	Start the 0.1 Hz sine test.
	When it finishes, enter the end z and the end load (from the Sensotec readout) in the spreadsheet. Read the maximum load value and the minimum load value of the last cycle from the LabView display (by "sliding" the load graph to the left using the time-axis slider.) Enter these values in the "Max" and "Min" columns of the spreadsheet: the peak-to-peak value will be automatically computed and displayed in the next column. Also measure the peak-to-peak load of the last cycle directly on the strip chart. Enter the value in the "0.1 Hz p-p Chart (g)" column. Set the Play Sine Motion Frequency and Number of Cycles to: **0.02 Hz** Frequency **3** Number of cycles
20:30	Start the 0.02 Hz sine test.
	Again, when it finishes, enter the end z and the end load (from the Sensotec readout) in the spreadsheet. Read the maximum load value and the minimum load value of the last cycle from the LabView display (by "sliding" the load graph to the left using the time-axis slider.) Enter these values in the "Max" and "Min" columns of the spreadsheet: the peak-to-peak value will be automatically computed and displayed in the next column.

	Also measure the peak-to-peak load of the last cycle directly on the strip chart. Enter the value in the "0.02 Hz p-p Chart (g)" column.
	Use Simple Motion to lift the indenter up way-high, well clear of the surface. Record the time in the "Liftoff Time" column.

Lather, rinse, repeat for each location to be tested.
When done, enjoy a cold, refreshing beverage!

Appendix C

Mechanical testing apparatus data

Linseis L2200 strip chart recorder frequency response calibration data

	0.25 V p-p sine input (10% full-scale)		1 V p-p sine input (40% full-scale)		2.5 V p-p sine input (100% full-scale)	
Frequency (Hz)	Chart Amplitude (V)	Amplitude Normalized to 0.02 Hz	Chart Amplitude (V)	Amplitude Normalized to 0.02 Hz	Chart Amplitude (V)	Amplitude Normalized to 0.02 Hz
0.02	0.248	1	0.996	1	0.2495	1
0.05					0.2492	1.00
0.1	0.245	0.99	0.995	1.00	0.249	1.00
0.2			0.99	0.99		
0.25	0.244	0.98	0.99	0.99	0.2478	0.99
0.3			0.989	0.99		
0.4			0.98	0.98		
0.5	0.24	0.97	0.975	0.98	0.2449	0.98
0.6			0.969	0.97		
0.7			0.96	0.96		
0.75	0.236	0.95	0.958	0.96	0.24	0.96
0.8			0.955	0.96		
0.9			0.948	0.95		
1	0.23	0.93	0.938	0.94	0.2342	0.94
1.1			0.921	0.92		
1.25	0.222	0.90	0.909	0.91	0.2265	0.91
1.3			0.9	0.90		
1.4			0.89	0.89		
1.5	0.215	0.87	0.875	0.88	0.2178	0.87
1.75	0.207	0.83			0.2091	0.84
2	0.198	0.80	0.8	0.80	0.1981	0.79

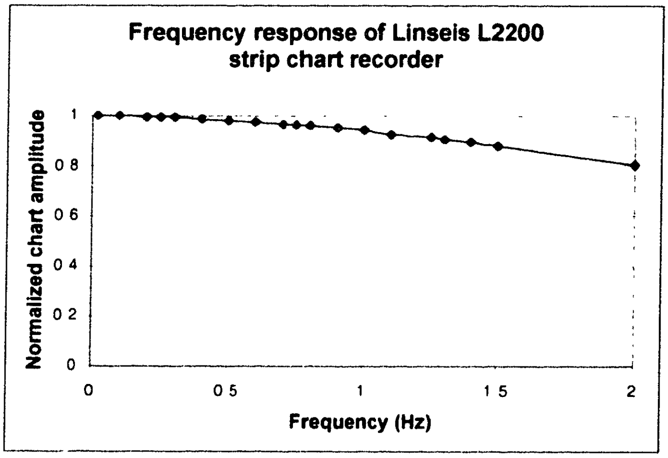

Linseis L6514 strip chart recorder frequency response calibration data

	.308 V p-p sine input (62% full-scale)	
Frequency (Hz)	Chart Ampli- tude (V)	Amplitude Normalized to 0.1 Hz
0.1	0.308	1.00
0.2	0.307	1.00
0.25	0.306	0.99
0.4	0.303	0.98
0.6	0.298	0.97
0.8	0.291	0.94
1	0.282	0.92
1.2	0.272	0.88
1.5	0.256	0.83
2	0.226	0.73
2.5	0.192	0.62
3	0.156	0.51

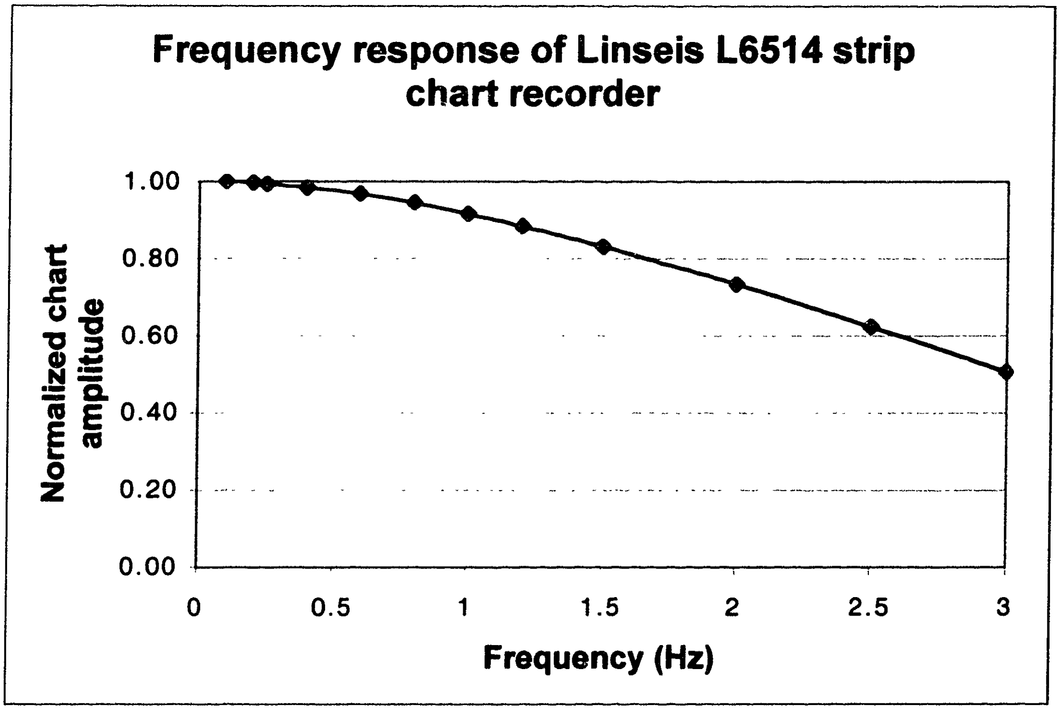

JoeTron2000 Quadrature-to-Analog Converter Calibration Data

Pressmaster Displacement (mm)	**JoeTron2000 Analog Voltage Output (mV)**
0	0.2
0.101	31.5
0.1995	61.7
0.3	92.1
0.4005	122.7
0.5	153.3
0.5995	183.75
0.7	214.25
0.7995	244.6
0.9005	275.25
0.9995	305.9

Result: 305.4 mV/mm (output voltage increment/displacement input)

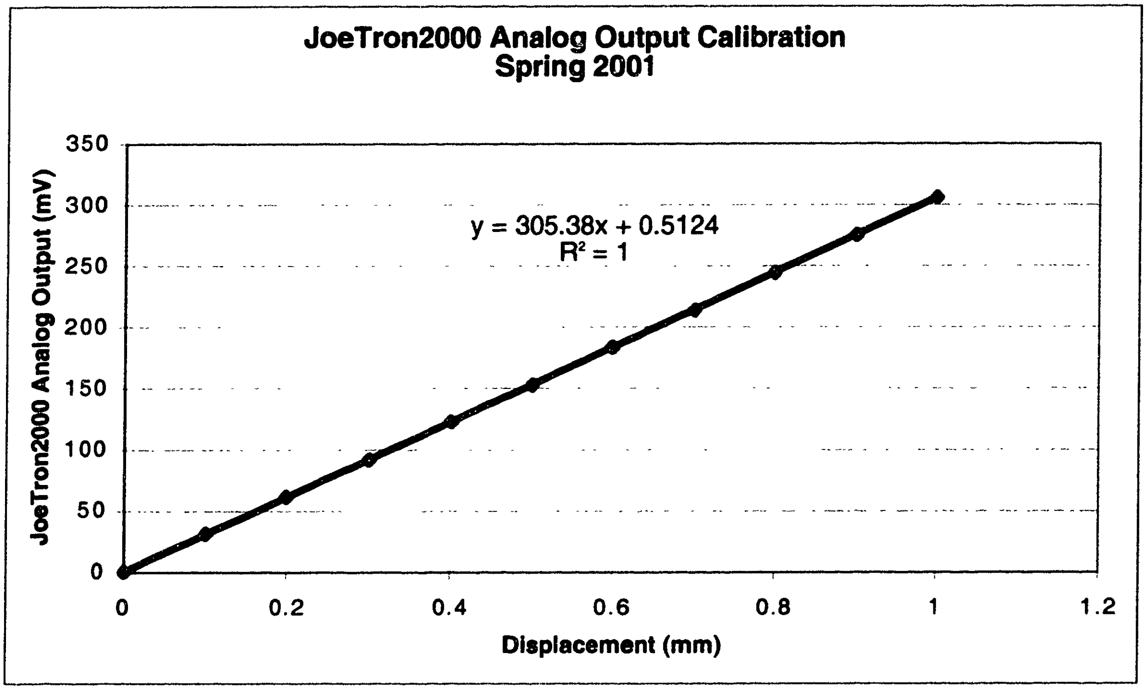

Appendix D

Analysis of strain along the shaft of a surgical probe

In order to determine the type and optimize the placement of strain gauges to be used in the instrumented surgical probe, an analysis was first made of the expected strain the shaft of the probe would experience in response to typical loads during probing of an articular surface.

Referring to Figure D-1, the probe shaft can be analyzed as a tapered, cylindrical beam, rigidly fixed at the handle and with a load W applied at the tip. Applying standard analysis for a bending beam (Young 1989), the longitudinal stress σ at the top or bottom surface of the probe at a distance x from the tip can be shown to be:

$$\sigma = \frac{MR}{I}$$

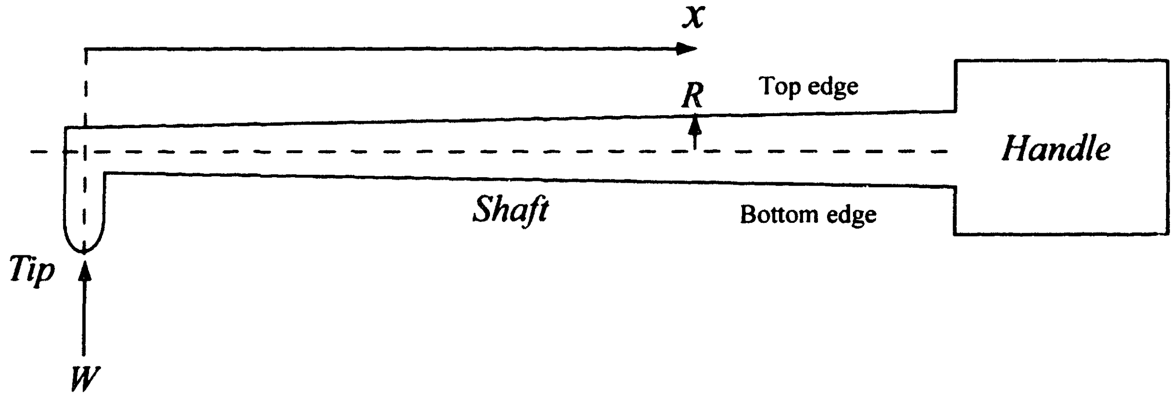

Figure D-1 Diagram for analysis of strain along shaft of surgical probe. W = load applied to tip of probe. x = distance from center of tip to a point along shaft. R = radius of shaft at x. (Not to scale.)

where M is the bending moment at x, R is the radius of the shaft at x, and I is the moment of inertia of the section of the shaft with respect to the central axis. For a positive W (as defined in Figure D-1), the stress is compressive at the top edge of the shaft and tensile at the bottom edge. Using the relations:

$$M = W\,x$$

and

$$I = \frac{\pi}{4} R^4 \quad \text{(for a shaft of circular cross-section)}$$

we obtain:

$$\sigma = \frac{4W\,x}{\pi R^3}$$

The resulting strain e at the top or bottom surface of the probe is:

$$e = \frac{\sigma}{E}$$

where E is the modulus of elasticity of the shaft material. (The Acufex Model 010001 probe is made of surgical stainless steel; an exact value of E for the specific alloy used in the probe was not obtainable, so a nominal value for stainless steel of $E = 195 \cdot 10^9$ Pa was used.)

A rough estimate was made that during *in vivo* arthroscopic probing, the force applied at the probe tip is on the order of one to several ounces. This was done by observation and interviews of surgeons in the operating room during arthroscopic probing and manual probing by the author (under guidance by the attending surgeon). Using the above relationships and a nominal load of 100 g (approximately 3 ounces), the value of strain was computed at locations along the probe shaft from 2 cm to 10 cm from the tip. (The total length of the probe from tip to handle is 11.5 cm.) To obtain R at each position along the shaft, the diameter was measured with an electronic digital caliper (Fowler & NSK Max-Cal). The results are tabulated in Table D-1.

An interesting feature of the longitudinal stress and strain is that these parameters vary by only approximately +/- 10% from $x = 2$ cm to $x = 8$ cm. This is a result of the steady increase in shaft diameter between these locations. Strain reached a maximum close to the handle, indicating that maximum sensitivity of the instrumented probe would be achieved by placing the strain gages on the shaft as close to the handle as practicable.

Distance from tip, x (cm)	Shaft radius, R (mm)	Shaft surface stress σ for 100 g load (Pa)	Shaft surface strain e for 100 g load
2.0	2.0	$25 \cdot 10^6$	$128 \cdot 10^{-6}$
4.0	2.4	$29 \cdot 10^6$	$148 \cdot 10^{-6}$
6.0	2.765	$28 \cdot 10^6$	$145 \cdot 10^{-6}$
8.0	2.98	$30 \cdot 10^6$	$155 \cdot 10^{-6}$
10.0	2.98	$38 \cdot 10^6$	$193 \cdot 10^{-6}$

Table D-1 Calculated stress and strain at 5 locations along shaft of Acufex Model 010001 arthroscopic probe when loaded with 100 g at the tip.

Bibliography

Allen, R. G., D. Burstein and M. L. Gray (1999). Monitoring glycosaminoglycan replenishment in cartilage explants with gadolinium-enhanced magnetic resonance imaging. *J Orthop Res*, **17**(3): 430-6.

Allen, R. G., S. R. Eisenberg and M. L. Gray (1998). Quantitative measurement of the biological response of cartilage to mechanical deformation. *Methods in molecular medicine, Vol. 18: Tissue engineering methods and protocols.* J. R. Morgan and M. L. Yarmush, editors. Totowa, N.J., Humana Press Inc.: 521-542.

Appleyard, R. C., M. V. Swain, S. Khanna and G. A. Murrell (2001). The accuracy and reliability of a novel handheld dynamic indentation probe for analysing articular cartilage. *Phys Med Biol*, **46**(2): 541-50.

Armitage, P. and G. Berry (1987). Statistical methods in medical research, 2nd edition. 2nd ed. Oxford, Blackwell Scientific Publications: 273-279.

Armstrong, C. G., W. M. Lai and V. C. Mow (1984). An analysis of the unconfined compression of articular cartilage. *J Biomech Eng*, **106**(2): 165-73.

Arnoczky, S. P., J. A. Dodds and T. L. Wickiewicz (1996). Basic science of the knee. *Operative Arthroscopy*. J. B. McGinty, R. B. Caspari, R. W. Jackson and G. G. Poehling, editors. Philadelphia, Lippincott-Raven: 211-239.

Askew, M. J. and V. C. Mow (1978). The biomechanical function of the collagen fibril ultrastructure of articular cartilage. *J Biomech Eng*, **100**: 105-15.

Ateshian, G. A., L. J. Soslowsky and V. C. Mow (1991). Quantitation of articular surface topography and cartilage thickness in knee joints using stereophotogrammetry. *J Biomech*, **24**(8): 761-76.

Athanasiou, K. A., M. P. Rosenwasser, J. A. Buckwalter, T. I. Malinin and V. C. Mow (1991). Interspecies comparisons of in situ intrinsic mechanical properties of distal femoral cartilage. *J Orthop Res*, **9**(3): 330-40.

Azar, F. M. and J. R. Andrews (1997). Diagnostic arthroscopy of the knee. *Diagnostic and operative arthroscopy*. J. R. Andrews and L. A. Timmerman, editors. Philadelphia, W. B. Saunders Company: 227-253.

Bader, D. L., G. E. Kempson, J. Egan, W. Gilbey and A. J. Barrett (1992). The effects of selective matrix degradation on the short-term compressive properties of adult human articular cartilage. *Biochim Biophys Acta*, **1116**(2): 147-54.

Bae, W. C., M. M. Temple, K. L. Rivard, G. Niederauer and R. L. Sah (2002). Indentation testing of human articular cartilage: sensitivity to indices of degeneration. *Trans Orthop Res Soc*, **27**: 252.

Bageac, A. C., M. L. Gray, M. Zhang, A. R. Poole and D. Burstein (1999). *Development of an MRI surrogate for immunohistochemical staining of collagen damage in cartilage*. 5th international conference on magnetic resonance microscopy, Heidelberg, Germany, Groupement Ampere.

Bashir, A., M. L. Gray, R. D. Boutin and D. Burstein (1997). Glycosaminoglycan in articular cartilage: in vivo assessment with delayed Gd(DTPA)(2-)-enhanced MR imaging. *Radiology*, **205**(2): 551-8.

Bashir, A., M. L. Gray and D. Burstein (1996). Gd-DTPA2- as a measure of cartilage degradation. *Magn Reson Med*, **36**(5): 665-73.

Bashir, A., M. L. Gray, J. Hartke and D. Burstein (1999). Nondestructive imaging of human cartilage glycosaminoglycan concentration by MRI. *Magn Reson Med*, **41**(5): 857-65.

Beauregard, G. L. (1996). *Sensorimotor interactions in the haptic perception of virtual objects*. Ph.D. Thesis, Department of Biomedical Engineering, Boston University, Boston.

Berkenblit, S. I., E. H. Frank, E. P. Salant and A. J. Grodzinsky (1994). Nondestructive detection of cartilage degeneration using electromechanical surface spectroscopy. *J Biomech Eng*, **116**(4): 384-92.

Black, J., C. A. Shadle, J. R. Parsons and C. T. Brighton (1979). Articular cartilage preservation and storage. II. Mechanical indentation testing of viable, stored articular cartilage. *Arthritis Rheum*, **22**(10): 1102-8.

Bray, R. C., C. B. Frank and A. Miniaci (1996). The structure and function of diarthrodial joints. *Operative arthroscopy.* J. B. McGinty, R. B. Caspari, R. W. Jackson and G. G. Poehling, editors. Philadelphia, Lippincott-Raven: 105-143.

Burstein, D., A. Bashir and M. L. Gray (2000). MRI techniques in early stages of cartilage disease. *Invest Radiol,* **35**(10): 622-38.

Burstein, D., J. Velyvis, K. T. Scott, K. W. Stock, Y. J. Kim, D. Jaramillo, R. D. Boutin and M. L. Gray (2001). Protocol issues for delayed Gd(DTPA)(2-)-enhanced MRI (dGEMRIC) for clinical evaluation of articular cartilage. *Magn Reson Med,* **45**(1): 36-41.

Centers for Disease Control and Prevention (2001). Targeting arthritis: the nation's leading cause of disability. http://www.cdc.gov/nccdphp/arthritis.pdf Accessed January 3, 2002.

Clark, J. M. (1991). Variation of collagen fiber alignment in a joint surface: a scanning electron microscope study of the tibial plateau in dog, rabbit, and man. *J Orthop Res,* **9**(2): 246-57.

Cohen, B. (1992). *Anisotropic hydrated soft tissues in finite deformation and the biomechanics of the growth plate.* Ph.D. thesis, Columbia University.

Cohen, B., T. R. Gardner and G. A. Ateshian (1993). The influence of transverse isotropy on cartilage indentation behavior. A study of the human humeral head. *Trans Orthop Res Soc,* **18**: 185.

Coletti, J. M., W. H. Akeson and S. L. Woo (1972). A comparison of the physical behavior of normal articular cartilage and the arthroplasty surface. *J Bone Joint Surg Am,* **54**(1): 147-60.

Conway, W. F., C. W. Hayes, T. Loughran, W. G. Totty, L. K. Griffeth, G. Y. el-Khoury and F. G. Shellock (1991). Cross-sectional imaging of the patellofemoral joint and surrounding structures. *Radiographics,* **11**(2): 195-217.

Dashefsky, J. H. (1987). Arthroscopic measurement of chondromalacia of patella cartilage using a microminiature pressure transducer. *Arthroscopy,* **3**(2): 80-5.

Dawson, S. L. and J. A. Kaufman (1998). The imperative for medical simulation. *Proceedings of the IEEE,* **86**(3): 479-483.

DiSilvestro, M. R. and J. K. Suh (2001). A cross-validation of the biphasic poroviscoelastic model of articular cartilage in unconfined compression, indentation, and confined compression. *J Biomech,* **34**(4): 519-25.

Durfee, W. K., C. M. Hendrix, P. Cheng and G. Varughese (1997). Influence of haptic and visual displays on the estimation of virtual environment stiffness. *Proceedings of the ASME Dynamic Systems and Control Division.*

Eberhardt, A. W., L. M. Keer, J. L. Lewis and V. Vithoontien (1990). An analytical model of joint contact. *J Biomech Eng*, **112**(4): 407-13.

Franz, T., E. M. Hasler, R. Hagg, C. Weiler, R. P. Jakob and P. Mainil-Varlet (2001). In situ compressive stiffness, biochemical composition, and structural integrity of articular cartilage of the human knee joint. *Osteoarthritis Cartilage*, **9**(6): 582-92.

Fu, F. H., I. Youn and J. K. Suh (1998). *Clinical evaluation of mechanical properties of articular cartilage using a newly developed arthroscopic ultrasonic indentation probe*. 2nd Symposium of the International Cartilage Repair Society (ICRS), Boston.

Fung, Y. C. (1972). Stress–strain-history relations of soft tissues in simple elongation. *Biomechanics: Its foundations and objectives*. Y. C. Fung, N. Perrone and M. Anliker, editors. Englewood Cliffs, N.J., Prentice-Hall: 181-208.

Fung, Y. C. (1993). *Biomechanics: Mechanical properties of living tissues*. New York, Springer-Verlag.

Gibson, S., C. Fyock, E. Grimson, T. Kanade, R. Kikinis, H. Lauer, N. McKenzie, A. Mor, S. Nakajima, H. Ohkami, R. Osborne, J. Samosky and A. Sawada (1998). Volumetric object modeling for surgical simulation. *Med Image Anal*, **2**(2): 121-32.

Goldsmith, A. A., A. Hayes and S. E. Clift (1996). Application of finite elements to the stress analysis of articular cartilage. *Med Eng Phys*, **18**(2): 89-98.

Grunder, W., M. Biesold, M. Wagner and A. Werner (1998). Improved nuclear magnetic resonance microscopic visualization of joint cartilage using liposome entrapped contrast agents. *Invest Radiol*, **33**(4): 193-202.

Harris, E. D., H. G. Parker, E. L. Radin and S. M. Krane (1972). Effects of proteolytic enzymes on structural and mechanical properties of cartilage. *Arthritis Rheum*, **15**(5): 497-503.

Hayes, W. C., L. M. Keer, G. Herrmann and L. F. Mockros (1972). A mathematical analysis for indentation tests of articular cartilage. *J Biomech*, **5**(5): 541-51.

Hayes, W. C. and L. F. Mockros (1971). Viscoelastic properties of human articular cartilage. *J Appl Physiol*, **31**(4): 562-8.

Hertz, H. (1895a). Über die Berührung fester elastischer Körper. *Gesammelte Werke*, **1**: 155-173.

Hertz, H. (1895b). Über die Berührung fester elastischer Körper und über die Härte. *Gesammelte Werke*, **1**: 174-196.

Hoch, D. H., A. J. Grodzinsky, T. J. Koob, M. L. Albert and D. R. Eyre (1983). Early changes in material properties of rabbit articular cartilage after meniscectomy. *J Orthop Res*, **1**(1): 4-12.

Hori, R. Y. and L. F. Mockros (1976). Indentation tests of human articular cartilage. *J Biomech*, **9**(4): 259-68.

Jones, L. A. and I. W. Hunter (1990). A perceptual analysis of stiffness. *Exp Brain Res*, **79**(1): 150-6.

Jones, L. A. and I. W. Hunter (1993). A perceptual analysis of viscosity. *Exp Brain Res*, **94**(2): 343-51.

Joyce, M. E. and J. R. Andrews (1997). Normal and pathologic arthroscopic anatomy of the knee. *Diagnostic and operative arthroscopy*. J. R. Andrews and L. A. Timmerman, editors. Philadelphia, W. B. Saunders Company: 254-173.

Jurvelin, J., A. M. Saamanen, J. Arokoski, H. J. Helminen, I. Kiviranta and M. Tammi (1988). Biomechanical properties of the canine knee articular cartilage as related to matrix proteoglycans and collagen. *Engineering in Medicine*, **17**(4): 157-62.

Kapur, T., P. A. Beardsley, S. F. Gibson, W. E. L. Grimson and W. M. Wells (1998). Model based segmentation of clinical knee MRI. *IEEE International Workshop on Model Based 3D Image Analysis*.

Kapur, T., W. E. L. Grimson, R. Kikinis and W. M. Wells (1998). Enhanced spatial priors for segmentation of magnetic resonance imagery. *Proceedings of MICCAI '98*: 457-468.

Kempson, G. E. (1975). The effects of proteoglycan and collagen degradation on the mechanical properties of adult human articular cartilage. *Dynamics of connective tissue macromolecules*. P. M. C. Burleigh and A. R. Poole, editors. Amsterdam, North Holland Publishing Co. **532:** 277-307.

Kempson, G. E., H. Muir, S. A. Swanson and M. A. Freeman (1970). Correlations between stiffness and the chemical constituents of cartilage on the human femoral head. *Biochim Biophys Acta*, **215**: 70-71.

Kempson, G. E., C. J. Spivey, S. A. Swanson and M. A. Freeman (1971). Patterns of cartilage stiffness on normal and degenerate human femoral heads. *J Biomech*, **4**(6): 597-609.

Korhonen, R. K., M. Wong, J. Arokoski, R. Lindgren, H. J. Helminen, E. B. Hunziker and J. S. Jurvelin (2002). Importance of the superficial tissue layer for the indentation stiffness of articular cartilage. *Med Eng Phys*, **24**(2): 99-108.

Kwan, M. K., W. M. Lai and V. C. Mow (1990). A finite deformation theory for cartilage and other soft hydrated connective tissues--I. Equilibrium results. *J Biomech*, **23**(2): 145-55.

Lai, W. M. and V. C. Mow (1980). Drag-induced compression of articular cartilage during a permeation experiment. *Biorheology*, **17**(1-2): 111-23.

Lai, W. M., V. C. Mow and V. Roth (1981). Effects of nonlinear strain-dependent permeability and rate of compression on the stress behavior of articular cartilage. *J Biomech Eng*, **103**(2): 61-6.

Lai, W. M., V. C. Mow and W. Zhu (1993). Constitutive modeling of articular cartilage and biomacromolecular solutions. *J Biomech Eng*, **115**(4B): 474-80.

Lécuyer, A., J.-M. Burkhardt, S. Coquillart and P. Coiffet (2001). "Boundary of Illusion": an experiment of sensory integration with a pseudo-haptic system. *Proceedings of IEEE Virtual Reality*: 115-122.

Lyyra, T., J. P. Arokoski, N. Oksala, A. Vihko, M. Hyttinen, J. S. Jurvelin and I. Kiviranta (1999). Experimental validation of arthroscopic cartilage stiffness measurement using enzymatically degraded cartilage samples. *Phys Med Biol*, **44**(2): 525-35.

Lyyra, T., J. Jurvelin, P. Pitkanen, U. Vaatainen and I. Kiviranta (1995). Indentation instrument for the measurement of cartilage stiffness under arthroscopic control. *Med Eng Phys*, **17**(5): 395-9.

Mak, A. F. (1986). The apparent viscoelastic behavior of articular cartilage--the contributions from the intrinsic matrix viscoelasticity and interstitial fluid flows. *J Biomech Eng*, **108**(2): 123-30.

Mak, A. F., W. M. Lai and V. C. Mow (1987). Biphasic indentation of articular cartilage--I. Theoretical analysis. *J Biomech*, **20**(7): 703-14.

Maroudas, A., P. Bullough, S. A. Swanson and M. A. Freeman (1968). The permeability of articular cartilage. *J Bone Joint Surg Br*, **50**(1): 166-77.

Metcalf, R. W. and H. J. Sweeny (1996). Education in arthroscopy. *Operative arthroscopy*. 2nd ed. J. B. McGinty, R. B. Caspari, R. W. Jackson and G. G. Poehling, editors. Philadelphia, Lippincott-Raven: 93-104.

Mizrahi, J., A. Maroudas, Y. Lanir, I. Ziv and T. J. Webber (1986). The "instantaneous" deformation of cartilage: effects of collagen fiber orientation and osmotic stress. *Biorheology*, **23**(4): 311-30.

Mow, V. C., M. C. Gibbs, W. M. Lai, W. B. Zhu and K. A. Athanasiou (1989). Biphasic indentation of articular cartilage--II. A numerical algorithm and an experimental study. *J Biomech*, **22**(8-9): 853-61.

Mow, V. C., S. C. Kuei, W. M. Lai and C. G. Armstrong (1980). Biphasic creep and stress relaxation of articular cartilage in compression: theory and experiments. *J Biomech Eng*, **102**(1): 73-84.

Mow, V. C., M. K. Kwan, W. M. Lai and M. H. Holmes (1986). A finite deformation theory for nonlinearly permeable soft hydrated biological tissues. *Frontiers in Biomechanics*. S. L. Woo, editor. New York, Springer-Verlag: 153-179.

Niederauer, M. Q., S. Cristante, G. M. Niederauer, R. P. Wilkes, S. M. Singh, D. F. Messina, M. A. Walter, B. D. Boyan, J. C. DeLee and G. Niederauer (1998). *A novel instrument for quantitatively measuring the stiffness of articular cartilage*. Transactions of the 44th Annual Meeting of the Orthopaedic Research Society, New Orleans, Louisiana.

Nieminen, M. T., J. Töyräs, M. S. Laasanen, J. Rieppo, J. Silvennoinen, H. J. Helminen and J. S. Jurvelin (2001). MRI quantitation of proteoglycans predicts cartilage stiffness in bovine humeral head. *Trans Orthop Res Soc*, **26**: 127.

Nieminen, M. T., J. Toyras, J. Rieppo, J. M. Hakumaki, J. Silvennoinen, H. J. Helminen and J. S. Jurvelin (2000). Quantitative MR microscopy of enzymatically degraded articular cartilage. *Magn Reson Med*, **43**(5): 676-81.

Ota, D., B. Loftin, T. Saito, R. Lea and J. Keller (1995). Virtual reality in surgical education. *Computers in Biology and Medicine*, **25**(2): 127-137.

Parsons, J. R. and J. Black (1977). The viscoelastic shear behavior of normal rabbit articular cartilage. *J Biomech*, **10**(1): 21-9.

Praemer, A. (1998). Personal communication, August 5, 1998. Data extracted and analyzed by American Academy of Orthopaedic Surgery, Department of Research and Scientific Affairs. Source: National Center for Health Statistics, 1995 National Hospital Discharge Survey and 1995 National Survey of Ambulatory Surgery.

Roland, P. E. and H. Ladegaard-Pedersen (1977). A quantitative analysis of sensations of tension and of kinaesthesia in man. Evidence for a peripherally originating muscular sense and for a sense of effort. *Brain*, **100**(4): 671-92.

Sah, R. L., Y. J. Kim, J. Y. Doong, A. J. Grodzinsky, A. H. Plaas and J. D. Sandy (1989). Biosynthetic response of cartilage explants to dynamic compression. *J Orthop Res*, **7**(5): 619-36.

Satava, R. M. (1993). Virtual reality surgical simulator: The first steps. *Surgical Endoscopy*, **7**: 203-205.

Satava, R. M. and S. B. Jones (1998). Current and future applications of virtual reality for medicine. *Proceedings of the IEEE*, **86**(3): 484-489.

Shahriaree, H. (1992). Arthroscopic technique and normal anatomy. *O'Connor's textbook of arthroscopic surgery*. 2nd ed. Philadelphia, J. B. Lippincott: 255-283.

Shepherd, D. E. and B. B. Seedhom (1999). The 'instantaneous' compressive modulus of human articular cartilage in joints of the lower limb. *Rheumatology (Oxford)*, **38**(2): 124-32.

Simon, B. R., R. S. Coats and S. L. Woo (1984). Relaxation and creep quasilinear viscoelastic models for normal articular cartilage. *J Biomech Eng*, **106**(2): 159-64.

Spilker, R. L. and J. F. Suh (1990). Formulation and evaluation of a finite element model for the biphasic model of hydrated soft tissues. *Comp. and Struc.*, **35**(4): 425-439.

Spilker, R. L., J. K. Suh and V. C. Mow (1992). A finite element analysis of the indentation stress-relaxation response of linear biphasic articular cartilage. *J Biomech Eng*, **114**(2): 191-201.

Srinivasan, M. A., G. L. Beauregard and D. L. Brock (1996). The impact of visual information on the haptic perception of stiffness in virtual environments. *Proceedings of the ASME Dynamic Systems and Control Division*, **58**: 555-559.

Tan, H. Z., N. I. Durlach, G. L. Beauregard and M. A. Srinivasan (1995). Manual discrimination of compliance using active pinch grasp: the roles of force and work cues. *Percept Psychophys*, **57**(4): 495-510.

Tan, H. Z., X. D. Pang and N. I. Durlach (1992). Manual resolution of length, force and compliance. *Advances in Robotics, Proceedings of the ASME Dynamics and Control Division*, **42**: 13-18.

Tiderius, C. J., L. E. Olsson, P. Leander, H. De Verdier and L. Dahlberg (1999). Gadolinium (Gd-DTPA^{2-}) enhanced MRI can differentiate between arthroscopically healthy and degenerated human knee joint cartilage. *Trans Orthop Res Soc*, **24**.

Tiderius, C. J., L. E. Olsson, H. Verdier, P. Leander, O. Ekberg and L. Dahlberg (2001). Gd-DTPA^{2-}-enhanced MRI of femoral knee cartilage: a dose-response study in healthy volunteers. *Magn Reson Med (in press).*

Timoshenko, S. and J. N. Goodier (1970). Theory of elasticity. 3rd ed. New York, McGraw-Hill: 409-414.

Tkaczuk, H. (1986). Human cartilage stiffness. In vivo studies. *Clinical Orthopaedics and Related Research*(206): 301-12.

Tkaczuk, H., H. Norrbom and H. Werelind (1982). A cartilage elastometer for use in the living subject. *J Med Eng Technol*, **6**(3): 104-7.

Trattnig, S., V. Mlynarik, M. Breitenseher, M. Huber, A. Zembsch, T. Rand and H. Imhof (1999). MRI visualization of proteoglycan depletion in articular cartilage via intravenous administration of Gd-DTPA. *Magn Reson Imaging*, **17**(4): 577-83.

Treppo, S., E. C. Quan, N. Batra, E. H. Frank and A. J. Grodzinsky (1998). *Development of a surface electromechanical spectroscopy probe for in-vivo cartilage diagnostics.* 2nd Symposium of the International Cartilage Repair Society (ICRS), Boston.

Wagner, M., A. Werner and W. Grunder (1999). Visualization of collagenase-induced cartilage degradation using NMR microscopy. *Invest Radiol*, **34**(10): 607-14.

Waters, N. E. (1965). The indentation of thin rubber sheets by spherical indentors. *British Journal of Applied Physics*, **16**: 557-563.

Williams, A. A. (2001). *Regeneration of cartilage glycosaminoglycan after degradation by interleukin-1.* M.S. Thesis, Department of Electrical Engineering and Computer Science, Massachusetts Institute of Technology, Cambridge, MA.

Winalski, C. S., P. Aliabadi, R. J. Wright, S. Shortkroff, C. B. Sledge and B. N. Weissman (1993). Enhancement of joint fluid with intravenously administered gadopentetate dimeglumine: technique, rationale, and implications. *Radiology*, **187**(1): 179-85.

Woo, S. L., B. R. Simon, S. C. Kuei and W. H. Akeson (1980). Quasi-linear viscoelastic properties of normal articular cartilage. *J Biomech Eng*, **102**(2): 85-90.

Wu, W.-C., C. Basdogan and M. A. Srinivasan (1999). Visual, haptic, and bimodal perception of size and stiffness in virtual environments. *Proceedings of the ASME Dynamics and Control Division*, **67**: 19-26.

Xia, Y. (1998). Relaxation anisotropy in cartilage by NMR microscopy (muMRI) at 14-microm resolution. *Magn Reson Med*, **39**(6): 941-9.

Young, W. C. (1989). *Roark's Formulas for Stress and Strain*. 6th ed. New York, McGraw-Hill.

THESIS PROCESSING SLIP

FIXED FIELD: ill. ______________ name ______________

index ______________ biblio ______________

► **COPIES:** [✓ Archives] Aero Dewey Barker Hum

Lindgren Music Rotch Science [✓ Sche-Plough]

TITLE VARIES: ► ☐ ______________

NAME VARIES: ► ☐ ______________

IMPRINT: (COPYRIGHT) ______________

► **COLLATION:** ______________

► **ADD: DEGREE:** ________ ► **DEPT.:** ______________

► **ADD: DEGREE:** ________ ► **DEPT.:** ______________

SUPERVISORS: ______________

[illegible]

NOTES:

cat'r: date:

page:

► [illegible]

► **DEPT:** HST

► **YEAR:** 2002 ► **DEGREE:** Ph.D.

► **NAME:** [illegible]

[illegible]